

Universiteit
Leiden
The Netherlands

Development of hyaluronan-based dissolving microneedle arrays for dermal vaccination

Leone, M.

Citation

Leone, M. (2020, December 10). *Development of hyaluronan-based dissolving microneedle arrays for dermal vaccination*. Retrieved from https://hdl.handle.net/1887/138252

Version:	Publisher's Version
License:	Licence agreement concerning inclusion of doctoral thesis in the Institutional Repository of the University of Leiden
Downloaded from:	https://hdl.handle.net/1887/138252

Note: To cite this publication please use the final published version (if applicable).

Cover Page



Universiteit Leiden



The handle http://hdl.handle.net/1887/138252 holds various files of this Leiden University dissertation.

Author: Leone, M.
Title: Development of hyaluronan-based dissolving microneedle arrays for dermal vaccination
Issue date: 2020-12-10

Development of hyaluronan-based dissolving microneedle arrays for dermal vaccination

Mara Leone

Development of hyaluronan-based dissolving microneedle arrays for dermal vaccination

PhD thesis with summary in Dutch

©2020 Mara Leone. All rights reserved. No part of this thesis may be reproduced or transmitted in any form or by any means without written permission of the author.

Cover： the fluorescence microscopy images provide a view parallel to the skin surface and depict fluorescein amine-labeled hyaluronan (green), rhodamine B-labeled trimethyl chitosan (white) and lumogallion-labeled diphtheria toxoid (red) released in *ex vivo* human skin.

Cover design: Mara Leone

Printing: Off Page, Amsterdam

ISBN: 978-94-93197-35-0

Development of hyaluronan-based dissolving microneedle arrays for dermal vaccination

PROEFSCHRIFT

ter verkrijging van

de graad van Doctor aan de Universiteit Leiden,

op gezag van de Rector Magnificus prof.mr. C.J.J.M. Stolker,

volgens besluit van het College voor Promoties

te verdedigen op donderdag 10 december 2020

klokke 10:00 uur

door

Mara Leone

Geboren te Avellino, Italy

in 1987

Promotoren Prof. Dr. G.F.A. Kersten

Prof. Dr. J.A. Bouwstra

Promotiecommissie Prof. Dr. H. Irth, Universiteit Leiden (voorzitter)

Prof. Dr. A. P. IJzerman, Universiteit Leiden (secretaris)

Prof. Dr. C. W. J. Oomens, Universiteit Eindhoven

Prof. Dr. Ir. W. E. Hennink, Universiteit Utrecht

Prof. Dr. A.L.W. Huckriede, Rijksuniversiteit Groningen

Dr. A. Moore, University College Cork, Ireland

The research described in this thesis was performed at the division BioTherapeutics of the Leiden Academic Centre for Drug Research (LACDR), Leiden University (Leiden, The Netherlands). The research was financially supported by Intravacc (Bilthoven, The Netherlands).

To my family,

to Paolo,

for being always by my side

giving me strength, support and endless love

TABLE OF CONTENTS

Chapter 1

General introduction, aim and outline of this thesis 1

Chapter 2

Dissolving Microneedle Patches for Dermal Vaccination 9

Chapter 3

Universal Applicator for Digitally-Controlled Pressing Force and Impact Velocity Insertion of Microneedles into Skin 41

Chapter 4

Hyaluronan-based dissolving microneedles with high antigen content for intradermal vaccination: Formulation, physicochemical characterization and immunogenicity assessment 67

Chapter 5

Hyaluronan molecular weight: Effects on dissolution time of dissolving microneedles in the skin and on immunogenicity of antigen 99

Chapter 6

Diphtheria toxoid dissolving microneedle vaccination: adjuvant screening and effect of repeated-fractional dose administration 119

Chapter 7

Summarizing discussion and prospects 147

Appendices

Nederlandse samenvatting 157

Curriculum Vitae 165

List of publications 167

Chapter 1

General introduction, aim and outline of this thesis

GENERAL INTRODUCTION

Vaccination

Vaccination is one of the most effective healthcare interventions lowering mortality and morbidity and as a result increasing life expectancy [1]. The introduction of vaccines led to the eradication of smallpox, while eradication of polio is on its way and other important infectious diseases such as measles are under control in vaccinated populations [2]. Although many successes can be related to effective vaccines and vaccination programs, each year almost 3 million children still die of diseases caused by infections that could be prevented by vaccination [2]. A large proportion of deaths occurs in low-income countries [1]. Vaccination costs related to the production, transport, need for cold-chain and for trained personnel capable to administer the vaccine all contribute to total system costs, making vaccination too expensive for developing countries [3, 4]. A reduction in the vaccination coverage is also related to avoidance of injections because of fear for pain, needle-phobia and stress experienced during vaccination [5]. To overcome these problems, research on a minimally invasive strategy of vaccine administration has been addressed focusing on nasal [6], oral [7], pulmonary [8] and intradermal route of vaccination [9]. Intradermal vaccination has been considered particularly attractive because the skin is easy to access and a very immune competent organ containing antigen presenting cells (APCs) as Langerhans cells (LCs) and dermal dendritic cells (dDCs) [10, 11], making the skin an attractive vaccination site. However, the skin presents a barrier located in the upper layer, the *stratum corneum*, that protects the body against the entrance of foreign substances [12]. An effective method to enable vaccine administration via the skin is the use of microneedles (MNs), conceived for the first time by ALZA corporation and described in a patent in 1976 [13].

Microneedles

MNs have a size of up to 1 mm in length. They are designed to pierce the physical barrier, the *stratum corneum*, and to avoid the generation of pain because the MN tips do not reach pain receptors in the skin [14-16]. A further potential advantage of MNs consists in reducing the vaccination costs by i) avoiding the need of trained personnel to be applied [14, 17] and ii) resulting in a dose-sparing potential as the skin is a potent immune competent organ [18-21].

Generally, MNs are classified in six groups [22-25]:

i) Solid MNs designed for pretreatment of the skin. After the formation of microholes in the skin, the MNs are removed and a vaccine loaded patch is applied on the pierced skin to allow the diffusion of the vaccine along the conduits into the skin. Although a very straightforward method, the diffusion of the vaccine from the skin surface to and through the microholes made by the MNs is slow and inefficient due to the small diameter of the microholes and the limited number of microneedles in the patch. Thus, over a reasonable time

period, only a small fraction of the applied vaccine is delivered into the skin. Furthermore, the microholes may close soon after the removal of the MNs limiting the diffusion time [26]. To avoid this inconvenience, new MN systems have been developed including hollow, coated, porous, dissolving and hydrogel-forming MNs.

ii) Hollow MNs contain a bore through which the vaccine formulation can be injected into the skin. One of the advantage of using hollow MNs is that the skin depth and injection volume and injection rate can be precisely controlled [15]. However, one big challenge is to avoid leakage due to the short needle length inserted in the skin. Furthermore, dry formulation need a reconstitution step previous injection [17]. Additionally, the use of harmful chemicals, as hydrofluoric acid and concentrated sulfuric acid, may be included in the production process of hollow MNs [27, 28].

iii) Coated MNs have the vaccine coated on their surface and upon insertion the vaccine is released into the skin. Although only a very low amount of vaccine can be coated, due to the limited surface area of MNs, this may be sufficient to evoke a protective immune response [29]. Coatings are usually applied by: i) dip coating method [30, 31], ii) gas jet drying approach producing a thin coating and thus reducing vaccine wastage [32] or iii) layer-by-layer coating approach in which the intended amount of vaccine can be coated by adjusting the number of layers [33-35].

iv) Porous MNs with the vaccine deposited in a porous MN matrix release the vaccine by diffusion of the vaccine in solution from the pores into the skin after piercing. However, porous structures are generally more fragile than solid structures [36] and may easily break remaining in the skin. This may be a problem when the matrix is made of no-biodegradable material as silicon [37, 38]. Therefore, biodegradable materials are preferred such as microporous calcium phosphate coating stainless steel solid MNs [39].

v) Hydrogel-forming MNs that after insertion into the skin take up interstitial fluids from the tissue that triggers the release of the vaccine into the skin. These MNs are prepared from crosslinked polymers that rapidly take up skin interstitial fluid upon skin insertion to form continuous hydrogel conduits from the array to the dermal microcirculation. With this approach, the delivery of vaccine is controlled by the crosslink density of the hydrogel system [40].

vi) Dissolving MNs are made of hydrophilic material, such as polymers or sugars, mixed with the active pharmaceutical ingredient. After insertion into the skin, the MNs can completely dissolve thereby releasing the vaccine.

This thesis focuses on dissolving microneedles (dMNs). They have the advantage to completely dissolve in the skin avoiding sharp needle waste left behind after use [17] and thus avoiding potential infections due to the needle re-use especially in developing countries. Moreover, for vaccine in solid state, as for coated and dissolving MNs, it may be

possible to circumvent the need for a cold-chain to keep the antigen stable during storage and shipping [30].

Microneedle application

Microneedles can be applied onto the skin either manually or by the use of an applicator. The manual application, however, especially for short MNs (< 550 μm), may results in both a low penetration efficiency in the skin and a low reproducibility of skin piercing [41, 42] and therefore an applicator is required for this type of microneedles for a controlled application [43] in terms of penetration force or velocity.

AIM AND OUTLINE OF THIS THESIS

The aim of this thesis was to develop dissolving MNs for dermal vaccine delivery. The study objectives include:

1. An overview of dMNs for a proper understanding of the dMN subject present in the following research chapters;

2. The use of a digitally-controlled applicator as a tool to investigate mechanical variables and their effect on insertion efficiency of a wide variety of MNs in the skin and consequent delivery of the antigen in the skin;

3. The optimization of dMN fabrication and investigation of antigen loading capacity of dMNs;

4. The evaluation of the effects of the molecular weight of hyaluronan (dMNs matrix material) on the immune response for a proper choice in the fabrication of dMNs;

5. The determination of the effects of different antigen(-adjuvant) administration modalities by dMNs, such as single dose or repeated fractional doses administration, on the immune response.

Chapter 2 provides a review of the current status of dMN development. This includes a screening of the materials used for the fabrication of dMNs, a description of the dMN manufacturing methods and an analysis of the parameters that must be evaluated to assess dMN quality. Furthermore, this chapter describes the immunogenicity of antigens administered by dMNs both in preclinical and in clinical studies.

The research described in *Chapter 3* focuses on the investigation of penetration efficiency and antigen release in the skin after MN application by the use of a digitally-controlled

applicator for a reproducible piercing of the skin. To this end, different application settings were set digitally in the applicator to determine the optimal insertion parameters for a variety of MN arrays from different manufacturers.

In *Chapter 4*, optimisation of the manufacturing of dMNs is described. A novel dMN fabrication method was developed and the effects of ovalbumin loading on dMNs physicochemical properties, such as dMN appearance, antigen stability after dMN fabrication, penetration efficiency of dMN in the skin, dissolution time of dMN in the skin, quantification of the amount of antigen delivered in the skin after dMN dissolution and mechanical integrity of dMNs after storage, were investigated. Finally, immunogenicity of OVA delivered by dMNs was determined in mice and compared with the immunogenicity of OVA administered via the conventional subcutaneous route.

The selected base material for the dMNs studied in this thesis is high molecular weight hyaluronan (HA). In the literature examples of immune modulating properties of low-molecular weight HA have been reported. The effect of HA molecular weights (HA-MWs) on the immune response against OVA are described in *Chapter 5*. After assessment of potential immune-modulatory effects following immunization with fluid formulations containing HA with different molecular weight, the suitability of HA-MWs to fabricate mechanically robust and functional dMNs was assessed.

Even though dermal immunization is in general very effective, adjuvants may be needed to optimise immune responses either quantitatively or qualitatively. Therefore, in *Chapter 6* an adjuvant screening for dermal vaccination was performed by vaccine microinjections using hollow MNs. Diphtheria toxoid was used as antigen. After selection of two promising adjuvants, dMNs loading diphtheria toxoid (DT), in the presence or absence of adjuvants, were fabricated and characterized *in vitro* and *in vivo*. In addition to a single full dose immunization, the effect of administering several fractional doses in several days was tested.

Chapter 7 provides a summary of the main findings of this thesis and the future prospects of dMNs-based immunization are discussed.

REFERENCES

1. Andre FE, Booy R, Bock HL, Clemens J, Datta SK, John TJ, Lee BW, Lolekha S, Peltola H, Ruff TA, Santosham M, Schmitt HJ. Vaccination greatly reduces disease, disability, death and inequity worldwide. Bull World Health Organ. 2008;86(2):140-146.
2. Greenwood B. The contribution of vaccination to global health: past, present and future. Philos Trans R Soc Lond B Biol Sci. 2014;369(1645):20130433.
3. Le Gargasson JB, Nyonator FK, Adibo M, Gessner BD, Colombini A. Costs of routine immunization and the introduction of new and underutilized vaccines in Ghana. Vaccine. 2015;33 Suppl 1:A40-46.
4. WHO. Stability of vaccines. Available from: https://www.who.int/biologicals/vaccines/stability_of_vaccines_ref_mats/en/.
5. Giudice EL, Campbell JD. Needle-free vaccine delivery. Adv Drug Deliv Rev. 2006;58(1):68-89.
6. Slutter B, Hagenaars N, Jiskoot W. Rational design of nasal vaccines. J Drug Target. 2008;16(1):1-17.
7. Simerska P, Moyle PM, Olive C, Toth I. Oral vaccine delivery--new strategies and technologies. Curr Drug Deliv. 2009;6(4):347-358.
8. Lu DM, Hickey AJ. Pulmonary vaccine delivery. Expert Rev Vaccines. 2007;6(2):213-226.
9. Mikszta JA, Laurent PE. Cutaneous delivery of prophylactic and therapeutic vaccines: historical perspective and future outlook. Expert Rev Vaccines. 2008;7(9):1329-1339.
10. Engelke L, Winter G, Hook S, Engert J. Recent insights into cutaneous immunization: How to vaccinate via the skin. Vaccine. 2015;33(37):4663-4674.
11. Kaurav M, Minz S, Sahu K, Kumar M, Madan J, Pandey RS. Nanoparticulate mediated transcutaneous immunization: Myth or reality. Nanomedicine. 2016;12(4):1063-1081.
12. Grice EA, Segre JA. The skin microbiome. Nat Rev Microbiol. 2011;9(4):244-253.
13. Martin S. Gerstel VAP. Drug delivery device In: Patent US, editor.: Alza Corporation, Palo Alto, Calif.; 1976.
14. Leone M, Monkare J, Bouwstra JA, Kersten G. Dissolving Microneedle Patches for Dermal Vaccination. Pharm Res. 2017.
15. van der Maaden K, Jiskoot W, Bouwstra J. Microneedle technologies for (trans)dermal drug and vaccine delivery. J Control Release. 2012;161(2):645-655.
16. Hegde NR, Kaveri SV, Bayry J. Recent advances in the administration of vaccines for infectious diseases: microneedles as painless delivery devices for mass vaccination. Drug Discov Today. 2011;16(23-24):1061-1068.
17. Kim YC, Park JH, Prausnitz MR. Microneedles for drug and vaccine delivery. Adv Drug Deliv Rev. 2012;64(14):1547-1568.
18. Vassilieva EV, Kalluri H, McAllister D, Taherbhai MT, Esser ES, Pewin WP, Pulit-Penaloza JA, Prausnitz MR, Compans RW, Skountzou I. Improved immunogenicity of individual influenza vaccine components delivered with a novel dissolving microneedle patch stable at room temperature. Drug Deliv Transl Re. 2015;5(4):360-371.
19. Vrdoljak A, Allen EA, Ferrara F, Temperton NJ, Crean AM, Moore AC. Induction of broad immunity by thermostabilised vaccines incorporated in dissolvable microneedles using novel fabrication methods. J Control Release. 2016;225:192-204.
20. Matriano JA, Cormier M, Johnson J, Young WA, Buttery M, Nyam K, Daddona PE. Macroflux microprojection array patch technology: a new and efficient approach for intracutaneous immunization. Pharm Res. 2002;19(1):63-70.
21. Alarcon JB, Hartley AW, Harvey NG, Mikszta JA. Preclinical evaluation of microneedle technology for intradermal delivery of influenza vaccines. Clin Vaccine Immunol. 2007;14(4):375-381.
22. Larraneta E, Lutton REM, Woolfson AD, Donnelly RF. Microneedle arrays as transdermal and intradermal drug delivery systems: Materials science, manufacture and commercial development. Mat Sci Eng R. 2016;104:1-32.
23. Larraneta E, McCrudden MTC, Courtenay AJ, Donnelly RF. Microneedles: A New Frontier in

Nanomedicine Delivery. Pharm Res-Dordr. 2016;33(5):1055-1073.
24. van der Maaden K, Luttge R, Vos PJ, Bouwstra J, Kersten G, Ploemen I. Microneedle-based drug and vaccine delivery via nanoporous microneedle arrays. Drug Deliv Transl Re. 2015;5(4):397-406.
25. Tuan-Mahmood TM, McCrudden MT, Torrisi BM, McAlister E, Garland MJ, Singh TR, Donnelly RF. Microneedles for intradermal and transdermal drug delivery. Eur J Pharm Sci. 2013;50(5):623-637.
26. Bal S, Kruithof AC, Liebl H, Tomerius M, Bouwstra J, Lademann J, Meinke M. In vivo visualization of microneedle conduits in human skin using laser scanning microscopy. Laser Phys Lett. 2010;7(3):242-246.
27. van der Maaden K, Trietsch SJ, Kraan H, Varypataki EM, Romeijn S, Zwier R, van der Linden HJ, Kersten G, Hankemeier T, Jiskoot W, Bouwstra J. Novel hollow microneedle technology for depth-controlled microinjection-mediated dermal vaccination: a study with polio vaccine in rats. Pharm Res. 2014;31(7):1846-1854.
28. Schipper P, van der Maaden K, Romeijn S, Oomens C, Kersten G, Jiskoot W, Bouwstra J. Determination of Depth-Dependent Intradermal Immunogenicity of Adjuvanted Inactivated Polio Vaccine Delivered by Microinjections via Hollow Microneedles. Pharm Res. 2016;33(9):2269-2279.
29. Du G, Woythe L, van der Maaden K, Leone M, Romeijn S, Kros A, Kersten G, Jiskoot W, Bouwstra JA. Coated and Hollow Microneedle-Mediated Intradermal Immunization in Mice with Diphtheria Toxoid Loaded Mesoporous Silica Nanoparticles. Pharm Res. 2018;35(10):189.
30. Gill HS, Prausnitz MR. Coated microneedles for transdermal delivery. J Control Release. 2007;117(2):227-237.
31. Gill HS, Prausnitz MR. Coating formulations for microneedles. Pharm Res. 2007;24(7):1369-1380.
32. Chen X, Prow TW, Crichton ML, Jenkins DW, Roberts MS, Frazer IH, Fernando GJ, Kendall MA. Dry-coated microprojection array patches for targeted delivery of immunotherapeutics to the skin. J Control Release. 2009;139(3):212-220.
33. DeMuth PC, Moon JJ, Suh H, Hammond PT, Irvine DJ. Releasable Layer-by-Layer Assembly of Stabilized Lipid Nanocapsules on Microneedles for Enhanced Transcutaneous Vaccine Delivery. Acs Nano. 2012;6(9):8041-8051.
34. van der Maaden K, Sekerdag E, Schipper P, Kersten G, Jiskoot W, Bouwstra J. Layer-by-Layer Assembly of Inactivated Poliovirus and N-Trimethyl Chitosan on pH-Sensitive Microneedles for Dermal Vaccination. Langmuir. 2015;31(31):8654-8660.
35. van der Maaden K, Yu HX, Sliedregt K, Zwier R, Leboux R, Oguri M, Kros A, Jiskoot W, Bouwstra JA. Nanolayered chemical modification of silicon surfaces with ionizable surface groups for pH-triggered protein adsorption and release: application to microneedles. J Mater Chem B. 2013;1(35):4466-4477.
36. Park JH, Choi SO, Kamath R, Yoon YK, Allen MG, Prausnitz MR. Polymer particle-based micromolding to fabricate novel microstructures. Biomed Microdevices. 2007;9(2):223-234.
37. D. Scholten MS, F. Laermer, A. Feyh. Manufacturing method for a porous microneedle array and corresponding porous microneedle array and corresponding substrate composite. In: Application USP, editor.: Robert Bosch GmbH. Stuttgart (DE).
38. M.G. Allen MRP, D.V. McAllister, F.P.M. Cros. Microneedle Devices and Methods of Manufacture and Use Thereof. In: Patent US, editor.: Georgia Tech Research Corporation, Atlanta, GA (US).
39. Shirkhanzadeh M. Microneedles coated with porous calcium phosphate ceramics: effective vehicles for transdermal delivery of solid trehalose. J Mater Sci Mater Med. 2005;16(1):37-45.
40. Donnelly RF, Singh TR, Garland MJ, Migalska K, Majithiya R, McCrudden CM, Kole PL, Mahmood TM, McCarthy HO, Woolfson AD. Hydrogel-Forming Microneedle Arrays for Enhanced Transdermal Drug Delivery. Adv Funct Mater. 2012;22(23):4879-4890.

41. Verbaan FJ, Bal SM, van den Berg DJ, Dijksman JA, van Hecke M, Verpoorten H, van den Berg A, Luttge R, Bouwstra JA. Improved piercing of microneedle arrays in dermatomed human skin by an impact insertion method. J Control Release. 2008;128(1):80-88.
42. Verbaan FJ, Bal SM, van den Berg DJ, Groenink WHH, Verpoorten H, Luttge R, Bouwstra JA. Assembled microneedle arrays enhance the transport of compounds varying over a large range of molecular weight across human dermatomed skin. J Control Release. 2007;117(2):238-245.
43. van der Maaden K, Sekerdag E, Jiskoot W, Bouwstra J. Impact-insertion applicator improves reliability of skin penetration by solid microneedle arrays. Aaps J. 2014;16(4):681-684.

Chapter 2

Dissolving microneedle patches for dermal vaccination

Adapted from Pharm. Res. 2017 (34):2223-2240

Mara Leone[1], Juha Mönkäre[1], Joke A. Bouwstra[1,*], Gideon Kersten[1,2,*]

[1] Division of Drug Delivery Technology, Cluster BioTherapeutics, Leiden Academic Centre for Drug Research, Leiden University, Leiden, the Netherlands

[2] Department of Analytical Development and Formulation, Intravacc, Bilthoven, the Netherlands

[*] These authors contributed equally.

ABSTRACT

The dermal route is an attractive route for vaccine delivery due to the easy skin accessibility and a dense network of immune cells in the skin. The development of microneedles is crucial to take advantage of the skin immunization and simultaneously to overcome problems related to vaccination by conventional needles (e.g. pain, needle-stick injuries or needle re-use). This review focuses on dissolving microneedles that after penetration into the skin dissolve releasing the encapsulated antigen. The microneedle patch fabrication techniques and their challenges are discussed as well as the microneedle characterization methods and antigen stability aspects. The immunogenicity of antigens formulated in dissolving microneedles are addressed. Finally, the early clinical development is discussed.

Keywords: antigen stability, dissolving microneedle fabrication, dissolving microneedle characterization, skin immunization, vaccine delivery.

1. INTRODUCTION

Vaccination is one of the most successful medical interventions in history, reducing mortality and morbidity for several infectious diseases to almost zero in areas where vaccines are being used [1,2]. Most vaccines are administered intramuscularly or subcutaneously (Figure 1) by injection that may cause pain and discomfort and avoidance by people with needle-phobia [4–7]. Furthermore, the hypodermic needles used to administer the vaccine by these routes generates hazardous waste and can lead to needle stick-injuries and needle re-use. The latter can spread infectious diseases such as Hepatitis B and AIDS particularly in the developing countries [8]. Furthermore, the use of innovative vaccine delivery systems could offer several other advantages such as antigen thermostability, fewer booster immunizations and, as a consequence, increase of the vaccination adherence and a reduced burden on healthcare personnel. These latter advantages would especially be beneficial in mass vaccination campaigns, such as in case of outbreaks, when feasible and fast immunizations schemes are necessary [4].

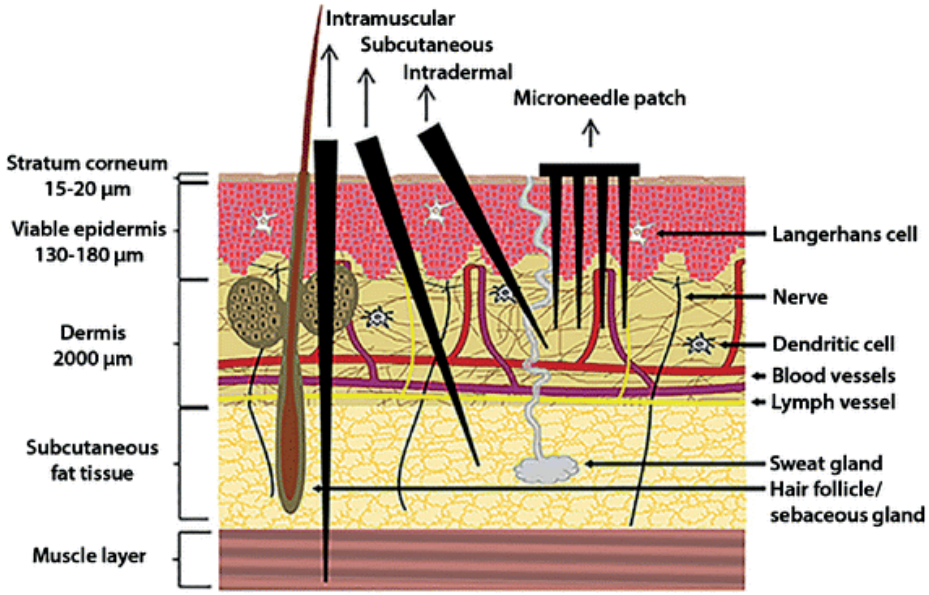


Figure 1. Schematic representation of microneedle insertion and conventional (intramuscular, subcutaneous and intradermal) injections onto the human skin are shown. Microneedles penetrate the *stratum corneum* reaching the viable epidermis. The hypodermic needles puncture the skin during insertion into the subcutaneous or muscle tissues. Adapted from [3].

Since the skin is a very immune-competent organ and easily accessible, dermal vaccine delivery is an attractive alternative. The viable epidermis and dermis contain many antigen presenting cells (APCs) such as Langerhans cells (LCs) and dermal dendritic cells (dDCs) (Figure 1) [9,10]. These APCs capture antigens and subsequently migrate to the draining

lymph nodes to present the antigen to the T-cells to activate Ag-specific T-cells and B-cells for systemic immune response. Besides LCs and dDCs, epidermal keratinocytes are also involved in the immune response by producing cytokines and chemokines (e.g. TNF-α and IL-1β) to enhance maturation of APCs and migration to the lymph nodes [11].

Although the skin surface is easily accessible, the skin (Figure 1) is designed to protect the human body against entry of foreign organisms or toxic substances [3,12]. Therefore, the top-layer of the skin, the *stratum corneum* (in humans 15–20 μm thick), forms a significant physical barrier for vaccine delivery. Consequently, the delivery of high-molecular weight (>500 Da) compounds such as antigens require methods enabling their penetration into the skin [13]. Several methods such as powder and fluid jet injection, thermal microporation, sonoporation, transfollicular delivery and microneedles [9] have been proposed to deliver antigens into the skin. Recently, microneedles (MNs) have gained great attention for dermal vaccination. MNs are needle-like microstructures, up to 1 mm in length [3], typically assembled in variable numbers on a patch. They pierce the *stratum corneum* and underlying tissue to deliver the antigen into the epidermis or dermis while they are short enough not to reach pain receptors and thus pain sensation can be avoided [7]. Furthermore, the immunization with MNs may not require the healthcare personnel [5,6,11] and does not generate sharp needle wastage after immunization.

The first microneedles were conceptualized for drug delivery in 1976 [14] but only during the last 20 years microneedles have been actively developed. MNs can be classified in the following groups: hollow, coated, porous, hydrogel-forming, dissolving microneedles (dMNs) and MNs for pretreatment [15–18]. dMNs consist of fast-dissolving materials (e.g. polymers or sugars) as a matrix material and the drug/antigen is mixed in the matrix. After insertion into the skin, they dissolve releasing simultaneously the active pharmaceutical ingredient [3,6,15,16,19].

The scope of this review is to evaluate the use of dMNs as vaccine delivery systems to overcome the limitations of traditional subcutaneous (s.c.), intramuscular (i.m.) or intradermal (i.d.) injections. Preparation methods for dMNs, their characterization and immunological properties will be described underlining the potential and novelty of this new micro-technology.

2. MATERIALS AND MANUFACTURING METHODS

2.1. Materials

Matrix material should possess the following characteristics: biocompatible, biodegradable, low toxicity, strength/toughness and cheap [17,20]. Many materials have been used to produce dMNs (Table 1). Head to head comparisons of the materials used for dMN production have not been reported as far as we know. The selection of the matrix material

may be based on practical considerations rather than rational design. Apart from safety, factors to consider include obtaining MNs capable to pierce the skin, compatibility with the active compound, compatibility with the manufacturing procedure (acceptable viscosity before drying or spraying and reasonable solidification time) and a potential to scale-up of dMN patches for mass production [16]. The most frequently used matrix materials are sodium hyaluronate, that is naturally present in the skin, and sodium carboxymethylcellulose [21–23,31–33]. Both are approved as inactive materials by FDA for parenteral drug products. Other materials include poly(vinylalcohol) (PVA) [42], poly(vinylpyrrolidone) (PVP) [43], methylvinylether-co-maleic anhydride (PMVE/MA) (Gantrez AN-139®) [44,45] and low molecular weight sugars like maltose [46,47] and trehalose [48]. dMNs have also been prepared from biodegradable polymers such as polylactic-co-glycolic acid (PLGA) [46], polylactic acid (PLA) [49] and polyglycolic acid (PGA) [50]. However, due to their slow dissolution rate in skin and a preparation method using high temperatures [34] and organic solvents, these polymers are less suitable as matrix material. The back-plate of the dMN patch can be made by using the same [51] or different materials [30,42] as the needles. Furthermore, the back-plate can be reinforced or the ease of handling can be increased by applying an adhesive tape [38,42,52–54]. Besides matrix material, other excipients might be included [30, 32, 33] to improve the antigen stability or mechanical strength of the dMNs (Table 1).

Table 1. Overview of matrix materials and antigens used for dMN vaccination studies. Back-plate materials are not listed in this table.

dMN composition	Antigen (Ag)	Adjuvant (Adj)	Ref.
sodium hyaluronate	OVA		[21]
sodium hyaluronate	adeno virus		[21]
sodium hyaluronate, dextran 70 and polyvidone	TT/DT		[22]
sodium hyaluronate	TT/DT		[23]
sodium hyaluronate	SE36 recombinant molecule (malaria vaccine)		[23]
sodium hyaluronate	trivalent influenza		[23]
sodium hyaluronate	EV71 virus-like particles		[24]

dMN composition	Antigen (Ag)	Adjuvant (Adj)	Ref.
PVP	OVA	CpG OND / co-encapsulation in cationic liposome	[25]
PVP	whole inactivated influenza virus		[26]
PVP	plasmid vector VR2012 encoding the middle envelope proteins of HBV	CpG ODN / Co-encapsulation in cationic liposome	[27]
Gantrez® AN-139	OVA	encapsulation in PLGA NPs	[28]
Gantrez® AN-139 and polysorbate 80	HIV-1 CN54gp140	MPLA	[29]
sucrose and threonine / maltodextrin	IPV		[30]
sucrose, threonine and CMC	live-attenuated measles vaccine		[31]
Na-CMC and trehalose	monovalent subunit influenza vaccine / trivalent subunit influenza vaccine		[32]
Na-CMC, sucrose and lactose	adenovirus expressing OVA / adenovirus expressing HIV-1 CN54 gag		[33]
PAA	OVA	poly(I:C) loaded NPs	[34]
PAA	OVA	silk depot loading OVA / poly(I:C)	[35]
sodium chondroitin sulfate	OVA		[36]
chitosan	OVA		[37]

dMN composition	Antigen (Ag)	Adjuvant (Adj)	Ref.
trehalose and PVA	inactivated split trivalent influenza vaccine		[38]
dextran 70 and sorbitol	trivalent subunit influenza vaccine		[39]
fish gelatin and sucrose	subunit monovalent influenza vaccines		[40]
PVA and sucrose	DNA plasmid expressing rabies G protein		[41]

CpG OD, CpG oligodeoxynucleotides; DT, diphtheria toxoid; EV71, Enterovirus 71; Gantrez® AN-139, copolymer of methylvinylether-co-maleic anhydride (PMVE/MA); HIV, human immunodeficiency virus; HBV, hepatitis B virus; IPV, inactivated polio vaccine; MPLA, monophosphoryl lipid A; NPs, nanoparticles; Na-CMC, Sodium carboxymethylcellulose; OVA, ovalbumin; PAA, poly(acrylic acid); PLGA, poly-D,L-lactide-co-glycolide; poly(I:C), polyinosinic-polycytidylic acid; PVA, poly(vinylalcohol); PVP, poly(vinylpyrrolidone); TT, tetanus toxoid.

Antigens that have been used include almost all vaccine types, ranging from peptides and proteins [21–23] to DNA vectors encoding antigenic proteins [27,33,41] and attenuated or inactivated viruses [26,30,31]. Antigens are generally dispersed directly in the dMN matrix [21–23,31,32] but they can also be encapsulated in nanoparticles or in a cross-linked structure [25,28,35] to potentiate or alter the immune response [25,34,35]. Furthermore, adjuvant can be incorporated in the dMNs [55].

2.2. Manufacturing methods

2.2.1. Micromolding

The most common fabrication method of dMNs is micromolding in which dMNs are prepared using a polydimethylsiloxane (PDMS) mold (Figure 2). First, the PDMS mold is typically produced from a silicon or metallic master mold [17] that is obtained by using techniques such as etching [56], lithography [57], thermal drawing [58] and laser micromachining [59,60]. PDMS is a hydrophobic flexible material, which can very accurately reproduce the master structure as a negative template [17]. The mold can be re-used for dMN fabrications after appropriate cleaning. The first step in preparing dMNs using the PDMS mold is the addition of the polymer/antigen mixture in the mold. This is typically done manually at the research setting but the mold can also be filled by using an atomized spray [48]. After filling of the mold, vacuum and/or centrifugation steps are performed to fill the PDMS microcavities with the polymer/antigen mixture [61]. Finally, the solution in the mold is dried at slightly elevated temperature [62,63]. The drying step can be replaced by photopolymerization if photocrosslinkable material is used [60].

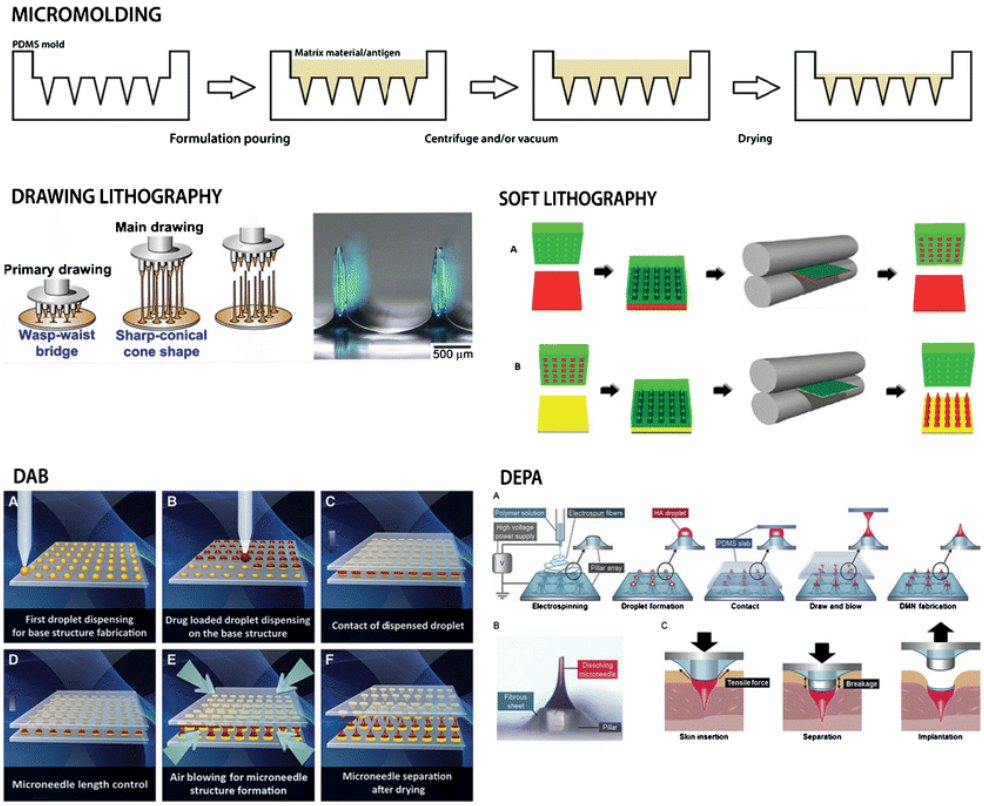


Figure 2. dMN Manufacturing Methods. See main text for details. Adapted from [66–69]. DAB, droplet-born air blowing; DEPA, dMN on an electrospun pillar array.

The micromolding can be a straightforward technique in the laboratory because it requires little additional equipment. Furthermore, the absence of harsh conditions (e.g. high temperature or organic solvents) is an advantage when working with sensitive antigens [64]. However, it might not be suitable for industrial scale-up or continuous manufacturing if steps such as manual removal of air bubbles from the microcavities after vacuum or centrifugation are needed or if the production method will result in too much vaccine wastage (see Antigen Wastage section).

2.2.2. Lithography

Drawing lithography

This technique is based on extensional (stretching) deformation of polymeric material from a 2-dimensional to a 3-dimensional structure. Melted polymer is dispensed on a fixed plate and elongated by drawing pillars in the upper-moving plate (Figure 2) [65,66]. The polymer

viscosity is progressively increased by cooling until the glass transition temperature of the polymer is reached. Finally, further cooling induces a solid polymer providing the suitable dMN strength for the skin piercing [19,66]. The advantage of this fast fabrication method is the minimal polymer wastage due to the dispensed drops on the plate. However, only a limited number of polymers have suitable glass transition temperatures for this method [65]. More importantly, this technique is not appropriate for thermolabile antigens because melting and transition temperatures are high during the manufacturing (e.g. for maltose >95°C [66]).

Soft lithography

In soft lithography dMNs are fabricated by first pairing a polymer film with the mold with microcavities and passing them through a heated nip. Next, the filled mold is placed on a flexible, water-soluble substrate and passed through the heated nip. After separation of the mold, a dMN patch on the substrate remains (Figure 2). Instead of heated nip, photocuring can be also used [67]. Similarly to drawing lithography, this manufacturing method claims excellent scalability, low cost and short preparation time. However, the high temperature used for the fabrication can be still critical while using a thermolabile antigen mixed with the matrix.

2.2.3. Droplet-born air blowing and dMN on an electrospun pillar array

In droplet-born air blowing (DAB), a droplet of polymer solution without drug and another droplet of drug solution are dispensed together on two plates. The upper plate is moved downwards so that the droplets are touching and thereafter plates are withdrawn to a distance corresponding to the two dMN lengths of the lower and upper plate (Figure 2). The polymer solutions are dried with air flow producing a dMN patch on each plate (Figure 2) [68]. The advantages include low temperature (4 – 25 ° C) and fast (≤ 10 min) fabrication and minimal drug and polymer wastage.

A variant of DAB is dMN on an electrospun pillar array (DEPA). The flat plate is replaced here by a pillar array covered by a fibrous sheet. Then, polymer formulation droplets are dispensed on the pillar array and placed in contact with a PDMS slab to pull and elongate the droplets obtaining microneedles (Figure 2). Finally, elongated droplets are dried by air flow.

2.3. General challenges of dMN preparation

2.3.1. Antigen wastage

Dermal vaccination is attractive especially for the antigen dose sparing to evoke an immune response. However, the optimization of the manufacturing methods is crucial to reduce antigen wastage. During micromolding part of the antigen is lost in the PDMS mold due to

low volume filling of the microcavities relative to the system volume needed [70]. It is often mentioned that excess of solution from the mold can be collected in order to recycle [35,51,63]. However, the saved antigen amount is often not reported in the literature and more importantly the quality of the recovered antigen may be difficult to guarantee hampering reuse of the vaccine formulation.

One possibility to reduce the antigen loss during the micromolding is to use polymer/antigen solution only for the dMNs and to produce a backplate only from the matrix material or even from other material. The backplate material should possess higher viscosity than that of the needles to reduce the diffusion of the antigen from the dMNs during preparation and drying [51]. In stability studies presence of antigen in the needles and its absence in the backplate should be monitored to demonstrate lack of diffusion of antigen to the backplate during storage [62]. However, in literature this aspect is generally not addressed. In fabrication methods like drawing lithography, DAB and DEPA, the antigen is dispensed in drops, thus the antigen wastage can be potentially reduced drastically. However, it is not reported if antigen can be lost in the dispensing instrument.

2.3.2. Antigen and adjuvant loading

Besides reproducible loading [61] and dose homogeneity, dMNs should contain a sufficient high antigen and adjuvant dose, which can be challenging due to very low volumes of dMN tips. This can be particularly challenging in the case of antigens encapsulated in nanoparticles, an approach to improve immunogenicity of dermally delivered subunit antigens [28]. Another aspect to consider is the delivery efficiency, i.e. the relation between the antigen amount incorporated into the dMNs and the antigen dose actually delivered into the skin. Unfortunately, these aspects are often not described in detail in the literature, although systems have been and are in development to maximize delivery (see next section). This makes comparison of different concepts difficult if not impossible. An additional issue is the physico-chemical properties of the adjuvant, that determines whether the adjuvant can be mixed properly with the matrix material.

2.3.3. Fabrication aimed to improve delivery efficiency

In order to facilitate the delivery of the entire intended antigen dose into the skin, some modified fabrications have been developed. These include micromolding of arrowhead dMNs mounted on mechanically strong shafts [37,63] or dMNs presenting an elongated base increasing the needle length [51]. Drawing lithography has been modified by dispensing melted polymer on a fixed plate presenting pedestals [71]. DEPA presents patch pillars to improve the delivery efficiency. After patch application into the skin, dMNs separate from the pillars due to a tensile breaking force of the fibrous sheet between the pillar and the

dMN (Figure 2). This allows a proper implantation of the dMNs into the skin and removal of the remaining back plate without the need to wait dMN dissolution [69].

2.3.4. Antigen degradation

Other critical steps during the dMN preparation are related to the high temperature reached in some manufacturing methods. The micromolding usually is done at mild temperatures. However, when using methods such as drawing and soft lithography, temperatures around 100°C may be required. Such a temperature can be critical when using thermolabile antigens mixed to the matrix. Alternatively, photocurable polymers like acrylate-based polymers [72] and poly (ethylene glycol) diacrylate (PEGDA) [73–75] may be used. However, radiation should not damage proteins or DNA of vaccines. In all methods, a drying step is included which can be detrimental for protein antigens even at moderate temperatures [76].

2.3.5. Sterility

Because dMNs deliver antigen into the viable skin, they should be sterile and have low endotoxin content [77]. Since the final product is dry, a sterile filtration step, if at all possible, should be done on final fluid bulk, implying that the actual patch manufacturing should be performed under aseptic conditions [77]. Alternatively, sterilization of patches by gamma irradiation may be considered, although this can damage the antigen [77] and may be difficult to validate. Based on FDA guidelines for medical devices in direct contact with lymphatic tissue, the endotoxin content in dMNs should be <20EU/device [78].

3. CHARACTERIZATION OF DISSOLVING MICRONEEDLES

A number of unique parameters must be determined to assess dMN quality (Table 2). Since there are no licensed products on the market, no MN monographs exist in pharmacopoeias [79]. Below, aspects that may be of importance are discussed.

Table 2. dMN characterization methods

Characteristic	Characterization method
Appearance	Microscopy techniques
Antigen distribution in MNs	Confocal microscopy
Water content	Thermogravimetric analyser Karl Fischer Moisture balance
Antigen stability	Immunogenicity Antigenicity: ELISA, SRID, virus titration Physico-chemical characterization: intrinsic fluorescence, CD, SDS-PAGE Aggregation: HP-SEC, NTA, MFI, AF4, TEM, DLS
Mechanical strength	Displacement-force test station
Skin piercing efficiency	Skin staining and histological sections
Dissolution of MNs	Dissolution of MNs in vitro Change in MN tip length after skin insertion
Antigen localization into the skin	Microscope analysis of skin sections or confocal microscopy analysis of intact skin Analysis of histological skin sections
Antigen quantification	Quantification of antigen concentration after in vitro dissolution of dMNs by suitable methods (e.g. UV-vis, fluorescence or ELISA) Quantification of antigen delivered into the skin by e.g. radioactivity or infrared imaging
Stability after storage	Forced (elevated humidity and temperature) and real time stability testing

AF4, asymmetrical flow field–flow fractionation; CD, circular dichroism; DLS, dynamic light scattering; ELISA, enzyme-linked immunosorbent assay; HP-SEC, size exclusion chromatography; MFI , micro-flow imaging; NTA, nanoparticle tracking analysis; SDS-PAGE, sodium dodecyl sulfate-polyacrylamide gel electrophoresis; SRID, single radial immunodiffusion assay; TEM, transmission electron microscopy; UV-Vis, ultraviolet–visible spectroscopy.

3.1. Appearance

Shape and sharpness of MNs are typically investigated by microscopic techniques such as light and scanning electron microscopy [80–84]. During product development, microscopy can be used also to analyze the distribution of fluorescent-labelled antigen in the MNs [61].

3.2. Water content

dMNs are dry formulations and it is important to measure their water content by using methods such as Karl Fisher titration (a coulorimetric or volumetric titration to determine trace amounts of water in the sample), thermogravimetric analysis or moisture balance [85]. The water content can influence mechanical properties, protein stability and dissolution kinetics [81]. The generally recommended water content for freeze-dried vaccines is less than 3% (w/w) [79], that could be also taken as guideline for dMNs.

3.3. Antigen stability

Stability of the antigen should be assessed both after the manufacturing of dMNs [86] as well as after the storage [22,24,31,38,39]. The type of stability indicating assays depends on the antigen as well as the type of immunity that should be induced (e.g. for antibody responses the tertiary structure of protein is important). Protein conformation can be assessed by spectroscopic techniques such as circular dichroism [80] and fluorescence spectroscopy [61]. Protein backbone integrity can be analyzed also by SDS-PAGE [25]. However, this method is not suitable to examine the protein unfolding, indicating the loss of B-cell epitopes. The obvious way to analyse B-cell epitopes is by measuring antigenicity with immunoassays such as ELISA. In case of incorporation of DNA in dMNs, agarose gel electrophoresis and *in vitro* transfection can be performed to measure the DNA supercoiling and efficacy respectively [41].

The aggregation of protein antigens or particulate vaccines can be investigated by several methods such as size exclusion chromatography (HP-SEC) [61], asymmetrical flow field–flow fractionation (AF4) [61], micro-flow imaging (MFI) [61], transmission electron microscopy (TEM) [24], dynamic light scattering (DLS) [24] and nanoparticle tracking analysis (NTA). For live attenuated or vector vaccines the viability of virus or bacterium may be sufficient because the antigen will replicate after immunization and so the vaccine potency can be determined by measuring the titer of live antigen [31]. Finally, immunogenicity studies are crucial to determine vaccine potency [26]. A limiting factor for characterization and quality control may be the small sample sizes and matrix effects due to high concentrations of matrix component after dissolution of the dMNs.

So far, a few studies have systematically analyzed vaccine stability in dMNs. Mistilis et al. showed that the buffer composition and preparation conditions (e.g. drying temperature) must be carefully selected to retain the vaccine stability of subunit influenza vaccine [85]. ELISA analysis of hemagglutinin activity showed that ammonium acetate buffer (pH 7.0) and HEPES retained the antigenicity much better in solution and dry state than when using phosphate-buffers. In addition, surfactants destabilized the antigen especially in liquid formulation prior to dMN fabrication and they may cause crystallization of the MN matrix damaging the antigen [85]. Antigen encapsulation plays also a role in the antigen stabilization. Similar antigen-specific CD8+ proliferative responses for OVA-PLGA NPs in dMNs before and after 10 weeks storage at ambient conditions were obtained [28]. In contrast, groups immunized with 10 weeks stored monomeric OVA in dMNs showed a decrease in T-cell response in comparison with the group immunized with non-stored one [28].

3.4. dMN mechanical strength and skin penetration

The mechanical properties of MNs (e.g. strength or facture force) should be analyzed to determine whether dMNs are strong enough and do not fracture during skin penetration [87], unless it is intended so. Measurements of dMN displacement-force can be performed by using a displacement-force test station to compare different matrix materials or geometry [80,83] or the effect of storage conditions [24]. Subsequent skin penetration studies are typically analyzed on *ex vivo* human [61] or porcine skin [88]. However, it is also important to consider the *in vitro-in vivo* correlation of the subcutaneous layers as these layers can also affect microneedle performance. For this purpose, artificial gel-layers can be used to resemble the *in vivo* situation more closely [89]. After MN application and removal from the skin, the skin is stained with dye (e.g. trypan blue). Additionally, *stratum corneum* can be stripped and the number of penetrating tips per patch can be determined. The penetration of single MN through the skin layers can be examined in a detailed way by analysing histological cross-sections of skin, although this is a more laborious approach [37,51,80] and not suitable for routine analysis. The depth of deposition of fluorescently-labelled antigen in the skin can be investigated by confocal microscopy [61] or fluorescence microscopy by using skin cryo-sections [24].

3.5. dMN dissolution

The analysis of the dissolution process of MNs is crucial for reproducible antigen disposition in the skin. The dMN dissolution time can be investigated *in vitro* by immersing MNs in buffer (e.g. PBS) [82]. This allows the assessment of the quantity and quality of the dissolved antigen. When focusing on dissolution in the skin, the optimal application time of dMN in the skin can be determined by analyzing MN length after the pre-determined application

periods [24,80,81]. The dMN dissolution in *ex vivo* skin typically resembles the *in vivo* use of MNs. However, it is important to analyze the dissolution also in preclinical studies and in the early clinical development because temperature and humidity conditions may be difficult to mimic in *ex vivo* conditions. Careful preclinical evaluation does not take away the need to study microneedle dissolution in a clinical setting. The contribution of physiological and mechanical properties of the skin at the application site (e.g. thickness, elasticity, etc) to the dMN dissolution rate and antigen delivery may be substantial and should be investigated in the future. Besides reproducible *in vivo* dissolution the actual dose delivered should be determined. Actual dose delivered can be substantially lower than the theoretical maximal dose since the base of the microneedle has a tendency not to dissolve completely. This is an economical risk. In that respect arrow-shaped microneedles having a smaller base, could have advantages above cone-shaped needles.

3.6. Quantification of antigen/adjuvant dose

3.6.1. In vitro analysis

The quantification of antigen dose in dMNs is often very challenging and it can be done *in vitro* by cutting the dMNs from the baseplate and dissolving them [81] or embedding the dMN patch in parafilm and allow MN tips to dissolve in PBS [90]. Then, the antigen quantification can be performed for example by fluorescence [81,90], UV-vis analysis [90] or ELISA. The antigen amount in the dMNs can be also determined by dissolving the entire patch (MNs and back-plate) and calculate the volume of the needles based on the needle dimensions. In this case, a prior analysis should demonstrate homogeneous antigen distribution in the entire patch. However, these *in vitro* techniques are difficult to validate. Furthermore, when using an adjuvant, this should also be quantified to confirm its dose, similarly to antigen.

3.6.2. Ex vivo and in vivo analysis

The antigen dose delivered into the skin and the reproducibility of the antigen delivery can be determined in *ex vivo* or *in vivo* studies [63], either indirectly by measuring the remaining antigen in the dissolved MNs or directly by measuring the antigen in the skin. Direct quantification can be performed by using either radioactivity [91] or infrared imaging.

4. IMMUNOGENICITY OF ANTIGENS ADMINISTERED BY dMNs: PRECLINICAL STUDIES

The first successful vaccination with dissolving microneedles was reported in 2010 [55]. Table 3 gives a summary of the reported immunization studies. Depending on the antigen, a humoral and/or cellular response is important for a therapeutic effect.

Table 3. Immunization studies with dMNs.

Antigen/ Adjuvant (dose)	Animal model	Immunization site and application method	Immunization scheme	Immune response analyzed	dMNs result vs other groups	Ref.
OVA 1 µg	C57Bl/6 and Wistar ST rats	Back skin Handheld applicator	4 times every 2 weeks	Ab response	IgG levels equal or superior to s.c. or i.d. group	[21]
OVA 10 µg, 100 µg	BALB/c mice	Dorsal skin Manual application	2 times every 2 weeks	Ab response	IgG levels comparable to i.d. group	[36]
OVA 15 µg 50 ng poly(I:C) in PLGA NPs	C57Bl/6	Dorsal ear skin No applicator mentioned	2 times every 35 days	Ab and T-cell response	IgG levels comparable to the i.m. and i.d. groups at day 63 $CD8^+$ T-cells similar to i.d. groups and higher than i.m. after booster dose Central memory $CD8^+$ T-cells higher than i.d. and i.m. groups	[34]
OVA 9 µg poly(I:C) 150 ng	C57Bl/6	Dorsal ear skin No applicator mentioned	Single vaccination for dMNs Boost on day 28 for i.d. injection	Ab and T-cell response	Both $CD8^+$ and IgG response higher than with i.d. injection Central memory $CD8^+$ T-cells higher than i.d. group	[35]
OVA 1 mg	Sprague Dawley (SD) rats	Back skin Homemade applicator	Single vaccination	Ab response	IgG levels higher than i.m. group	[37]
OVA 2 µg CpG OND 10 µg co-encapsulated in cationic liposome	BALB/c mice	Abdomen skin Homemade applicator	2 vaccinations after 3 weeks	Ab response	IgG levels higher than i.m. group	[25]
PLGA NP-encapsulated OVA 10 µg	C57Bl/6	Dorsal ears skin Manual insertion	Single vaccination	T-cell response and challange	In dMN group: CD8+ T-cell response with central and effector memory profiles. Growth of melanoma tumor through the Th1 IFN-γ mediated response suppressed Protection against respiratory challenge with OVA-expressing virus	[28]

Antigen/ Adjuvant (dose)	Animal model	Immunization site and application method	Immunization scheme	Immune response analyzed	dMNs result vs other groups	Ref.
OVA 7.6 µg / Quil-A 0.2 µg (2 patches per mouse)	C57Bl/6	Ventral ear skin Spring applicator	Single vaccination	Ab response	IgG levels (lower dose than i.m.) higher after 102 days than i.m. group	[55]
OVA 0.4 µg / Quil-A 0.01 µg (1 patch per mouse)					IgG levels (lower dose than i.m.) comparable after 102 days than i.m. group	
Split virus influenza vaccine 0.06 µg (1 patch per mouse) Split virus influenza vaccine 0.12 µg (2 patch per mouse)	C57Bl/6	Ventral ear skin Spring applicator	Single vaccination	Ab response	IgG levels (lower dose than i.m.) lower than i.m. group	[55]
Inactivated Influenza virus 6 µg	BALB/c mice	Dorsal skin Manually inserted	Single vaccination	Ab and T-cell response	IgG levels slightly lower (after 14 days) and then similar (after 28 days) than i.m. group HAI similar to i.m. group Cellular response similar to the i.m. route	[26]
Inactivated split TIV 0.375 µg HA	BALB/c mice	Ear Manual application	Single vaccination	Ab response	Anti-HA IgG response higher than i.m. group	[38]
Inactivated split TIV 3 µg HA					Anti-HA IgG comparable but more durable than i.m group HI titers comparable to i.m. group	
Influenza vaccine H1N1 0.1 µg and 1 µg HA	BALB/c mice	Not reported	2 times after 4 weeks	Ab response	HI and IgG titers higher than i.m. group Microneutralization titers lower than i.m. group	[32]
TIV 0.1 µg HA					HI titers after the boost lower than i.m. group	
Cell culture-derived influenza subunit trivalent vaccine 3 x 2.5 µg HA and 3 x 10.8 µg HA	Hartley guinea pigs	Dorsal skin Spring-based applicator	2 times after 3 weeks	Ab response	IgG and HI titers comparable to i.m. group	[39]
H1N1 3 µg of HA	BALB/c mice	Dorsal skin Manually inserted	Single vaccination	Ab response	HAI, IgG and VNT higher than i.m. group	[40]
H3N2 3 µg of HA					HAI titers higher than i.m. group VNT and IgG titers similar to i.m. group	
B 3 µg of HA					HAI, IgG and VNT higher than i.m. group	
Ad type 5 - OVA vector (4.3×10^8 VP)	C57Bl/6 and B6	Dorsal surface of the foot, ear or back skin Manual application	Single vaccination	T-cell response	SIINFEKL- specific CD8+ T-cells indistinguishable with i.d., s.c. and i.m. groups	[33]
Ad type 5 – HIV/gag vector (4.3×10^8 VP)					CD8+ T-cell frequencies comparable with i.d. group	

Antigen/ Adjuvant (dose)	Animal model	Immunization site and application method	Immunization scheme	Immune response analyzed	dMNs result vs other groups	Ref.
Ad (7.7 x 10^9 VP)	Hairless rats	Back skin Handheld Applicator	3 times after 2 weeks	Ab response	IgG titers equal to s.c. group	[21]
EV71 VLP 1 µg	BALB/c mice	Dorsal skin Applicator	3 times after 2 weeks	Ab, T-cell response and challenge	IgG and VNT comparable to i.m.(10 µg) and higher than s.c. (10 µg) after the third vaccination 100 % survival after challenge Stronger T-cell response than i.m. and s.c. (both 10 µg)	[24]
IPV type 1 (47 D-antigen units)	Rhesus Macaques	Upper back skin Manual insertion	2 times after 8 weeks	Ab response	No difference in IgG responses with i.m. group	[30]
IPV type 2 (9 D-antigen units)					No difference in IgG responses with i.m. group	
IPV type 3 (38 D-antigen units)					IgG lower than in the i.m. group. This difference is due to a mistake in the IPV type 3 quantification: the real dose in the patch was 3x lower than 38 D-antigen units	
Divalent toxoid vaccine (TT 20 µg and DT 10 µg)	Wistar ST rats	Back skin Handheld applicator	5 times after 2 weeks	Ab response	Both anti-TT and anti-DT IgG titers after dMNs stored vaccination comparable with those induced by freshly prepared dMNs	[22]
Measles Vaccine (3100 TCID50)	Rhesus Macaques	Upper back skin Manual application	Single vaccination	Ab response	VNT titers equivalent to that of s.c. group	[31]
Vector encoding the middle envelope proteins of HBV 10 µg CpG ODN 10 µg Encapsulation (with or without Adj) in cationic liposomes	BALB/c mice	Abdominal skin Manual application	2 times after 3 weeks	Ab response	IgG comparable to i.m. group	[27]
DNA plasmid expressing rabies G protein 50 µg	Beagle dogs	Inner ear pinna Application by thumb	2 times after 4 weeks	Ab response	VNT titers comparable (42 days after the prime) and higher (56 days after the prime) than i.m. group	[41]
DNA plasmid expressing rabies G protein 5 µg					VNT titers lower than i.m. group	

Antigen/ Adjuvant (dose)	Animal model	Immunization site and application method	Immunization scheme	Immune response analyzed	dMNs result vs other groups	Ref.
HIV-1 CN54gp140 10 μg MPLA (20 μg)	BalB/c	Ear Application by thumb	4 times after 2 weeks	Ab response	IgG titers lower than s.c. group	[29]

Ad, adenovirus; B, Brisbane; CpG ODN, CpG oligodeoxynucleotides; DT, diphtheria toxoid; EV71, Enterovirus 71; HA, hemagglutinin; HBV, hepatitis B virus; HIV, human immunodeficiency virus; HN, hemagglutinin and neuraminidase; IPV, inactivated polio vaccine; MPLA, monophosphoryl lipid A; NPs, nanoparticles; OVA, ovalbumin, PLGA, poly-D,L-lactide-co-glycolide; poly(I:C), polyinosinic-polycytidylic acid; TIV, trivalent influenza vaccine; TT, tetanus toxoid; VLP, virus like particles; VNT, virus neutralization test; VP, virus particles.

4.1. Animal models and application method

Mice are the most frequently used animal model, particularly BalB/c [23,25–27,29,32,36,38,40] or C57BL/6 [21,28,33–35,55] strains. Transgenic T-cell receptor mouse models (e.g. OT-I mouse for examining CD8+ T-cell response) can be also used as immunological model [92–94]. However, animal models with skin anatomy that mimics more closely human skin may be more relevant, for example guinea pigs for influenza [39], beagle dogs for rabies vaccination [41] and rhesus macaques for measles and polio vaccination [30,31].

The dMN patch can be applied either manually, particularly if MN length is over 500 μm, [26–31,33,36,38,40,41] or by using an applicator [21,22,25,37,39,55]. The advantages of the manual application are simple administration and reduced costs [30]. However, efficient skin piercing after manual application might be limited to longer MNs (>550 μm) while shorter MNs (300 μm) might require an applicator [95,96]. Besides the penetration efficiency, an applicator improves the reproducibility of the piercing, that is expected to lead to a more reproducible delivery of the vaccine [97].

4.2. Humoral immune response

4.2.1. OVA

The model antigen ovalbumin (OVA) is most commonly used in dMN immunization studies due to its relatively low cost and excellent stability [98] and the strong immunogenicity in mice. However, these beneficial characteristics mean that the results obtained with OVA may obscure formulation problems with more relevant vaccine antigens. Several studies with OVA-containing dMNs have shown that IgG responses are either equal or superior to the ones obtained by s.c., i.m. or traditional i.d. injection of the same dose [21,25,28,34,36,37,55]. Furthermore, non adjuvanted OVA dMNs (10 μg) showed a higher response than topical application of cholera toxin-adjuvanted OVA (100 μg) on intact skin

[36]. This indicates the importance of a direct delivery of the entire antigen dose into the skin to induce an immune response.

In another study, OVA loaded chitosan dMNs elicited higher IgG response than i.m. injection of OVA solution after single immunization in rats. This can be explained by a gradual degradation of chitosan microneedles creating a depot effect in the skin [37]. The OVA containing chitosan microneedles were mounted on a PLA support. After application, the chitosan microneedle tips were released from the support, forming a depot in the skin. Even two weeks after the dMN application, chitosan and OVA were still present in rat skin. Similarly, single immunization with cross-linked silk/poly(acrylic acid) (PAA) dMNs evoked higher IgG response than the i.d. injection of OVA [35]. However, in this case sustained release from the cross-linked silk in the PAA dMNs (100% within 12 days) did not improve the response compared to fast release from PAA dMNs (100% within 6 days) [35]. Similarly, single immunization with Quil-A adjuvanted OVA dMNs resulted in stronger long-lasting IgG response than Quil-A adjuvanted OVA after i.m immunization [55]. Twenty-eight days after a single immunization, dMNs (dose 7.6 μg) had similar IgG response to i.m injection (15 μg) despite the lower dose. At day 102, the IgG response of dMNs (7.6 μg) was higher than that of i.m (15 μg), and even more interestingly low-dose dMNs (0.4 μg) had similar response to i.m. immunization (15 μg) [55]. However, it must be noted that dMN patches were applied at two sites (both ears) while i.m injection was performed only at one site. Draining to two lymph nodes may have an effect on the magnitude of the response. Also, the ear is a very sensitive location for dermal vaccination probably for the short distance to one major draining lymph node [99].

The use of dMNs have been shown to affect the Th1/Th2 balance. Single immunization with cross-linked silk/PAA dMNs evoked strong IgG1 and IgG2c response while i.d. injection elicit only IgG1 response, and thus dMN immunization shifted Th1/Th2 balance toward Th1 [35]. These results were supported by another study where hyaluronan-based OVA dMNs were compared to s.c. and i.d. injections in mice [21]. In contrast, in rats no IgG2c response was detected neither after dMN, s.c., or i.d. immunization in the same study [21]. Additionally, in another study the shift in Th1/Th2 balance was not observed after dMN immunization in mice [25]. As conclusion, dMN vaccination may affect the Th1/Th2 balance but further studies are needed since the number of publications on this subject is limited.

4.2.2. Influenza

Immunization with influenza vaccine loaded dMNs resulted often in higher [38, 40] or comparable [26] IgG response than i.m. administration. However, Kommareddy et al. showed that dMNs evoked lower IgG response than i.m. immunization after the boost, although the response induced by dMNs was higher after the prime [32]. However, in other studies contradicting results were found. Haemagglutination inhibition titers and antibodies

and neutralizing antibody titers after the dMN immunization were similar [26] or superior [40] to i.m. immunization. Stabilization of the antigen by addition of sucrose [40] may have allowed to obtain a higher antibody titers than the previous work [26]. Furthermore, the difference with the above mentioned study [32] could be explained by the use of a different assay (ELISA assay) than the one routinely used to investigate the influenza vaccine quality (single radial immunodiffusion (SRID) assay). Interestingly, the dry matrix of dMNs can stabilize the antigen up to one year in comparison to liquid formulation [38]. In summary, most studies show that influenza vaccination by dMNs can evoke comparable or even superior responses than i.m. immunization.

4.2.3. Other antigens

Different types of antigen, such as vector, live attenuated and inactivated vaccines, have been loaded in dMNs and evaluated *in vivo*. An example is the vaccination of rats with the model antigen adenovirus (Ad) loaded dMNs: Ad-specific IgG titers observed were comparable to the s.c. group, while topical application showed no IgG response [21]. In a study examining the dose-sparing effect, mice were immunized with dMNs loaded with 1/10th the dose of Enterovirus71 (EV71) – virus-like particles compared to immunization with a full dose i.m. and s.c. injected vaccine. Antibody and neutralizing titers both revealed comparable responses to i.m. and higher responses than s.c. after the three immunizations. Furthermore, the dMN group, together with s.c. and i.m. groups, survived the lethal virus challenge showing the protective effect of the dMNs [24]. Rhesus macaques were used as animal model to examine the immune response after vaccination with inactivated polio vaccine (IPV) [30] and live-attenuated measles vaccine [31]. In both cases, neutralizing antibody titers after dMN immunization were comparable to that after s.c. (measles) and i.m. (IPV) immunization.

In the case of dMNs loaded with DNA containing the rabies G-protein gene, comparable neutralizing antibody titers with i.m. were detected after a booster. No evidence of the dose sparing in dMNs was found since the antibody titers of 10-fold lower dose were clearly weaker than those of full dose in dMNs [41]. The co-encapsulation of plasmid vector against hepatitis B virus (HBV) and CpG in cationic liposomes in dMNs resulted in slightly higher IgG titers than free antigen and adjuvant in dMNs [27]. It should be considered that the characteristics of liposomes changed after loading in dMNs (increase in size and decrease in Z-potential). However, the immune responses were generally similar between dMN and i.m immunization, and adjuvant and liposomes did not affect the IgG1/IgG2a balance [27].

4.3. Cellular immune response

De Muth et al. have reported two studies in which dMN immunization elicited high CD8+ T-cell responses. Mice were immunized with dMNs made of fast-dissolving PAA containing OVA mixed with PLGA microparticles (size 1.6 μm) encapsulating poly(I:C) [34] or cross-linked silk structure of OVA and poly(I:C) [35]. The latter results in a binary release profile: a burst of OVA after dMN dissolution followed by a sustained OVA release from the cross-linked silk structure. Both studies indicated that the CD8+ T-cells producing IFN-γ and TNF-α, upon peptide stimulation, are increased by dermal sustained release (>16 days) from dMNs in comparison with i.m. injection of sustained release of poly(I:C) from PLGA microparticles [34], or with i.d. injection of soluble OVA and poly(I:C) [35]. Furthermore, when comparing the different dMNs, the sustained release of cross-linked silk/PAA microneedles additionally increased the CD8+ response in comparison with fast release of PAA microneedles [35]. In addition, a prime immunization with dMNs can produce a similar fraction of functional CD8+ T-cells as a prime and boost with i.d. injection [35]. Despite a larger effector CD8+ T-cell response, dMN delivery also resulted in a more rapid transition to central memory CD8+ T-cells than i.m. and i.d. injections, suggesting the additional expansion of CD8+ T-cells after dMN delivery did not solely result in more terminally differentiated effector cells [34, 35]. However, sustained release from dMNs did not further improve the memory response [35]. A long-term memory immune response was reported also after vaccination by Na-CMC dMNs loading recombinant adenovirus vector encoding HIV-1 gag. Vaccination by dMNs generated CD8+ memory T-cells comparable with the intradermal injection [100]. Supporting results have been found also with other MN technologies inducing a better long-term memory response than s.c. [101] or i.d. [102] injections.

The PLGA NPs dMN concept may have potential for therapeutic cancer vaccination: dMN immunization suppressed the growth of melanoma tumor, evoked in mice by injecting OVA-tumor cells, through antigen-specific CD8+ T cells [28]. Furthermore, OVA-PLGA NPs dMN immunization protected against respiratory viral challenge with a recombinant Sendai virus expressing OVA [28]. The vaccine depot and particulate vaccines may induce a better T-cell immune protection because the response correlates with antigen persistence [103], the sustained antigen release [104] or particulate nature of vaccine. To elucidate the immunological mechanism, it was shown that Langerhans cells are required for cytotoxic CD8+ responses [28, 105]. Langerhans cells apparently efficiently process the OVA loaded in the microparticles which leads to cross presentation by MHC class I molecules. To support this explanation, the role of Langerhans cells was less significant for soluble OVA compared to particulate OVA [105].

In another study with dMNs loaded with EV71 virus-like particles, vaccination by dMNs loading 10 times lower antigen dose than i.m. and s.c. injections could promote stronger EV71-specific T-cell response than the conventional injections [24].

Viral vectors are able to induce strong T-cell responses after dMN immunization. dMNs with human adenovirus expressing ovalbumin were compared to i.d, i.m. and s.c. injections. The T-cell responses were similar in all groups [33]. Similarly, CD8+ T-cell responses were comparable after mice were immunized with rAdHu5 vector encoding a HIV-1 Gag gene by dMNs or i.d. injection [33].

4.4. dMN immunization: factors influencing the immunogenicity

4.4.1. Adjuvants

Several adjuvants have been used in dMNs and they are similar to those used for other administration routes except aluminum based adjuvants and emulsions. Aluminium based adjuvants may cause local adverse effects like granuloma formation and therefore is not suitable for delivery to the skin [106]. Emulsions cannot be formulated in dry formulations like dMN because water is a structural part of the formulation. Molecular immune modulators, such as CpG [25,27], poly(I:C) [34], Quil-A [55], monophosphoryl lipid A (MPLA) [29] and imiquimod [107] have been used in dMNs. In general, a significant increase in the immune response is observed when an adjuvant is included in dMNs [25,27], although sometimes the control group without the adjuvant is lacking. Unfortunately, the rationale of selection a certain adjuvant and its dose has not often been addressed.

Delivery systems can be formulated into dMNs (see previous section). Similarly to other administration routes, encapsulation of antigen (and adjuvant) in nanoparticles or liposomes can enhance the immune response after delivery with dMNs [25,27,28] as described above (Humoral Immune Response and Cellular Immune Response Sections). Adjuvants are often needed with modern subunit vaccines but their use might be avoided with attenuated viruses and viral vectors. Absence of adjuvant would also facilitate batch release since adjuvant quantification is not needed and antigen quantity is often limited to a simple plaque titration or colony count as opposed to an immunogenicity test in experimental animals.

4.4.2. MNs spacing and MN geometry

Modelling studies have indicated that the MNs spacing may affect the immune response by contributing to the optimal antigen concentration released into the skin to activate APC located between the MNs [108]. However, this is not experimentally confirmed and factors not accounted for in the model may contribute significantly to the immunogenicity.

The MN length may influence the population of APCs activated so that shorter MNs could activate LCs in the epidermis and longer MNs could activate dDCs in the dermis [108]. *In vivo* studies with 1 µg OVA showed that IgG response after vaccination by dMNs of 300 and 800

μm in length is higher than using dMNs of 200 μm in length [21]. On the other hand, the variation of injection depth with hollow MNs did not affect the immune response [109] However, while a controlled antigen dose was released at different skin depth by hollow microneedles [109], not clear is the antigen dose released into the skin from the dMN of different lengths [21]. This could explain the difference in the immune response.

Apart from MN length, needle density may be an important variable with respect to immunogenicity. The needles cause minor damage and cell death, initiating a pathway acting as "natural immune enhancer" mediated by the release of damage-associated molecular patterns (DAMPs) [110]. In fact, the same antigen dose released by coated MNs elicited higher response than a single i.d. injection [110].

5. CLINICAL DEVELOPMENT OF DISSOLVING MICRONEEDLES

dMNs are a relatively new vaccine delivery system with no licensed vaccines and few results from clinical studies. Two phase 1 (safety) studies with microneedles without antigen have been performed so far. In the first, hyaluronan microneedles (length 300, 500 and 800 μm, 200 dMNs on a 0.8 cm^2 patch) have been applied on 17 subjects [53] Despite a successful dMN penetration into the skin by using an applicator, the microneedles required 6 h of application for nearly complete dissolution in all subjects, which may be too long for routine immunization. In the second study, PVA microneedles (length 650 μm, 100 dMNs on a 1 cm^2 patch) have been applied on 15 subjects [111]. In this case, an average of 100% piercing efficiency of MNs into the skin without any applicator use was reached. However, variance in the microneedle volume dissolved, especially among subjects using self-administration, underlined the importance of using an applicator to have a controlled force and an impact during application. Few subjects [53] or all of them [111] showed a slight erythema after dMN application that disappeared within 7 days. However, longer dMNs of 500 and 800 μm caused purpura, indicating capillary damage, in 50% of the volunteers but shorter 300 μm dMNs did not induce any purpura [53]. No swelling at the application site [111] or systemic adverse events were observed [53]. Additionally, it was also concluded that dMN application caused hardly [53] or no pain [111].

In another clinical phase 1 study, trivalent influenza hemagglutinins vaccination with sodium hyaluronate dMNs (800 μm, 200 dMNs on a 0.8 cm^2 patch, spring-type applicator used) was investigated in healthy subjects [112]. dMNs loaded with 3 x 15 μg of influenza antigens on a single patch, were compared with the same dose administered by s.c. injection. During the prime immunization a proper dMN dissolution was observed in only seven subjects out of 20 and only these subjects were included in the final analysis. Furthermore, the applicator settings were changed to obtained a more efficient application in the second vaccination. After the prime, the anti-HI antibody titers against influenza A HA-antigens (H1N1 and H3N2 strains) were equivalent in the dMN and s.c. groups, except that for the B strain that showed

higher titers in the dMN group also observed in preclinical studies [32]. More IFN-γ-producing peripheral blood mononuclear cells were detected after s.c. than dMN immunization [112]. However, the low number of subjects in dMN group limits the conclusions. Regarding the safety, erythema detected in the dMN group was higher than the s.c. one and more pronounced than in the previous clinical studies [53,111]. Purpura was observed in 50% of the subjects both in the dMN and the s.c. group. However, no adverse systemic events were observed [112].

These studies prove that the applicator and its settings have a crucial role for MN penetration and subsequent dissolution into the skin. Alternatively, encapsulation of the antigen only in the microneedle tip can enable a complete antigen delivery even with incomplete microneedle dissolution (e.g., localizing the antigen in the upper 70% of the MNs, a 70% dissolution would correspond to 100% antigen delivery).

Besides above mentioned studies, at least one other study has been performed to investigate safety and immunogenicity of influenza vaccination with dMNs but the results are not yet published [113].

6. CONCLUSIONS AND PROSPECTS

dMN vaccination can offer important advantages such as dose sparing, pain-free immunization and avoidance of needle-stick injuries. Furthermore, it can extend the vaccination coverage in developing countries by potentially offering improved vaccine stability, reduction of vaccine wastage and of burden on trained personnel. However, several improvements are still needed in some areas of dMN development before the regulatory acceptance and industrial scale-up are feasible. Fabrication methods require further optimization to enable the minimal wastage of antigen that is often claimed but rarely reported in the literature, and not yet proven on at least pilot scale production level. Analytical challenges include potency testing and stability testing during fabrication and storage, and quantification and reproducibility of antigen/adjuvant dose delivered in the skin. dMN immunization has generated comparable or higher and more durable antibody and cellular responses than conventional immunizations in preclinical studies. Additionally, sustained release of antigen from nanoparticles or cross-linked structures in dMNs showed to induce a better cellular immune response than fast release from dMNs or liquid solution, although the sustained release from dMNs did not improve further the humoral response than fast release from dMNs. However, further studies should be performed to support this conclusion. In the future, more systematic studies, such as identification of optimal adjuvants and analysis of effect of dMN geometry, may be necessary to optimize dMN immunization. Until now, three clinical phase 1 studies have been reported and showed that skin irritation and patch application are hurdles that need to be solved in future applications. The ideal dMN patch (Table 4) does not exist yet but encouraging progress has been made.

More work is needed to further develop dMNs into safe, efficacious, affordable and widely used products.

Table 4. Target product profile of the ideal dMN patch.

Total systems costs lower than injected vaccine
Competitive production costs
Simple to produce
Stable outside the cold chain
Higher immunogenicity / dose sparing / single shot
Minimum waste
No applicator needed
Fail-proof application/check on full dose delivery
Short application time
Less adverse effects
Affordable

ACKNOWLEDGEMENTS AND DISCLOSURES

This work was sponsored by Intravacc.

REFERENCES

1. Bal SM, Ding Z, van Riet E, Jiskoot W, Bouwstra JA. Advances in transcutaneous vaccine delivery: do all ways lead to Rome? J Control Release. 2010;148(3):266–82.
2. Hilleman MR. Vaccines in historic evolution and perspective: a narrative of vaccine discoveries. Vaccine. 2000;18(15):1436–47.
3. van der Maaden K, Jiskoot W, Bouwstra J. Microneedle technologies for (trans)dermal drug and vaccine delivery. J Control Release. 2012;161(2):645–55.
4. Kersten G, Hirschberg H. Needle-free vaccine delivery. Expert Opin Drug Del. 2007;4(5):459–74.
5. Kim YC, Park JH, Prausnitz MR. Microneedles for drug and vaccine delivery. Adv Drug Deliv Rev. 2012;64(14):1547–68.
6. Ita K. Transdermal delivery of drugs with microneedles: strategies and outcomes. J Drug Deliv Sci Tec. 2015;29:16–23.
7. Hegde NR, Kaveri SV, Bayry J. Recent advances in the administration of vaccines for infectious diseases: microneedles as painless delivery devices for mass vaccination. Drug Discov Today. 2011;16(23–24):1061–8.
8. Hauri AM, Armstrong GL, Hutin YJF. The global burden of disease attributable to contaminated injections given in health care settings. Int J STD AIDS. 2004;15(1):7–16.
9. Engelke L, Winter G, Hook S, Engert J. Recent insights into cutaneous immunization: how to vaccinate via the skin. Vaccine. 2015;33(37):4663–74.
10. Kaurav M, Minz S, Sahu K, Kumar M, Madan J, Pandey RS. Nanoparticulate mediated transcutaneous immunization: myth or reality. Nanomedicine. 2016;12(4):1063–81.
11. Matsuo K, Hirobe S, Okada N, Nakagawa S. Frontiers of transcutaneous vaccination systems: novel technologies and devices for vaccine delivery. Vaccine. 2013;31(19):2403–15.
12. Grice EA, Segre JA. The skin microbiome. Nat Rev Microbiol. 2011;9(4):244–53.
13. Prausnitz MR, Mitragotri S, Langer R. Current status and future potential of transdermal drug delivery. Nat Rev Drug Discov. 2004;3(2):115–24.
14. Martin S. Gerstel VAP. Drug delivery device In: Patent US, editor. United States: Alza Corporation, Palo Alto, Calif.; 1976.
15. Larraneta E, McCrudden MTC, Courtenay AJ, Donnelly RF. Microneedles: a new frontier in Nanomedicine delivery. Pharm Res-Dordr. 2016;33(5):1055–73.
16. Tuan-Mahmood TM, McCrudden MTC, Torrisi BM, McAlister E, Garland MJ, Singh TRR, et al. Microneedles for intradermal and transdermal drug delivery. Eur J Pharm Sci. 2013;50(5):623–37.
17. Larraneta E, Lutton REM, Woolfson AD, Donnelly RF. Microneedle arrays as transdermal and intradermal drug delivery systems: materials science, manufacture and commercial development. Mater Sci Eng R. 2016;104:1–32.
18. van der Maaden K, Luttge R, Vos PJ, Bouwstra J, Kersten G, Ploemen I. Microneedle-based drug and vaccine delivery via nanoporous microneedle arrays. Drug Deliv Transl Re. 2015;5(4):397–406.
19. Indermun S, Luttge R, Choonara YE, Kumar P, du Toit LC, Modi G, et al. Current advances in the fabrication of microneedles for transdermal delivery. J Control Release. 2014;185:130–8.
20. McCrudden MT, Alkilani AZ, McCrudden CM, McAlister E, McCarthy HO, Woolfson AD, et al. Design and physicochemical characterisation of novel dissolving polymeric microneedle arrays for transdermal delivery of high dose, low molecular weight drugs. J Control Release. 2014;180:71–80.
21. Matsuo K, Yokota Y, Zhai Y, Quan YS, Kamiyama F, Mukai Y, et al. A low-invasive and effective transcutaneous immunization system using a novel dissolving microneedle array for soluble and particulate antigens (vol 161, pg 10, 2012). J Control Release. 2014;184:9–9.
22. Hiraishi Y, Nakagawa T, Quan YS, Kamiyama F, Hirobe S, Okada N, et al. Performance and characteristics evaluation of a sodium hyaluronate-based microneedle patch for a transcutaneous drug delivery system. Int J

Pharm. 2013;441(1–2):570–9.
23. Matsuo K, Hirobe S, Yokota Y, Ayabe Y, Seto M, Quan YS, et al. Transcutaneous immunization using a dissolving microneedle array protects against tetanus, diphtheria, malaria, and influenza (vol 160, pg 495, 2012). J Control Release. 2014;184:18–9.
24. Zhu Z, Ye X, Ku Z, Liu Q, Shen C, Luo H, et al. Transcutaneous immunization via rapidly dissolvable microneedles protects against hand-foot-and-mouth disease caused by enterovirus 71. J Control Release. 2016;243:291–302.
25. Guo L, Chen JM, Qiu YQ, Zhang SH, Xu B, Gao YH. Enhanced transcutaneous immunization via dissolving microneedle array loaded with liposome encapsulated antigen and adjuvant. Int J Pharm. 2013;447(1–2):22–30.
26. Sullivan SP, Koutsonanos DG, Martin MD, Lee JW, Zarnitsyn V, Choi SO, et al. Dissolving polymer microneedle patches for influenza vaccination. Nat Med. 2010;16(8):915–U116.
27. Qiu Y, Guo L, Zhang S, Xu B, Gao Y, Hu Y, et al. DNA-based vaccination against hepatitis B virus using dissolving microneedle arrays adjuvanted by cationic liposomes and CpG ODN. Drug Deliv. 2015:1–8.
28. Zaric M, Lyubomska O, Touzelet O, Poux C, Al-Zahrani S, Fay F, et al. Skin dendritic cell targeting via microneedle arrays laden with antigen-encapsulated Poly-D,L-lactide-co-Glycolide nanoparticles induces efficient antitumor and antiviral immune responses. ACS Nano. 2013;7(3):2042–55.
29. Pattani A, McKay PF, Donnelly RF, Garland MJ, Migalska K, Cassidy CM, et al. Microneedle mediated intradermal delivery of Adjuvanted recombinant HIV-1 CN54gp140 effectively primes mucosal boost inoculations. AIDS Res Hum Retrovir. 2011;27(10):A69–9.
30. Edens C, Dybdahl-Sissoko NC, Weldon WC, Oberste MS, Prausnitz MR. Inactivated polio vaccination using a microneedle patch is immunogenic in the rhesus macaque. Vaccine. 2015;33(37):4683–90.
31. Edens C, Collins ML, Goodson JL, Rota PA, Prausnitz MR. A microneedle patch containing measles vaccine is immunogenic in non-human primates. Vaccine. 2015;33(37):4712–8.
32. Kommareddy S, Baudner BC, Oh S, Kwon SY, Singh M, O'Hagan DT. Dissolvable microneedle patches for the delivery of cell-culture-derived influenza vaccine antigens. J Pharm Sci-Us. 2012;101(3):1021–7.
33. Bachy V, Hervouet C, Becker PD, Chorro L, Carlin LM, Herath S, et al. Langerin negative dendritic cells promote potent CD8+ T-cell priming by skin delivery of live adenovirus vaccine microneedle arrays. Proc Natl Acad Sci U S A. 2013;110(8):3041–6.
34. DeMuth PC, Garcia-Beltran WF, Ai-Ling ML, Hammond PT, Irvine DJ. Composite dissolving microneedles for coordinated control of antigen and adjuvant delivery kinetics in transcutaneous vaccination. Adv Funct Mater. 2013;23(2):161–72.
35. DeMuth PC, Min Y, Irvine DJ, Hammond PT. Implantable silk composite microneedles for programmable vaccine release kinetics and enhanced immunogenicity in transcutaneous immunization. Adv Healthc Mater. 2014;3(1):47–58.
36. Naito S, Ito Y, Kiyohara T, Kataoka M, Ochiai M, Takada K. Antigen-loaded dissolving microneedle array as a novel tool for percutaneous vaccination. Vaccine. 2012;30(6):1191–7.
37. Chen MC, Huang SF, Lai KY, Ling MH. Fully embeddable chitosan microneedles as a sustained release depot for intradermal vaccination. Biomaterials. 2013;34(12):3077–86.
38. Vrdoljak A, Allen EA, Ferrara F, Temperton NJ, Crean AM, Moore AC. Induction of broad immunity by thermostabilised vaccines incorporated in dissolvable microneedles using novel fabrication methods. J Control Release. 2016;225:192–204.
39. Bonificio A, Ghartey-Tagoe E, Gallorini S, Baudner B, Chen GH, Singh P, et al. Fabrication of cell culture-derived influenza vaccine dissolvable microstructures and evaluation of immunogenicity in guinea pigs. Vaccine. 2015;33(25):2930–8.
40. Vassilieva EV, Kalluri H, McAllister D, Taherbhai MT, Esser ES, Pewin WP, et al. Improved immunogenicity of individual

influenza vaccine components delivered with a novel dissolving microneedle patch stable at room temperature. Drug Deliv Transl Re. 2015;5(4):360–71.

41. Arya JM, Dewitt K, Scott-Garrard M, Chiang YW, Prausnitz MR. Rabies vaccination in dogs using a dissolving microneedle patch. J Control Release. 2016;239:19–26.
42. Allen EA, O'Mahony C, Cronin M, O'Mahony T, Moore AC, Crean AM. Dissolvable microneedle fabrication using piezoelectric dispensing technology. Int J Pharm. 2016;500(1–2):1–10.
43. Quinn HL, Bonham L, Hughes CM, Donnelly RF. Design of a Dissolving Microneedle Platform for transdermal delivery of a fixed-dose combination of cardiovascular drugs. J Pharm Sci-Us. 2015;104(10):3490–500.
44. Caffarel-Salvador E, Kearney MC, Mairs R, Gallo L, Stewart SA, Brady AJ, et al. Methylene blue-loaded dissolving microneedles: potential use in photodynamic antimicrobial chemotherapy of infected wounds. Pharmaceutics. 2015;7(4):397–412.
45. Gomaa YA, Garland MJ, McInnes F, El-Khordagui LK, Wilson C, Donnelly RF. Laser-engineered dissolving microneedles for active transdermal delivery of nadroparin calcium. Eur J Pharm Biopharm. 2012;82(2):299–307.
46. Wu X, Chen Y, Gui S, Wu X, Chen L, Cao Y, et al. Sinomenine hydrochloride-loaded dissolving microneedles enhanced its absorption in rabbits. Pharm Dev Technol. 2015:1–7.
47. Vemulapalli V, Yang Y, Friden PM, Banga AK. Synergistic effect of iontophoresis and soluble microneedles for transdermal delivery of methotrexate. J Pharm Pharmacol. 2008;60(1):27–33.
48. McGrath MG, Vucen S, Vrdoljak A, Kelly A, O'Mahony C, Crean AM, et al. Production of dissolvable microneedles using an atomised spray process: effect of microneedle composition on skin penetration. Eur J Pharm Biopharm. 2014;86(2):200–11.
49. Park JH, Choi SO, Seo S, Choy YB, Prausnitz MR. A microneedle roller for transdermal drug delivery. Eur J Pharm Biopharm. 2010;76(2):282–9.
50. Park JH, Allen MG, Prausnitz MR. Biodegradable polymer microneedles: fabrication, mechanics and transdermal drug delivery. Conf Proc IEEE Eng Med Biol Soc. 2004;4:2654–7.
51. Chu LY, Choi SO, Prausnitz MR. Fabrication of dissolving polymer microneedles for controlled drug encapsulation and delivery: bubble and pedestal microneedle designs. J Pharm Sci. 2010;99(10):4228–38.
52. Liu S, Jin MN, Uuan YSQ, Kamiyama F, Kusamori K, Katsumi H, et al. Transdermal delivery of relatively high molecular weight drugs using novel self-dissolving microneedle arrays fabricated from hyaluronic acid and their characteristics and safety after application to the skin. Eur J Pharm Biopharm. 2014;86(2):267–76.
53. Hirobe S, Azukizawa H, Matsuo K, Zhai Y, Quan YS, Kamiyama F, et al. Development and clinical study of a self-dissolving microneedle patch for transcutaneous immunization device. Pharm Res-Dordr. 2013;30(10):2664–74.
54. Liu S, Jin MN, Quan YS, Kamiyama F, Katsumi H, Sakane T, et al. The development and characteristics of novel microneedle arrays fabricated from hyaluronic acid, and their application in the transdermal delivery of insulin. J Control Release. 2012;161(3):933–41.
55. Raphael AP, Prow TW, Crichton ML, Chen XF, Fernando GIP, Kendall MAF. Targeted, needle-free vaccinations in skin using multi layered. Densely-Packed Dissolving Microprojection Arrays Small. 2010;6(16):1785–93.
56. Lippmann JM, Geiger EJ, Pisano AP. Polymer investment molding: method for fabricating hollow, microscale parts. Sensor Actuat a-Phys. 2007;134(1):2–10.
57. Perennes F, Marmiroli B, Matteucci M, Tormen M, Vaccari L, Di Fabrizio E. Sharp beveled tip hollow microneedle arrays fabricated by LIGA and 3D soft lithography with polyvinyl alcohol. J Micromech Microeng. 2006;16(3):473–9.
58. Lee J, Park SH, Seo IH, Lee KJ, Ryu W. Rapid and repeatable fabrication of high a/R silk fibroin microneedles using thermally-drawn micromolds. Eur J Pharm Biopharm. 2015;94:11–9.
59. Gomaa YA, Morrow DI, Garland MJ, Donnelly

RF, El-Khordagui LK, Meidan VM. Effects of microneedle length, density, insertion time and multiple applications on human skin barrier function: assessments by transepidermal water loss. Toxicol in Vitro. 2010;24(7):1971–8.
60. Park Y, Park J, Chu GS, Kim KS, Sung JH, Kim B. Transdermal delivery of cosmetic ingredients using dissolving polymer microneedle arrays. Biotechnol Bioproc E. 2015;20(3):543–9.
61. Monkare J, Reza Nejadnik M, Baccouche K, Romeijn S, Jiskoot W, Bouwstra JA. IgG-loaded hyaluronan-based dissolving microneedles for intradermal protein delivery. J Control Release. 2015;218:53–62.
62. Wang QQ, Yao GT, Dong P, Gong ZH, Li G, Zhang KJ, et al. Investigation on fabrication process of dissolving microneedle arrays to improve effective needle drug distribution. Eur J Pharm Sci. 2015;66:148–56.
63. Chu LY, Prausnitz MR. Separable arrowhead microneedles. J Control Release. 2011;149(3):242–9.
64. Ita K. Transdermal delivery of drugs with microneedles-potential and challenges. Pharmaceutics. 2015;7(3):90–105.
65. Lee K, Jung H. Drawing lithography for microneedles: a review of fundamentals and biomedical applications. Biomaterials. 2012;33(30):7309–26.
66. Lee K, Lee CY, Jung H. Dissolving microneedles for transdermal drug administration prepared by stepwise controlled drawing of maltose. Biomaterials. 2011;32(11):3134–40.
67. Moga KA, Bickford LR, Geil RD, Dunn SS, Pandya AA, Wang YP, et al. Rapidly-dissolvable microneedle patches via a highly scalable and reproducible soft lithography approach. Adv Mater. 2013;25(36):5060–6.
68. Kim JD, Kim M, Yang H, Lee K, Jung H. Droplet-born air blowing: novel dissolving microneedle fabrication. J Control Release. 2013;170(3):430–6.
69. Yang H, Kim S, Huh I, Kim S, Lahiji SF, Kim M, et al. Rapid implantation of dissolving microneedles on an electrospun pillar array. Biomaterials. 2015;64:70–7.
70. McCaffrey J, McCrudden CM, Ali AA, Massey AS, McBride JW, McCrudden MTC, et al. Transcending epithelial and intracellular biological barriers; a prototype DNA delivery device. J Control Release. 2016;226:238–47.
71. Xiang ZL, Wang H, Pant A, Pastorin G, Lee C. Development of vertical SU-8 microtubes integrated with dissolvable tips for transdermal drug delivery. Biomicrofluidics. 2013;7(2).
72. Narayan RJ, Doraiswamy A, Chrisey DB, Chichkov BN. Medical prototyping using two photon polymerization. Mater Today. 2010;13(12):42–8.
73. Kochhar JS, Goh WJ, Chan SY, Kang LF. A simple method of microneedle array fabrication for transdermal drug delivery. Drug Dev Ind Pharm. 2013;39(2):299–309.
74. Kochhar JS, Zou S, Chan SY, Kang LF. Protein encapsulation in polymeric microneedles by photolithography. Int J Nanomedicine. 2012;7:3143–54.
75. Gittard SD, Ovsianikov A, Akar H, Chichkov B, Monteiro-Riviere NA, Stafslien S, et al. Two photon polymerization-Micromolding of polyethylene glycol-gentamicin sulfate microneedles. Adv Eng Mater. 2010;12(4):B77–82.
76. Prestrelski SJ, Tedeschi N, Arakawa T, Carpenter JF. Dehydration-induced conformational transitions in proteins and their inhibition by stabilizers. Biophys J. 1993;65(2):661–71.
77. McCrudden MTC, Alkilani AZ, Courtenay AJ, McCrudden CM, McCloskey B, Walker C, et al. Considerations in the sterile manufacture of polymeric microneedle arrays. Drug Deliv Transl Re. 2015;5(1):3–14.
78. Guidance for industry, pyrogen and endotoxin testing question and answers 2012. In.; 2014.
79. European Pharmacopeia; 2013.
80. Lee JW, Park JH, Prausnitz MR. Dissolving microneedles for transdermal drug delivery. Biomaterials. 2008;29(13):2113–24.
81. Thakur RR, Tekko IA, Al-Shammari F, Ali AA, McCarthy H, Donnelly RF. Rapidly dissolving polymeric microneedles for minimally invasive intraocular drug delivery. Drug Deliv Transl Res. 2016;6(6):800–15.
82. Kim YPB. Skin permeability of compounds loaded within dissolving microneedles

dependent on composition of sodium hyaluronate and carboxymethyl cellulose. Korean J Chem Eng. 2016:1–6.
83. Demir YK, Akan Z, Kerimoglu O. Characterization of polymeric microneedle arrays for transdermal drug delivery. PLoS One. 2013;8(10):e77289.
84. Donnelly RF, Morrow DI, Fay F, Scott CJ, Abdelghany S, Singh RR, et al. Microneedle-mediated intradermal nanoparticle delivery: potential for enhanced local administration of hydrophobic pre-formed photosensitisers. Photodiagn Photodyn Ther. 2010;7(4):222–31.
85. Mistilis MJ, Bommarius AS, Prausnitz MR. Development of a thermostable microneedle patch for influenza vaccination. J Pharm Sci-Us. 2015;104(2):740–9.
86. Kommareddy S, Baudner BC, Oh S, Kwon SY, Singh M, O'Hagan DT. Dissolvable microneedle patches for the delivery of cell-culture-derived influenza vaccine antigens. J Pharm Sci. 2012;101(3):1021–7.
87. Davis SP, Landis BJ, Adams ZH, Allen MG, Prausnitz MR. Insertion of microneedles into skin: measurement and prediction of insertion force and needle fracture force. J Biomech. 2004;37(8):1155–63.
88. Sullivan SP, Murthy N, Prausnitz MR. Minimally invasive protein delivery with rapidly dissolving polymer microneedles. Adv Mater. 2008;20(5):933–8.
89. Moronkeji K, Todd S, Dawidowska I, Barrett SD, Akhtar R. The role of subcutaneous tissue stiffness on microneedle performance in a representative in vitro model of skin. J Control Release. 2016.
90. Larraneta E, Stewart S, Fallows SJ, Birkhauer LL, McCrudden MT, Woolfson AD, et al. A facile system to evaluate in vitro drug release from dissolving microneedle arrays. Int J Pharm. 2016;497(1–2):62–9.
91. van der Maaden K, Varypataki EM, Romeijn S, Ossendorp F, Jiskoot W, Bouwstra J. Ovalbumin-coated pH-sensitive microneedle arrays effectively induce ovalbumin-specific antibody and T-cell responses in mice. Eur J Pharm Biopharm. 2014;88(2):310–5.
92. De Koker S, De Geest BG, Singh SK, De Rycke R, Naessens T, Van Kooyk Y, et al. Polyelectrolyte microcapsules as antigen delivery vehicles to dendritic cells: uptake, processing, and cross-presentation of encapsulated antigens. Angew Chem Int Ed. 2009;48(45):8485–9.
93. Jung S, Unutmaz D, Wong P, Sano G. De los Santos K, Sparwasser T, Wu S, Vuthoori S, Ko K, Zavala F, Pamer EG, Littman DR, Lang RA. In vivo depletion of CD11c+ dendritic cells abrogates priming of CD8+ T cells by exogenous cell-associated antigens. Immunity. 2002;17(2):211–20.
94. Badovinac VP, Haring JS, Harty JT. Initial T cell receptor transgenic cell precursor frequency dictates critical aspects of the CD8(+) T cell response to infection. Immunity. 2007;26(6):827–41.
95. Verbaan FJ, Bal SM, van den Berg DJ, Groenink WHH, Verpoorten H, Luttge R, et al. Assembled microneedle arrays enhance the transport of compounds varying over a large range of molecular weight across human dermatomed skin. J Control Release. 2007;117(2):238–45.
96. Verbaan FJ, Bal SM, van den Berg DJ, Dijksman JA, van Hecke M, Verpoorten H, et al. Improved piercing of microneedle arrays in dermatomed human skin by an impact insertion method. J Control Release. 2008;128(1):80–8.
97. van der Maaden K, Sekerdag E, Jiskoot W, Bouwstra J. Impact-insertion applicator improves reliability of skin penetration by solid microneedle arrays. AAPS J. 2014;16(4):681–4.
98. Sugimoto Y, Sanuki S, Ohsako S, Higashimoto Y, Kondo M, Kurawaki J, et al. Ovalbumin in developing chicken eggs migrates from egg white to embryonic organs while changing its conformation and thermal stability. J Biol Chem. 1999;274(16):11030–7.
99. van der Maaden K, Varypataki EM, Yu H, Romeijn S, Jiskoot W, Bouwstra J. Parameter optimization toward optimal microneedle-based dermal vaccination. Eur J Pharm Sci. 2014;64:18–25.
100. Becker PD, Hervouet C, Mason GM, Kwon SY, Klavinskis LS. Skin vaccination with live virus vectored microneedle arrays induce long lived CD8(+) T cell memory. Vaccine. 2015;33(37):4691–8.

101. Carey JB, Pearson FE, Vrdoljak A, McGrath MG, Crean AM, Walsh PT, et al. Microneedle array design determines the induction of protective memory CD8+ T cell responses induced by a recombinant live malaria vaccine in mice. PLoS One. 2011;6(7):e22442.
102. Koutsonanos DG, del Pilar MM, Zarnitsyn VG, Jacob J, Prausnitz MR, Compans RW, et al. Serological memory and long-term protection to novel H1N1 influenza virus after skin vaccination. J Infect Dis. 2011;204(4):582–91.
103. Ochsenbein AF, Karrer U, Klenerman P, Althage A, Ciurea A, Shen H, et al. A comparison of T cell memory against the same antigen induced by virus versus intracellular bacteria. Proc Natl Acad Sci U S A. 1999;96(16):9293–8.
104. Demento SL, Cui W, Criscione JM, Stern E, Tulipan J, Kaech SM, et al. Role of sustained antigen release from nanoparticle vaccines in shaping the T cell memory phenotype. Biomaterials. 2012;33(19):4957–64.
105. Zaric M, Lyubomska O, Poux C, Hanna ML, McCrudden MT, Malissen B, et al. Dissolving microneedle delivery of nanoparticle-encapsulated antigen elicits efficient cross-priming and Th1 immune responses by murine Langerhans cells. J Invest Dermatol. 2015;135(2):425–34.
106. Vogelbruch M, Nuss B, Korner M, Kapp A, Kiehl P, Bohm W. Aluminium-induced granulomas after inaccurate intradermal hyposensitization injections of aluminium-adsorbed depot preparations. Allergy. 2000;55(9):883–7.
107. McCrudden MT, Torrisi BM, Al-Zahrani S, McCrudden CM, Zaric M, Scott CJ, et al. Laser-engineered dissolving microneedle arrays for protein delivery: potential for enhanced intradermal vaccination. J Pharm Pharmacol. 2015;67(3):409–25.
108. Romgens AM, Bader DL, Bouwstra JA, Oomens CW. Predicting the optimal geometry of microneedles and their array for dermal vaccination using a computational model. Comput Methods Biomech Biomed Engin. 2016;19(15):1599–609.
109. Schipper P, van der Maaden K, Romeijn S, Oomens C, Kersten G, Jiskoot W, et al. Determination of depth-dependent intradermal immunogenicity of Adjuvanted inactivated polio vaccine delivered by microinjections via hollow microneedles. Pharm Res. 2016;33(9):2269–79.
110. Depelsenaire ACI, Meliga SC, McNeilly CL, Pearson FE, Coffey JW, Haigh OL, et al. Colocalization of cell death with antigen deposition in skin enhances vaccine immunogenicity. J Invest Dermatol. 2014;134(9):2361–70.
111. Arya J, Henry S, Kalluri H, McAllister DV, Pewin WP, Prausnitz MR. Tolerability, usability and acceptability of dissolving microneedle patch administration in human subjects. Biomaterials. 2017;128:1–7.
112. Hirobe S, Azukizawa H, Hanafusa T, Matsuo K, Quan YS, Kamiyama F, et al. Clinical study and stability assessment of a novel transcutaneous influenza vaccination using a dissolving microneedle patch. Biomaterials. 2015;57:50–8.
113. A Phase I Study of the Safety, Reactogenicity, Acceptability and Immunogenicity of Inactivated Influenza Vaccine Delivered by Microneedle Patch or by Hypodermic Needle. In.; 2015.

Chapter 3

Universal applicator for digitally-controlled pressing force and impact velocity insertion of microneedles into skin

Adapted from Pharmaceutics 2018, 10(4), 211

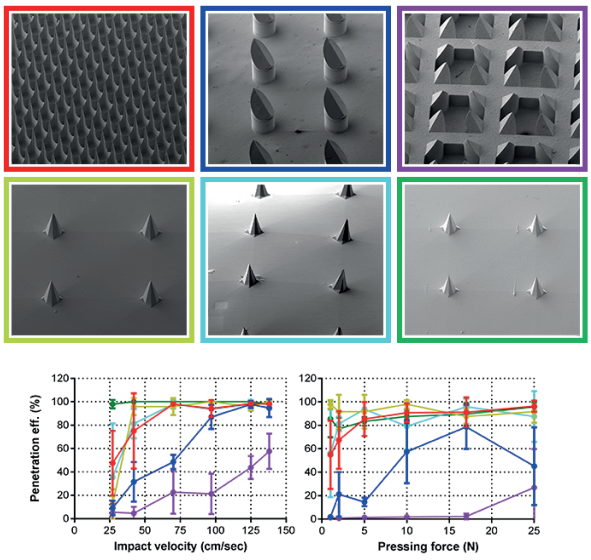
Mara Leone[1], Bart H. Van Oorschot[2], M. Reza Nejadnik[1], Andrea Bocchino[3], Matteo Rosato[3], Gideon Kersten[1,4], Conor O'Mahony[3], Joke Bouwstra[1] and Koen Van der Maaden[1,2]

[1] Division of BioTherapeutics, Leiden Academic Centre for Drug Research, Leiden University, Leiden, The Netherlands
[2] uPRAX Microsolutions B.V., Delft, The Netherlands
[3]Tyndall National Institute, University College Cork, Cork, Ireland
[4]Institute for Translational Vaccinology, Bilthoven, The Netherlands

ABSTRACT

Microneedle technologies have been developed for dermal drug and vaccine delivery, including hollow-, solid-, coated-, and dissolving microneedles. Microneedles have been made in many different geometries and of many different materials, all of which may influence their skin-penetrating ability. To ensure reproducible and effective drug and vaccine delivery via microneedles, the optimal insertion parameters should be known. Therefore, a digitally-controlled microneedle applicator was developed to insert microneedles into the skin via impact insertion (velocity) or via pressing force insertion. Six microneedle arrays with different geometries and/or materials were applied onto *ex vivo* human skin with varying velocities or pressing forces. Penetration efficiency and delivered antigen dose into the skin after application of microneedles were determined. In general, microneedles pierced the skin more efficiently when applied by impact application as compared to application via pressing force. However, the angle of application of the applicator on the skin can affect the velocity of the impact, influencing the penetration efficiency of microneedles. Regarding the antigen delivery into the skin, the delivered dose was increasing by increasing the velocity or pressure, and thus, increasing the penetration efficiency. These data demonstrate that an applicator is an important tool to determine optimal application conditions with *ex vivo* human skin.

GRAPHICAL ABSTRACT



Keywords: microneedle arrays, impact applicator, pressing force applicator, skin penetration, (trans)dermal drug/vaccine delivery.

1. INTRODUCTION

Drug and vaccine delivery via the skin offers several advantages over conventional administration routes (i.e., oral and parenteral), including prevention of drug and vaccine degradation by the gastro-intestinal tract, elimination of pain and discomfort, acceptability by people with needle-phobia, avoidance of hazardous waste, needle-stick injuries, and needle re-use [1-7]. However, the top layer of the skin, the *stratum corneum*, limits delivery via the skin of high-molecular weight drugs and vaccines (>500 Da), as well as biotherapeutics, such as peptides, proteins, hormones, and growth factors [6-8]. To enable drug and vaccine delivery via the skin, different techniques, such as powder and fluid jet injection, thermal and liquid microporation, sonoporation, and microneedles have been proposed [9-12]. The use of microneedles has been shown to be very attractive to overcome the *stratum corneum*, thereby enabling drug and vaccine delivery into and through the skin. Microneedles are needle-like structures shorter than 1 mm. Depending on their material, sharpness, and method of application, microneedles can penetrate the skin, thereby creating transient pores reaching the epidermis or dermis but not reaching pain receptors, enabling pain-free intradermal delivery of macromolecules [2,5,13,14]. Different microneedle technologies have been developed for drug and vaccine delivery via the skin, including (a) hollow microneedles for injections of liquid drugs or vaccine formulations, and (b) solid microneedles classified as (i) microneedles for skin pretreatment, and (ii) porous, coated, hydrogel-forming microneedles and dissolving (polymeric) microneedles that, after insertion into the skin, release the drug or vaccine [15-18]. These different microneedle types have been made with many different geometries (e.g., length, sharpness, diameter, density), and have been made of different materials (e.g., glass, silicon, stainless steel, titanium, sugar, (synthetic) polymer), which all may influence their skin penetrating ability.

The two frequently used methods of microneedle application are by pressing force or impact application [6]. Application by pressing force can be performed manually [19-22] or by an applicator [23]. To apply microneedles by impact application, using a predetermined velocity or impact energy, an applicator is needed [24-26]. It has been shown that an impact applicator [26] or a controlled pressing force applicator [23] ensures improved reproducibility of microneedle piercing of the *stratum corneum*, independent of the user, compared to manual application by pressing force of the thumb.

The aims of this study were to (i) develop a microneedle applicator that supports control of the parameters to insert microneedles via impact application or pressing force into skin, and (ii) evaluate the applicator for optimal microneedle insertion using a panel of different microneedle arrays (MNAs). Therefore, in this study a digitally-controlled microneedle applicator was developed, and was subsequently used to optimize the piercing of skin by different types of solid microneedles (i.e., different materials and geometries). The universal applicator uses an electronically-controlled unit to insert microneedles into the skin either by impact-insertion with a variable impact velocity, or by applying a variable pressing force. To evaluate the optimal insertion parameters for a variety of microneedle types, staining of

the skin with trypan blue was performed to investigate the microneedle penetration efficiency, while an ovalbumin formulation was used to demonstrate efficacy of antigen delivery into the skin after microneedle application as pretreatment. This work shows that each microneedle type has different specific settings (impact velocity or pressing force) for optimal application on the skin.

2. MATERIALS AND METHODS

2.1. Materials

Milli-Q water (18.2 MΩ/cm, Millipore Co., Bedford, MA, USA) was used for the preparation of aqueous solutions. Trypan blue solution 0.4% (w/v) and infrared dye (IRDye 800CW) were purchased from Sigma Aldrich and LI-COR (Lincoln, NE, USA), respectively. Polydimethylsiloxane (PDMS, Sylgard 184) was obtained from Dow Corning (Midland, MI, USA). 10 mM phosphate buffer (7.7 mM Na_2HPO_4, 2.3 mM NaH_2PO_4, pH 7.4) was prepared in the laboratory. Hyaluronan (sodium hyaluronate, average Mw was 150 kDa) was purchased from Lifecore Biomedical (Chaska, MN, USA). Vinylpolysiloxanes A-silicone (Elite Double 32a Normal) was purchased from the Zhermack Group (Badia Polesine, Italy) and two-component epoxy glue from Bison International B.V. (Goes, The Netherlands). 4 × 4 silicon microneedle arrays were obtained from Tyndall National Institute (Cork, Ireland), 24 × 24 silicon microneedle arrays were gifted from Bosch GmbH (Stuttgart, Germany), and ceramic alumina microneedle arrays (MLT-200 and MLT-475) were obtained from MyLife Technologies (MLT, Leiden BioScience Park, Leiden, The Netherlands). Conventional transparent tape Avery 440 Gloss Transparent Removable was obtained from Avery Dennison (Glendale, CA, USA).

2.2. Human skin

Human abdomen skin was obtained within 24 h after cosmetic surgery from local hospitals after informed consent from the donors, and handled according to the Declaration of Helsinki Principles. After removal of the fat, the skin was stored at −80 °C until use. Prior to the microneedle application studies, the skin was thawed in an incubator at 37 °C for one hour in a petri dish with a wet tissue to prevent dehydration. Next, the skin was stretched and fixed on Parafilm-covered Styrofoam. Finally, the skin was sequentially cleaned with 70% ethanol and Milli-Q water.

2.3. Production of dissolving microneedle arrays

Dissolving MNAs (dMNAs) were fabricated by micromolding technique, pouring a solution of 10% (w/v) hyaluronan (HA) in 10 mM phosphate buffer (pH 7.4) in a PDMS mold. The PDMS mold was prepared by pouring and letting cure a PDMS solution consisting of a mixture of a silicone elastomer and silicone elastomer curing agent (10:1 ratio) on a template presenting Tyndall MNAs [27] (see Table 1). dMNA and dMNA featuring a back-plate part (dMNA-BP) of vinylpolysiloxane and epoxy glue were prepared using two different PDMS mold designs (Figure 1) [27].

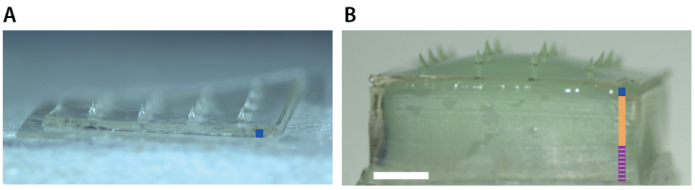


Figure 1. Bright field microscopy image (1.25× magnification) of a hyaluronan dissolving microneedle array (dMNA) without **(A)** and with a bi-layered back-plate **(B)**. Dark blue lines in **(A,B)** indicate the thin hyaluronan (HA) layer, the bright orange and purple stripped lines in **B** indicate silicone and glue layers, respectively. Scale bar (white line) represents 1 mm.

2.4. Microneedle arrays

In this study, a set of microneedle arrays with varying properties (e.g., microneedle length, microneedle geometry, density, surface area, material, etc.) were obtained or prepared (see Table 1) to evaluate their piercing ability using the newly-developed applicator (see sections below).

Table 1. Material and geometry of the microneedle arrays used in this study. Abbreviations: dissolving microneedle (dMNA); bi-layered back-plate (BP); microneedles (MNs).

Microneedle Array	Material	Array Geometry	Microneedle Length (µm)	Microneedle Density (cm^{-1})	Backplate surface (mm^2)	Number of MNs
Bosch	Silicon	Square (5x5 mm)	320	2304	25	576
MLT-475	Ceramic	Circular (d=9 mm)	475	150	69	105
MLT-200	Ceramic	Circular (d=9 mm)	200	600	69	414
Tyndall	Silicon	Square (5x5 mm)	300	64	25	16
dMNA	Hyaluronan	Square (5x5 mm)	300	64	25	16
dMNA-BP	Hyaluronan	Square (5x5 mm)	300	64	25	16

Microneedle were examined by scanning electron microscopy (SEM, Nova NanoSEM-200, FEI, Hillsboro, OR, USA) after coating with a layer of 15 nm platinum/palladium (Sputter Coater 208HR, Cressington, Watford, UK). The instrument was operated at 5.00 kV, and images were taken at magnifications of 80, 300, and 10,000 times. The tip diameters of microneedles were measured on SEM images using ZEN 2011 blue edition software, version: 2.0.14283.302 (Carl Zeiss Microscopy GmbH).

2.5. Applicator design

A microneedle applicator was developed (uPRAX Microsolutions B.V., Delft, The Netherlands), as shown in Figure 2, to apply microneedles either via pressing force or impact insertion into the skin (see sections below). As shown in Figure 2A, the applicator contains an electromagnetic actuator (solenoid). The mass mapp of the movable part of the applicator (25 g) is important for calculating the impact energy (Equation 1) upon microneedle impact, where v is the velocity of the microneedle mount at impact:

$$\text{Impact energy} = \tfrac{1}{2} \times m_{app}\, v^2 = J \qquad \text{(Eqn. 1)}$$

The movable part of the actuator contains a plunger (23 g) onto which a microneedle mount (2 g) is attached, which will move 1.3 cm (=stroke) in the vertical direction upon activation. The outer housing contains a skin-contact surface and a height-adjustment bolt that is connected to the inner housing. The electromagnetic actuator is mounted in the inner housing that has an adjustable position relative to the outer housing. The position of the inner housing is moved towards the skin contact surface by turning the allen key for height adjustment counterclockwise, and moving the inner housing upwards by turning the allen key clockwise (Figure 2B). The electromagnetic actuator has two important positions: (i) the zero position, when the actuator does not have (enough) electric power, and (ii) a maximum extended position, when the actuator has enough electric power to stay in this position (Figure 2C).

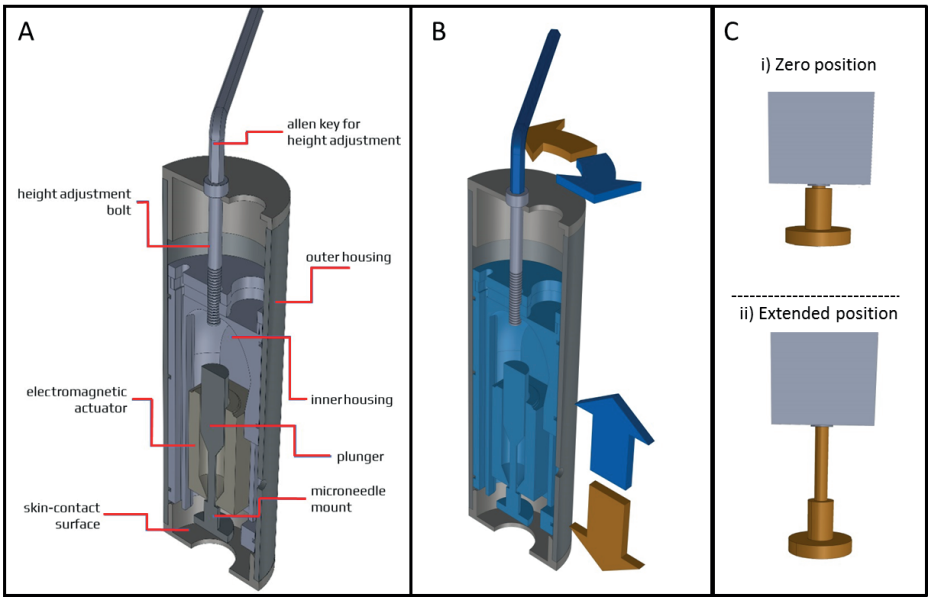


Figure 2. Design of the applicator **(A)** of which the inner housing (including the microneedle mount onto which microneedle arrays (MNAs) can be attached) can move towards the skin-contact surface by turning an allen key counterclockwise (brown arrows) and moving upwards by turning the allen key clockwise (blue arrows) **(B)**. The electromagnetic actuator moving the microneedle mount **(C)**.

2.6. Pressing force and impact insertion application

To apply MNAs by pressing force, the microneedle mount (onto which MNAs are attached (not shown in the image)) is protruding through the skin contact surface, while the electromagnetic actuator is in the extended position (Figure 3A-i). Next, the microneedle mount is pressed onto the skin by hand force (Figure 3A-ii). By exceeding the predetermined actuator's holding force (see below), the microneedle mount is retracted into the applicator (Figure 3A-iii).

To apply MNAs by impact application, the position of the inner housing should be adjusted in such a way that the skin contact surface is in line with the microneedle mount when the electromagnetic actuator is in its maximum position (Figure 2C-ii). The applicator's skin contact surface is first placed onto the skin when the electromagnetic actuator is in its retracted position (Figure 3B-i). Next, upon activation of the electromagnetic actuator, the microneedle mount moves towards the skin into the extended position with a predetermined impact velocity (see below) (Figure 3B-ii). Finally, the microneedle mount automatically retracts into the applicator upon reaching the set application time (Figure 3B-iii).

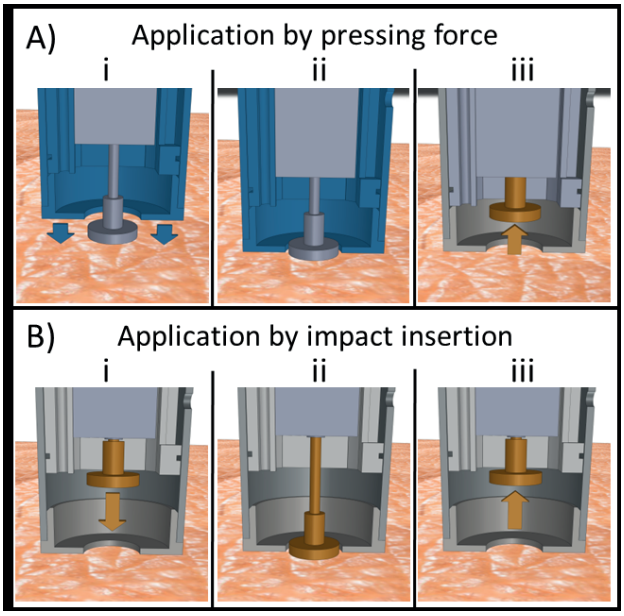


Figure 3. Application of microneedles onto skin by **(A)** pressing force: (i) electromagnetic actuator in the extended position, (ii) microneedle mount pressed onto the skin by hand force, (iii) microneedle mount retracted into the applicator; **(B)** impact insertion: (i) electromagnetic actuator in its retracted position, (ii) microneedle mount propelled into extended position, (iii) microneedle mount retracted into the applicator (see main text for explanation).

2.7. Microneedle applicator controller

A digitally-controlled applicator controller unit was developed to have precise control over the settings of microneedle application via the applicator. The applicator controller unit was programmed to modulate the duty cycle of a pulse width modulated (PWM) signal at a frequency of 10.5 kHz. The PWM signal was used to regulate the power of the applicator's electromagnetic actuator by switching a 24 V, 1 A power source via a transistor. Based on the mode of application, pressing force, or impact insertion, the pulse width was modulated to adjust the actuators holding force (see below) or the movement of the microneedle mount from the zero position to the extended position (see Figure 2C), thereby regulating the impact velocity (see below for further explanation). Furthermore, when the applicator is used for impact application, the applicator controller unit provides control over the application time (i.e., the time that a microneedle is retained onto the skin).

2.8. Force calibration for pressing force application

To control the pressing force by which MNAs can be applied onto the skin, the holding force of the electromagnetic actuator was regulated. When the electromagnetic actuator is in its extended position (Figure 2C-ii), it has a holding force that is dependent on the electric power it receives. This means that the electromagnetic actuator will stay in the extended position until a pressing force applied onto the microneedle mount exceeds the solenoid's holding force (the plunger will not be in its optimal electromagnetic field, and thereby, the force is reduced), which results in the actuator returning to the zero position (see Figure 2C-ii). To this end, the pressing force ($F_{pressing\ force}$) at which the electromagnetic actuator retracts to the zero position was determined by using the Equation 2:

$$F = m \times g \qquad \text{(Eqn. 2)}$$

where m is the mass measured by pressing the microneedle mount on a balance as a function of the pulse width value until microneedle mount detraction, and g is the gravitational acceleration.

The pressing force was fitted in GraphPad Prism 7 (GraphPad, San Diego, CA, USA) as a function of the duty cycle of the PWM using linear regression ($F_{pressing\ force}$ = slope × PWM − Force). By programming these linear regression parameters (A, B) in the applicator controller unit, the pulse width was set for a chosen pressing force of the applicator.

2.9. Calibration of impact velocity for impact insertion

In order to control the velocity at the impact of microneedle application, the average velocity as a function of the duty cycle of the PWM was determined. To this end, high speed imaging was used (FASTCAM Mini UX100, Motion Engineering Company, Inc. (Westfield, India) at 8000 frames per second). As shown in Figure 4, a reference (ruler) was attached to a 3D printed skin contact surface, and the microneedle mount was marked with a white spot. The position of this spot was tracked over consecutive frames to determine the traveled distance and the velocity of the microneedle mount as a function of time using the Tracker software version 5.0.1 (freely available from https:physlets.org/tracker). To calibrate the impact velocity of the microneedle applicator, high-speed imaging was performed in tenfold for each different pulse width (PWM_{width}). The impact velocity (v_{imp}) was defined as the average velocity at impact (which was at a displacement of the microneedle mount of 12.5–13 mm). Next, the PWM_{width} was plotted as a function of v_{imp}, which was fitted using nonlinear regression (v_{imp} = (Y0 − Plateau) × exp(−K × PWM_{width}) + Plateau) in GraphPad Prism 7. The calibration parameters (Y0; Plateau; K) were programmed in the applicator controller unit to set the pulse width for a chosen impact velocity.

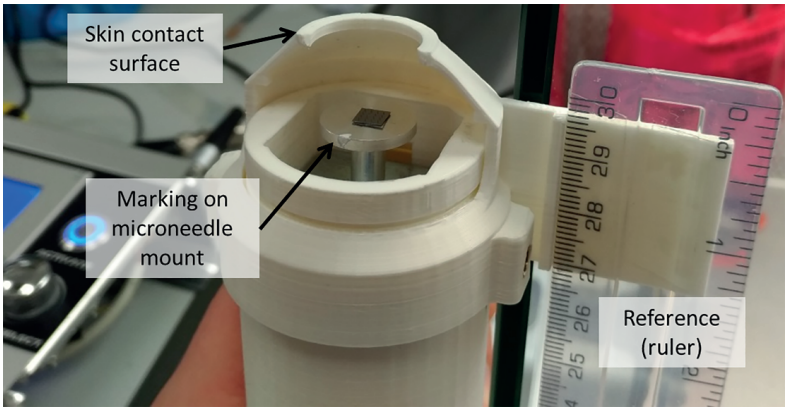


Figure 4. Microneedle applicator used for high-speed imaging.

2.10. Influence of the applicator's angle as a function of the pulse width

The angle of an impact applicator related to the gravitational force might influence the impact velocity and impact energy of the applicator, and thereby, the penetration efficiency of MNAs. Therefore, the velocity of the electromagnetic actuator as a function of the pulse width was investigated under different angles ranging from 0°–180° (where at 0° the microneedle mount is moving in the same direction as the gravitational force and at 180° in the opposite direction). The impact velocity was determined using high-speed imaging and the tracking software as described above.

2.11. Application of MNAs onto *ex vivo* human skin

In this study, all microneedles were mounted onto the microneedle mount of the applicator by using double-sided adhesive tape (Tesa®). To investigate the optimal manner of application of a set of MNAs with different properties via impact insertion or pressing force, MNAs were applied with different velocities and pressing forces, respectively. MNAs applied by impact application were applied with 6 different impact velocities measured by high speed camera: 27, 42, 70, 97, 125, and 138 cm/s, and a fixed array retraction after 1.00 s. Each microneedle array was applied three times on a different site of *ex vivo* human skin from a single donor. The insertion parameters of different MNAs by pressing force was investigated by applying each array in triplicate using 6 different pressing forces: 1, 2, 5, 10, 17, and 25 Newton, and an application time of 5 s per microneedle.

2.12. Determination of penetration efficiency by a trypan blue assay

To determine the penetration efficiency by the different microneedle arrays, a drop of 70 µL 1.2 mg/ml trypan blue was applied for 1 h on microneedle-pierced skin. Next, the *stratum corneum* was removed by tape-stripping until the skin appeared shiny (approximately 10 times stripping) to prevent overestimation of the penetration efficiency [26]. Subsequently, the skin was imaged by microscopy and the resulting microscopic images were analyzed using ImageJ software version 1.48v (freely available at http://rsb.info.nih.gov/ij/) to determine the amount of skin piercings. The penetration efficiency (PE) was calculated by using Equation 3 [26]:

$$PE = (\text{number of piercings}/\text{number of microneedles per array}) \times 100\% \qquad \text{(Eqn. 3)}$$

2.13. Calculation of penetration parameters

The MNAs used in this study had different properties. To calculate the optimal insertion parameters for the different microneedle geometries, the EC50 value for the different microneedle arrays was calculated per MNA, per individual microneedle, and MNA (back-plate) surface area. The EC50 value corresponded to the required impact energy or pressing force to pierce 50% of the microneedles of a MNA into the skin, and was calculated in GraphPad Prism 7 using a dose-response 3-parameter fit, which was constrained with: bottom asymptote penetration efficiency = 0; top asymptote penetration efficiency < 101 and hill slope < 0.2.

2.14. Normalization of penetration efficiency

To optimize the rate of antigen delivery and/or sampling when using MNAs, the MNA geometry may need adjustment (i.e., increase the number of microneedles, the surface area of an array or the microneedle length). This will lead to altered MNA insertion parameters. Therefore, to estimate the insertion parameters of a MNA when the number of microneedles or MNA surface area changes (while retaining a microneedle-specific geometry), we attempted to normalize the impact energy and pressing force per microneedle, with the assumptions that all microneedles from a single array pierce the skin in the same manner and the energy and force are homogeneously distributed per single microneedle of one array. Furthermore, when normalizing for the MNA (back-plate) surface area, we assumed that the energy and force are homogeneously distributed over the back-plate surface area (rather than on the individual microneedles).

2.15. Delivery of fluorescently labeled ovalbumin into pierced skin

To investigate the relationship between the penetration efficiency and the delivery of an antigen into the skin as a function of the impact velocity and insertion force, the model antigen ovalbumin was used. To this end, ovalbumin was labeled with IRDye 800CW (OVA-IR800) according to the manufacturer's instructions. A molar ratio of ovalbumin, IR800 of 2:1 (10 mg ovalbumin: 0.5 mg IRDye 800CW), was used. Next, 10 mg/ml ovalbumin in carbonate buffer (100 mM, pH 9) was added to 0.5 mg IRDye 800CW and pipetted in an Eppendorf Thermomixer R (Sigma-Aldrich, St. Louis, MO, USA) for 1 h at 300 RPM at room temperature. The unreacted dye was removed by using a 5 mL desalt column (LI-COR Biosciences, Lincoln, NE, USA). The infrared signal of labeled ovalbumin was measured on a Tecan Infinite M1000 plate reader (Männedorf, Switserland) at excitation and emission wavelengths of 774 nm and 789 nm, respectively. A concentration of 6.8 mg/ml OVA-IR800 (68% labeling efficiency) was obtained.

After application of the different MNAs with different impact velocity and application forces, a drop of 70 µL 20 mg/ml OVA-IR800 was applied. After 2 h, the excess of liquid was removed and the skin was tape-stripped. In order to quantify the dose of OVA-IR800 delivered into the skin after MNA pretreatment, a calibration curve of OVA-IR800 in *ex vivo* skin was prepared. Intradermal microinjections at a depth of 150 µm of an OVA-IR800 solution of 10 µg/ml with injection volumes ranging from 0.5–20 µL (5–200 ng) were performed, using a microinjection system as reported previously [28].

The near-infrared fluorescence of the delivered OVA-IR800 was measured in a Perkin-Elmer IVIS Lumina Series III in vivo imaging system (Waltham, MA, USA) using an indocyanine green background (ICG bkg) excitation filter and an ICG emission filter and an acquisition time 10 s. Living Image software version 4.3.1.0 (Perkin-Elmer, Waltham, MA, USA) was used for image acquisition and analysis. Fluorescence data were processed using region of interest (ROI) analysis, with background subtraction consisting of a control region of *ex vivo* human skin.

3. RESULTS

3.1. Microneedles appearance

To visualize the differences in microneedle geometry and surface properties of the different MNAs, SEM imaging was performed (Figure 5), and the tip diameter was measured (Table 2). The Bosch MNAs have a high microneedle density, and the silicon surface is rougher than for other microneedle types. A Bosch tetrahedral structure presents a narrow tip diameter, making it the sharpest microneedle in the MNA set. MLT-475 and MLT-200 are nanoporous (made of alumina nanoparticles), and therefore, have a rough surface. The MLT-475 shape is similar to conventional hypodermic needles, whereas MLT-200 consists of groups of four needles positioned in a square. These two microneedle types present the largest tip

diameter in comparison with the other microneedle types. Tyndall, dMNAs, and dMNAs-BP have a smooth surface and an identical octahedral geometry due to the PDMS mold that is based on the Tyndall MNAs to fabricate dMNAs and dMNAs-BP.

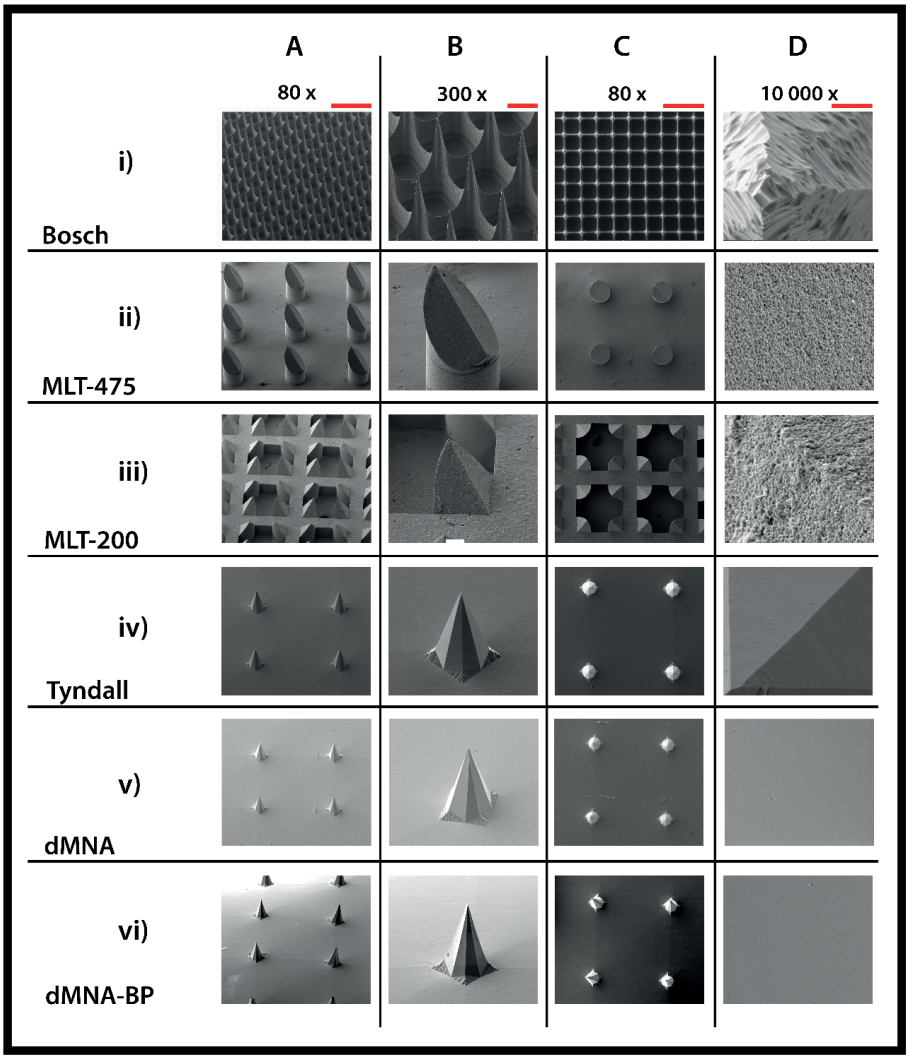


Figure 5. Scanning electron microscopy images of microneedle arrays (MNAs) with different geometries and lengths: Bosch of 320 µm (i), MLT-475 of 475 µm (ii), MLT-200 of 200 µm (iii), and Tyndall (iv) dMNA (v) and dMNA-BP (vi) of 300 µm. MNAs were imaged from a lateral view **(A,B)**, and from the top side **(C,D)**. Scale bars represent 500 µm (80×) **(A,C)**, 100 µm (300×) **(B)**, and 4 µm (10,000×) **(D)**.

Table 2. Microneedle tip diameters of different MNAs measured using the SEM images. Data are shown as mean ± SD, n = 5 (except Tyndall, dMNAs and dMNAs-BP with n = 4).

	Bosch	MLT-200	MLT-475	Tyndall	dMNA	dMNA-BP
Tip diameter (µm)	1.2 ± 0.3	7.5 ± 1.0	7.6 ± 0.9	3.8 ± 0.4	4.3 ± 0.7	4.0 ± 0.3

3.2. Applicator setting: velocity

The relationship between applicator setting (pulse width) and output (velocity and travel distance) was determined by high-speed imaging in combination with tracking software. As shown in Figure 6A, the distance of the microneedle mount from the zero position (S = 0 mm) to the extended position (S = 13 mm) as a function of time was determined using different pulse widths. This shows that a pulse width of 80 (dimensionless 8 bit (0 to 255) value) or more is required to move the microneedle mount into the extended position, which is required to impact the microneedles onto the skin. Furthermore, from this figure, the time of flight (i.e., the time required to move the solenoid from the zero position to the extended position of 13 mm) was determined as a function of the pulse width. In Figure 6B, the traveled distance of the microneedle mount was plotted as a function of the velocity, showing that the maximum velocity of the microneedle mount was reached when the microneedle mount traveled a distance of 8–10 mm when using pulse widths of 150 or more. However, when using pulse widths of 100 or lower, the maximum velocity was higher than the impact velocity (because the spring in the solenoid, which returns the microneedle mount back in the zero position when there is no power on the solenoid, decelerates the microneedle mount). Therefore, to calibrate the applicator and to calculate the impact energy (see Table 3), the impact velocity was used.

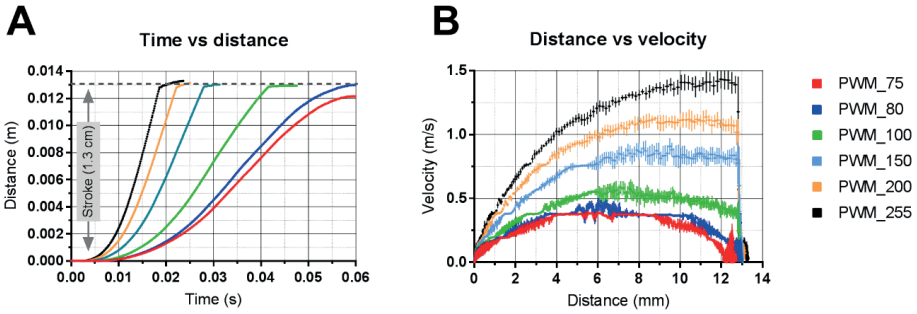


Figure 6. Analysis of high-speed imaging data (8000 fps) to determine the traveled distance (A) and the velocity as a function of the position of the microneedle mount at different pulse widths (B). Data are shown as mean ± SD, n = 10.

3.3. Calibration of applicator

The applicator was calibrated for pressing force and impact velocity to automatically set the pulse width for a chosen pressing force or impact velocity. To this end, the pressing force of the applicator was determined as a function of the pulse width, as shown in Figure 7A. Subsequently, the regression curve variables (Force = 0.392 × PWM_{width} + 3.16) were programmed into the applicator controller unit to set the pulse width for a chosen pressing force between 1 and 25 Newton. Next, the applicator's impact velocity (extracted from Figure 6) was plotted as a function of the pulse width, as shown in Figure 7B. To set the applicator's velocity, the regression curve variables (v_{imp} = (−0.9421 − 2.139) × exp(−0.005599 × PWM_{width}) + 2.139) were programmed into the applicator controller.

In order to determine the reproducibility in impact velocity or pressing force delivered by the applicator, the relative standard deviation (RSD) per each impact velocity or pressing force value was calculated. Then, the set of RSD was averaged. An average RSD of 8.9% and 3.4% were obtained for pressing force and impact velocity application, respectively.

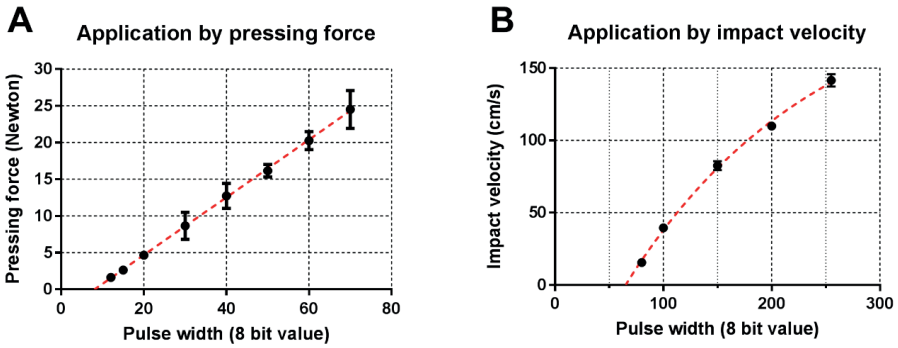


Figure 7. Regression curves used to set the applicator's pulse width as a function of the chosen pressing force **(A)** and impact velocity **(B)** at a pulse frequency of 10.5 kHz. Data are shown as mean ± SD, n = 3 **(A)** and n = 10 **(B)**.

3.4. Influence of the applicator's angle on the impact velocity

The angle of an impact applicator relative to the gravitational force might influence the applicator's impact velocity and impact energy, and thereby, the penetration efficiency of MNAs. Therefore, the applicator's impact velocity was investigated as a function of the angle (related to the gravitational force) and pulse width (Figure 8). At low pulse widths (<80), the microneedle mount did not reach the extended position (Figure 6A); thus, no relation between impact velocity and applicator's angle can be defined. At medium pulse widths (90–170), the impact velocity is highly dependent on the applicator's angle. Finally, using high

pulse widths (>170) results in reproducible velocities that are less dependent on the angle of the applicator.

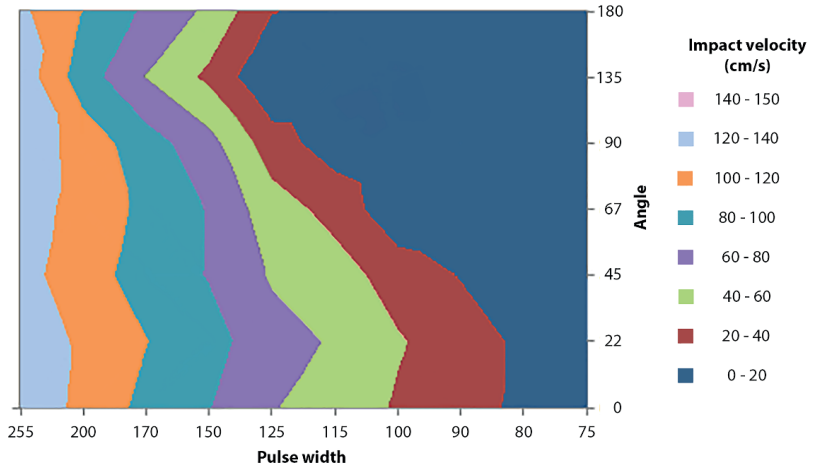


Figure 8. The impact velocity of the microneedle mount (in impact insertion mode) as a function of pulse width (8 bit dimensionless value; 0–255) and angle from the direction of the gravitational force (mean, n = 3, except for 0° which was n = 10).

3.5. Penetration of human skin by pressing force and impact application

The penetration of *ex vivo* human skin as a function of pressing force and impact application was investigated for six MNA designs (see Table 1 and Figure 9). The parameters that were used to apply the six different (MNAs) by impact application are summarized in Table 3.

For microneedles with a tetrahedral structure, like Bosch, and octahedral structure, like Tyndall, dissolving and dissolving-BP, both impact velocity and pressing force allowed a penetration efficiency of *ex vivo* human skin close to 100%. The structure and MNA surface area of MLT-475 allows a high penetration efficiency at an impact velocity above 100 cm/s. Nevertheless, application by pressing force resulted in a lower and less reproducible penetration efficiency. Similarly for MLT-200, a better penetration was obtained using the impact application as compared to pressing the MNAs into the skin. However, the design and high MNA surface area of MLT-200 did not result in higher penetration efficiencies than 60% using the settings wherein the applicator was calibrated.

Furthermore, the reproducibility in piercing at the best impact velocity or pressing force value per each MNA was investigated by calculating the RSD of the penetration efficiency at the highest impact velocity and pressing force values (Table 4).

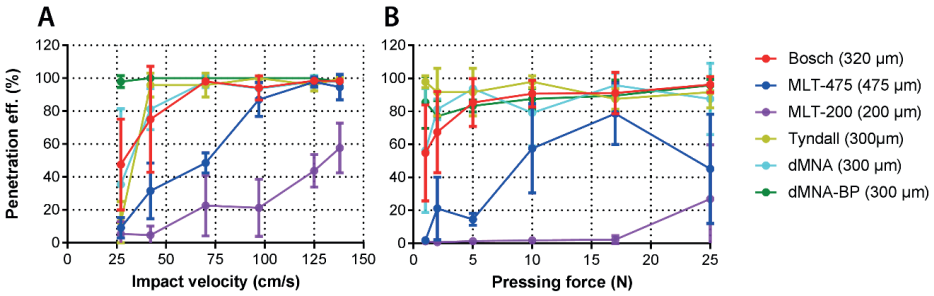


Figure 9. Penetration efficiency (in percentage) of MNs on *ex vivo* human skin as a function of the microneedle impact velocity **(A)** and pressing force **(B)**. Data are shown as mean ± SD, n = 3.

Table 3. MNA application parameters used to investigate skin piercing of the six different MNAs via impact insertion.

Pulse width (8 bit value)	Impact velocity (cm/s)	Impact energy (mJ)
90	27.40	0.94
104	42.50	2.16
136	70.60	6.06
174	97.40	11.85
221	125.70	19.43
250	138.10	23.84

Table 4. Relative standard deviation (RSD) of impact velocity or pressing force calculated for each microneedle array (MNA) application at 125–138 cm/s and 17–25 N.

	Bosch (300 µm)	MLT-475 (475 µm)	MLT-200 (200 µm)	Tyndall (300 µm)	dMNA (300 µm)	dMNA-BP (300 µm)
RSD (%) (125-138 cm/s)	1	6	25	2	4	2
RSD (%) (17-25 N)	9	42	121	9	16	7

3.6. Calculation of penetration parameters

Differences in MNAs geometry (microneedle shape and length, square or circular MNA, MNA area, and number and density of microneedles) and material (silicon, alumina, or hyaluronate) did not make possible a direct comparison of the penetration efficiencies of the different types of microneedles. However, the applicator could be set to find the optimal penetration properties to pierce the microneedles effectively and reproducibly (relatively low SD), and determine the piercing properties (EC50).

Penetration properties were calculated as EC50 values, and the corresponding pressing forces and impact energies were normalized per single microneedle and per MNA surface

area (see Figure 10 and Table 5). A more reproducible piercing can be obtained when the applicator is set for impact velocity as compared to pressing force (Figure 10). When the application is in pressing force mode, the piercing is still effective, especially for high pressing forces and tetrahedral and octahedral geometries, but with reduced reproducibility.

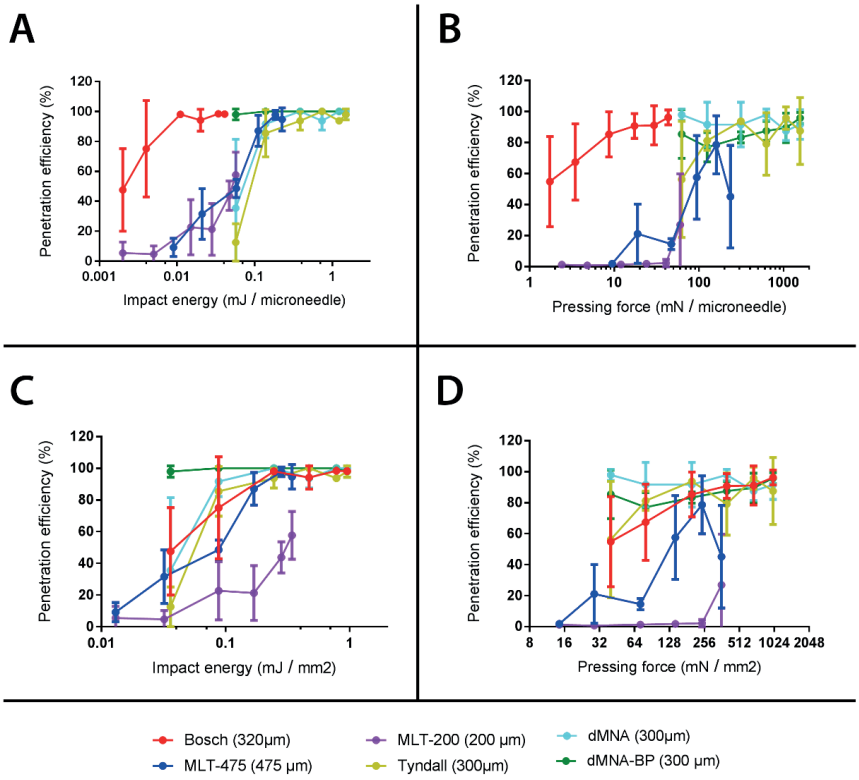


Figure 10. Penetration efficiency (in percentage) on *ex vivo* human skin as a function of the microneedle impact energy **(A,C)** and pressing force **(B,D)** both normalized for microneedle number (MN) **(A,B)** and microneedle array surface area (MNA surface) **(C,D)**. Data are shown as mean ± SD (n = 3).

Table 5. EC50 values calculated from the penetration efficiency as a function of impact energy or pressing force. The EC50 values are reported per microneedle array or normalized per microneedle and per microneedle array surface area.

	Impact energy per:			Pressing force per:		
	MNA (mJ)	Individual MN (mJ)	mm^2 (mJ)	MNA (N)	Individual MN (mN)	mm^2 (mN)
Bosch (300 µm)	0.97	0.002	0.04	1.4	2.4	56.0
MLT-475 (475 µm)	5.47	0.052	0.08	6.3	59.8	91.4
MLT-200 (200 µm)	21.85	0.053	0.31	>25.0*	>60.1*	>360.2*
Tyndall (300 µm)	<1.00*	<0.063	<0.04	<1.0*	<62.5*	<40.0*
dMNA (300 µm)	1.28	0.080	0.05	<1.0*	<62.5*	<40.0*
dMNA-BP (300 µm)	<1.00*	<0.063	<0.04	<1.0*	<62.5*	<40.0*

*: the EC50 values could not be calculated because higher or lower than respectively the maximum or minimum impact velocity or pressing force used.

3.7. Relation between penetration efficiency and antigen dose delivered into the skin

The relation between the penetration efficiency and the delivered dose of antigen into the skin as a function of the impact velocity and pressing force for different types of MNAs was investigated (Figure 11). For some MNAs, the penetration efficiency reached its maximum, but the amount of delivered ovalbumin was still increasing with further increasing impact velocities or application forces. Furthermore, despite fact that the penetration efficiency increased as a function of the impact velocity and the application force using the MLT-200 MNAs, the delivered amount of ovalbumin did not proportionally increase with the penetration efficiency. However, in general, the amount of ovalbumin delivered into the skin increased proportionally with an increasing penetration efficiency as a result of increasing impact velocities and pressing forces.

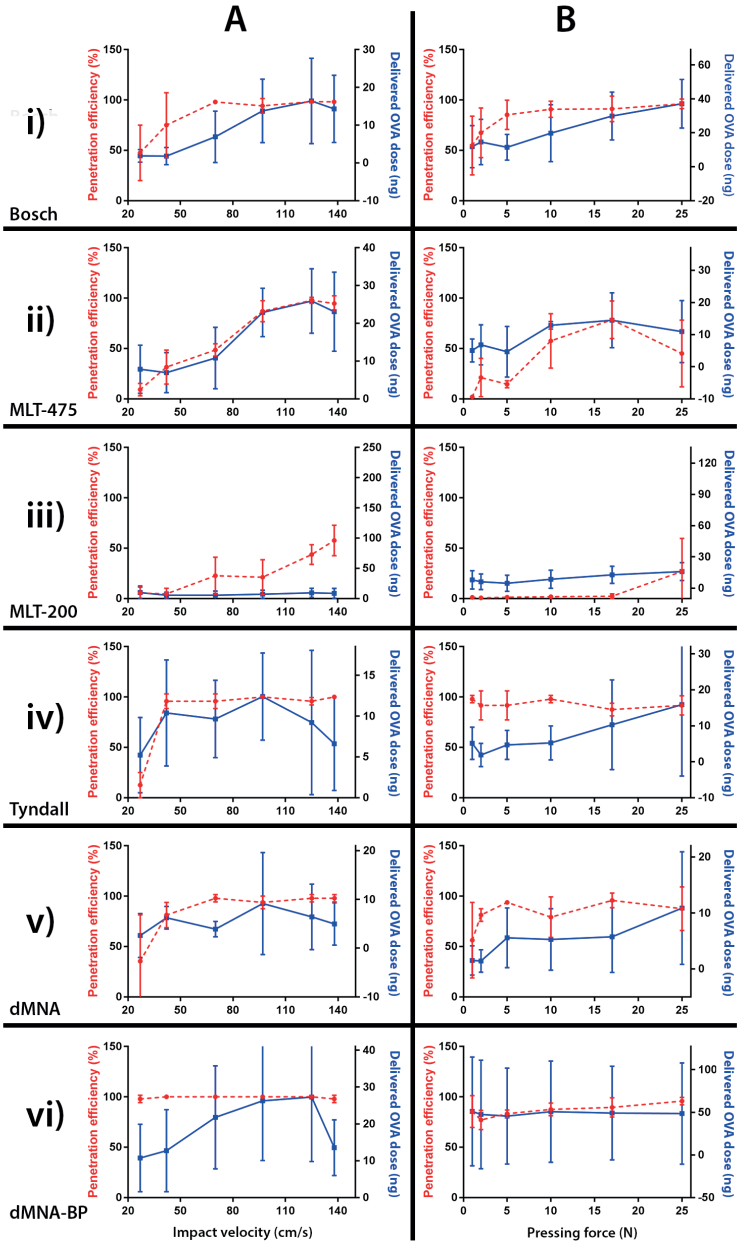


Figure 11. Penetration efficiency (in percentage) (red dotted line) and delivered dose of ovalbumin-IRDye 800CW (maximum dose delivery value matching the corresponding penetration efficiency value) (blue continuous line) into *in vitro* human skin as a function of the microneedle impact velocity **(A)** or pressing force **(B)**. Six different microneedle arrays (MNAs) were used, having different geometries and lengths: Bosch of 320 µm (i), MLT-475 of 475 µm (ii), MLT-200 of 200 µm (iii), and Tyndall (iv) dMNA (v) and dMNA-BP (vi) of 300 µm. Data are shown as mean ± SD (n = 3). OVA, ovalbumin.

4. DISCUSSION

In the literature, most microneedle applicators are used to apply MNAs via pressing force or impact application [6,19-26]. However, these applicators do not provide precise control over the pressing force or impact velocity of microneedle application. Applicators with precise control over such parameters can be used to get fundamental insights into critical application parameters of specific microneedle designs. Therefore, the aims of this study were to (i) develop a digitally-controlled microneedle applicator that supports control of the insertion parameters of microneedles into skin via impact application or via pressing force, and (ii) evaluate the applicator for the optimal application of microneedles (effective and reproducible skin piercing) using a set of six different MNAs with varying properties (e.g., length, density, material, MNA surface).

4.1. Microneedle applicator

It has been reported that long microneedles (>550 μm) could pierce skin effectively upon manual application, while microneedles of 300 μm and shorter generally require an impact applicator to pierce the skin effectively [29,30]. Importantly, the use of an applicator can result in lower inter- and intra-individual (several applications from the same person or from different people) variation as compared to manual application without an applicator [23,26]. Considering the reported studies, this work aimed to underline the importance of a device to assist the microneedle insertion if relatively short microneedles are used, and to determine the optimal settings (impact velocity and/or pressing force) for an efficient and reproducible piercing of different MNAs into the skin.

In order to achieve efficient and reproducible skin penetration, the delivered impact velocity and pressing force should be reproducible. In this study, it was shown that a chosen pressing force was reproducibly delivered by the applicator (average relative standard deviation of 8.9%), and was linearly dependent on the pulse width (Figure 7A). Furthermore, regarding impact application, it was shown that a pulse width below 80 did not allow the microneedle mount to reach the extended position, and will thereby not result in the microneedles impacting the skin. After accelerating of the microneedle mount (until approximately 4–8 mm) at pulse widths of 100 and lower, the velocity was decreasing towards the extended position (Figure 6B). However, using pulse widths between 90 and 255 resulted in very reproducible impact velocities (average relative standard deviation of 3.4%) between 30 and 140 cm/s (Figure 7B).

Skin penetration by microneedles is dependent on the impact velocity. However, in this study, it was shown that the angle of the applicator related to the gravitational force influences the impact velocity. Therefore, these data show the importance of designing applicators that deliver sufficient energy to reach an impact velocity that results in efficient

and reproducible microneedle piercing, or ensure that impact applicators are only used at a specific angle.

Summarizing, the developed applicator was able to accurately deliver a chosen impact velocity and pressing force with high reproducibility.

4.2. Skin penetration by microneedles

For microneedle-based drug and vaccine delivery, it is important that microneedles pierce the skin effectively and reproducibly. In general, the investigated MNAs gave a high penetration efficiency both when applied by impact velocity and by pressing force. By using impact application, the penetration efficiency was mostly reaching 100%, while it reached 80% when using application by pressing force. This was also observed in our previous study using microneedles with a length of 200 µm (576 microneedles/array on a back-plate of 5 × 5 mm) [26]. This was very evident for MLT-200 and MLT-475: the impact application was more efficient compared to application by pressing force. This better performance in penetration efficiency by impact application may be related to the lower sharpness and to the roughness of the material (see SEM imaging) increasing the friction of the microneedle during penetration, or to the microneedle design, which has been shown to play an important role in mechanical properties of microneedles [20,31]. Furthermore, the microneedle length can have a strong impact on the penetration. In a previous study [26] Bosch microneedles with similar design as those used in the present study (MNA surface, density and material) showed an EC50 of 3.5 N/array with a lower penetration efficiency than the Bosch microneedles in the present study (EC50 1.4 N/array), which were only slightly longer, i.e., 320 µm vs 200 µm. Similarly, the MLT-200 µm microneedles require more than 25 N/array, whereas the longer MLT-475 µm needles had an EC50 of 8.0 N/array. Furthermore, applying microneedles by pressing force (17 and 25 N) (with respect to the penetration efficiency) resulted in reproducible skin penetration for Bosch, Tyndall, and dMNA(-BP) microneedles (Figure 9B). Moreover, using impact velocity (125 and 138 cm/s) resulted in very reproducible skin penetration for all investigated microneedles except MLT-200 (Figure 9A). Summarizing, applying microneedles via impact application generally results in higher penetration efficiencies with higher reproducibility.

It is interesting to note how the presence of a curved MNA surface (back-plate) can improve the penetration efficiency both by impact and pressing force application. This was the case of dMNA-BP differentiating from the dMNA only for the presence of a convex surface area where the MNs are located [27]. The convex surface may enable a better positioning of the microneedles towards the skin surface when pressed by the array, increasing the capability of microneedles to penetrate the skin.

The EC50 values calculated for the different microneedle geometries could be used as guidance for developing applicators for microneedles with altered numbers of microneedles and surface areas while retaining the microneedle geometry.

4.3. Delivery of a model antigen in relation with the penetration efficiency

The standard deviations of the quantification of the delivered amount of antigen were rather high, which was partially caused by the measurement method (in this study the antigen-signal to background ratio was [1.3:1]) and by a short antigen application time on microneedle-treated skin, thereby not leading to a steady state diffusion. However, the amount of ovalbumin delivered in the skin showed that there is generally a relationship between the increase in penetration efficiency and increase in delivered amount of antigen with increasing impact velocities and pressing forces. Therefore, these data indicate that using the penetration efficiency could be a good value to estimate the required impact velocity and pressing force to obtain effective drug and vaccine delivery when using the "poke and patch" approach [32].

5. CONCLUSIONS

We have developed an applicator that reproducibly delivers a chosen pressing force and impact velocity. This applicator can be used to determine the optimal insertion parameters of a variety of microneedle arrays, and could therefore be a valuable tool for microneedle researchers. Moreover, using this applicator results in effective and reproducible piercing of *ex vivo* human skin with microneedles prepared with different shapes and materials.

Author Contributions

M.L. and K.v.d.M. conceived, designed and performed the experiments, analysed the data and wrote the paper; G.K., J.B., and C.O. contributed to the scientific content/discussions during the construction of the manuscript. B.H.v.O. designed and fabricated the applicator. C.O. provided the equipment for high-speed imaging and interpreting this data. A.B. and M.R. set-up and performed the high-speed imaging experiments. M.R.N. performed the SEM imaging. G.K., and J.B. supported in reagents, materials and tools to quantify the penetration efficiency and the delivery of the fluorescently labelled protein into skin.

Conflicts of Interest

K.v.d.M. and B.H.v.O. are co-founders of uPRAX Microsolutions. The other authors declare no conflict of interest.

REFERENCES

1. Hauri, A.M.; Armstrong, G.L.; Hutin, Y.J.F. The global burden of disease attributable to contaminated injections given in health care settings. Int. J. STD AIDS 2004, 15, 7–16.
2. Hegde, N.R.; Kaveri, S.V.; Bayry, J. Recent advances in the administration of vaccines for infectious diseases: Microneedles as painless delivery devices for mass vaccination. Drug Discov. Today 2011, 16, 1061–1068.
3. Ita, K. Transdermal delivery of drugs with microneedles: Strategies and outcomes. J. Drug Deliv. Sci. Technol. 2015, 29, 16–23.
4. Kersten, G.; Hirschberg, H. Needle-free vaccine delivery. Expert Opin. Drug Deliv. 2007, 4, 459–474.
5. Kim, Y.C.; Park, J.H.; Prausnitz, M.R. Microneedles for drug and vaccine delivery. Adv. Drug Deliv. Rev. 2012, 64, 1547–1568.
6. Leone, M.; Monkare, J.; Bouwstra, J.A.; Kersten, G. Dissolving Microneedle Patches for Dermal Vaccination. Pharm. Res. 2017.
7. Singh, T.R.; Dunne, N.J.; Cunningham, E.; Donnelly, R.F. Review of patents on microneedle applicators. Recent Pat. Drug Deliv. Formul. 2011, 5, 11–23.
8. Prausnitz, M.R.; Mitragotri, S.; Langer, R. Current status and future potential of transdermal drug delivery. Nat. Rev. Drug Discov. 2004, 3, 115–124.
9. Arora, A.; Prausnitz, M.R.; Mitragotri, S. Micro-scale devices for transdermal drug delivery. Int. J. Pharm. 2008, 364, 227–236.
10. Engelke, L.; Winter, G.; Hook, S.; Engert, J. Recent insights into cutaneous immunization: How to vaccinate via the skin. Vaccine 2015, 33, 4663–4674.
11. Kalia, Y.N.; Naik, A.; Garrison, J.; Guy, R.H. Iontophoretic drug delivery. Adv. Drug Deliv. Rev. 2004, 56, 619–658.
12. Prausnitz, M.R.; Bose, V.G.; Langer, R.; Weaver, J.C. Electroporation of mammalian skin: A mechanism to enhance transdermal drug delivery. Proc. Natl. Acad. Sci. USA 1993, 90, 10504–10508.
13. Haq, M.I.; Smith, E.; John, D.N.; Kalavala, M.; Edwards, C.; Anstey, A.; Morrissey, A.; Birchall, J.C. Clinical administration of microneedles: Skin puncture, pain and sensation. Biomed. Microdevices 2009, 11, 35–47.
14. Roxhed, N.; Samel, B.; Nordquist, L.; Griss, P.; Stemme, G. Painless drug delivery through microneedle-based transdermal patches featuring active infusion. IEEE Trans. Biomed. Eng. 2008, 55, 1063–1071.
15. Larraneta, E.; Lutton, R.E.M.; Woolfson, A.D.; Donnelly, R.F. Microneedle arrays as transdermal and intradermal drug delivery systems: Materials science, manufacture and commercial development. Mater. Sci. Eng. R 2016, 104, 1–32.
16. Larraneta, E.; McCrudden, M.T.C.; Courtenay, A.J.; Donnelly, R.F. Microneedles: A New Frontier in Nanomedicine Delivery. Pharm. Res. 2016, 33, 1055–1073.
17. Tuan-Mahmood, T.M.; McCrudden, M.T.; Torrisi, B.M.; McAlister, E.; Garland, M.J.; Singh, T.R.; Donnelly, R.F. Microneedles for intradermal and transdermal drug delivery. Eur. J. Pharm. Sci. 2013, 50, 623–637.
18. Van der Maaden, K.; Luttge, R.; Vos, P.J.; Bouwstra, J.; Kersten, G.; Ploemen, I. Microneedle-based drug and vaccine delivery via nanoporous microneedle arrays. Drug Deliv. Transl. Res. 2015, 5, 397–406.
19. Edens, C.; Dybdahl-Sissoko, N.C.; Weldon, W.C.; Oberste, M.S.; Prausnitz, M.R. Inactivated polio vaccination using a microneedle patch is immunogenic in the rhesus macaque. Vaccine 2015, 33, 4683–4690.
20. Qiu, Y.; Guo, L.; Zhang, S.; Xu, B.; Gao, Y.; Hu, Y.; Hou, J.; Bai, B.; Shen, H.; Mao, P. DNA-based vaccination against hepatitis B virus using dissolving microneedle arrays adjuvanted by cationic liposomes and CpG ODN. Drug Deliv. 2015, 23, 2391–2398.
21. Vassilieva, E.V.; Kalluri, H.; McAllister, D.; Taherbhai, M.T.; Esser, E.S.; Pewin, W.P.; Pulit-Penaloza, J.A.; Prausnitz, M.R.; Compans, R.W.; Skountzou, I. Improved immunogenicity of individual influenza vaccine components delivered with a novel dissolving microneedle patch stable at room temperature. Drug Deliv. Transl. Res. 2015, 5, 360–371.

22. Vrdoljak, A.; Allen, E.A.; Ferrara, F.; Temperton, N.J.; Crean, A.M.; Moore, A.C. Induction of broad immunity by thermostabilised vaccines incorporated in dissolvable microneedles using novel fabrication methods. J. Control. Release 2016, 225, 192–204.
23. Norman, J.J.; Arya, J.M.; McClain, M.A.; Frew, P.M.; Meltzer, M.I.; Prausnitz, M.R. Microneedle patches: Usability and acceptability for self-vaccination against influenza. Vaccine 2014, 32, 1856–1862.
24. Bonificio, A.; Ghartey-Tagoe, E.; Gallorini, S.; Baudner, B.; Chen, G.H.; Singh, P.; O'Hagan, D.T.; Kommareddy, S. Fabrication of cell culture-derived influenza vaccine dissolvable microstructures and evaluation of immunogenicity in guinea pigs. Vaccine 2015, 33, 2930–2938.
25. Raphael, A.P.; Prow, T.W.; Crichton, M.L.; Chen, X.F.; Fernando, G.I.P.; Kendall, M.A.F. Targeted, Needle-Free Vaccinations in Skin using Multi layered, Densely-Packed Dissolving Microprojection Arrays. Small 2010, 6, 1785–1793.
26. Van der Maaden, K.; Sekerdag, E.; Jiskoot, W.; Bouwstra, J. Impact-insertion applicator improves reliability of skin penetration by solid microneedle arrays. AAPS J. 2014, 16, 681–684.
27. M. Leone, M.I. Priester, S. Romeijn, M.R. Nejadnik, J. Monkare, C. O'Mahony, W. Jiskoot, G. Kersten, J.A. Bouwstra, Hyaluronan-based dissolving microneedles with high antigen content for intradermal vaccination: Formulation, physicochemical characterization and immunogenicity assessment, Eur J Pharm Biopharm, 134 (2019) 49-59.
28. Van der Maaden, K.; Heuts, J.; Camps, M.; Pontier, M.; Terwisscha van Scheltinga, A.; Jiskoot, W.; Ossendorp, F.; Bouwstra, J. Hollow microneedle-mediated micro-injections of a liposomal HPV E743-63 synthetic long peptide vaccine for efficient induction of cytotoxic and T-helper responses. J. Control. Release 2018, 269, 347–354.
29. Verbaan, F.J.; Bal, S.M.; van den Berg, D.J.; Groenink, W.H.; Verpoorten, H.; Luttge, R.; Bouwstra, J.A. Assembled microneedle arrays enhance the transport of compounds varying over a large range of molecular weight across human dermatomed skin. J. Control. Release 2007, 117, 238–245.
30. Verbaan, F.J.; Bal, S.M.; van den Berg, D.J.; Dijksman, J.A.; van Hecke, M.; Verpoorten, H.; van den Berg, A.; Luttge, R.; Bouwstra, J.A. Improved piercing of microneedle arrays in dermatomed human skin by an impact insertion method. J. Control. Release 2008, 128, 80–88.
31. Lee, J.W.; Park, J.H.; Prausnitz, M.R. Dissolving microneedles for transdermal drug delivery. Biomaterials 2008, 29, 2113–2124.
32. Van der Maaden, K.; Jiskoot, W.; Bouwstra, J. Microneedle technologies for (trans)dermal drug and vaccine delivery. J. Control. Release 2012, 161, 645–655.

Chapter 4

Hyaluronan-based dissolving microneedles with high antigen content for intradermal vaccination: formulation, physicochemical characterization and immunogenicity assessment

Adapted from Eur J Pharm Biopharm 2019 (134):49-59

Mara Leone[1], Marjolein I. Priester[1], Stefan Romeijn[1], M. Reza Nejadnik[1], Juha Mönkäre[1], Conor O'Mahony[2], Wim Jiskoot[1], Gideon Kersten[1,3,*], Joke A. Bouwstra[1,*]

[1] Division of BioTherapeutics, Leiden Academic Centre for Drug Research (LACDR), Leiden University, Leiden, the Netherlands

[2] Tyndall National Institute, University College Cork, Cork, Ireland

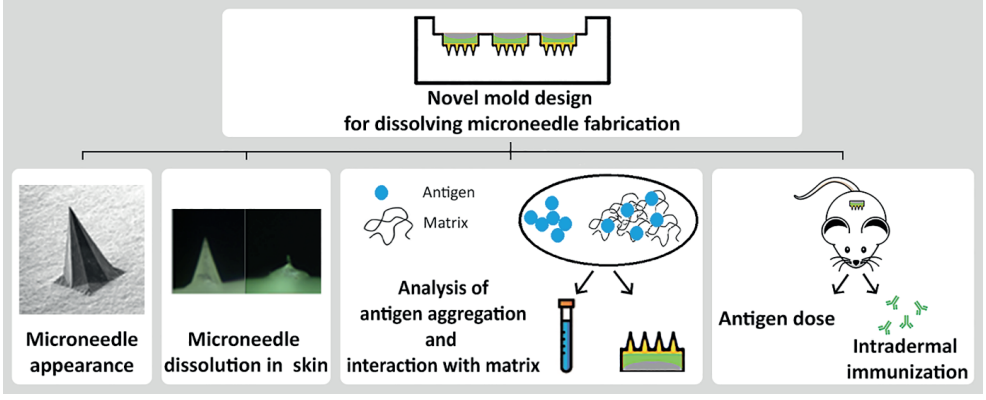
[3] Institute for Translational Vaccinology (Intravacc), Bilthoven, the Netherlands

[*] These authors contributed equally.

ABSTRACT

The purpose of this study was to optimize the manufacturing of dissolving microneedles (dMNs) and to increase the antigen loading in dMNs to investigate the effect on their physicochemical properties. To achieve this, a novel single-array wells polydimethylsiloxane mold was designed, minimizing antigen wastage during fabrication and achieving homogeneous antigen distribution among the dMN arrays. Using this mold, hyaluronan (HA)-based dMNs were fabricated and tested for maximal ovalbumin (OVA) content. dMNs could be fabricated with an OVA:HA ratio as high as 1:1 (w/w), without compromising their properties such as shape and penetration into the *ex vivo* human skin, even after storage at high humidity and temperature. High antigen loading did not induce protein aggregation during dMN fabrication as demonstrated by complementary analytical methods. However, the dissolution rate in *ex vivo* human skin decreased with increasing antigen loading. About 2.7 µg OVA could be delivered in mice by using a single array with an OVA:HA ratio of 1:3 (w/w). Intradermal vaccination with dMNs induced an immune response similar as subcutaneous injection and faster than after hollow microneedle injection. In conclusion, results suggest that (i) the polydimethylsiloxane mold design has an impact on the manufacturing of dMNs, (ii) the increase in antigen loading in dMNs affects the microneedle dissolution and (iii) dMNs are a valid alternative for vaccine administration over conventional injection.

GRAPHICAL ABSTRACT



Keywords: dissolving microneedles, hyaluronan, antigen loading, antigen aggregation, vaccine delivery, skin immunization.

1. INTRODUCTION

The skin is an attractive target for vaccination since it is a very immune-competent organ. Several types of antigen presenting cells (APCs) such as Langerhans cells (LCs) and dermal dendritic cells (dDCs) are present in the skin [1,2]. They capture antigens and migrate to the draining lymph nodes for antigen-presentation to T-cells, evoking antigen-specific T-cell and B-cell activation. Pain-free delivery of antigen into the skin, however, is a challenge, but can be achieved by using microneedles. Microneedles (MNs) are microstructures (up to 1 mm in length [3]) capable to pierce the skin and deliver the antigen in the epidermis and dermis [3-7]. For pain-free delivery they should not reach the nerve endings in the skin [8]. Furthermore, immunization with MNs would not necessarily require healthcare personnel [4, 9-11].

Dissolving microneedles (dMNs) are a microneedle type consisting of fast-dissolving excipient, such as polymers or sugars, as matrix mixed with the active compound. They dissolve in the skin after insertion thereby releasing the active ingredient [3-7]. Several studies have demonstrated that vaccines delivered intradermally via dMNs can generate immune responses at least as strong as those generated by subcutaneous or intramuscular injections [11-16]. However, the advantages of dMNs include low cost of matrix materials [17] and avoidance of sharp needle wastage after immunization make dMNs an attractive delivery system for intradermal vaccination. Additionally, the dry state of dMNs in combination with stabilizing excipients can lead to vaccine thermostability [18].

Dissolving MNs are often fabricated by micromolding in which a polydimethylsiloxane (PDMS) mold is used to pour the vaccine/matrix formulation [13]. The PDMS mold design is crucial for an efficient and consistent fabrication, ideally leading to minimal loss of active material and a homogenous distribution of the antigen among the simultaneously produced microneedle arrays without antigen aggregation [19]. Furthermore, the mold design is important in determining the optimal matrix concentration for the dMN fabrication. Although different matrix materials have been tested and compared for the dMN fabrication [20,21], optimization of the formulation with respect to antigen loading and mechanical properties has to our knowledge not been reported. A more detailed analysis regarding the loading capacity of dMNs is relevant to encapsulate a sufficient amount of antigen to evoke an effective immune response. Furthermore, an increase in antigen concentration, besides drying steps during fabrication, may considerably compromise the protein stability as previously reported [19, 22-28]. The stability of protein in microneedle arrays has to be well determined, because presence of protein degradants such as aggregates may compromise safety and efficacy of the vaccine.

This study aimed to (i) reduce the antigen waste during dMN fabrication and achieve dose uniformity within a batch of arrays, (ii) maximize the antigen loading in dMNs while maintaining a sufficient dMN sharpness and stiffness to pierce human skin and minimizing antigen aggregation during fabrication, and iii) obtain dMNs that deliver a sufficient dose of

antigen in mouse skin *in vivo* to induce an immune response comparable with conventional injection. To this end, hyaluronan (HA) was used as matrix material for dMN fabrication and ovalbumin (OVA) was used as model antigen.

2. MATERIALS AND METHODS

2.1. Materials

Hyaluronan (HA) (sodium hyaluronate, average Mw 150 kDa) was purchased from Lifecore Biomedical (Chaska, MN, USA) and OVA (Grade V) was obtained from Sigma-Aldrich (St. Louis, MO, USA). Vinylpolysiloxanes A-silicone (Elite Double 32a Normal) and the two-component epoxy glue (Bison, Goes, The Netherlands) were obtained from The Zhermack Group (Badia Polesine, Italy) and Bison International B.V. (Goes, The Netherlands), respectively. Polydimethylsiloxane (PDMS, Sylgard 184) was obtained from Dow Corning (Midland, MI, USA). Solid silicon MNs, fabricated using a potassium hydroxide wet-etching process [29], were kindly provided by the Tyndall Institute (Cork, Ireland). PBS pH 7.4 for subcutaneous and hMN injections was obtained from B. Braun, Melsungen, Germany. Immunization studies and ELISA were performed by using endotoxin-free OVA (endotoxin level < 1 EU/mg) from Invivogen (Toulouse, France). 10 mM PB (7.7 mM Na_2HPO_4, 2.3 mM NaH_2PO_4, pH 7.4) was prepared in the laboratory.

2.2. Dissolving microneedles

2.2.1. Polydimethylsiloxane mold fabrication

The fabrication of dMNs by micromolding requires the use of a polydimethylsiloxane (PDMS) mold. The PDMS mold was fabricated by using a template of poly(methyl metacrylate) (PMMA). The PMMA template, made by milling on a HAAS VF1 VMC (Vertical Milling Machine, USA), presented nine square pedestals of 5.4 × 5.4 mm with a height of 2.5 mm. On top of each pedestal a single solid silicon microneedle array (16 MNs in 5.4 × 5.4 mm array, 300 µm length and 200 µm base diameter) was fixed (see Figure 1). Next, a PDMS solution consisting of a mixture of a silicone elastomer and curing agent, was prepared in a 10:1 ratio (w/w) following the manufacturer's instruction. The solution was mixed, degassed in a vacuum and subsequently poured on top of the PMMA template. Then the template was vacuumed and finally placed at 60 °C overnight to cure. The following day, the mold was carefully removed from the PMMA template (Figure 1).

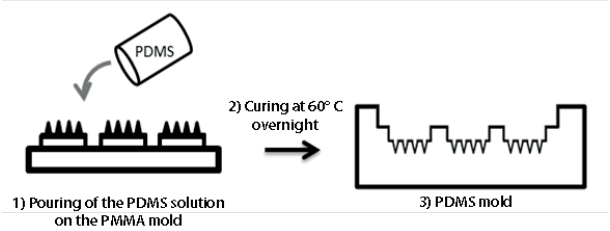


Figure 1. PDMS mold fabrication.

2.2.2. Preparation of dissolving microneedles

For the dMN preparation, the HA was dissolved in PB (10 mM, pH 7.4) and the solution was stored overnight to ensure the complete dissolution of HA. The next day, OVA in PB was added. Microneedle preparation was performed by pouring a selected OVA/HA solution in each well of the PDMS mold. Air bubbles were removed by vacuum cycles and to ensure complete filling of the micro-holes, the mold was placed in a centrifuge (1575 g, 37 °C, 3 h) (Beckman Coulter Allegra X-12R Indianapolis, IN, USA). Subsequently, additional OVA/HA solution was added to each well and steps of vacuum and centrifugation were repeated. Finally, the arrays were dried at 37 °C overnight.

To investigate the effect of the antigen loading in dMNs, a total of 12 OVA/HA compositions were used. These are provided in (Table 1).

Table 1. Overview of the different formulation compositions used to prepare the dMNs. In the Formulation approach A, the amount of HA was kept at 100 mg/ml while the amount of OVA varied. In the Formulation approach B, the amount of solids (OVA plus HA) was kept constant at 100 mg/ml but the ratio OVA/HA was changed. The control consisted of 10% HA. The compositions refer to the liquid formulations before dMN fabrication.

Composition	Formulation approach A				Formulation approach B							Control
OVA/HA (% w/v)	2.5/10	5/10	7/10	10/10	2.5/7.5	5/5	6/4	7/3	8/2	9/1	10/0	0/10
OVA (mg/ml)	25	50	70	100	25	50	60	70	80	90	100	0
HA (mg/ml)	100	100	100	100	75	50	40	30	20	10	0	100

After the overnight drying, an antigen-free bi-layered back-plate was prepared for all dMNs. A mixture of vinylpolysiloxane base and catalyst was prepared in a 1:1 ratio. The silicone solution was poured in each well and left curing for 20 min at room temperature (RT) to form the first layer of the back-plate. Next, a solution of two-components glue was placed

on top of the silicone layer. A sheet of solid PDMS and a 200 g weight were subsequently placed on top of the layers during the setting of the glue (2 h at 37 °C) to obtain a flat back-plate. Finally, the arrays were removed from the PDMS mold, and stored at RT in a desiccator until use.

2.3. Dissolving microneedle characterization

Microneedles were inspected by light microscopy (Stemi 2000-C, Carl Zeiss Microscopy GmbH, Göttingen, Germany) for shape, sharpness and for absence of empty cavities at the microneedle base after cutting tips transversely by using a stainless surgical blade (Swann-Morton, Sheffield, England). For high-resolution imaging, scanning electron microscopy (SEM, Nova NanoSEM-200, FEI, Hillsboro, OR, USA) was used. Prior to SEM imaging, the microneedle arrays were covered with a layer of 15 nm platinum/palladium (Sputter Coater 208HR, Cressington, Watford, UK). The instrument was operated at 5.00 kV and images were taken at magnifications between 300 and 600×.

2.4. Human skin

Human abdomen skin was obtained within 24 h after cosmetic surgery from local hospitals. After manual removal of the excess fat, the skin was stored at −80 °C until use. Before use, the skin was thawed in a humid petri dish at 37 °C for at least one hour and stretched with pins on parafilm-covered Styrofoam. The skin was cleaned with Milli-Q and 70% ethanol before the start of the experiment.

2.5. Microneedle penetration of *ex vivo* human skin

The arrays were applied by using an impact insertion applicator with a constant velocity of 0.54 m/s (Leiden University - applicator with uPRAX controller version 0.3) to ensure a reproducible piercing of dMNs [30]. After 18 s, the array was removed and 70 µl of 0.4% (w/v) trypan blue solution was applied on the penetration site for 1 h. After removal of the trypan blue solution with dry paper tissue, tape-stripping (approximately 10 strips) was performed (Avery 440 Gloss Transparent Removable, Avery Dennison) to remove the *stratum corneum* until the skin had a shiny appearance (Supplementary data, Figure S1). In this way only dMN penetration that reached the viable epidermis is taken into account [30]. Three arrays of each dMN composition were tested for their ability to penetrate *ex vivo* human skin from three different donors (i.e., n = 9 arrays for each dMN composition). The number of blue spots, indicating holes created by a microneedle, were counted for each individual array and divided by the total number of MNs on the array to obtain the penetration efficiency (PE) of each dMN composition (Equation 1) [30]:

$$\text{Penetration efficiency (\%)} = (\text{Number of blue spots}/16) \times 100\% \qquad \text{(Eqn. 1)}$$

2.6. Mechanical integrity of dissolving microneedles after storage

To examine the mechanical integrity after storage, three dMN arrays per each composition were exposed to different humidity and temperature in a desiccator as indicated in Table 2.

Table 2. Storage conditions of dMNs.

Storage period	Temperature (°Celsius)	Humidity (% Relative Humidity)
60 days	4	0
	Room temperature	0
	37	0
	60	0
4 hours	Room temperature	60
	Room temperature	82

To ensure 0% relative humidity (RH), microneedle arrays were stored over silica gel and to achieve 60 and 82 RH%, oversaturated salt solutions of sodium bromide and potassium chloride were used, respectively [31]. Prior arrays storage, the relative humidity was registered overnight every 20 min (Supplementary data, Figure S2) by using a data logger (EL-USB-2-LCD+, Lascar Electronics, Salisbury, UK) and a digital thermos-hygrometer (TFA-Fostmann GmbH & Co., Wertheim, Germany) to ensure constant humidity conditions in time. For each condition, five arrays per dMN composition were stored. After storage, two arrays were used for the visual characterization of dMNs and three arrays were used to investigate the capability of dMNs to pierce the *ex vivo* human skin as described in paragraph 2.6.

2.7. Microneedle dissolution in *ex vivo* human skin

Microneedles were pierced into the skin as described above and kept in the skin for 1 min, 5 min, 10 min or 20 min. Thereafter, arrays with remaining dMN tips were removed and stored in a desiccator until light microscopy analysis was carried out to determine the remaining microneedle tip length. Three arrays of each dMN composition were tested on three different skin donors for each time point (i.e., n = 3 arrays for each time point). The dissolved MN tip volume was calculated for each dMN composition (Supplementary data, Figure S3) and compared.

2.8. Analysis of protein stability

For the protein stability analysis, microneedle arrays (stored for less than one week in a desiccator RH 0% at room temperature) of all OVA/HA compositions (6 patches, one per composition) were dissolved overnight in PBS pH 7.4. Buffer volume was adjusted to obtain 0.5 mg/ml of OVA concentration.

2.8.1. Asymmetrical flow field-flow fractionation

In order to analyze the state of the antigen after microneedle dissolution, asymmetrical flow field-flow fractionation (AF4) was performed. The analysis was performed on all the compositions of OVA/HA both in solutions prior to microneedle fabrication and their corresponding microneedle arrays dissolved in PBS. Controls of OVA-only and HA-only, both in solution and as dissolved array, were also analyzed. AF4 measurements were performed on an Agilent 1200 system with a UV detector (280 nm) (Agilent Technologies, Palo Alto, California) combined with Wyatt Eclipse for AF4 separation and a multiangle laser light scattering (MALLS) detector (Wyatt Technology Europe GmbH, Dernbach, Germany). For the separation, a small channel equipped with a 350 µm spacer of medium width and a regenerated cellulose membrane with a cut-off of 10 kDa was used. The injection volume was 50 µl and the mobile phase was a solution of 50 mM of $NaNO_3$. In order to separate the aggregates in the samples (eluting later) from the monomer/dimers (eluting earlier), the samples were injected into the channel, followed by 1 min focus-flow. Thereafter, elution in the channel started with a cross-flow of 3 ml/min for 12 min. Then, after a total AF4 program time of 19 min, the cross-flow stopped to elute all remaining aggregates. The detector flow during elution was set to 1 ml/min. Calculation of the percentage of aggregates in the sample was done by calculating the area under the curve (AUC) of the aggregate peaks of the elugrams dividing by the total AUC of all peaks ('monomer and/or dimer' and 'aggregates') with Chemstation software from Agilent. The molecular weight of the species was calculated by relating the MALLS signal to UV according to the built-in functions in the Astra software version 5.3.2.22 (Wyatt Technology Europe GmbH, Dernbach, Germany).

2.8.2. Flow imaging microscopy analysis

A Micro-Flow Imaging (MFI) system (MFI5200, ProteinSimple, Santa Clara, USA), equipped with a silane coated flow cell (1.41 × 1.76 × 0.1 mm) and controlled by the MFI View System Software (MVSS) version 2, was used for flow imaging microscopy analysis. The system was flushed thoroughly with ultrapure water and PBS prior to each measurement to reduce the background counts of particles. After the rinsing step, the cleanliness of the field of view was checked visually. The background was zeroed by flowing PBS and performing the 'optimize illumination' procedure. Samples of 0.5 ml with a pre-run volume of 0.2 ml were analyzed at

a flow rate of 0.17 ml/min and a fixed camera rate of 22 flashes per second. The data recorded by the MVSS was analyzed with MFI View Analysis Suite (MVAS) version 1.2 after stuck particle removal procedure was performed by the software. The equivalent circular diameter (ECD), which is the diameter of a spherical particle that has an equivalent projection area as the particle imaged by MFI, was calculated as a measure of the particle size. The particle concentrations (particles/ml) were obtained and plotted in function of the particle size.

2.8.3. Nanoparticle tracking analysis

Nanoparticle tracking analysis (NTA) was performed at room temperature with a NanoSight LM20 (NanoSight Ltd., Amesbury, United Kingdom) equipped with a 640 nm laser and operating at an angle of 173° with respect to the flow cell (100 × 80 × 10 μm). Samples were injected into the chamber by an automatic pump (Harvard Apparatus, catalog no. 98–4362, Holliston, USA) using a sterile 1 ml syringe (BD Discardit II, New Jersey).

The following settings were used for tracking of the particles: background extract on; brightness 0; gain 1.00; blur size 3 × 3; detection threshold 10, viscosity equal to that of water. All other parameters were set to the automatic adjustment mode. For each sample a 90 s video was captured with shutter set at 1495 and gain at 680. The video was analyzed by using the NTA 2.0 Build 127 software.

2.9. Mice

Female BALB/c (H2d) (Charles River (Maastricht, The Netherlands), 8–11 weeks old at the beginning of the studies, were maintained under standardized conditions in the LACDR animal facility. The mice were randomly assigned to groups of 8 mice. Quantification and immunization studies were approved by the ethical committee on animal experiments of Leiden University (License number 14241).

2.10. Quantification of ovalbumin delivery in mouse skin *in vivo*

2.10.1. Preparation of infrared labeled ovalbumin

To quantify OVA release in mouse skin *in vivo*, OVA was labeled with an infrared dye (IRDye 800CW, LI-COR, Lincoln, Nebraska USA) (OVA-IR800) according to the manufacturer's instructions. The infrared signal of labeled OVA was measured by Tecan Infinite M1000 plate reader (Männedorf, Switzerland) at excitation and emission wavelengths of 774 nm and 789 nm, respectively.

2.10.2. Ovalbumin quantification

Based on the dissolution studies in *ex vivo* human skin, microneedle arrays of 2.5% OVA and 7.5% HA (n = 9) were selected for quantification of OVA in mouse skin *in vivo* and 5% of the total OVA was replaced with OVA-IR800.

The dMNs were inserted into anaesthetized female BALB/c (H2d) (Charles River (Maastricht, The Netherlands)) shaved flank skin for a period of 20 min after which the array was removed. Mice were euthanized and the near-infrared fluorescence of the delivered OVA-IR800 was measured in a Perkin-Elmer IVIS Lumina Series III *in vivo* imaging system (Waltham, MA, USA), by using a ICG bkg excitation filter and an ICG emission filter, acquisition time 4 s, F-stop 2, binning 4 and field of view of 12.5 cm. Perkin-Elmer Living Image software version 4.3.1.0 was used for image acquisition and analysis. Infrared data were processed using region of interest (ROI) analysis with background subtraction consisting of a control region of the skin.

To enable the quantification of the delivered amount of OVA-IR800, a calibration curve in *ex vivo* mouse skin was made by injecting different volumes of a formulation containing an OVA:HA ratio of 1:3 (w/w). Intradermal microinjections of OVA-IR800 were performed at OVA-IR800 doses between 62.5 and 1000 ng by using the in house fabricated hollow microneedle (hMN) injection system reported elsewhere [32-34].

2.11. Immunizations

To evaluate the functionality of dMNs as vaccination method, the dMNs with a composition of 2.5% OVA and 7.5% HA was chosen to perform immunization study. The immunization groups (n = 8) are reported in Table 3.

Table 3. Immunization study parameters.

Immunization route	Application method	Group name	OVA dose (µg)
Intradermal	**Dissolving MNs**	OVA/HA dMNs[a]	2.7
	Single hollow MN (10 µl, 120 µm injection depth)	OVA hMN	4.0
		OVA/HA hMN[b]	4.0
Subcutaneous	**Conventional 26G needle (100 µl)**	OVA sc	4.0
		PBS sc[c]	-

[a] 2.5% OVA/7.5% HA group as determined by OVA delivery from fluorescently labeled OVA-IR800 in mouse skin *in vivo*.

[b] 12 µg HA, resembling the OVA:HA ratio of dMNs group.

[c] PBS pH 7.4 (as negative control)

For single hollow microneedle injection and the dMN array application specially designed applicators were used as described previously [30, 32-34]. Immunizations were performed at day 1 (prime immunization), day 21 (boost immunization) and day 42 (2nd boost immunization). One day prior to the immunizations by dMN and hMN systems, the mice were shaved on the flank (approximately 4 cm^2). On the same day, venous blood (200 µl) was collected by tail vein incision in a 0.8 ml MiniCollect® tube. The blood was stored on ice before centrifugation (3000 g, room temperature, 10 min) to isolate serum, which was stored at −80 °C until analysis. Prior to vaccination, mice were anaesthetized by intraperitoneal injection of 150 mg/kg ketamine and 10 mg/kg xylazine. At day 63, all mice were bled by incision of abdominal/thoracic artery followed by scarification by cervical dislocation. Blood samples in 2.5 ml Vacuette® tubes were stored on ice before centrifugation at 1800 g (4 °C, 10 min) to isolate serum, which was stored at −80 °C until analysis.

2.12. Serum IgG assay

OVA-specific antibodies were determined by ELISA as described earlier [35]. OVA coated ELISA plate wells were blocked with bovine serum albumin (BSA) (Sigma-Aldrich, Zwijndrecht, the Netherlands) and subsequently, three-fold serial dilutions of serum were added to the plates and incubated for 1.5 h at 37 °C. The plates were incubated with horseradish peroxidase-conjugated goat antibodies against IgG total, IgG1 and IgG2a (Southern Biotech, Birmingham, AL, USA) for 1 h at 37 °C. 1-step TM ultra 3,3',5,5'-tetramethylbenzidine (TMB) (Thermo-Fischer Scientific, Waltham, USA) was used as substrate and the reaction was stopped with sulfuric acid (H2SO4) (95–98%) (JT Baker, Deventer, The Netherlands). The absorbance was measured at 450 nm on a Tecan Infinite M1000 plate reader (Männedorf, Switzerland) and the antibody titers were expressed as the log10 value of the mid-point dilution of a complete s-shaped absorbance-log dilution curve of the diluted serum level.

2.13. Statistical analysis

Microneedle penetration efficiency was analyzed by Kruskal–Wallis test with Dunn's multiple comparison test. Level of significance was set at $p < 0.05$. The remaining dMN length after dissolution at different time points was analyzed by two-way ANOVA with a Tukey's post-test ($p < 0.05$). IgG titers were analyzed using one-way ANOVA with Bonferroni post-test suitable in the software Prism (Graphpad, San Diego, USA). A p-value less than 0.001 was considered to be significant.

3. RESULTS

3.1. Polydimethylsiloxane mold optimization and dissolving microneedle fabrication

A novel PMMA template was designed so that in the PDMS mold each individual dMN array was fabricated in a separate well, referred to as single-array well design (Figure 2A). This has the advantage over our previously designed template resulting in multi-arrays well PDMS design [19] that (1) each well undergoes the same physical processing during the preparation of the dMN arrays, (2) dMN arrays of different compositions can be prepared in one fabrication process run and (3) the antigen loss could be reduced by pouring the matrix/antigen solution on each array-space (well), herewith avoiding to waste the solution on areas in between the wells. A comparison between the single-array well design and the multi-arrays well design is provided in Supplementary data, Figure S4.

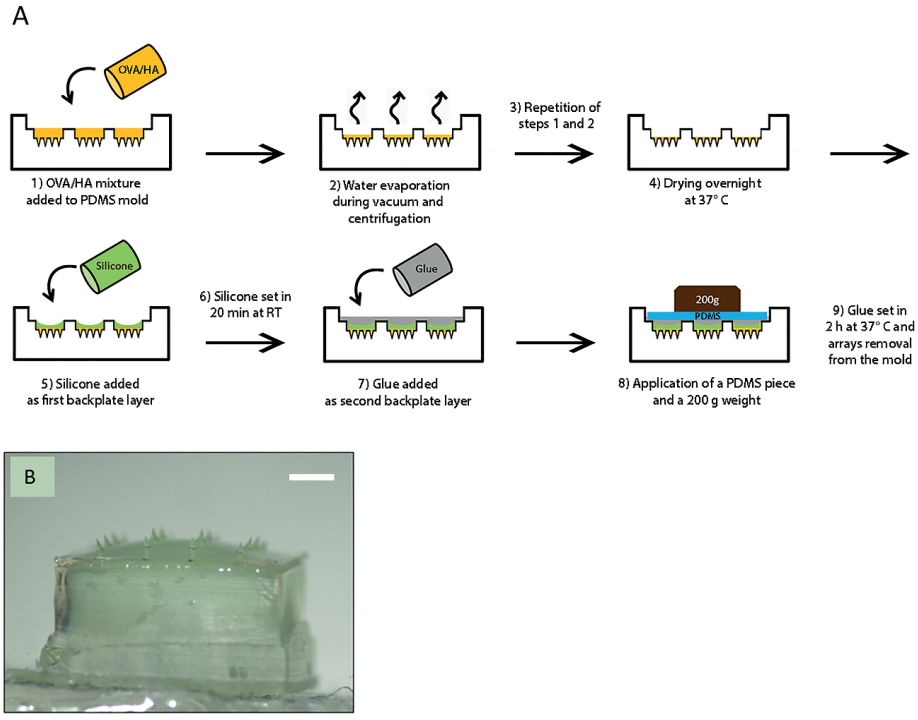


Figure 2. (A) Preparation scheme of dMNs and bi-layered back-plate using a single-array well mold. **(B)** Brightfield microscope images (1.25×) of a dissolving microneedle array with bi-layered back-plate (scale bar 1 mm). PDMS, Polydimethylsiloxane; RT, room temperature.

The single-array well PDMS design allowed the preparation of an antigen-free back-plate and thus less antigen is required for MN preparation. The antigen-free bi-layered back-plate consisted of a first layer of silicone and a second layer of glue (Figure 2A-B) and increases the easiness of MN array handling.

The PDMS mold was used to select the optimal HA concentration as control (Supplementary data, Figure S5) for the dMN fabrication. dMNs with HA concentration below 10% (w/v) in preparation mixture, showed empty cavities at the base of MN tip, whereas the use of concentrations of 10% (w/v) HA or above it resulted in dMNs without empty cavities at the base. The 10% HA concentration was selected as HA control because solutions with higher HA concentration were too viscous and thus difficult to handle. It was further observed that 10% (w/v) total solid content, i.e. reached by HA and OVA together content combined, could still give microneedles without empty cavities at the base (see Formulation approach B, Figure 3B).

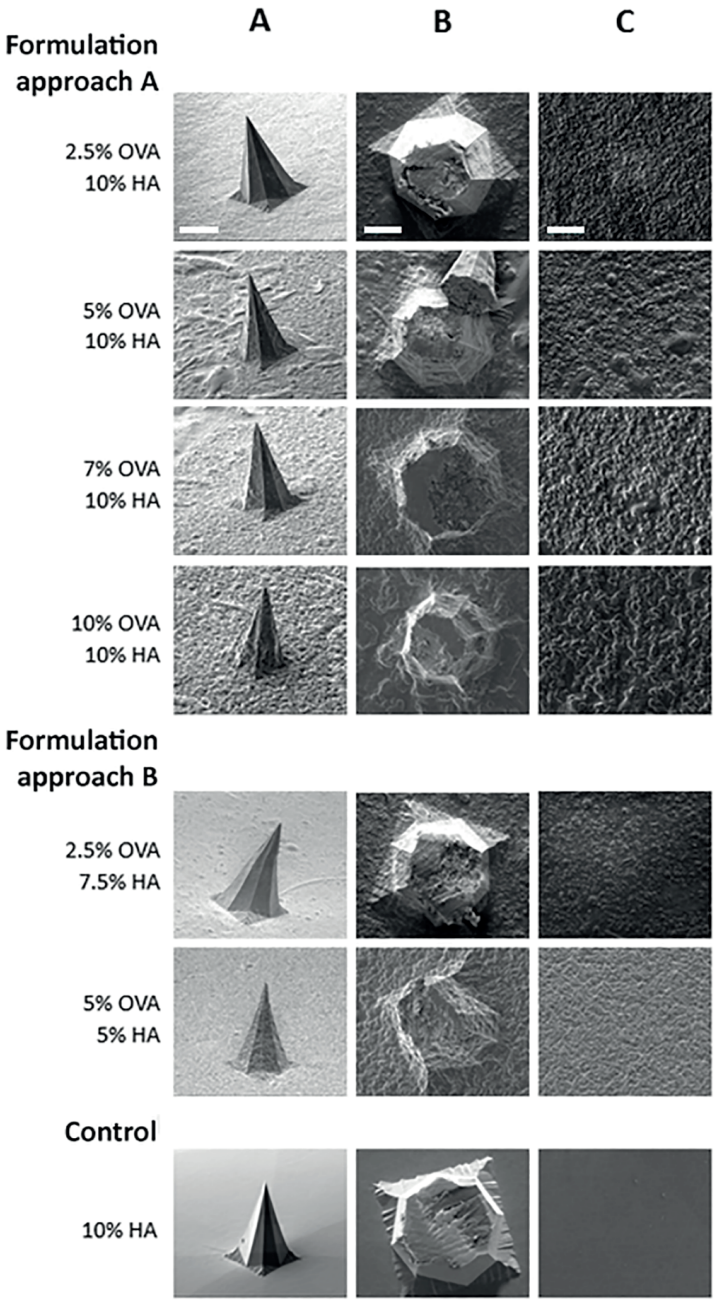


Figure 3. SEM images show increasing OVA concentration up to a weight ratio of 1:1 with HA allows the preparation of symmetrical and sharp dMNs. **(A)** dMNs lateral view (300×, scale bar 100 μm), **(B)** cut dMNs, upper view (600×, scale bar 50 μm) and **(C)** surface structure dMNs (600×, scale bar 50 μm).

3.2. Appearance of dissolving microneedles

To assess whether high antigen loading affects the quality of the dMNs, dMN arrays were prepared with increasing antigen content (Table 1). It was possible to increase the OVA content in the dMNs up to an OVA:HA ratio of 1:1 (w/w) (10% OVA/10% HA or 5% OVA/5% HA) without observing a decrease in the microneedle sharpness (Figure 3A). However, increasing the OVA content beyond 50% of total HA and OVA concentration led to inconsistencies in fabrication. The arrays were fragile, contained ruptures, and it was not possible to remove intact arrays from the PDMS mold (data not shown).

SEM (Figure 3B) and brightfield (data not shown) analysis of transversal-cut dMN showed no empty cavities in the inner side of MNs up to an OVA:HA ratio of 1:1 (w/w) in both approaches, indicating a homogeneous filling of the PDMS micro-holes during dMN fabrication.

For both Formulation approach A and B, changes in the surface structure in comparison with the HA only control were observed (Figure 3C). Increasing OVA content in dMNs increased the surface roughness in comparison with the control (10% HA), which had a smooth surface. However, this did not affect the sharpness and shape of dMNs.

3.3. Penetration ability of microneedle arrays into *ex vivo* human skin

To investigate whether differences in dMN composition affect the dMN penetration of the skin, the arrays were applied onto *ex vivo* human skin. Regardless of the composition, all dMNs penetrated the skin, with a penetration efficiency of almost 100% for all the compositions (Table 4).

Table 4. Penetration efficiency of dMN with different compositions. All data are presented as mean ± SD (n = 9). No significant difference ($p > 0.05$) was found by Kruskall–Wallis test with Dunn's multiple comparison test.

Sample	Penetration efficiency (%)
2.5% OVA/10% HA	99.3 ± 2.1
5% OVA/10% HA	100.0 ± 0.0
7% OVA/10% HA	100.0 ± 0.0
10% OVA/10% HA	98.6 ± 2.7
2.5% OVA/7.5% HA	100.0 ± 0.0
5% OVA/5% HA	96.8 ± 4.7
10% HA	99.3 ± 2.1

3.4. Mechanical integrity of dissolving microneedles after storage

As dMN arrays may be exposed to various temperature and humidity conditions during shipment, storage and administration, the effect of these conditions was investigated. Microscope analysis showed that storage at different temperature and humidity conditions (Table 2) did not affect the sharpness of the dMNs (data not shown). Furthermore, the storage conditions did not alter the skin penetration efficiency of the dMNs, which remained close to 100% for all dMN compositions and storage conditions (Table 5).

Table 5. Penetration efficiency of dMNs after storage. dMNs were stored (n = 3 per dMN composition) under the conditions indicated. All data are presented as mean ± SD. No significant difference ($p > 0.05$) was found by Kruskal–Wallis test with Dunn's multiple comparison test.

	4°C 0% RH	RT 0% RH	37°C 0% RH	60°C 0% RH	RT 60% RH	RT 82% RH
SAMPLE	**60 days**				**4 hours**	
Formulation approach A						
10% OVA/10% HA	100 ± 0.0	100 ± 0.0	87.5 ± 16.5	100 ± 0.0	97.9 ± 3.6	97.9 ± 3.6
2.5% OVA/10% HA	100 ± 0.0	100 ± 0.0	100 ± 0.0	100 ± 0.0	97.9 ± 3.6	100 ± 0.0
Formulation approach B						
2.5% OVA/7.5% HA	100 ± 0.0	100 ± 0.0	100 ± 0.0	100 ± 0.0	97.9 ± 3.6	100 ± 0.0
5% OVA/5% HA	97.9 ± 3.6	100 ± 0.0	97.9 ± 3.6	100 ± 0.0	91.7 ± 3.6	97.9 ± 3.6
Control						
10% HA	100 ± 0.0	100 ± 0.0	95.8 ± 7.2	97.9 ± 3.6	97.9 ± 3.6	95.8 ± 7.2

RH, Relative humidity; RT, Room temperature.

3.5. Microneedle dissolution in *ex vivo* human skin

Analysis of the dissolved MN volume percentage after an application of 1, 5, 10 or 20 min showed that the dissolution rate depends on the dMN composition.

All dMN compositions showed a gradual dissolution as a function of time (Figure 4A). For compositions with an OVA concentration in the liquid starting formulation higher than 2.5% (w/v) as 5% OVA/5% HA, 5% OVA/10% HA, 7% OVA/10% HA and 10% OVA/10% HA, a comparable dissolution rate was reached after 1, 5, 10 and 20 min respectively (Figure 4B). The leftover was still high in comparison with that of the control (10% HA) (Figure 4A).

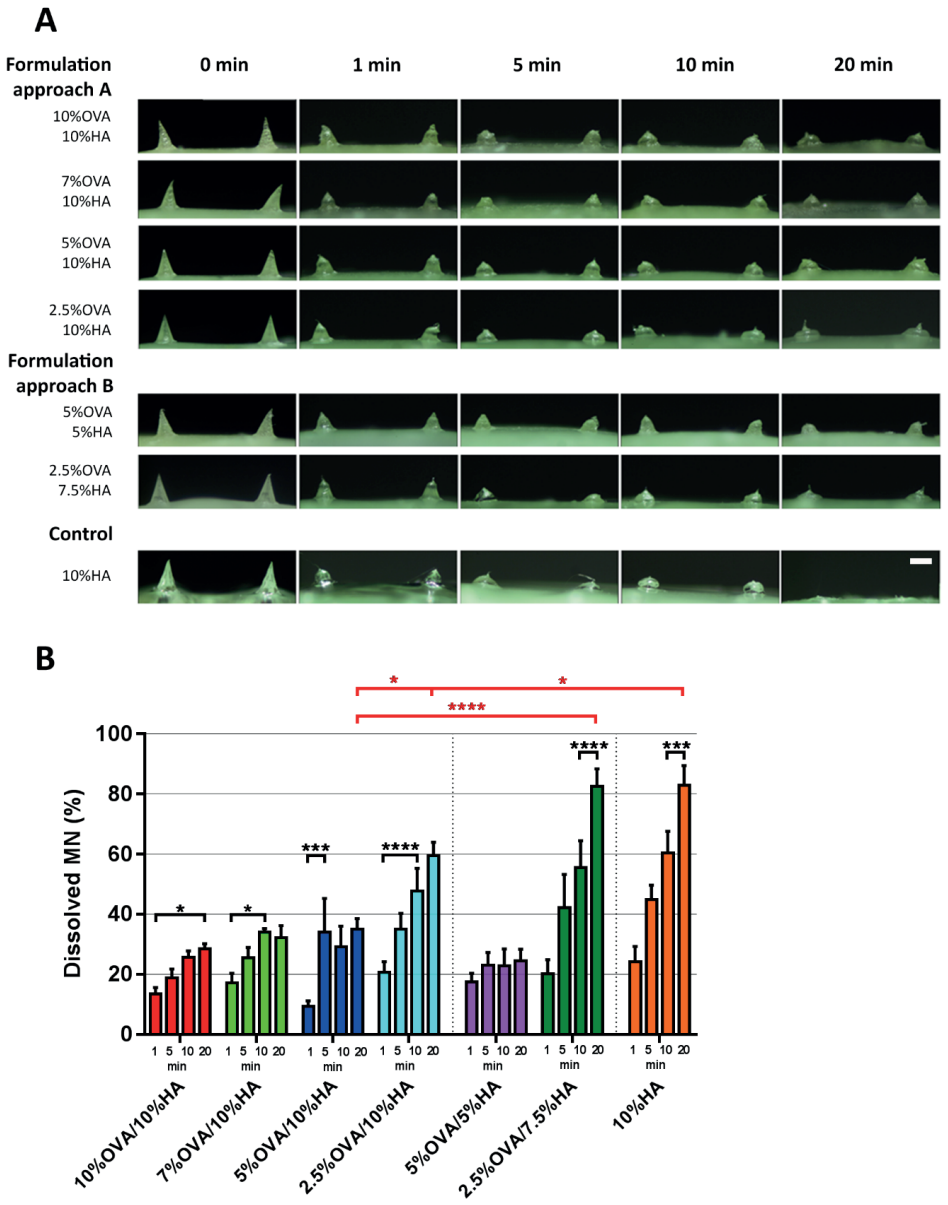


Figure 4. dMN dissolution in *ex vivo* human skin. **(A)** Representative light microscope images of dMNs before dissolution (0 min) and after 1, 5, 10 and 20 min dissolution in *ex vivo* human skin (40×). Scale bar is 200 µm; **(B)** Effect of time (1, 5, 10 and 20 min) on dissolution (statistics in black), showed per each dMN composition. Effect of formulation on dissolution (red statistics). Significance (*$p < 0.05$, ***$p < 0.001$ and ****$p < 0.0001$) was determined by a two-way ANOVA with a Tukey's post-test ($n = 3$). All data are presented as mean ± SEM.

The 2.5 %OVA/7.5% HA dMNs dissolved almost completely within 20 min after application, similarly to the control (Figure 4A and B). Although prepared with an equal OVA concentration in the liquid starting formulation as the 2.5% OVA/7.5% HA dMNs, the 2.5% OVA/10% HA dMNs reached maximal dissolution rate after 10 min resulting statistically different from the control (Figure 4B). As the 2.5% OVA/7.5% HA dMNs dissolved nearly completely after 20 min, we selected this composition for further studies.

3.6. Protein stability

The dMN fabrication conditions are mild, e.g., high temperature and extreme pH conditions are avoided, making chemical degradation unlikely to occur. Nevertheless, the antigen may encounter stress during the dMN preparation. The drying at high antigen concentrations may cause aggregation. To investigate whether submicron aggregates were formed during the dMN fabrication, AF4 analysis was performed. Figure 5A presents the UV elugrams of an OVA standard solution, a solution of 2.5% OVA/7.5% HA prior to dMN fabrication, and the same composition after dMN manufacturing and dissolving the MN array in PBS. Figure 5A shows how the OVA monomer eluted at 11.5 min, the OVA dimer eluted at 13.0 min and a small peak eluted after stopping the cross-flow at 19 min, indicating that OVA standard solution contained a minor fraction of aggregates with an average molecular weight of 2820 kDa calculated by MALLS detection. The 2.5% OVA/7.5% HA dissolved MN solution eluted at 12.1 min with a broader peak than OVA standard solution, indicating that OVA interacts with HA. However, the 2.5% OVA/7.5% HA starting solution showed a considerably broader peak (11.0–19.0 min), suggesting an even stronger interaction between OVA and HA. Furthermore, the peak of 2.5% OVA/7.5% HA solution after cross-flow stopping at 19.0 min indicates that the aggregate content and/or complexes between OVA and HA were considerably higher as compared to the 2.5% OVA/7.5% HA dissolved MN solution. All other compositions showed the same trend as the shown composition (data not shown). The dissolved HA-free dMNs, comprising only OVA (10% OVA w/v), showed an identical UV elugram as the OVA standard solution (results not shown), demonstrating that the drying/reconstitution process had no impact on the monomer/dimer content of plain OVA without HA present. Altogether, these results indicate a clear transient and reversible interaction between OVA and HA in solution, causing delayed elution of OVA both for OVA/HA solution prior to dMN fabrication and to a lesser extent for the corresponding dissolved MN array.

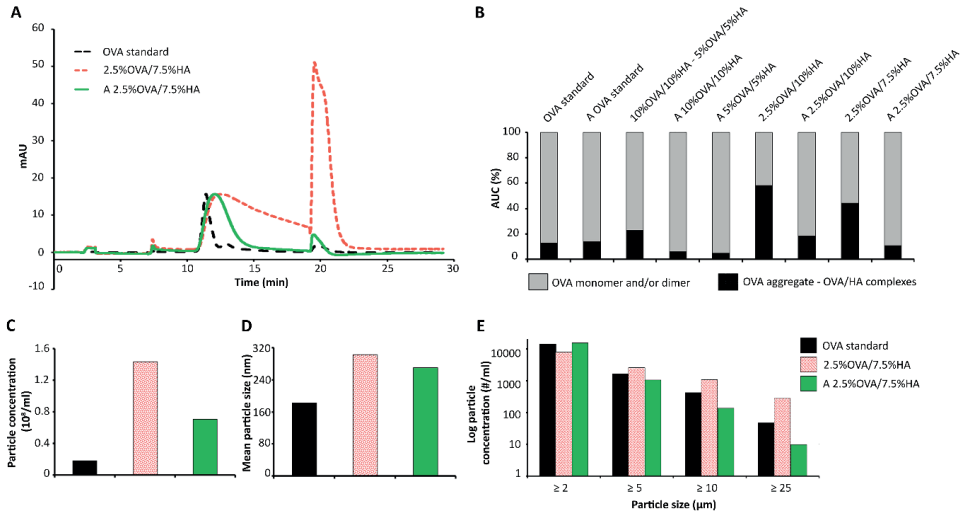


Figure 5. Protein aggregation analysis by AF4, NTA and MFI. **(A)** AF4 UV-based (280 nm) elugrams, normalized for the OVA standard solution peak at 11.5 min, of OVA standard solution (OVA standard, dark dashed line), 2.5% OVA/7.5% HA composition in solution prior to dMN fabrication (2.5%OVA/7.5%HA, light red dotted line) and its associated array dissolved in PBS (A 2.5%OVA/7.5%HA, green solid line); **(B)** Relative amount of OVA in aggregated and/or OVA/HA complexes (dark bars) and monomer and/or dimer state (light bars) calculated from the area under the curve of the AF4 UV elugrams for all OVA/HA compositions and OVA standard control; **(C–D)** Results of NTA of particle concentration and mean particle size, respectively, for the composition 2.5% OVA/7.5% HA both in solution prior to fabrication of dMNs and after array dissolution in PBS (A 2.5% OVA/7.5% HA); **(E)** Results of MFI shown as cumulative particle concentration vs particle size for the composition 2.5% OVA/7.5% HA before and after dMN fabrication. A, array.

The relative peak areas of monomer and/or dimer and aggregates expressed as percentages for each sample are shown in Figure 5B. It is evident that OVA/HA starting material contains more aggregates as compared to dissolved arrays for all compositions. Furthermore, the lower the OVA:HA ratio, in both solution and dissolved MN, the more OVA aggregates and/or OVA/HA complexes are found (see Figure 5B), again indicating an interaction of HA with OVA.

To rule out any particle formation that might have been missed during AF4 analysis, NTA and MFI analyses were performed for all compositions to monitor the presence of larger, nano- and micron-size aggregates, respectively. NTA showed that nanoparticle concentrations and particle sizes (Figure 5C and D, respectively, all other compositions showed similar trend (data not shown)) in the solutions of the dissolved arrays were lower than in the solutions prior to preparation of dMNs, corroborating the AF4 results. MFI analysis pointed in the same direction, i.e., it showed a lower micronsize particle content for all size ranges for the dissolved array compositions as compared to the freshly prepared OVA/HA mixtures and

even OVA standard solution (Figure 5E, all other compositions showed similar trend (data not shown)).

3.7. *In vivo* studies

As information on the delivered dose in the skin is crucial for designing immunization studies, the amount of OVA delivered into mouse skin *in vivo* after dMN array application was determined by using infrared labeled OVA. The dMN array with a composition of 2.5 %OVA/7.5% HA, that was selected for its optimal dissolution capability, was shown to deliver dose of 2.7 ± 1.3 µg (mean ± SD, n = 9) of OVA per array. The corresponding dissolved MN volume was of 76.4 ± 4.1% (mean ± SD, n = 9).

In order to investigate the immunogenicity of OVA delivered by dMNs in comparison with conventional subcutaneous injection, mice were immunized with OVA-dMNs (2.5% OVA/7.5% HA). As control, OVA (4 µg) was administered subcutaneously. In addition, hollow MNs were used to inject an exact dose of OVA with or without HA to investigate whether HA affects the immune response.

As shown in Figure 6, OVA administered via dMNs was equally immunogenic as subcutaneously injected OVA after both the prime and the two booster immunizations. For both groups, the first booster resulted in an overall increase in IgG total titers of about 2 log scales, whereas the second booster did not have a substantial additional effect on the total IgG titers. Interestingly, the IgG total responses were initially higher in the dMN group as compared to the mice receiving intradermally administered OVA with one hollow MN (OVA and OVA/HA). Only after the first or the second boost the IgG total titers of the hMN group OVA/HA and hMN group OVA respectively reached a comparable level as the dMN and s.c. groups. The presence of HA did not seem to have a major effect on the IgG total levels. The concentrations of OVA-specific IgG1 resembled closely the IgG total titers after each immunization point and IgG2a titers were absent (Supplementary data, Figure S6).

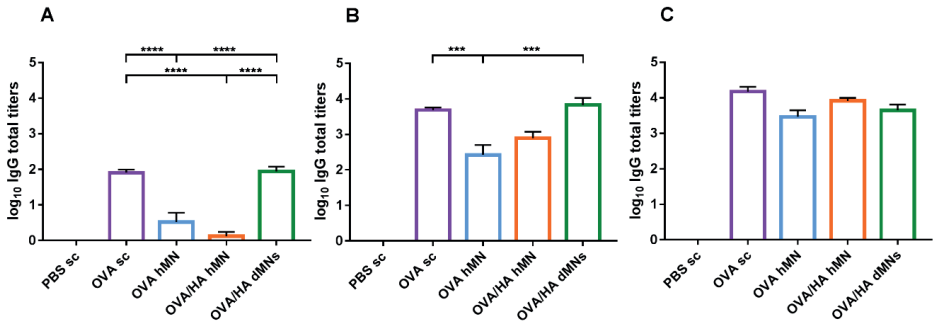


Figure 6. OVA-specific IgG antibody responses after vaccination. Mice were vaccinated either intradermally using dMNs (OVA/HA dMNs), hollow microneedle without HA (OVA hMN) and hollow microneedle with HA (OVA/HA hMN) or subcutaneously (OVA sc and PBS sc). Sera collected from the mice were assayed for OVA-specific IgG total titers after prime **(A)**, 1st boost **(B)** and 2nd boost **(C)**. Results are shown as mean ± SEM and statistical significance was determined by a one-way ANOVA with a Bonferroni post-test (***$p < 0.001$ and ****$p < 0.0001$).

4. DISCUSSION

The design of the PDMS mold plays an important role in the fabrication of dMNs. An optimization of the design by creating single-array well in the PDMS mold may have several advantages, such as a reduction in antigen waste during fabrication and an avoidance of heterogeneous distribution of the antigen content among the arrays of the single mold. It has been shown that the distribution of the protein within arrays prepared with a multi-arrays well design of a mold was not equal, most probably due to centrifugation forces in preparing the microneedle arrays [19]. In addition, this novel single-array well design allowed to work with different formulations during the same manufacturing run and to fabricate an antigen-free back-plate easy to handle. In the multi-arrays well PDMS mold the fabrication of an antigen-free back-plate for each single array was not possible because no single isolated arrays were prepared during manufacturing. The single-array well mold design was used in preliminary studies to identify the optimal HA concentration for a fabrication of cavity-free dMNs. Introducing an empty cavity at the microneedle base has been considered as a strategy to improve the delivery efficiency reducing the drug remaining in the microneedle after dissolution [36]. However, the size of the cavity is difficult to control, potentially leading to non-homogeneous dosing and reduced and variable needle strength. In our present study the optimal matrix concentration for cavity-free dMNs was 10% HA (w/v), while in a previous study using the multi-arrays well design mold and the same polymer, the arrays were fabricated by using lower HA concentrations [19]. This illustrates that for each mold design the polymer concentration should be optimized.

It was examined whether high protein antigen concentrations can be used in this novel way of producing the microneedles. A sufficient antigen dose is often required for achieving the desired effect and limited dose is one of main challenges of dMNs. It was observed that increasing the OVA content beyond 50% of total HA and OVA concentration led to fragile arrays. This may be related to a lack sufficient HA, which is needed for the structure of the microneedles provided by the polysaccharide hyaluronan network. Importantly, an increase in antigen content with a OVA:HA ratio from 1:4 up to a 1:1 (w/w) resulted in sharp dMNs that could efficiently penetrate the *ex vivo* human skin in a reproducible way. The penetration efficiency of almost 100% for all the compositions, enabled by the curved surface of the array and the presence of a back-plate [37], was comparable to that obtained in a previous study with silicon MNs applied via the same applicator [30].

Although the protein stability in dMNs is of critical importance, studies addressing this issue are scarce and they focus mainly on obtaining an immune response after dMN application to show preserved functionality after fabrication [13]. This, however, is an indirect and inaccurate way of monitoring antigen stability, as the immunogenicity of degraded antigens as well as antigen dose-response relationships are usually unknown. In this study, it was shown that the presented dMN fabrication method induced limited aggregation, even at very high OVA loading. This indicates that the conditions used during the micromolding were mild, as opposed to other fabrication methods [38, 39]. However, whether the same protein stability can be preserved for antigens different than OVA should be investigated. Remarkably, after dMN fabrication there was less aggregated OVA than in the OVA/HA solution used to produce the dMNs. This was observed for all OVA/HA solutions tested. Furthermore, AF4 showed a slight shift in elution time of OVA in the presence of HA, indicating some interaction between OVA and HA. This is in line with our previous study in which we showed reversible association between IgG and HA to occur [19]. The reason that this interaction was stronger in the solution before drying compared to dissolved needles may be caused by the fact that the needles were dissolved in PBS, resulting in increased ionic strength and, as consequence, in less electrostatic interactions between OVA and HA.

One important limitation that was encountered with a high OVA content (>2.5% (w/v)) in the arrays was a slower and reduced dMN dissolution in the skin. Increasing the hydrophilic polymer fraction did not avoid this, suggesting that the total OVA/HA concentration in the solution prior fabrication is affecting the dissolution of microneedles. However, when the selected 2.5% OVA/7.5% HA dMNs were used, the dissolution rate of dMNs was reasonably high. Moreover, the dissolved MN volume reached after application for 20 min in mouse skin *in vivo* (76.4 ± 4.1%) and in *ex vivo* human skin (82.6 ± 14.2%) were equal, proving a similar dissolution of dMNs in two different skin types. Interestingly, our studies demonstrate a faster dissolution of the control (10% HA) and 2.5% OVA/7.5% HA dMNs in comparison with HA dMNs reported in literature, such as 60 min and 120 min for complete dissolution of 300 µm and 800 µm length dMNs respectively [14, 40, 41]. This difference in dissolution time might be explained by differences in preparation conditions, although in some papers these

are not specified in detail. Also, the molecular weight of the HA used may be different. Other variables affecting dissolution time are the presence of excipients in dMNs [40], the type and quality of the skin used for dMN application (e.g., mice [14, 40] or rats [14, 41]), the use of an applicator, applicator settings and the experimental details of dissolution studies (*ex vivo* or *in vivo*).

Importantly, storage at different temperature or humidity values did not affect the dMN integrity. Contrasting results were reported by Hiraishi et al., who showed that high humidity caused dMN bending during use which prevented skin piercing [40]. However, in that case longer conical dMNs (800 μm) were tested and the MN design may play a role resulting the tetrahedral design of dMNs from the present study stronger [15, 42].

Prior to the immunization studies, the dose of OVA delivered in mouse skin *in vivo* from the selected 2.5% OVA/7.5% HA dMNs was quantified and estimated to be approximately 3 μg. This dose is in the range of a human dose of some licensed vaccines. Functionality of dMNs and retention of OVA after fabrication were proved through *in vivo* studies, showing comparable immunogenicity between dMNs and subcutaneous groups. Furthermore, the role of the HA as immunomodulator was investigated because of contrasting results in the literature [43-48]. The presence of HA with a mean molecular weight of 150 kDa did not affect the immune response, suggesting its inert nature as matrix material.

Finally, the higher response in the dMNs group than in the OVA hMN group after prime and first boost immunizations indicate that OVA administration by dMNs results in a faster response than administration by hMN. This may be due to a slower release of the antigen into the skin from dMNs than from hMN due to the dissolution step. Moreover, the different numbers of needles penetrating the skin may play a role: a hollow MN delivers the antigen as a small bolus at one site, whereas the dMNs deposit 16 small doses over a larger area. The slower release together with the broader antigen distribution and a potentially higher tissue damage and cell death [13, 49] from dMNs may result in a faster and higher response. The lack of IgG2a response was expected as no adjuvant was added to the MN formulation [50]. This may be subject of a follow-up study.

5. CONCLUSIONS

In summary, our study demonstrates that the design of the PDMS mold is a critical parameter in the fabrication of dMNs and that high antigen content in HA-based dMNs does not affect the sharpness and capability to pierce the skin of dMNs. dMNs can be manufactured with ovalbumin:hyaluronan ratio as high as 1:1 (w/w) without aggregate formation. However, the higher the antigen loading the lower is the dissolution rate of dMNs in the skin. Finally, vaccination by means of dMNs was shown to evoke a comparable response as by conventional subcutaneous injection and a faster response than hMN injection, illustrating the potential of dMNs for intradermal vaccine delivery.

Conflict of interest

Wim Jiskoot is a scientific advisor at Coriolis Pharma, Martinsried, Germany.

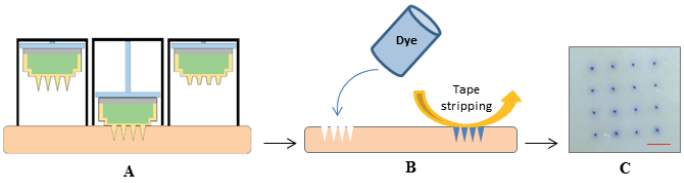
REFERENCES

1. L. Engelke, G. Winter, S. Hook, J. Engert, Recent insights into cutaneous immunization: how to vaccinate via the skin, Vaccine, 33 (2015), pp. 4663-4674
2. M. Kaurav, S. Minz, K. Sahu, M. Kumar, J. Madan, R.S. Pandey, Nanoparticulate mediated transcutaneous immunization: myth or reality, Nanomedicine, 12 (2016), pp. 1063-1081
3. K. van der Maaden, W. Jiskoot, J. Bouwstra, Microneedle technologies for (trans)dermal drug and vaccine delivery, J. Control Release, 161 (2012), pp. 645-655
4. K. Ita, Transdermal delivery of drugs with microneedles: Strategies and outcomes, J. Drug Deliv. Sci. Tec., 29 (2015), pp. 16-23
5. S. Indermun, R. Luttge, Y.E. Choonara, P. Kumar, L.C. du Toit, G. Modi, V. Pillay, Current advances in the fabrication of microneedles for transdermal delivery, J. Control Release, 185 (2014), pp. 130-138
6. E. Larraneta, M.T.C. McCrudden, A.J. Courtenay, R.F. Donnelly, Microneedles: a new frontier in nanomedicine delivery, Pharm. Res.-Dordr., 33 (2016), pp. 1055-1073
7. T.M. Tuan-Mahmood, M.T.C. McCrudden, B.M. Torrisi, E. McAlister, M.J. Garland, T.R.R. Singh, R.F. Donnelly, Microneedles for intradermal and transdermal drug delivery, Eur. J. Pharm. Sci., 50 (2013), pp. 623-637
8. N.R. Hegde, S.V. Kaveri, J. Bayry, Recent advances in the administration of vaccines for infectious diseases: microneedles as painless delivery devices for mass vaccination, Drug Discov. Today, 16 (2011), pp. 1061-1068
9. Y.C. Kim, J.H. Park, M.R. Prausnitz, Microneedles for drug and vaccine delivery, Adv. Drug Deliver Rev., 64 (2012), pp. 1547-1568
10. K. Matsuo, S. Hirobe, N. Okada, S. Nakagawa, Frontiers of transcutaneous vaccination systems: novel technologies and devices for vaccine delivery, Vaccine, 31 (2013), pp. 2403-2415
11. N.G. Rouphael, M. Paine, R. Mosley, S. Henry, D.V. McAllister, H. Kalluri, W. Pewin, P.M. Frew, T. Yu, N.J. Thornburg, S. Kabbani, L. Lai, E.V. Vassilieva, I. Skountzou, R.W. Compans, M.J. Mulligan, M.R. Prausnitz, T.-M.S. Group, The safety, immunogenicity, and acceptability of inactivated influenza vaccine delivered by microneedle patch (TIV-MNP 2015): a randomised, partly blinded, placebo-controlled, phase 1 trial, Lancet, 390 (2017), pp. 649-658
12. C. Edens, M.L. Collins, J.L. Goodson, P.A. Rota, M.R. Prausnitz, A microneedle patch containing measles vaccine is immunogenic in non-human primates, Vaccine, 33 (2015), pp. 4712-4718
13. M. Leone, J. Monkare, J.A. Bouwstra, G. Kersten, Dissolving microneedle patches for dermal vaccination, Pharm. Res., 34 (2017), pp. 2223-2240
14. K. Matsuo, Y. Yokota, Y. Zhai, Y.S. Quan, F. Kamiyama, Y. Mukai, N. Okada, S. Nakagawa, A low-invasive and effective transcutaneous immunization system using a novel dissolving microneedle array for soluble and particulate antigens, J. Control Release, 161 (2012), pp. 10-17
15. Y. Qiu, L. Guo, S. Zhang, B. Xu, Y. Gao, Y. Hu, J. Hou, B. Bai, H. Shen, P. Mao, DNA-based vaccination against hepatitis B virus using dissolving microneedle arrays adjuvanted by cationic liposomes and CpG ODN, Drug Deliv. (2015), pp. 1-8
16. E.V. Vassilieva, H. Kalluri, D. McAllister, M.T. Taherbhai, E.S. Esser, W.P. Pewin, J.A. Pulit-Penaloza, M.R. Prausnitz, R.W. Compans, I. Skountzou, Improved immunogenicity of individual influenza vaccine components delivered with a novel dissolving microneedle patch stable at room temperature, Drug Deliv. Transl. Re, 5 (2015), pp. 360-371
17. E. Larraneta, R.E.M. Lutton, A.D. Woolfson, R.F. Donnelly, Microneedle arrays as transdermal and intradermal drug delivery systems: materials science, manufacture and commercial development, Mat. Sci. Eng. R, 104 (2016), pp. 1-32
18. J. Arya, M.R. Prausnitz, Microneedle patches for vaccination in developing countries, J. Control Release, 240 (2015), pp. 135-141

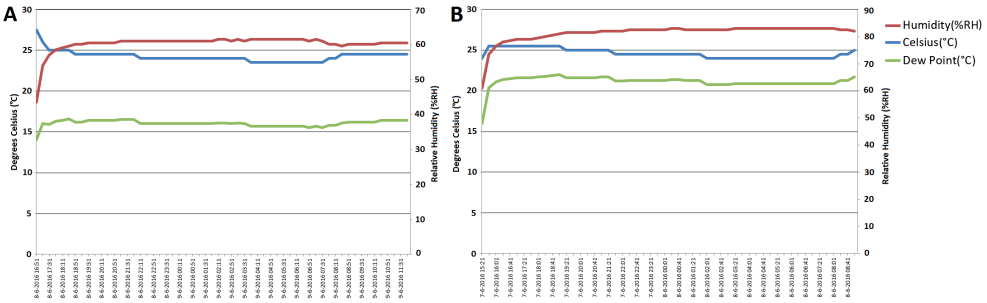
19. J. Monkare, M. Reza Nejadnik, K. Baccouche, S. Romeijn, W. Jiskoot, J.A. Bouwstra, IgG-loaded hyaluronan-based dissolving microneedles for intradermal protein delivery, J Control Release, 218 (2015), pp. 53-62
20. Y.K. Demir, Z. Akan, O. Kerimoglu, Characterization of polymeric microneedle arrays for transdermal drug delivery, PLoS ONE, 8 (2013), p. e77289
21. M.T. McCrudden, A.Z. Alkilani, C.M. McCrudden, E. McAlister, H.O. McCarthy, A.D. Woolfson, R.F. Donnelly, Design and physicochemical characterisation of novel dissolving polymeric microneedle arrays for transdermal delivery of high dose, low molecular weight drugs, J. Control Release, 180 (2014), pp. 71-80
22. S.D. Allison, A. Dong, J.F. Carpenter, Counteracting effects of thiocyanate and sucrose on chymotrypsinogen secondary structure and aggregation during freezing, drying, and rehydration, Biophys. J., 71 (1996), pp. 2022-2032
23. M. Katakam, L.N. Bell, A.K. Banga, Effect of surfactants on the physical stability of recombinant human growth hormone, J. Pharm. Sci., 84 (1995), pp. 713-716
24. S.J. Prestrelski, N. Tedeschi, T. Arakawa, J.F. Carpenter, Dehydration-induced conformational transitions in proteins and their inhibition by stabilizers, Biophys. J., 65 (1993), pp. 661-671
25. A.K.a.T. Takagi, Formation of Intermolecular β-sheet structure during heat denaturation of ovalbumin, J. Agric. Food. Chem., 36 (1988), pp. 1156-1159
26. W. Wang, Protein aggregation and its inhibition in biopharmaceutics, Int. J. Pharm., 289 (2005), pp. 1-30
27. W. Wang, S. Nema, D. Teagarden, Protein aggregation–pathways and influencing factors, Int. J. Pharm., 390 (2010), pp. 89-99
28. T. Arakawa, S.J. Prestrelski, W.C. Kenney, J.F. Carpenter, Factors affecting short-term and long-term stabilities of proteins, Adv. Drug Deliv. Rev., 46 (2001), pp. 307-326
29. N. Wilke, M.L. Reed, A. Morrissey, The evolution from convex corner undercut towards microneedle formation: theory and experimental verification, J. Micromech. Microeng., 16 (2006), pp. 808-814
30. K. van der Maaden, E. Sekerdag, W. Jiskoot, J. Bouwstra, Impact-insertion applicator improves reliability of skin penetration by solid microneedle arrays, Aaps J., 16 (2014), pp. 681-684
31. R. Blaine, Humidity Fixed Points, in: TA Instruments, 2004.
32. P. Schipper, K. van der Maaden, S. Romeijn, C. Oomens, G. Kersten, W. Jiskoot, J. Bouwstra, Repeated fractional intradermal dosing of an inactivated polio vaccine by a single hollow microneedle leads to superior immune responses, J. Control Release, 242 (2016), pp. 141-147
33. P. Schipper, K. van der Maaden, S. Romeijn, C. Oomens, G. Kersten, W. Jiskoot, J. Bouwstra, Determination of depth-dependent intradermal immunogenicity of adjuvanted inactivated polio vaccine delivered by microinjections via hollow microneedles, Pharm. Res., 33 (2016), pp. 2269-2279
34. K. van der Maaden, S.J. Trietsch, H. Kraan, E.M. Varypataki, S. Romeijn, R. Zwier, H.J. van der Linden, G. Kersten, T. Hankemeier, W. Jiskoot, J. Bouwstra, Novel hollow microneedle technology for depth-controlled microinjection-mediated dermal vaccination: a study with polio vaccine in rats, Pharm. Res., 31 (2014), pp. 1846-1854
35. L. Guo, J.M. Chen, Y.Q. Qiu, S.H. Zhang, B. Xu, Y.H. Gao, Enhanced transcutaneous immunization via dissolving microneedle array loaded with liposome encapsulated antigen and adjuvant, Int. J. Pharmaceut., 447 (2013), pp. 22-30
36. L.Y. Chu, S.O. Choi, M.R. Prausnitz, Fabrication of dissolving polymer microneedles for controlled drug encapsulation and delivery: Bubble and pedestal microneedle designs, J. Pharm. Sci., 99 (2010), pp. 4228-4238
37. M. Leone, B.H. van Oorschot, M.R. Nejadnik, A. Bocchino, M. Rosato, G. Kersten, C. O'Mahony, J. Bouwstra, K. van der Maaden, Universal applicator for digitally-controlled pressing force and impact velocity insertion of microneedles into skin, Pharmaceutics, 10 (2018)

38. K. Lee, C.Y. Lee, H. Jung, Dissolving microneedles for transdermal drug administration prepared by stepwise controlled drawing of maltose, Biomaterials, 32 (2011), pp. 3134-3140
39. K.A. Moga, L.R. Bickford, R.D. Geil, S.S. Dunn, A.A. Pandya, Y.P. Wang, J.H. Fain, C.F. Archuleta, A.T. O'Neill, J.M. DeSimone, Rapidly-dissolvable microneedle patches via a highly scalable and reproducible soft lithography approach, Adv. Mater., 25 (2013), pp. 5060-5066
40. Y. Hiraishi, T. Nakagawa, Y.S. Quan, F. Kamiyama, S. Hirobe, N. Okada, S. Nakagawa, Performance and characteristics evaluation of a sodium hyaluronate-based microneedle patch for a transcutaneous drug delivery system, Int. J. Pharm., 441 (2013), pp. 570-579
41. S. Liu, M.N. Jin, Y.S. Quan, F. Kamiyama, H. Katsumi, T. Sakane, A. Yamamoto, The development and characteristics of novel microneedle arrays fabricated from hyaluronic acid, and their application in the transdermal delivery of insulin, J. Control Release, 161 (2012), pp. 933-941
42. J.W. Lee, J.H. Park, M.R. Prausnitz, Dissolving microneedles for transdermal drug delivery, Biomaterials, 29 (2008), pp. 2113-2124
43. D. Krejcova, M. Pekarova, B. Safrankova, L. Kubala, The effect of different molecular weight hyaluronan on macrophage physiology, Neuro Endocrinol Lett, 30 (Suppl 1) (2009), pp. 106-111
44. S. Mizrahy, S.R. Raz, M. Hasgaard, H. Liu, N. Soffer-Tsur, K. Cohen, R. Dvash, D. Landsman-Milo, M.G. Bremer, S.M. Moghimi, D. Peer, Hyaluronan-coated nanoparticles: the influence of the molecular weight on CD44-hyaluronan interactions and on the immune response, J. Control Release, 156 (2011), pp. 231-238
45. C. Termeer, F. Benedix, J. Sleeman, C. Fieber, U. Voith, T. Ahrens, K. Miyake, M. Freudenberg, C. Galanos, J.C. Simon, Oligosaccharides of hyaluronan activate dendritic cells via toll-like receptor 4, J. Exp. Med., 195 (2002), pp. 99-111
46. C. Termeer, J.P. Sleeman, J.C. Simon, Hyaluronan–magic glue for the regulation of the immune response?, Trends Immunol., 24 (2003), pp. 112-114
47. C.C. Termeer, J. Hennies, U. Voith, T. Ahrens, J.M. Weiss, P. Prehm, J.C. Simon, Oligosaccharides of hyaluronan are potent activators of dendritic cells, J. Immunol., 165 (2000), pp. 1863-1870
48. M.J. Wang, J.S. Kuo, W.W. Lee, H.Y. Huang, W.F. Chen, S.Z. Lin, Translational event mediates differential production of tumor necrosis factor-alpha in hyaluronan-stimulated microglia and macrophages, J. Neurochem., 97 (2006), pp. 857-871
49. A.C.I. Depelsenaire, S.C. Meliga, C.L. McNeilly, F.E. Pearson, J.W. Coffey, O.L. Haigh, C.J. Flaim, I.H. Frazer, M.A.F. Kendall, Colocalization of cell death with antigen deposition in skin enhances vaccine immunogenicity, J. Invest. Dermatol., 134 (2014), pp. 2361-2370
50. G.S. Du, R.M. Hathout, M. Nasr, M.R. Nejadnik, J. Tu, R.I. Koning, A.J. Koster, B. Slutter, A. Kros, W. Jiskoot, J.A. Bouwstra, J. Monkare, Intradermal vaccination with hollow microneedles: a comparative study of various protein antigen and adjuvant encapsulated nanoparticles, J. Control Release, 266 (2017), pp. 109-118

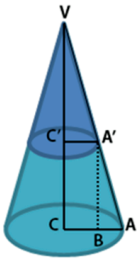
SUPPLEMENTARY MATERIAL



Supplementary Figure S1. Schematic representation of dissolving microneedle penetration and staining process. **(A)** The array is attached to the applicator piston. As the piston is lowered, the microneedles pierce the skin. After 18 seconds, the applicator piston is retrieved into its original position. **(B)** Pierced skin staining and SC removal by tape stripping. **(C)** Light microscope image (6.5x) of upper view of *ex vivo* human pierced skin. Each blue spot indicates effective microneedle penetration of the skin. Scale bar is 1 mm.



Supplementary Figure S2. Relative humidity values measured overnight every 20 min. Humidity graphs for sodium bromide **(A)** and potassium chloride **(B)**. The relative humidity, temperature and dew point of the solutions were measured by using a data logger (EL-USB-2-LCD+).



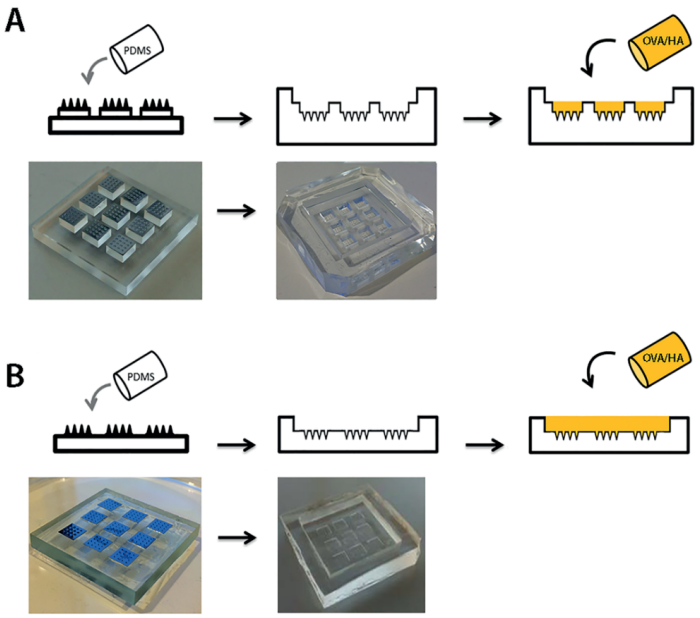
VC = H
VC' = h
CA = R
C'A' = r

ΔVC'A' and ΔVCA are similar

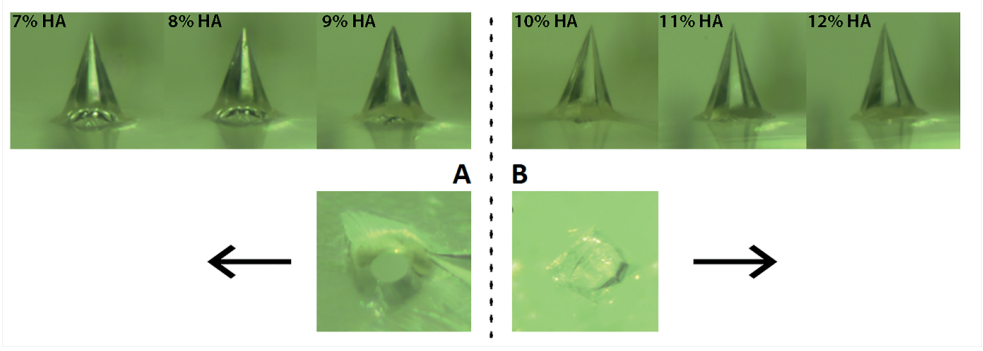
$$H : h = R : r \longrightarrow r = \frac{R \cdot h}{H} \qquad \text{(Equation 1)}$$

$$\textit{Dissolved cone volume} = \frac{1}{3} \cdot \pi \cdot r^2 \cdot h \qquad \text{(Equation 2)}$$

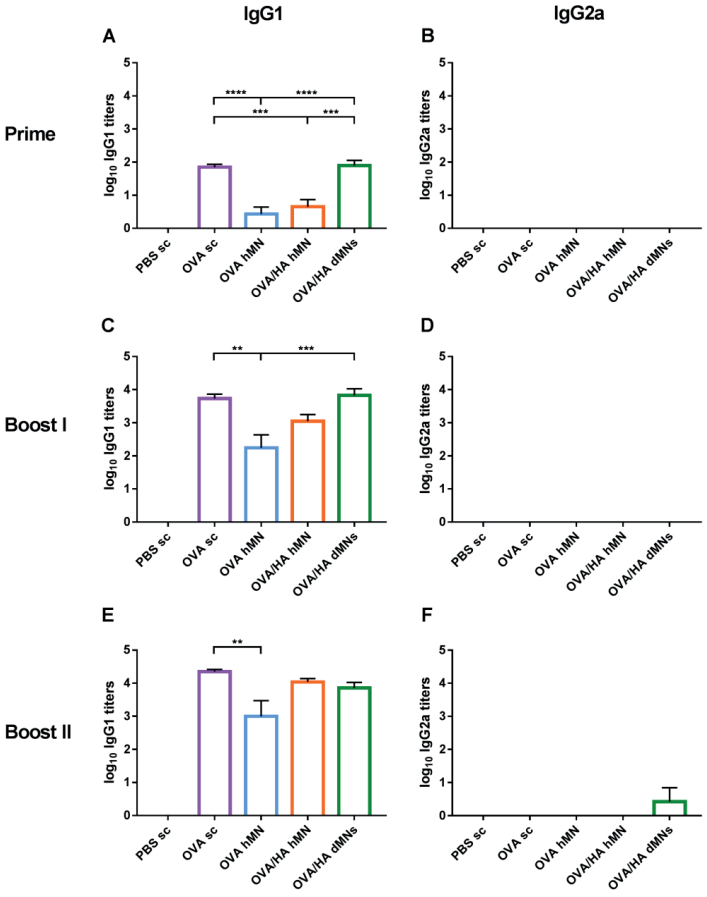
Supplementary Figure S3. Calculation of the dissolved MN percentage. To calculate the volume of the dissolved part of the needle the length of the dMN leftover was measured by using a microscope. Thus, the length of the MN dissolved part was calculated by subtracting the leftover from the original dMN length. Taking into account the original dMN length (H = 300 µm), the length of the dissolved part of the MN (h) and the radius of the base of the dMN (R = 100 µm), the top radius (r) can be calculated according to equation 1. Then, the volume of the dissolved part of the MN can be calculated (equation 2) and subsequently divided by the entire dMN volume to obtained the dissolved MN volume fraction.



Supplementary Figure S4. Polydimethylsiloxane molds. **(A)** Single-array well design. On the left, the poly(methyl metacrylate) (PMMA) template used for the fabrication of the polydimethylsiloxane (PDMS) mold. The PMMA mold presents pedestals on which silicon arrays are fixed. On the right, the resulting PDMS mold presenting wells with microholes in which the OVA/HA solution can be poured. **(B)** Multi-arrays well design. On the left the PMMA template, without pedestals, producing a PDMS mold (right) with the arrays sharing the same fabrication space in which the OVA/HA solution can be poured.



Supplementary Figure S5. Microscopic illustration of hyaluronan concentration optimization. Representative brightfield microscopy images (5x) of dMNs with increasing HA concentration (first row). In the second row, an upper view of a cut needle showing **(A)** a hole (observed for HA concentrations ≤ 9% (w/v)) and **(B)** without a hole (observed for HA concentrations > 9% (w/v)).



Supplementary Figure S6. OVA-specific IgG1 **(A, C, E)** and IgG2a **(B, D, F)** titers after prime **(A, B)**, 1st boost **(C, D)**, and 2nd boost **(E, F)** immunizations. Bars represent mean ± SEM, n = 8. **p < 0.01, ***p < 0.001, ****p<0.0001.

Chapter 5

Hyaluronan molecular weight: effects on dissolution time of dissolving microneedles in the skin and on immunogenicity of antigen

Adapted from Eur J Pharm Sci 2020 (146): 105269

Mara Leone[1], Stefan Romeijn[1], Bram Slütter[1], Conor O'Mahony[2], Gideon Kersten[1,3,*], Joke A. Bouwstra[1,*]

[1] Division of BioTherapeutics, Leiden Academic Centre for Drug Research (LACDR), Leiden University, Leiden, the Netherlands

[2] Tyndall National Institute, University College Cork, Cork, Ireland

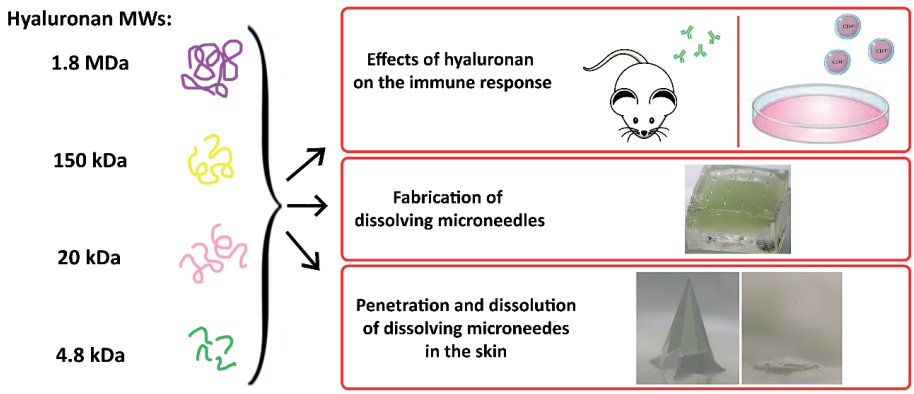
[3] Institute for Translational Vaccinology (Intravacc), Bilthoven, the Netherlands

[*] These authors contributed equally.

ABSTRACT

Biomaterials used as matrix for dissolving micro needles (dMNs) may affect the manufacturing process as well as the potency of the active pharmaceutical ingredient, e.g. the immunogenicity of incorporated vaccine antigens. The aim of this study was to investigate the effect of the molecular weight of hyaluronan, a polymer widely used in the fabrication of dMNs, ranging in molecular weight from 4.8 kDa to 1.8 MDa, on the dissolution of microneedles in the skin in time as well as the antibody response in mice and T-cell activation *in vitro*. Hyaluronan molecular weight (HA-MWs) did not affect antibody responses (when lower than 150 kDa) nor CD4+ T-cell responses against model antigen ovalbumin. However, the HA-MWs had an effect on the fabrication of dMNs. The 1.8 MDa HA was not suitable for the fabrication of dMNs. Similarly, the 4.8 kDa HA generated dMN arrays less robust compared to the other HA-MWs requiring optimization of the drying conditions. Finally, higher HA-MWs led to longer application time of dMN arrays for a complete dissolution of microneedles into the skin. Specifically, we identified 20 kDa HA as the optimal HA-MW for the fabrication of dMNs as with this MW the dMNs are robust and dissolve fast in the skin without affecting immunogenicity.

GRAPHICAL ABSTRACT



Keywords: dissolving microneedles, hyaluronan, molecular weight, immune response, dermal vaccine delivery.

1. INTRODUCTION

Microneedles are intensively studied for dermal and transdermal drug and vaccine delivery [1, 2]. Microneedles are needle-like structures up to 1 mm in length, capable of piercing the upper layer of the skin, the *stratum corneum*, enabling drug and vaccine delivery in a minimally invasive and painless way [3, 4]. Several microneedle concept are in development: i) hollow microneedles to inject liquid formulations through the bore of the microneedle, ii) microneedles for skin pretreatment to create microchannels prior application of a patch containing the drug or vaccine formulation, iii) porous, coated, hydrogel-forming microneedles and dissolving microneedles that release the drug or vaccine upon insertion into the skin [5-8]. Dissolving microneedles (dMNs), completely dissolve after insertion into the skin, thereby releasing the encapsulated drug or vaccine [3]. As an additional advantage, the dry state of dMNs combined with the presence of excipients can increase protein thermostability [3].

dMNs are produced from different materials, ranging from low molecular weight carbohydrates to biodegradable polymers [3]. The selection of the matrix material is based on different factors such as i) safety, ii) compatibility with the active compound and the manufacturing procedure, iii) capability of the manufactured dMNs to efficiently pierce the skin and subsequently dissolve in a short time period and iv) potential adjuvant properties. One of the most frequently used matrix material is the hyaluronan (HA) [3, 9-13]. High molecular weight HA is a non-toxic, biodegradable, biocompatible and non-inflammatory linear polysaccharide [14] naturally present in the skin and approved by the FDA as inactive material.

Although frequently used for microneedle manufacturing, the molecular weight of the polysaccharide HA is rarely addressed [1, 3, 9, 11, 12, 15-17]. There are indications however, that the molecular weight of the HA influences its immuno-adjuvant properties. Only high molecular weight HA (HMW-HA, MW 10^7 Da) is an ubiquitous extracellular matrix component [18, 19]. Low molecular weight HA (LMW-HA) (4- to 16-oligosaccharide size, 800 – 3200 Da [19, 20]) is able to activate immunocompetent cells such as macrophages [21] and DCs [19-23]. These activated human DCs are able to stimulate T-cell mediated immune responses [19, 20, 24]. The immune activation is mediated by the HA binding to specific receptors such as CD44, CD168, Toll-like receptor (TLR)-2 and TLR-4 [25-28]. The latter is a receptor associated with the innate immunity and the host defence against bacterial infection [20]. In the presence of antigens, a specific response may develop [29] and so the LMW-HA can act as an adjuvant during vaccination.

In a previous study from our group, the dissolving microneedle properties of the only 150 kDa HA, such as penetration and dissolution in the skin, have been reported [30].

The aim of this study was to determine whether i) HA with different MW had an effect on the immune response for both antibody (*in vivo* injections by hMN) and cellular (*in vitro* T-

cell exposure) responses and ii) it was possible to fabricate dMNs by micromolding from HA with different molecular weight. To this end, first the potential adjuvant effect of HA was assessed by i) performing immunization studies investigating the antibody response in mice injected with the model antigen ovalbumin (OVA) in presence of a range of different HA-MWs and ii) investigating T-cell activation *in vitro* upon exposure to several HA-MWs with OVA. Subsequently, different HA-MWs were used to fabricate dMNs assessing the compatibility of the matrix material of each MW with the manufacturing procedure. These dMNs were used to investigate their capability to pierce the skin and to dissolve in reasonable short time period.

2. MATERIALS AND METHODS

2.1 Materials

Hyaluronan (HA) (sodium hyaluronate, average Mw was 4.8 kDa, 20 kDa and 150 kDa (endotoxin level ≤ 0.05 EU/mg) or 1.8 MDa (endotoxin level ≤ 0.07 EU/mg)) was purchased from Lifecore Biomedical (Chaska, MN, USA). Immunization studies, ELISA and cell culturing were performed by using endotoxin-free ovalbumin (OVA) (endotoxin level < 1 EU/mg) from Invivogen (Toulouse, France). PBS pH 7.4 for hMN injections was obtained from B. Braun, Melsungen, Germany.

For cell culture, Ca^{2+}- and Mg^{2+}-free phosphate-buffered saline (PBS), Iscove's Modified Dulbecco's Medium (IMDM), Roswell Park Memorial Institute Medium (RPMI 1640), penicillin/streptomycin and l-glutamine were purchased from Lonza (Basel, Switzerland). Fetal calf serum (FCS) and granulocyte-macrophage colony-stimulating factor (GM-CSF) were purchased from GE Healthcare (Little Chalfont, UK) and PeptroTech (London, UK) respectively. Lipopolysaccharide (LPS) extracted from Salmonella typhosa, CFSE and β-mercaptoethanol were purchased from Sigma-Aldrich (Zwijndrecht, the Netherlands).

The antibodies CD25-APC (PC 61.5), CD69-PE (H1.2F3), Thy1.2-PE-Cy7 (53–2.1), CD4-eFluor450 (GK1.5), Vα2 TCR-PE (B20.1) and fixable viability dye-eFluor780 were purchased from eBioscience (Thermofisher Scientific, MA, USA).

For dissolving microneedle fabrication, 10 mM PB (7.7 mM Na_2HPO_4, 2.3 mM NaH_2PO_4, pH 7.4) was prepared in the laboratory. Vinylpolysiloxanes A-silicone (Elite Double 32a Normal) and the two-component epoxy glue (Bison, Goes, The Netherlands) were obtained from The Zhermack Group (Badia Polesine, Italy) and Bison International B.V. (Goes, The Netherlands), respectively. Polydimethylsiloxane (PDMS, Sylgard 184) was purchased from Dow Corning (Midland, MI, USA). Solid silicon MNs, obtained through a potassium hydroxide wet-etching process [31], were kindly provided by the Tyndall National Institute (Cork, Ireland). All the chemicals were of analytical grade and Milli-Q water (18 MΩ/cm, Millipore Co.) was used for the preparation of all solutions.

2.2 Animals

Immunization studies were performed using female BALB/c (H2d), 8-11 weeks old (Charles River, Maastricht, The Netherlands) and randomly assigned to groups of 8. The studies were approved by the ethical committee on animal experiments of Leiden University (License number (14176).

For *in vitro* T-cell activation studies, C57BL/6 and OT-II transgenic mice on a C57BL/6 background were purchased from Jackson Laboratory (CA, USA), bred in-house under standard laboratory conditions, and provided with food and water ad libitum. All animal work was performed in compliance with the Dutch government guidelines and the Directive 2010/63/EU of the European Parliament. Experiments were approved by the Ethics Committee for Animal Experiments of Leiden University (CCD number AVD106002017887).

2.3 Hollow microneedles

Hollow microneedles (hMNs) were prepared as described previously [32, 33] (a representative image of a hMN is reported in the Supplementary data, Figure S1). Briefly, polyimide-coated fused silica capillaries (Polymicro, Phoenix AZ, 375 µm outer diameter, 50 µm inner diameter) were filled with silicone oil in a vacuum oven (100 ° C) overnight. Subsequently, the capillaries were etched during 4 h in ≥ 48% hydrofluoric acid and the polyimide coating was removed from the ends of the capillaries by diving them into heated (250 °C) sulfuric acid for 5 min.

2.4 Immunization studies

BALB/c mice were anesthetized by intraperitoneal injection of 150 mg/kg ketamine and 10 mg/kg xylazine and the injection site was shaved (flank, approximately 4 cm^2). The same day, mice were immunized by intradermal hMN injection (120 µm injection depth) of 10 µl with 0.31 µg OVA with 3.1 µg HA for each HA-MW dissolved in PBS pH 7.4. Intradermal hMN injection of each HA-MWs without OVA and PBS were included as control. For controlled depth intradermal microinjections, a hollow-microneedle applicator was used as reported previously [32].

Immunizations were performed at day 1 (prime), day 22 (boost) and day 43 (2nd boost). Prior to each immunization, a blood sample was collected from the tail vein. At day 63, the blood sample was collected from the femoral artery and all mice were sacrificed. Serum was isolated from the samples and stored at - 80°C.

2.5 Determination of OVA-specific IgG antibodies

OVA-specific antibodies were analysed by a sandwich enzyme-linked immunosorbent assay (ELISA) as described earlier [10]. Briefly, well-plates were coated with OVA for 1.5 h at 37 °C and then blocked with bovine serum albumin (BSA) (Sigma-Aldrich, Zwijndrecht, the Netherlands). After the blocking, three-fold serial dilutions of serum were applied to the plates and incubated for 1.5 h at 37 °C. Then, the plates were incubated with horseradish peroxidase-conjugated goat antibodies against IgG total, IgG1 and IgG2a (Southern Biotech, Birmingham, AL, USA) for 1 h at 37 °C. Finally, 1-step TM ultra 3,3′,5,5′-tetramethylbenzidine (TMB) (Thermo-Fischer Scientific, Waltham, USA) was used as substrate and sulfuric acid (H_2SO_4) (95–98%) (JT Baker, Deventer, The Netherlands) was added to stop the reaction. The absorbance was measured at 450 nm on a Tecan Infinite M1000 plate reader (Männedorf, Switzerland) and the antibody titers were determined as the log10 value of the mid-point dilution of a complete s-shaped absorbance-log dilution curve of the diluted serum level.

2.6 Bone marrow-derived dendritic cells (BMDCs)

To examine T-cell activation *in vitro*, first bone marrow was isolated from the tibias and femurs of C57BL/6 female mouse. A single-cell suspension of bone marrow cells was obtained by using a 70 µm cell strainer (Greiner Bio-One B.V., Alphen aan den Rijn, NL). The cells were cultured in IMDM medium supplemented with 2 mM l-glutamine, 8% (v/v) FCS, 100 U/ml penicillin/streptomycin and 50 µM β-mercaptoethanol at 37 °C and 5% CO_2 in 95 mm Petri dishes (Greiner Bio-One B.V., Alphen aan den Rijn, NL) and 20 ng/ml GM-CSF for 10 days. Medium was refreshed every other day.

On day 11, the BMDCs were harvested from the petri dish and distributed into 96-well plates (100 µl/well, 10 000 cells/well). Then, 100 µl/well of formulations consisting of: i) 5 µg OVA, ii) 5 µg OVA mixed with 50 µg HA (per each molecular weight) or iii) 50 µg HA (per each molecular weight) were added to the wells. OVA (5 µg/well) + LPS (100 ng/well) or LPS (100 ng/well) were added as positive control; medium was included as negative control.

The BMDCs were exposed to the formulations overnight at 37 °C and 5% CO_2 and subsequently OVA-specific $CD4^+$ T-cells were transferred on BMDCs in co-culture experiments (see 2.6).

2.7 $CD4^+$ T-cell activation by antigen loaded BMDC

OT-II (OVA-specific $CD4^+$) T-cells were obtained from the spleen of OT-II transgenic C57BL/6 mouse. Single cell suspensions were obtained by forcing the spleens through a 70 µm strainer. After erythrocyte depletion with lysis-buffer (0.15 M NH_4Cl, 1 mM $KHCO_3$, 0.1 mM

Na_2EDTA; pH 7.3), staining with CFSE was performed. Briefly, cells were suspended in PBS containing 1 µM CFSE and incubate 10 min at room temperature. CFSE was neutralized by FCS addition and the cells were washed with RPMI to remove excess of CFSE.

At this point, the percentage of $CD4^+/Valpha^{2+}$ cells was determined by flow cytometry (BD FACSCanto-II, San Jose, CA). OT-II cells were transferred on BMDCs previously exposed to the formulations (50 000 cells/well).

On day 15, the cell surfaces were stained by incubating the cells with fixable viability dye-eFluor780 (1:1000) and fluorescently labelled antibodies specific for: Thy1.2-PE-Cy7 (1:500), CD25-APC (1:500), CD69-PE (1:500) and CD4-eFluor450 (1:500) for 30 min (100 µl/well) at 4 °C. After 30 min, the excess antibodies were washed by using FACS buffer. The cells were incubated with fixation and permeabilization solution (BD Biosciences) for 10 min at 4 °C. Finally, the cells were washed with FACS buffer and analysed by flow cytometry (BD FACSCanto-II, San Jose, CA). The data were analysed by using FlowJo software.

2.8 Fabrication of dissolving microneedles

dMN arrays were prepared as described previously [10]. HA 10% (w/v) was dissolved in phosphate buffer (10 mM, pH 7.4) and stored overnight. The next day, HA solution was poured in each well of the polydimethylsiloxane mold (PDMS, Sylgard 184, Dow Corning, Midland, MI, USA) to prepare dMN arrays (4 by 4 dMNs per array of 300 µm length and 100 µm base diameter). After several steps of vacuum and centrifuge, the 20 kDa and 150 kDa HA arrays were oven-dried overnight at 37°C. As this procedure result in fragile dMN arrays when using 4.8 kDa HA, these dMN arrays were dried at room temperature overnight. The next day, a backplate was produced by pouring a mixture of vinylpolysiloxane base and catalyst (in a 1:1 ratio) (Elite Double 32a Normal, Zhermack Group, Badia Polesine, Italy) and subsequently a two-component glue solution (Bison International B.V., Goes, The Netherlands) onto each array and left curing.

Finally, the arrays were removed from the PDMS mold and inspected for shape and sharpness by light microscopy (Stemi 2000-C, Carl Zeiss Microscopy GmbH, Göttingen, Germany).

2.9 Human skin

Human abdomen skin was obtained from a local hospital within 24 hours after cosmetic surgery according to the declaration of Helsinki. The fat excess was removed with a scalpel and the skin was stored at -80°C. Before use, the skin was thawed at 37°C for 1 h in a humid petri dish and stretched with pins on parafilm-covered styrofoam. Before starting the experiment, the skin was cleaned with Milli-Q and 70% ethanol.

2.10 Penetration of microneedles in *ex vivo* human skin

dMN arrays (n=3 per HA-MW) were applied onto the skin by impact velocity, as described elsewhere [10, 34], by using an impact insertion applicator with a constant velocity of 0.54 m/s (Leiden University - applicator with uPRAX controller version 0.3). The dMNs were kept in the skin for 18 seconds and withdrawn. Then, the pierced skin was treated with trypan blue, as previously described [35] and *stratum corneum* was removed by tape stripping. Finally, the blue spots were visualized using a light microscope (Axioskop and Stemi 2000-C, Carl Zeiss Microscopy GmbH, Göttingen, Germany) (a representative image of pierced skin is reported in the Supplementary data, Figure S2) and the penetration efficiency per array was calculated by dividing the number of blue spots by the number of dMNs on the array (16) (Equation 1).

$$\text{Penetration efficiency} = (\text{number of blue spots})/16 \times 100 \qquad \text{(Eqn. 1)}$$

2.11 Dissolution of microneedles in *ex vivo* human skin

A dMN array (n=7) was applied on the skin as described in section 2.10 and was kept in the skin for 1 min, 5 min, 10 min or 20 min. The microneedle length before and after dissolution was determined with a light microscope (Axioskop and Stemi 2000-C, Carl Zeiss Microscopy GmbH, Göttingen, Germany) equipped with a digital camera (Axiocam ICc 5, Carl Zeiss). In order to obtain the dMN dissolved volume for each insertion period, dissolved microneedle length was measured by ZEN 2012 blue edition software (Carl Zeiss Microscopy GmbH) and the dissolved MN volumes were calculated as reported in our previous study in supplementary Figure 3 [10].

2.12 Statistics

IgG titers and T-cell response were analysed using one-way ANOVA with respectively Bonferroni and Tukey's post-test suitable in the software Prism (Graphpad, San Diego, USA). A p-value less than 0.05 was considered to be significant.

Microneedle penetration efficiency was analysed by Kruskal-Wallis test with Dunn's multiple comparison test ($p < 0.05$).

The remaining dMN length after dissolution at different time points was analysed by two-way ANOVA with a Tukey's post-test ($p < 0.05$).

3. RESULTS

3.1 Immunization studies

The liquid formulations of OVA alone or mixed with different HA-MWs was intradermally injected by using hollow microneedles. During injection no problems with clogging or leakage were observed. The formation of a blister on the site of the injection indicated a successful intradermal delivery of the formulation. No adverse effects were observed.

The OVA-specific total IgG titers increased after each immunization (Figure 1A-C). The presence of HA, regardless of the molecular weight, did not increase the total IgG response compared to the injection of OVA only. After the first boost, a higher OVA specific IgG response in the mice immunized with OVA-HA 4.8 kDa was observed compared to the mice injected with OVA-HA 150 kDa ($p<0.01$). However, both OVA-HA 4.8 kDa and OVA-HA 1.8 MDa resulted in equal responses compared to the OVA only group. After the second boost, the group immunized with OVA-HA 1.8 MDa showed lower OVA-specific total IgG titers than OVA only and OVA-HA 4.8 kDa, suggesting a detrimental effect on adding high molecular weight HA. Overall, the presence of high MW HA seemed to reduce the immunogenicity of the antigen while the presence of HA regardless of the molecular weight did not enhance the immune response compared with OVA alone.

The IgG1 response (Figure 1 D-F) followed the same trend as the total IgG response: the presence of HA in different molecular weights did not change the response compared to OVA alone after each immunization. Intradermal injection of OVA, with or without HA, resulted in undetectable OVA specific IgG2a responses (data not shown).

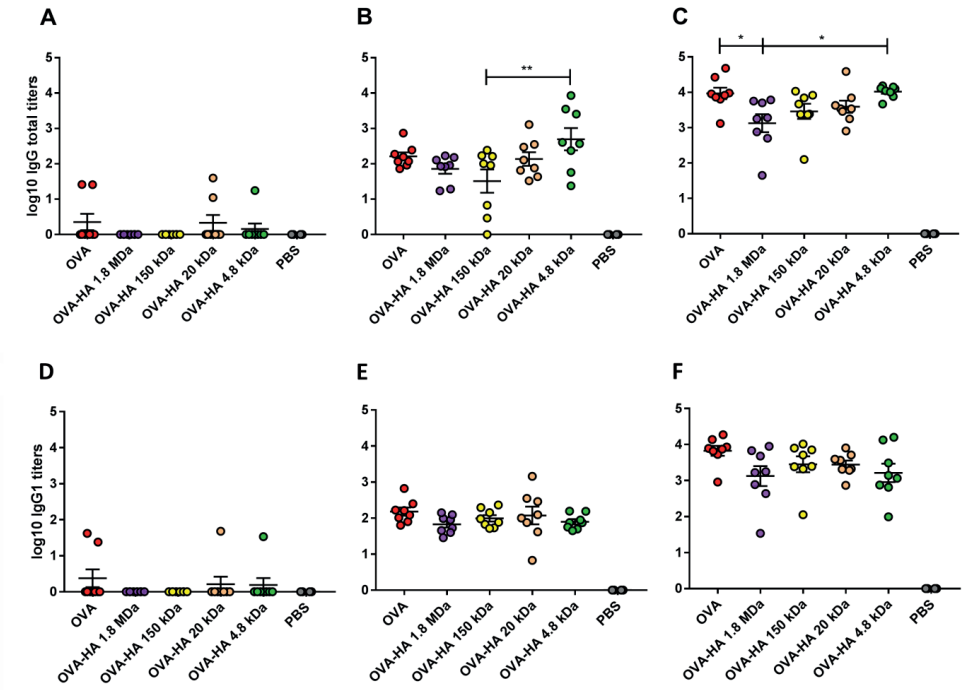


Figure 1. OVA-specific IgG total **(A-C)** and IgG1 **(D-F)** antibody titers measured in BALB/c mice on day 21 **(A and D)**, day 42 **(B and E)** and day 63 **(C and F)**. Bars represent mean ± SEM, n = 8. *p < 0.05, **p < 0.01. OVA, ovalbumin; HA, hyaluronan.

3.2 Analysis of CD4$^+$ T-cell activation *in vitro*

To determine whether the presence of different HA-MW, with or without OVA, affect cellular responses, OT-II T-cell (OVA-specific CD4$^+$ cells) activation studies were performed *in vitro*. As expected, addition of OVA induces OT-II proliferation, which is enhanced in the presence of LPS (Figure 2). The co-exposure of cells to OVA and HA however, regardless of the molecular weight, did not increase OT-II proliferation compared to OVA alone. In line with the antibody responses, this suggests that none of the tested HA polymer provided a measurable adjuvant effect.

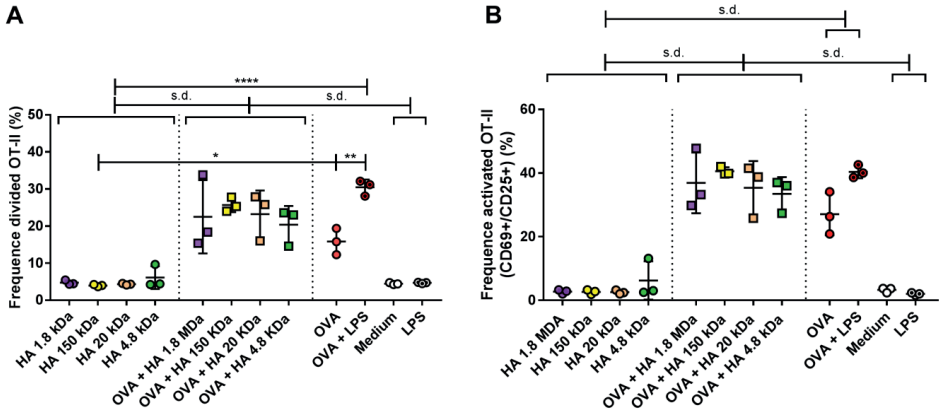


Figure 2. OT-II activation *in vitro*. **(A)** percentage of dividing cells, **(B)** percentage of $CD69^+/CD25^+$ cells. Bars represent mean ± SEM, n = 3. *p < 0.05, **p < 0.01. OVA, ovalbumin; HA, hyaluronan; LPS, lipopolysaccharide; s.d., significantly different.

3.3 Dissolving microneedle fabrication

The immunological analysis of the various HA polymers, suggests a preference for small MW polymer, as the high MW polymer show reduced antibody titers. Next we determined whether the MW of HA affected the fabrication of dissolving microneedles and their dissolution in the skin. Fabrication of dissolving microneedles was possible for the HA-MWs 150 kDa, 20 kDa and 4.8 kDa. The 10% (w/v) concentration of MW 1.8 MDa HA led to gel formation preventing the fabrication of microneedles. For the HA-MW 4.8 kDa, the fabrication of dissolving microneedles with a final step of drying at 37°C, as performed for the 150 kDa and 20 kDa HA, led to ruptures on the microneedle arrays surface (data not shown). Thus, the drying was performed at room temperature, resulting in intact microneedle arrays.

3.4 Penetration and dissolution of microneedles in *ex vivo* human skin

In order to assess whether the molecular weight of HA had an effect on the capability of microneedles to pierce and dissolve into the skin, first their ability to pierce *ex vivo* human skin was tested. Bright field analysis showed sharp microneedles regardless of the HA-MW (Figure 3A).The penetration efficiency of microneedles into the skin was not affected by the molecular weight of the HA. The 150 kDa microneedles showed a penetration efficiency of 96 ± 7%; 20 kDa and 4.8 kDa HA microneedles showed a penetration efficiency of 98 ± 4%, (mean ± SD, n=3).

Dissolution studies showed a gradual dissolution in time irrespective of the HA-MW (Figure 3A). However, while 20 kDa and 4.8 kDa HA dMNs completely dissolved within 20 minutes application in the skin (97 ± 2% and 100 ± 0% dissolved volumes respectively), the 150 kDa HA dMNs reached only 80% dissolved volume after the same application time (Figure 3A).

No differences in dissolved volumes between 20 kDa and 4.8 kDa HA microneedles at each application time were observed (Figure 3B), however the dissolved volume of the 150 kDa HA microneedles was significantly reduced at each time point compared to the other HA-MW microneedles. This resulted in a complete dissolution of the 20 kDa and 4.8 kDa HA microneedles after 10 minutes application, while the 150 kDa HA microneedles took 20 minutes to almost completely dissolve.

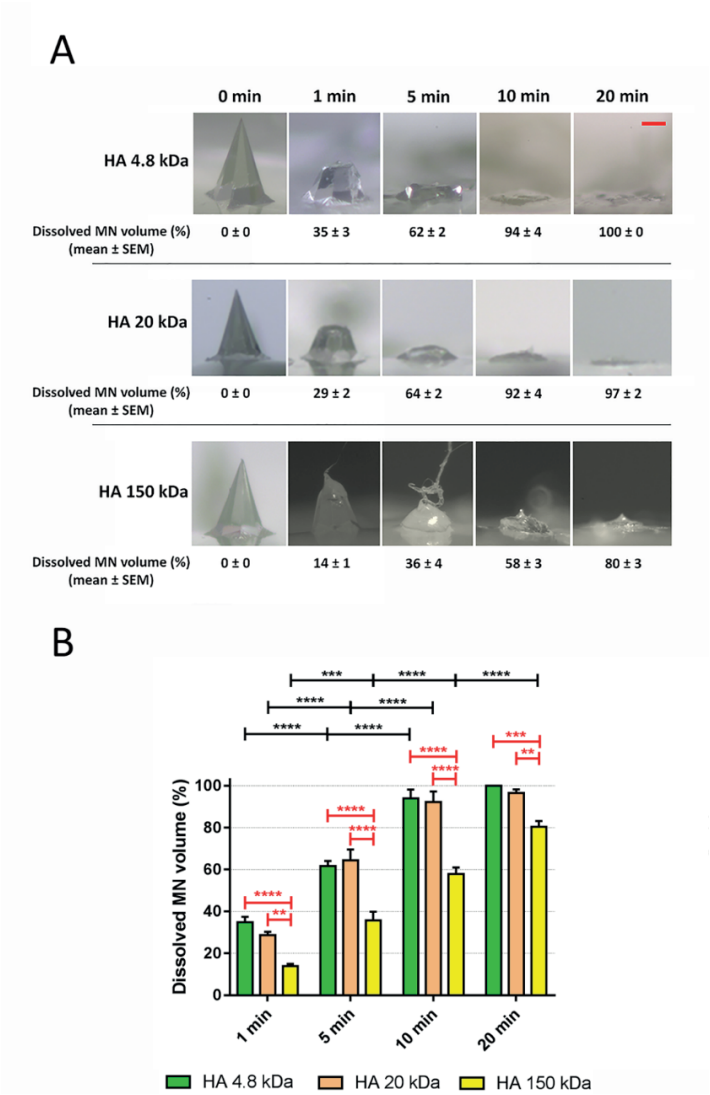


Figure 3. dMN dissolution in *ex vivo* human skin. **(A)** Representative bright field images (5x) of 10% (w/v) HA 4.8 kDa, 20 kDa and 150 kDa microneedle before application on the skin (0 min) and after 1, 5, 10 and 20 min dissolution in *ex vivo* human skin. Dissolved volumes are reported as mean ± SEM (n = 7). Scale bar 100 µm. **(B)** Effect of time (1, 5, 10 and 20 min) on dissolution per each HA-MW dMN type (statistics in black) and effect of HA-MWs on dissolution of dMNs at different time points (red statistics) are shown. Significance (**p<0.01, ***p<0.001 and ****p < 0.0001) was determined by a two-way ANOVA with a Tukey's post-test (n = 7). All data are presented as mean ± SEM. HA, hyaluronan.

4. DISCUSSION

When choosing the HA polymer for the fabrication of dMNs, it is relevant to investigate potential immune modulating effects besides effects related to the dMN manufacturing and physicochemical characteristics of dMNs such as capability to pierce the skin and dissolve quickly.

Although LMW-HA can have inflammatory properties in contrast to HMW-HA [19, 20, 22, 36, 37], to our knowledge, the role of HA-MW on the antibody response has not been reported yet. To this end, in the present study HA ranging from 4.8 kDa to 1.8 MDa mixed with OVA was injected intradermally in mice to assess the antibody response evoked. We did not observe an increase in antibody titers by adjuvanting with LMW-HA; however we did observe that HMW-HA (1.8 MDa) reduced the antibody level after the second boost compared to OVA only and LMW-HA 4.8 kDa HA mixed with OVA. This may be explained by reports that HMW-HA exerts an anti-inflammatory role reducing the side effects of vaccines [38, 39] and displays immunosuppressive properties [40-42]. To this end, it has been reported that HMW-HA up-regulates the transcription factor FOXP3 on regulatory T-cells (Treg) (e.g. $CD4^+$ $CD25^+$) [42] involved in the regulatory mechanism of autoantibody production [43] and likely antibody production. Although we did not investigate Treg activation in this study, they provide a potential mechanism regarding the lack of immunogenicity of HMW-HA.

The role of what in literature is defined as LMW-HA has been extensively investigated suggesting a pro-inflammatory effect *in vitro*: 4-6 oligosaccharides HA induced cytokine synthesis in dendritic cells [19, 20]; HA < 250 kDa induced inflammatory cytokines levels [36, 44-48]; HA ≤ 800 kDa led to activation of macrophages [37]. In this study, the effect of HA-MW was examined on the activation of $CD4^+$ T-cells. Although this is an *in vitro* system, it has shown to be predictive in the sense that formulations that induce strong *in vitro* response of OT-II cells also outperformed other formulations *in vivo* [49, 50]. Conversely to what has been reported in literature, changes in HA-MW did not influence the proliferation and activation of $CD4^+$ T-cells *in vitro*. Considerations justifying the referred controversial effects of HA preparations may be related to i) MW of HA that is not always measured accurately or is not homogeneous in the same HA population, for this reason an effect may be attributed to a minor population, ii) the presence of minor contaminants even in highly purified HA and iii) the conformational diversity of HA highly dependent on pH, temperature, salt concentration and specific cations [48]. Furthermore, the effects of HA-MW seems to be cell-specific and depending on the HA medium concentration [26, 48]. However, in literature there is not an optimal HA concentration reported and often the same concentration of different HA-MWs may have opposite effects on $CD4^+$ cellular response [42]. This lack of data should be addressed in future investigations, i.e. i) HAs in a wide range of concentrations with a dose/response on specific cell types and ii) cytokines produced by DCs

and $CD4^+$ T-cells after exposure to the HA formulations, to obtain additional information on the regulatory effect of HA.

Due to the absence of intrinsic adjuvant properties of HA, regardless of the molecular weight, all the HA-MWs were tested for potential effects on the manufacturing of dMNs and their capability to penetrate the skin and quickly dissolve. As reported in literature, a factor influencing the dMN dissolution time in the skin is the HA concentration [10, 51]. However, to our knowledge, the role of the HA-MW on the dMN dissolution in the skin is reported in the present study for the first time highlighting the novelty of this study. HA is being used in experimental drug delivery systems. The lack of immune activation of HA, regardless MW may be used to taylor drug release kinetics. However, although we did not show immunological effects, using low MW HA, may introduce safety concerns, since low MW fragments (oligomers) are associated with inflammatory responses [52].

Difficulties or impossibility in dMN fabrication when choosing too low (4.8 kDa) or high (1.8 MDa) HA-MWs, respectively, identified an optimal HA-MW in the middle range (20 kDa and 150 kDa). The 4.8 kDa HA could only be formulated into dMN by drying at room temperature to avoid ruptures of the dMN arrays. Although drying at low temperature (room temperature) can preserve the antigen stability, it may lead to long processing time not compatible with scalability in fabrication and to a higher residual moisture content in dMN than drying at high temperature, potentially resulting in decrease in antigen stability. The HA-MW 1.8 MDa formed a gel, due to the high viscosity, preventing further processing into dMNs. Furthermore, increase in HA-MW led to prolonged application time for a complete dMN dissolution into the skin.

Based on the result described above, the 20 kDa HA should be preferred to the 4.8 kDa and 150 kDa HA for the fabrication of dMNs.

5. CONCLUSIONS

The present study underlines the importance of defining a specific HA-MW for the fabrication of dMNs based on the investigation and assessment of the effects of the HA-MW on the immune response and on the physicochemical characteristics of dMNs such as capability to pierce the skin and dissolve quickly.

We consider, among the HA-MWs investigated, the medium-low HA-MW of 20 kDa the optimal MW as it results in robust dMNs characterized by a fast dissolving process in the skin and has no effect on the immunogenicity of the antigen.

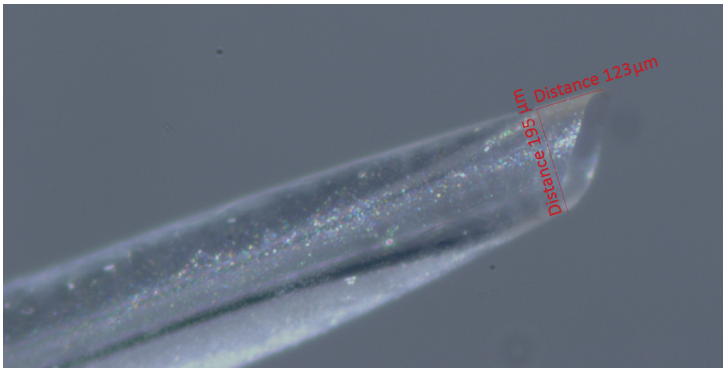
REFERENCES

1. S. Hirobe, H. Azukizawa, T. Hanafusa, K. Matsuo, Y.S. Quan, F. Kamiyama, I. Katayama, N. Okada, S. Nakagawa, Clinical study and stability assessment of a novel transcutaneous influenza vaccination using a dissolving microneedle patch, Biomaterials, 57 (2015) 50-58.
2. J. Arya, S. Henry, H. Kalluri, D.V. McAllister, W.P. Pewin, M.R. Prausnitz, Tolerability, usability and acceptability of dissolving microneedle patch administration in human subjects, Biomaterials, 128 (2017) 1-7.
3. M. Leone, J. Monkare, J.A. Bouwstra, G. Kersten, Dissolving Microneedle Patches for Dermal Vaccination, Pharm Res, 34 (2017) 2223-2240.
4. K. van der Maaden, W. Jiskoot, J. Bouwstra, Microneedle technologies for (trans)dermal drug and vaccine delivery, J Control Release, 161 (2012) 645-655.
5. E. Larraneta, R.E.M. Lutton, A.D. Woolfson, R.F. Donnelly, Microneedle arrays as transdermal and intradermal drug delivery systems: Materials science, manufacture and commercial development, Mat Sci Eng R, 104 (2016) 1-32.
6. E. Larraneta, M.T. McCrudden, A.J. Courtenay, R.F. Donnelly, Microneedles: A New Frontier in Nanomedicine Delivery, Pharm Res, 33 (2016) 1055-1073.
7. T.M. Tuan-Mahmood, M.T. McCrudden, B.M. Torrisi, E. McAlister, M.J. Garland, T.R. Singh, R.F. Donnelly, Microneedles for intradermal and transdermal drug delivery, Eur J Pharm Sci, 50 (2013) 623-637.
8. K. van der Maaden, R. Luttge, P.J. Vos, J. Bouwstra, G. Kersten, I. Ploemen, Microneedle-based drug and vaccine delivery via nanoporous microneedle arrays, Drug Deliv Transl Re, 5 (2015) 397-406.
9. S. Hirobe, H. Azukizawa, K. Matsuo, Y. Zhai, Y.S. Quan, F. Kamiyama, H. Suzuki, I. Katayama, N. Okada, S. Nakagawa, Development and Clinical Study of a Self-Dissolving Microneedle Patch for Transcutaneous Immunization Device, Pharm Res-Dordr, 30 (2013) 2664-2674.
10. M. Leone, M.I. Priester, S. Romeijn, M.R. Nejadnik, J. Monkare, C. O'Mahony, W. Jiskoot, G. Kersten, J.A. Bouwstra, Hyaluronan-based dissolving microneedles with high antigen content for intradermal vaccination: Formulation, physicochemical characterization and immunogenicity assessment, Eur J Pharm Biopharm, 134 (2019) 49-59.
11. K. Matsuo, S. Hirobe, Y. Yokota, Y. Ayabe, M. Seto, Y.S. Quan, F. Kamiyama, T. Tougan, T. Horii, Y. Mukai, N. Okada, S. Nakagawa, Transcutaneous immunization using a dissolving microneedle array protects against tetanus, diphtheria, malaria, and influenza (vol 160, pg 495, 2012), J Control Release, 184 (2014) 18-19.
12. K. Matsuo, Y. Yokota, Y. Zhai, Y.S. Quan, F. Kamiyama, Y. Mukai, N. Okada, S. Nakagawa, A low-invasive and effective transcutaneous immunization system using a novel dissolving microneedle array for soluble and particulate antigens (vol 161, pg 10, 2012), J Control Release, 184 (2014) 9-9.
13. Z. Zhu, X. Ye, Z. Ku, Q. Liu, C. Shen, H. Luo, H. Luan, C. Zhang, S. Tian, C. Lim, Z. Huang, H. Wang, Transcutaneous immunization via rapidly dissolvable microneedles protects against hand-foot-and-mouth disease caused by enterovirus 71, J Control Release, 243 (2016) 291-302.
14. E.J. Oh, K. Park, K.S. Kim, J. Kim, J.A. Yang, J.H. Kong, M.Y. Lee, A.S. Hoffman, S.K. Hahn, Target specific and long-acting delivery of protein, peptide, and nucleotide therapeutics using hyaluronic acid derivatives, J Control Release, 141 (2010) 2-12.
15. Y. Ito, S. Kashiwara, K. Fukushima, K. Takada, Two-layered dissolving microneedles for percutaneous delivery of sumatriptan in rats, Drug Dev Ind Pharm, 37 (2011) 1387-1393.
16. S. Liu, M.N. Jin, Y.S. Quan, F. Kamiyama, H. Katsumi, T. Sakane, A. Yamamoto, The development and characteristics of novel microneedle arrays fabricated from hyaluronic acid, and their application in the transdermal delivery of insulin, J Control Release, 161 (2012) 933-941.

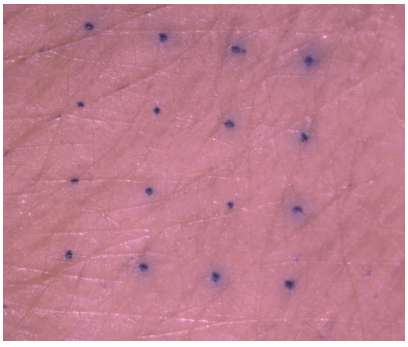
17. S. Liu, D. Wu, Y.S. Quan, F. Kamiyama, K. Kusamori, H. Katsumi, T. Sakane, A. Yamamoto, Improvement of Transdermal Delivery of Exendin-4 Using Novel Tip-Loaded Microneedle Arrays Fabricated from Hyaluronic Acid, Mol Pharm, 13 (2016) 272-279.
18. P.W. Noble, Hyaluronan and its catabolic products in tissue injury and repair, Matrix Biol, 21 (2002) 25-29.
19. C.C. Termeer, J. Hennies, U. Voith, T. Ahrens, J.M. Weiss, P. Prehm, J.C. Simon, Oligosaccharides of hyaluronan are potent activators of dendritic cells, J Immunol, 165 (2000) 1863-1870.
20. C. Termeer, F. Benedix, J. Sleeman, C. Fieber, U. Voith, T. Ahrens, K. Miyake, M. Freudenberg, C. Galanos, J.C. Simon, Oligosaccharides of Hyaluronan activate dendritic cells via toll-like receptor 4, J Exp Med, 195 (2002) 99-111.
21. U.M. Agren, R.H. Tammi, M.I. Tammi, Reactive oxygen species contribute to epidermal hyaluronan catabolism in human skin organ culture, Free Radic Biol Med, 23 (1997) 996-1001.
22. P.W. Noble, C.M. McKee, M. Cowman, H.S. Shin, Hyaluronan fragments activate an NF-kappa B/I-kappa B alpha autoregulatory loop in murine macrophages, J Exp Med, 183 (1996) 2373-2378.
23. J. Muto, Y. Morioka, K. Yamasaki, M. Kim, A. Garcia, A.F. Carlin, A. Varki, R.L. Gallo, Hyaluronan digestion controls DC migration from the skin, J Clin Invest, 124 (2014) 1309-1319.
24. D.N. Hart, Dendritic cells: unique leukocyte populations which control the primary immune response, Blood, 90 (1997) 3245-3287.
25. J. Lesley, N. Howes, A. Perschl, R. Hyman, Hyaluronan-Binding Function of Cd44 Is Transiently Activated on T-Cells during an in-Vivo Immune-Response, J Exp Med, 180 (1994) 383-387.
26. S. Mizrahy, S.R. Raz, M. Hasgaard, H. Liu, N. Soffer-Tsur, K. Cohen, R. Dvash, D. Landsman-Milo, M.G. Bremer, S.M. Moghimi, D. Peer, Hyaluronan-coated nanoparticles: the influence of the molecular weight on CD44-hyaluronan interactions and on the immune response, J Control Release, 156 (2011) 231-238.
27. D.H. Jiang, J.R. Liang, P.W. Noble, Hyaluronan as an Immune Regulator in Human Diseases, Physiol Rev, 91 (2011) 221-264.
28. C.S. Termeer, J. P.; Simon, J. C., Hyaluronan – magic glue for the regulation of the immune response?, TRENDS in Immunology, 24 (2003) 112-114.
29. H. Kono, K.L. Rock, How dying cells alert the immune system to danger, Nature Reviews Immunology, 8 (2008) 279-289.
30. M. Leone, M.I. Priester, S. Romeijn, M.R. Nejadnik, J. Monkare, C. O'Mahony, W. Jiskoot, G. Kersten, J.A. Bouwstra, Hyaluronan-based dissolving microneedles with high antigen content for intradermal vaccination: Formulation, physicochemical characterization and immunogenicity assessment, Eur J Pharm Biopharm, 134 (2019) 49-59.
31. N. Wilke, M.L. Reed, A. Morrissey, The evolution from convex corner undercut towards microneedle formation: theory and experimental verification, J Micromech Microeng, 16 (2006) 808-814.
32. P. Schipper, K. van der Maaden, S. Romeijn, C. Oomens, G. Kersten, W. Jiskoot, J. Bouwstra, Determination of Depth-Dependent Intradermal Immunogenicity of Adjuvanted Inactivated Polio Vaccine Delivered by Microinjections via Hollow Microneedles, Pharm Res, 33 (2016) 2269-2279.
33. K. van der Maaden, S.J. Trietsch, H. Kraan, E.M. Varypataki, S. Romeijn, R. Zwier, H.J. van der Linden, G. Kersten, T. Hankemeier, W. Jiskoot, J. Bouwstra, Novel hollow microneedle technology for depth-controlled microinjection-mediated dermal vaccination: a study with polio vaccine in rats, Pharm Res, 31 (2014) 1846-1854.
34. M. Leone, B.H. van Oorschot, M.R. Nejadnik, A. Bocchino, M. Rosato, G. Kersten, C. O'Mahony, J. Bouwstra, K. van der Maaden, Universal Applicator for Digitally-Controlled Pressing Force and Impact Velocity Insertion of Microneedles into Skin, Pharmaceutics, 10 (2018).

35. K. van der Maaden, E. Sekerdag, W. Jiskoot, J. Bouwstra, Impact-insertion applicator improves reliability of skin penetration by solid microneedle arrays, Aaps J, 16 (2014) 681-684.
36. A. D'Agostino, A. Stellavato, L. Corsuto, P. Diana, R. Filosa, A. La Gatta, M. De Rosa, C. Schiraldi, Is molecular size a discriminating factor in hyaluronan interaction with human cells?, Carbohyd Polym, 157 (2017) 21-30.
37. J.E. Rayahin, J.S. Buhrman, Y. Zhang, T.J. Koh, R.A. Gemeinhart, High and Low Molecular Weight Hyaluronic Acid Differentially Influence Macrophage Activation, Acs Biomater Sci Eng, 1 (2015) 481-493.
38. L. Topazio, R. Miano, V. Maurelli, G. Gaziev, M. Gacci, V. Iacovelli, E. Finazzi-Agro, Could Hyaluronic acid (HA) reduce Bacillus Calmette-Guerin (BCG) local side effects? Results of a pilot study, Bmc Urol, 14 (2014).
39. F. Zamboni, S. Vieira, R.L. Reis, J.M. Oliveira, M.N. Collins, The potential of hyaluronic acid in immunoprotection and immunomodulation: Chemistry, processing and function, Prog Mater Sci, 97 (2018) 97-122.
40. M. Litwiniuk, A. Krejner, T. Grzela, Hyaluronic Acid in Inflammation and Tissue Regeneration, Wounds, 28 (2016) 78-88.
41. T. Chanmee, P. Ontong, N. Itano, Hyaluronan: A modulator of the tumor microenvironment, Cancer Lett, 375 (2016) 20-30.
42. P.L. Bollyky, J.D. Lord, S.A. Masewicz, S.P. Evanko, J.H. Buckner, T.N. Wight, G.T. Nepom, Cutting edge: high molecular weight hyaluronan promotes the suppressive effects of CD4+CD25+ regulatory T cells, J Immunol, 179 (2007) 744-747.
43. W.T. Hsu, J.L. Suen, B.L. Chiang, The role of CD4(+)CD25(+) T cells in autoantibody production in murine lupus, Clin Exp Immunol, 145 (2006) 513-519.
44. J. Hodge-Dufour, P.W. Noble, M.R. Horton, C. Bao, M. Wysoka, M.D. Burdick, R.M. Strieter, G. Trinchieri, E. Pure, Induction of IL-12 and chemokines by hyaluronan requires adhesion-dependent priming of resident but not elicited macrophages, J Immunol, 159 (1997) 2492-2500.
45. M.R. Horton, M.D. Burdick, R.M. Strieter, G. Bao, P.W. Noble, Regulation of hyaluronan-induced chemokine gene expression by IL-10 and IFN-gamma in mouse macrophages, J Immunol, 160 (1998) 3023-3030.
46. C.M. McKee, M.B. Penno, M. Cowman, M.D. Burdick, R.M. Strieter, C. Bao, P.W. Noble, Hyaluronan (HA) fragments induce chemokine gene expression in alveolar macrophages. The role of HA size and CD44, J Clin Invest, 98 (1996) 2403-2413.
47. P.W. Noble, F.R. Lake, P.M. Henson, D.W. Riches, Hyaluronate activation of CD44 induces insulin-like growth factor-1 expression by a tumor necrosis factor-alpha-dependent mechanism in murine macrophages, J Clin Invest, 91 (1993) 2368-2377.
48. R. Stern, A.A. Asari, K.N. Sugahara, Hyaluronan fragments: an information-rich system, Eur J Cell Biol, 85 (2006) 699-715.
49. C. Keijzer, B. Slutter, R. van der Zee, W. Jiskoot, W. van Eden, F. Broere, PLGA, PLGA-TMC and TMC-TPP nanoparticles differentially modulate the outcome of nasal vaccination by inducing tolerance or enhancing humoral immunity, Plos One, 6 (2011) e26684.
50. N. Benne, J. van Duijn, F. Lozano Vigario, R.J.T. Leboux, P. van Veelen, J. Kuiper, W. Jiskoot, B. Slutter, Anionic 1,2-distearoyl-sn-glycero-3-phosphoglycerol (DSPG) liposomes induce antigen-specific regulatory T cells and prevent atherosclerosis in mice, J Control Release, 291 (2018) 135-146.
51. J. Monkare, M. Reza Nejadnik, K. Baccouche, S. Romeijn, W. Jiskoot, J.A. Bouwstra, IgG-loaded hyaluronan-based dissolving microneedles for intradermal protein delivery, J Control Release, 218 (2015) 53-62.
52. A. Passi, D. Vigetti, Hyaluronan as tunable drug delivery system, Adv Drug Deliver Rev, 146 (2019) 83-96.

SUPPLEMENTARY MATERIAL



Supplementary Figure S1. Representative bright field microscope image of a hMN. The diameter of approximately 195 µm and the microneedle tip of approximately 120 µm piercing in the skin are reported on the figure.



Supplementary Figure S2. Representative bright field microscope image of pierced *ex vivo* human skin after staining with trypan blue and *stratum corneum* stripping by tape.

Chapter 6

Diphtheria toxoid dissolving microneedle vaccination: adjuvant screening and effect of repeated-fractional dose administration

Adapted from Int J Pharm 2020 (580): 119182

Mara Leone[1], Stefan Romeijn[1], Guangsheng Du[1], Sylvia E. Le Dévédec[2], Hilde Vrieling[1,4], Conor O'Mahony[3], Joke A. Bouwstra[1,*], Gideon Kersten[1,4,*]

[1] Division of BioTherapeutics, Leiden Academic Centre for Drug Research, Leiden University, the Netherlandsb

[2] Division of Drug Discovery and Safety, Leiden Academic Centre for Drug Research, Leiden University, the Netherlands

[3] Tyndall National Institute, University College Cork, Cork, Ireland

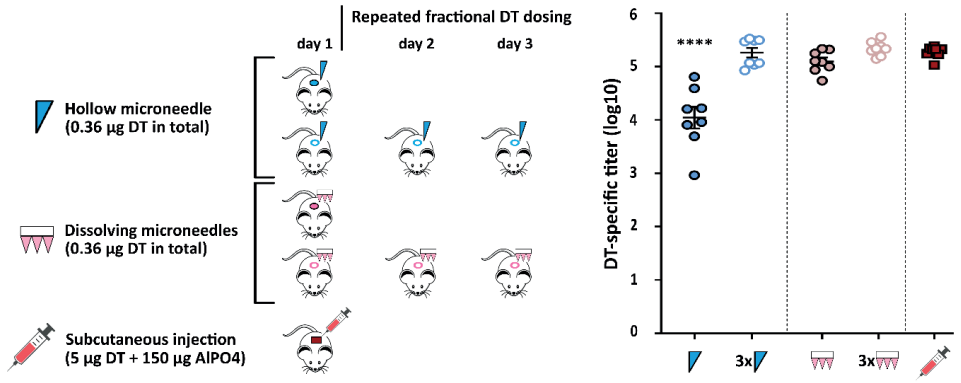
[4] Institute for Translational Vaccinology, Bilthoven, the Netherlands

[*] These authors contributed equally.

ABSTRACT

In this study the effect of repeated-fractional intradermal administration of diphtheria toxoid (DT) compared to a single administration in the presence or absence of adjuvants formulated in dissolving microneedles (dMNs) was investigated. Based on an adjuvant screening with a hollow microneedle (hMN) system, poly(I:C) and gibbsite, a nanoparticulate aluminum salt, were selected for further studies: they were co-encapsulated with DT in dMNs with either a full or fractional DT-adjuvant dose. Sharp dMNs were prepared regardless the composition and were capable to penetrate the skin, dissolve within 20 min and deposit the intended antigen-adjuvant dose, which remained in the skin for at least 5 h. Dermal immunization with hMN in repeated-fractional dosing (RFrD) resulted in a higher immune response than a single-full dose (SFD) administration. Vaccination by dMNs led overall to higher responses than hMN but did not show an enhanced response after RFrD compared to a SFD administration. Co-encapsulation of the adjuvant in dMNs did not increase the immune response further. Immunization by dMNs without adjuvant gave a comparable response to subcutaneously injected DT-$AlPO_4$ in a 15 times higher dose of DT, as well as subcutaneous injected DT-poly(I:C) in a similar DT dose. Summarizing, adjuvant-free dMNs showed to be a promising delivery tool for vaccination performed in SFD administration.

GRAPHICAL ABSTRACT



Keywords: dissolving microneedles, diphtheria toxoid, intradermal immunization, microneedles, aluminum-based adjuvants, repeated-fractional vaccine delivery.

1. INTRODUCTION

Vaccination has led to the control of devastating diseases such as smallpox, poliomyelitis, measles and hepatitis [1-3]. Most vaccines are injected intramuscularly or subcutaneously. However, classical injection can cause pain, distress, needle-stick injuries and requires trained personnel [4]. To overcome problems related to the hypodermic needles, less invasive technologies have been developed such as microneedles [4, 5]. Microneedles are structures up to 1 mm in length capable to penetrate the *stratum corneum*, the major skin barrier, in a pain-free way [4, 6], thereby delivering the antigen into the skin, a very immune competent organ populated with many antigen presenting cells. This may lead to antigen dose-sparing [4, 7] compared to the conventional routes of administration. Dissolving microneedles (dMNs) are a microneedle type that dissolve in the skin upon insertion thereby releasing the encapsulated vaccine [4]. Their dissolution in the skin allows to avoid sharp needle waste left behind after use and thus infections due to the needle re-use or needle-stick injuries are not possible [8]. Furthermore, for vaccine in the solid state it may be possible to circumvent the need for a cold-chain to keep the antigen stable during storage and shipping [9].

Vaccines consist of attenuated organisms, inactivated pathogens and toxins or subunit antigens. While attenuated vaccines may revert to the virulent form, inactivated and subunit vaccines are safer but generally less immunogenic [3, 10]. Thus, to potentiate the immune response using safer vaccines, together with the optimal administration route, adjuvants can be used, aiming for increased immunogenicity or antigen dose-sparing [4, 10, 11].

However, adjuvants can have drawbacks such as adverse effects and they may affect vaccine stability [11]. A previous study revealed that repeated administration of fractional doses of inactivated polio vaccine by means of a hollow microneedle (hMN) can lead to superior IgG responses without the use of adjuvants [12].

In this study, we examined whether the immunogenicity of diphtheria toxoid (DT) can be influenced by repeated dermal administration in comparison with a single dose without or with the addition of adjuvants. In a previous study the effect of repeated antigen dosing was assessed by using hMN [12]. In the present research, it was investigated whether repeated dosing by using dMNs and hMN had a similar effect on the immune response. To select the optimal adjuvant, the vaccination was performed by using a hMN intradermally in mice. This allowed to avoid time consuming dMN fabrication for all adjuvants and to screen a quite wide adjuvant set and to perform a relatively fast selection of them to encapsulate in the dMNs. Based on these studies, two adjuvants were selected for a follow-up study in which intradermal administration of DT and the adjuvant was performed in a single-full dose or in repeated-fractional dosing using either a hMN or dMNs.

2. MATERIALS AND METHODS

2.1 Materials

Hyaluronan (sodium hyaluronate, HA, average Mw was 150 kDa) was purchased from Lifecore Biomedical (Chaska, MN, USA). Diphtheria toxoid (DT) (12.25 mg/ml in phosphate buffered saline (PBS) pH 7.4) and diphtheria toxin (0.001 Lf/ml) were kindly provided by Intravacc (Bilthoven, The Netherlands). CpG ODN 1826 was purchased from Oligo Factory (Holliston, MA). Aluminum phosphate ($AlPO_4$) was purchased from Brenntag (Ballerup, Denmark). Fetal bovine serum (FBS) and cholera toxin (vibrio cholera) were obtained from Sigma-Aldrich (Zwijndrecht, The Netherlands). Glucose solution, L-Glutamine (200 mM), penicillin-streptomycin (10000 U/ml), and sodium bicarbonate were obtained from (Thermo-Fisher Scientific, Waltham, MA). Polyinosinic-polycytidylic acid (poly(I:C)) (low molecular weight) was purchased from Invivogen (Toulouse, France). Sterile phosphate buffered saline (PBS, 163.9 mM Na^+, 140.3 mM Cl^-, 8.7 mM HPO_4^{2-}, 1.8 mM $H_2PO_4^-$, pH 7.4) was ordered from Braun (Oss, The Netherlands). 10 mM phosphate buffer (PB, 7.7 mM Na_2HPO_4, 2.3 mM NaH_2PO_4, pH 7.4) was prepared in the laboratory. All the chemicals used were of analytical grade and distilled water (18 MΩ/cm, Millipore Co.) was used for the preparation of all solutions.

2.2 Synthesis of boehmite and gibbsite

Nanoparticulate aluminum salts boehmite and gibbsite were synthesized as described previously [13, 14]. Aluminium-iso-propoxide (80 mM) and aluminum-sec-butoxide (80 mM) were mixed in HCl (90 mM) and stirred for 10 days. The solution was hydrothermally treated at 150°C (boehmite) or 85°C (gibbsite) for 36h. The suspensions were dialyzed against water, autoclaved and stored at room temperature.

2.3 Preparation of formulations for hollow microneedle injections

In order to select the most promising adjuvants, various DT-adjuvant formulations were tested (Table 1) using a hMN injection system. DT was mixed in a concentration of 36 µg/ml with i) CpG ODN (36 µg/ml) or poly(I:C) (36 µg/ml) or cholera toxin (100 µg/ml) in PBS (pH 7.4), ii) the aluminum-based nanoparticles (alumNPs) gibbsite or boehmite (36 µg/ml Al^{3+} or 360 µg/ml Al^{3+}) in a sucrose (250 mM) containing histidine buffer (50 mM, pH 7.5). For the positive control, DT in a concentration of 500 µg/ml was mixed with $AlPO_4$ in a concentration of 15 mg/ml (DT-$AlPO_4$) in PBS (pH 7.4). AlumNPs and DT-$AlPO_4$ were incubated under continuous stirring at room temperature for 3 h to allow the DT adsorption on alumNPs or $AlPO_4$.

2.4 DT adsorption on alumNPs and $AlPO_4$

To determine the adsorption of free DT to alumNPs or $AlPO_4$, after the adsorption procedure the samples were centrifuged for 60 minutes at 35,000 × g at 4 °C in an Avanti J-20 XP centrifuge (Beckman Coulter). The DT in the supernatant was quantified by measuring the intrinsic fluorescence intensity of DT (λ_{ex} 280 nm/ λ_{em} 320 nm). The adsorption efficiency of DT was calculated according to the following equation:

$$\text{Adsorption efficieny } \% = (1 - \frac{M_{DT\ in\ supernatant}}{M_{DT\ total}}) \times 100\ \% \qquad \text{(Eqn. 1)}$$

where $M_{DT\ in\ supernatant}$ represents the mass of DT in supernatant after centrifugation, and $M_{DT\ total}$ is the total mass of DT used.

2.5 Particles size and zeta potential determination

For DT-alumNPs (DT in concentration of 36 µg/ml, alumNPs in concentrations of 36 µg/ml Al^{3+} or 360 µg/ml Al^{3+}) the particle size, polydispersity index (PDI) and zeta potential were determined by dynamic light scattering (DLS) and laser doppler velocimetry (Nano ZS® zetasizer, Malvern Instruments, Worcestershire, U.K.). To resemble the conditions for hMN injection and dMN arrays fabrication, samples were respectively prepared in 50 mM histidine (pH 7.5) or in 10 mM PB (pH 7.4).

2.6 Labeling of diphtheria, hyaluronan and alumNPs

2.6.1 Labeling for confocal microscopy

DT was labelled with Alexa Fluor 647® dye (AF647) (Life Technologies, Eugene, OR, USA) (λ_{ex} 651 nm, λ_{em} 672 nm) (DT-AF647) according to the manufacturer's instructions. Hyaluronan was labelled with fluoresceinamine (FAM) (Sigma-Aldrich, St. Louis, MO, USA) (isomer I, λ_{ex} 496 nm, λ_{em} 520 nm) (HA-FAM) following the method described by de Belder and Wik [15]. Gibbsite was labelled with lumogallion (Gib-LMG) (TCI Europe N.V., Antwerp, Belgium) (λ_{ex} 493 nm, λ_{em} 600 nm) following the method described by Mile et al [16].

2.6.2 Labeling for infrared detection

DT deposition in *ex vivo*-mouse and -human skin was quantified by using DT labelled with IRDye 800CW (LI-COR, Lincoln, Nebraska USA) (λ_{ex} 774 nm, λ_{em} 789 nm). DT labelling was performed according to the manufacturer's instructions.

2.7 Fabrication of dissolving microneedle arrays

dMN arrays (4x4 needles) were prepared as previously described [17, 18]. Briefly, 10% (w/v) HA was dissolved in PB (10 mM, pH 7.4) and stored overnight. The next day, 0.3% (w/v) DT for the full dose dMNs or 0.1% (w/v) DT for the fractional dose dMNs was added to the HA solution. The referred DT percentage for the full and fractional dose were defined to theoretically deliver 0.36 µg and 0.12 µg of DT respectively. The percentage was mathematically defined related to a previous publication [17]. For adjuvanted dMNs, the adjuvant in a weight ratio 1:1 with DT was added. For the DT adjuvanted with alumNPs, the alumNPs and DT were incubated under continuous stirring at room temperature for 3 h to allow the DT adsorption on alumNPs. Thus, the DT-alumNPs were added to the HA solution.

A polydimethylsiloxane mold (PDMS, Sylgard 184, Dow Corning, Midland, MI, USA) consisting of single-array wells was made using a master template presenting solid silicon MN arrays [17]. The PDMS mold was used to pour the HA-DT solution in each well. After several vacuum cycles and centrifugation steps, the dMN arrays were dried at 37°C overnight. The next day, an antigen-free backplate was produced by pouring a mixture of vinylpolysiloxane base and catalyst (1:1 ratio) (Elite Double 32a Normal, Zhermack Group, Badia Polesine, Italy). Subsequently a two-component glue solution (Bison International B.V., Goes, The Netherlands) was poured onto each array and left curing. Finally, the arrays were removed from the PDMS mold, cut into individual arrays and stored at room temperature in a desiccator until use.

To perform confocal imaging, in preparing the dMN arrays 100% of the DT and gibbsite amount and 4.5% of the hyaluronan amount were replaced with their labelled counterparts (DT-AF647, Gib-LMG and HA-FAM respectively). To perform near-infrared imaging of DT in the skin, 36% of the full dose of DT and 100% of the fractional dose of DT was labelled (DT-IR800).

2.8 Human skin

Human abdomen skin was obtained from a local hospital within 24 hours after cosmetic surgery. After removal of the fat excess with a scalpel, the skin was placed in the -80°C freezer until use. Before use, the skin was thawed in a petri dish containing a wet tissue at 37°C for 1 h and stretched with pins on parafilm-covered styrofoam. The skin was cleaned with distilled water and 70% ethanol before the start of the experiment.

Fresh *ex vivo* human skin was used within 24 hours after cosmetic surgery. After manual removal of the fat excess, the skin was cleaned with Milli-Q and 70% ethanol and stretched with pins on parafilm-covered Styrofoam to be used.

2.9 Penetration of microneedles in *ex vivo* human skin

dMN arrays (n=3) were applied onto the skin by impact velocity, as described elsewhere [18], by using an impact insertion applicator with a constant velocity of 0.40 m/s (Leiden University - applicator with uPRAX controller version 0.3) and kept in the skin during 18 sec. Penetration efficiency (PE) was determined by trypan blue treatment of pierced skin, as previously described [19]. After removal of the *stratum corneum* by stripping the blue spots were visualized using a light microscope. The penetration efficiency per array was calculated as follows (Equation 2), in which 16 is the number of microneedles per array:

$$\text{Penetration efficiency} = \frac{\text{Number of blue spots}}{16} \times 100 \qquad \text{(Eqn. 2)}$$

2.10 Dissolution of microneedles in *ex vivo* human skin

dMNs arrays (n=3) were applied on the skin as previously described (section 2.9) and were kept by the applicator for 20 min in the skin. The microneedle length before and after dissolution was determined with a light microscope (Axioskop and Stemi 2000-C, Carl Zeiss Microscopy GmbH, Göttingen, Germany) equipped with a digital camera (Axiocam ICc 5, Carl Zeiss). The images were analysed by ZEN 2012 blue edition software (Carl Zeiss Microscopy GmbH). The dissolved MN volumes were calculated as reported previously [17].

2.11 Quantification of diphtheria delivered in *ex vivo* mouse and human skin

Full dose dMN arrays (n=3 per skin type) and fractional dose dMN arrays (n=3 per skin type) were inserted into mouse or human skin *ex vivo* and the dMNs remained in the skin for 20 min. After dMN array removal, the near-infrared fluorescence of the delivered DT-IR800 was measured in a Perkin-Elmer IVIS Lumina Series III *in vivo* imaging system (Waltham, MA, USA), by using a ICG bkg excitation filter and an ICG emission filter and acquisition time 4 s, F-stop 2, binning 4 and field of view of 12.5 cm. Perkin-Elmer Living Image software version 4.3.1.0 was used for image acquisition and analysis. Fluorescence data were processed using region of interest (ROI) analysis with background subtraction consisting of a control region of the skin.

A calibration curve was generated in mouse and human skin by intradermal microinjections of DT-IR800 of 62.5 - 1000 ng with an in house fabricated hMN injection system with uPRAX controller version 0.3 (Leiden University) as reported elsewhere [12, 20, 21].

2.12 Confocal laser scanning microscopy

Confocal laser scanning microscopy (CLSM) was performed with a Nikon TE-2000-e inverted microscope equipped with a C1 confocal unit. Nikon Plan Apo 10 × and 4 × objectives (with a numerical aperture of 0.20 and 0.45 and working distance of 15.7 and 4 respectively) were used respectively for microneedle and skin visualization. Nikon NIS Elements version 4.20.00 64-bit software was used for acquisition and analysis of scans.

For dMN visualization, fluoresceinamine (FAM) and lumogallion (LMG) were excited at 488 nm and Alexa Fluor 647 at 633 nm. The xy resolution was 1.55 µm/pixel.

For antigen and nanoparticle localization in the skin, fluorescently labelled dMNs were inserted into *ex vivo* fresh human skin for 20 minutes. After removal of the remaining dMN array, time-lapse microscopy using CLSM as described above was performed with the skin in order to visualize hyaluronan, gibbsite or DT respectively. Each 30 min, sequentially xy scans (xy resolution of 6.21 µm/pixel) were taken with a spatial resolution of 10 µm in z-direction (z-axis of 0.7 mm) over a time period of 5 h.

2.13 Immunization studies

Immunization studies were performed using female BALB/c mice (H2d), 8-11 weeks old (Charles River, Maastricht, The Netherlands). The studies were approved by the ethical committee on animal experiments of Leiden University (License number 14241). The mice were randomly assigned to groups of 8.

Immunizations were given at day 1 (prime immunization), day 22 (boost immunization) and day 43 (2nd boost immunization). Before each intradermal immunization, the mice were shaved on the left flank (approximately 4 cm^2). A blood sample was collected, serum was isolated and stored at -80°C. Prior to vaccination, mice were anesthetized by intraperitoneal injection of 150 mg/kg ketamine and 10 mg/kg xylazine. At day 63, all mice were sacrificed and serum was collected.

2.13.1 Part I: adjuvant screening

The effect of adjuvants on the immunogenicity of dermally injected DT was assessed using hMN injection (Table 1). The inner diameter of the hMN was approximately of 150 µm and the length of the microneedle tip of approximately 120 µm. Injected volume was 10 µl at a controlled depth of 120 µm by using a specifically designed hMN injection system with uPRAX controller version 0.3 (Leiden University) [21]. Negative and positive controls included respectively intradermal injection of PBS by hMN and 100 µl subcutaneous injection of 5 µg DT and 150 µg $AlPO_4$ with a conventional 26G needle.

Table 1. Immunization study parameters for adjuvant screening. The dose of DT and adjuvant is provided together with the immunization route. Two ratios of DT and alumNPs were used.

Immunization route	**Intradermal by hollow microneedle**								**Subcutaneous**	
Group name[*)]	DT	DT-CT	DT-PI	DT-CpG ODN	DT-Gib		DT-Boe		PBS	DT- $AlPO_4$ sc
					1:1	1:10	1:1	1:10		
DT dose (µg)	0.36								-	5
Adjuvant dose (µg)	-	1	0.36		0.36[**)]	3.6 [**)]	0.36 [**)]	3.6 [**)]	-	150

[*)] DT, diphtheria toxoid; CT, cholera toxin; PI, poly(I:C); Gib, gibbsite; Boe, boehmite; $AlPO_4$, aluminum phosphate, [**)] Al^{3+} concentration.

2.13.2 Part II: single-full dose vs repeated-fractional doses

The effects of DT administration, with and without adjuvant, in repeated-fractional doses (RFrD) were investigated and compared to a single-full dose (SFD) injection (100% dose). The RFrD consisted of administration, in 3 consecutive days, of 1/3rd of the SFD of DT(-adjuvant) (3 x 33% doses). Intradermal vaccination in mice was performed using hMN (10 µl at a depth of 120 µm) and dMNs. Details of the formulations are reported in Table 2. PBS and DT- $AlPO_4$ groups were used as negative and positive control, respectively. An additional positive control of subcutaneous injection of 100 µl of 0.36 µg DT and 0.36 µg poly(I:C) was included.

Table 2. Immunization study parameters for administration kinetics investigation. The administration is in SFD (100%) or in 3 RFrD (3 x 33%).

Formulation	Formulation dose administration schedule	DT dose*) per array/injection (μg)
Intradermal administration: dissolving microneedles		
DT DT-Gib DT-PI E/E/DT**)	SFD	0.36
DT DT-Gib DT-PI	RFrD	0.12
Intradermal injection: hollow microneedles		
DT PBS/PBS/DT**)	SFD	0.36
DT	RFrD	0.12
PBS	-	-
Subcutaneous injection (conventional 26G needle)		
DT-PI	SFD	0.36
DT-$AlPO_4$	SFD	5

*) the DT and adjuvant dose are equal except for the subcutaneous injection with $AlPO_4$, in which 5 μg of DT and 150 μg $AlPO_4$ has been added in the formulation; **) application of an empty dMN array or injection of PBS on 2 consecutive days and DT administration in SFD on day 3. Abbreviations are DT, diphtheria toxoid; Gib, gibbsite; PI, poly(I:C); $AlPO_4$, aluminum phosphate; E, empty dMN array.

2.14 Determination of DT-specific serum IgG titers and diphtheria toxin-neutralizing antibody titers

DT-specific total IgG, IgG1 and IgG2a titers in serum were determined by ELISA as described previously [22]. Plates were coated with 140 ng DT per well and incubated overnight at 4 °C. After blocking with BSA (Sigma-Aldrich, Zwijndrecht, The Netherlands), sera samples were added in a three-fold serial dilution and the plates were incubated at 37 °C for 2 h. Detection of antibodies was performed with horseradish peroxidase-conjugated goat-anti-mouse IgG, IgG1 or IgG2a (Southern Biotech, Birmingham, AL) (1:5000 dilution) using 1-stepTM ultra 3,3',5,5'-tetramethylbenzidine (TMB) (Thermo-Fisher Scientific, Waltham, MA) as substrate. The reaction was stopped with 2 M sulfuric acid (JT Baker, Deventer, The Netherlands). Absorbance was measured at 450 nm. Antibody titers were expressed as the log10 value of the serum dilution at the mid-point of the S-shaped absorbance-dilution curve.

Toxin neutralizing capacity of antisera was measured in a Vero cell assay [23]. After complement inactivation by heating at 56 °C for 45 min, appropriate two-fold serial dilutions of serum samples were prepared in M199 medium (Sigma-Aldrich, Zwijndrecht, The Netherlands) (supplemented with 5% FBS (Sigma-Aldrich, Zwijndrecht, The Netherlands), 1 g/l glucose, 1.6 mM L-glutamine, 1.7 g/l sodium bicarbonate and 100 U/ml penicillin-streptomycin) and were applied to 96-well plates. Subsequently, 50 µl/well 0.001 Lf/ml diphtheria toxin diluted in complete culture medium was added and the plates were incubated at 37°C and 5% CO_2 for 2 h for toxin neutralization. Subsequently, 50 µl/well suspension of Vero cells were added (12,500 cells/well) and incubated at 37 °C in 5% CO_2 for 6 days. The number of wells containing viable Vero cells was determined by microscopy. The neutralizing antibody titers were expressed as the log2 value of the highest serum dilution that was still capable of protecting the Vero cells from the challenge of diphtheria toxin.

2.15 Statistical analysis

Data from antibody titers and neutralizing antibody titers were analyzed by one way ANOVA with Bonferroni post-test by using GraphPad Prism software (version 5.02). A $p < 0.05$ was considered to be significant.

3 RESULTS

3.1 Size and zeta potential of DT-alumNPs and adsorption efficiency of DT to alumNPs and to $AlPO_4$

DT-Gibbsite and DT-Boehmite were characterized in terms of particle size, polydispersity index (PDI) and zeta potential. DT-alumNPs were in the µm range, i.e. outside the measuring range of the DLS equipment, regardless the buffer composition (data not shown).

The effect of the type of particle on the zeta potential was examined. In histidine buffer, boehmite resulted in a positive surface charge, while gibbsite showed a negative zeta potential at the same concentration. When increasing the particle concentration the zeta potential became less negative for the boehmite and became positive for the gibbsite. The effect of the addition of DT on the zeta potential was also examined. It was observed that i) addition of DT to the alumNPs formulation resulted in a lower zeta potential than alumNPs only and ii) increasing the DT:alumNPs ratio from 1:1 to 1:10 by increasing the alumNP concentration resulted in a higher zeta potential, indicating a relative lower level of negatively charged DT on their surface compared with the slightly positively charged alumNPs (Table 3). No significant changes in zeta potential were observed within the first 24 h of storage (Table 3). The alumNPs in PB showed a more negative zeta potential than in histidine buffer.

The adsorption efficiency of DT on the alumNPs and $AlPO_4$ at 3 h after mixing was measured (Table 3). In solutions with DT : alumNPs 1:10 ratio more than 80% DT was adsorbed to the alumNPs. For a DT : alumNPs 1:1 ratio the DT adsorption on the alumNPs was less than 40%. This was also observed for the $AlPO_4$ particles. This indicated that at equal weight ratios the alumNP surface became saturated with DT.

Table 3. Zeta potential of DT-alumNPs and percentages of DT adsorption on alumNPs and $AlPO_4$ (n = 3). Data are average ± SEM.

		Time (h)			
		0	3	24	
Formulation	**Buffer**	**Zeta Potential (mV)**			**Adsorption efficiency (%)**
Gibbsite*)	PB	-24.7 ± 0.4	-	-	-
DT-Gibbsite*) 1:1		-32.6 ± 0.5	-32.8 ± 0.3	-32.1 ± 0.3	27.1 ± 0.5
Gibbsite*)	Histidine	-0.9 ± 0.3	-	-	-
DT-Gibbsite*) 1:1		-27.1 ± 0.1	-27.0 ± 0.2	-26.7 ± 0.2	11.4 ± 1.0
Gibbsite**)		17.6 ± 0.3	-	-	-
DT-Gibbsite**) 1:10		-22.8 ± 0.3	-22.5 ± 0.2	-19.0 ± 0.6	81.3 ± 0.1
Boehmite*)		3.4 ± 0.4	-	-	-
DT-Boehmite*) 1:1		-23.8 ± 0.2	-23.2 ± 0.2	-25.7 ± 0.1	25.5 ± 0.4
Boehmite**)		13.9 ± 0.5	-	-	-
DT-Boehmite**) 1:10		-15.4 ± 0.6	-8.5 ± 0.2	-4.7 ± 0.5	83.2 ± 0.1
DT-$AlPO_4$ 1:30	PBS	-	-	-	38.7 ± 0.3

*) 36 µg/ml Al^{3+}, **) 360 µg/ml Al^{3+}

3.2 Immunization study for adjuvant screening

In an immunization study using a hMN several adjuvants were screened on their efficiency to potentiate the immune response of DT. The selected adjuvants were CpG ODN, Poly(I:C), cholera toxin, gibbsite and boehmite (the latter two in DT : alumNPs ratios of 1:1 and 1:10).

After the prime, the groups DT-Gib 1:1 and DT-Boe 1:10 induced higher IgG titers than the DT group (Figure 1 A). The DT-Boe 1:10 group showed even a comparable response to the positive control DT-$AlPO_4$ (Figure 1 A).

At day 42, DT-specific total IgG titers increased further for all formulations (Figure 1 B). However, no significant adjuvant effect was observed in comparison with the DT control group (Figure 1 B). The DT-CT group had a comparable IgG response to the positive control DT-$AlPO_4$.

At day 63 (Figure 1 C), the response of all the groups was very close to the response of positive control DT-$AlPO_4$, despite a 15 fold lower dose (Figure 1 C). However, the addition of different adjuvants did not enhance further the response evoked by DT after three vaccinations (Figure 1 C).

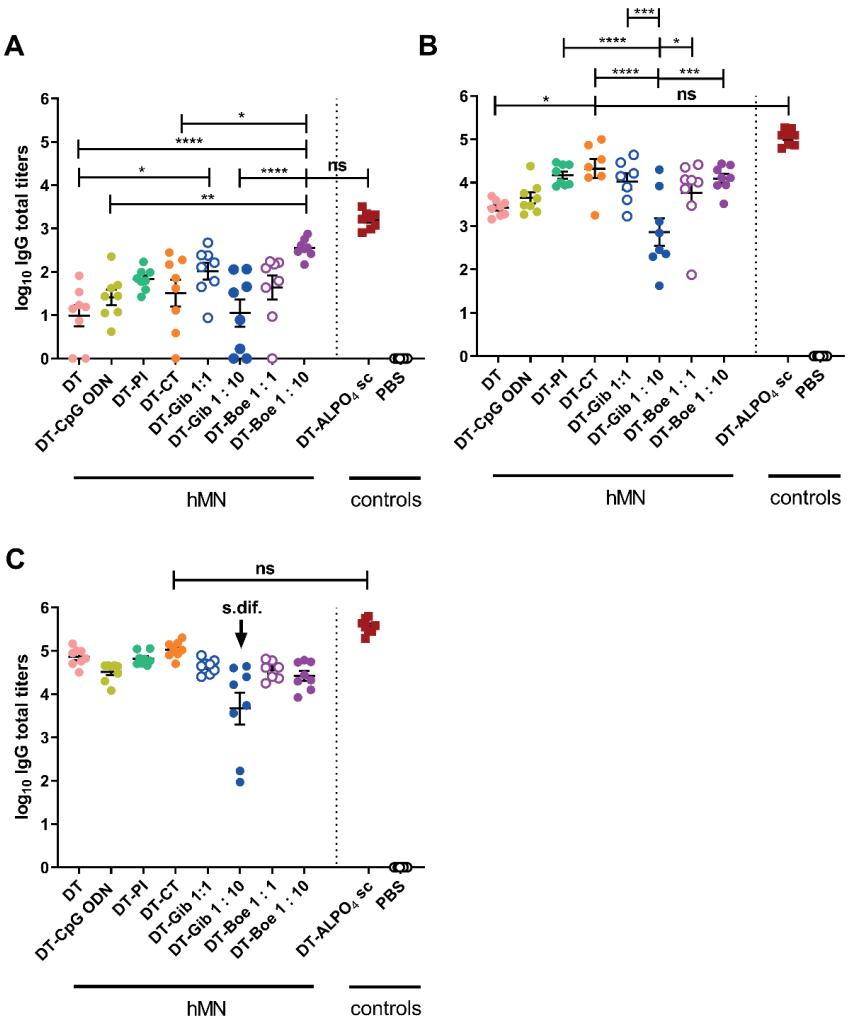


Figure 1. DT-specific total IgG titers on day 21 **(A)**, 42 **(B)** and 63 **(C)**. After each vaccination, the $AlPO_4$ was significantly different from each other group except the no significant (ns) group reported. After 63 days, the titers in the DT-Gib 1:10 group was significantly lower (s.dif.) compared to the titers in all the other groups. Bars represent mean ± SEM, n = 8. *p < 0.05, **p < 0.01, ***p < 0.001 and ****p < 0.0001. DT dose was 0.36 µg except DT-$AlPO_4$ sc: 5 µg. hMN, hollow microneedle; DT, diphtheria toxoid; PI, poly(I:C); CT, cholera toxin; Gib, gibbsite; Boe, boehmite; $AlPO_4$, aluminum phosphate.

Besides the IgG total response, the IgG1 and IgG2a responses were also measured. IgG1 and IgG2a ratios were not dependent on adjuvant type (Supplementary material, Figure S1) (p>0.05). This indicates that the Th2/Th1 balance was not influenced by the adjuvants.

The functionality of the antibody response was investigated by determining toxin neutralizing antibody titers in serum on day 63. The positive control DT-$ALPO_4$ showed higher levels of toxin-neutralizing antibodies than all other groups ($p<0.05$) (Figure 2). Overall, the addition of an adjuvant to DT did not improve the functional response. Similarly to the IgG total titers, DT-Gibbsite 1:10 was less immunogenic as compared to plain DT.

Based on neutralizing antibody results and the primary response, poly(I:C) and gibbsite (the formulation in 1:1 ratio with DT) were selected as adjuvants for the studies using dMNs.

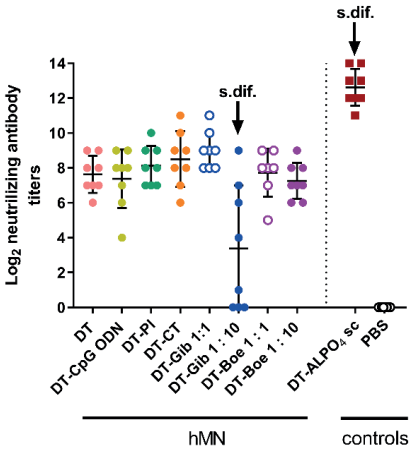


Figure 2. DT-neutralizing antibody titers. Results are shown for serum collected on day 63. The titers in the DT-Gib 1:10 group and the DT-$AlPO_4$ group were, respectively, significantly lower or higher (s.dif.) from the titers in all the other groups. Bars represent mean ± SEM, n = 8. hMN, hollow microneedle; DT, diphtheria toxoid; PI, poly(I:C); CT, cholera toxin; Gib, gibbsite; Boe, boehmite; $AlPO_4$, aluminum phosphate.

3.3 Dissolving microneedle: characterization and interaction with the skin

dMN arrays were prepared with DT in absence or presence of the selected adjuvant. Very sharp dMNs containing either DT, DT-PI or DT-Gib could be prepared (Figure 3) in a reproducible manner. The DT content (full dose or fractional dose) did not affect the shape either (Figure 3 and data not shown).

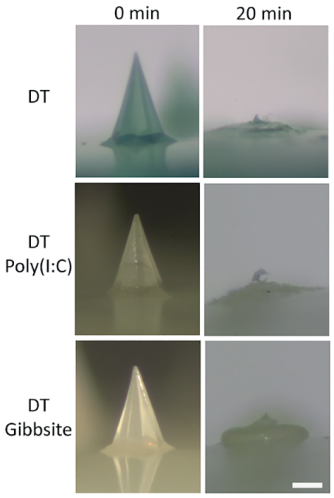


Figure 3. Brightfield microscope images (5x) of microneedles with DT, DT-PI and DT-Gib full dose content before application on the skin (0 min) and after 20 minutes dissolution into *ex vivo* human skin. Scale bar 100 µm.

Hyaluronan, DT and gibbsite were uniformly distributed within the dMN as investigated with confocal 3D imaging using fluorescently labelled components (Figure 4).

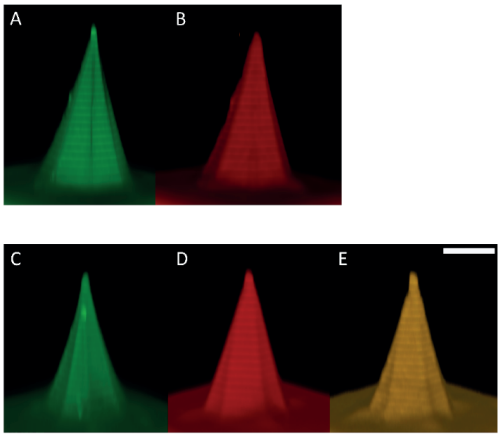


Figure 4. CLSM 3D images of the distribution of fluorescently labelled HA **(A)** and DT **(B)** in the hyaluronan-based dMNs containing DT; Fluorescently labelled HA **(C)**, DT **(D)** and Gib **(E)** in hyaluronan-based dMNs containing DT adsorbed gibbsite nanoparticles. Both dMNs **(A-B and C-E)** contained a full dose of DT or DT-Gib. Scale bar 100 µm.

dMN arrays prepared from full dose of either DT, DT-PI or DT-Gib were applied on *ex vivo* human skin. After withdrawal and application of trypan blue, the number of blue spots were determined and the penetration efficiency and the standard deviation were calculated being respectively 95.8 ± 7.2%, 89.6 ± 9.5% and 100.0 ± 0.0%, respectively (n = 3).

As shown in Figure 3, dMNs with DT or DT-PI incorporated dissolved completely in the skin within 20 min (100 ± 0% dissolved MN volume, mean ± sd), the dMNs with DT-Gib incorporated resulted in some dMN leftover (approximately 91 ± 1% dissolved volume, mean ± sd).

After 20 min microneedle dissolution in fresh human skin and withdrawal of the remaining dMN array, the hyaluronan, DT and gibbsite were visualized in the skin by CLSM during 5 hours each 30 minutes as function of depth parallel to the skin surface (Figure 5, only 0, 3 and 5 h time points are shown). All components were deposited and co-localized in the epidermis and top layers of the dermis. Furthermore, the delivered antigen without or with gibbsite remained at the site of administration for at least 5 h, whereas HA is mostly diffused away after 3 h or less.

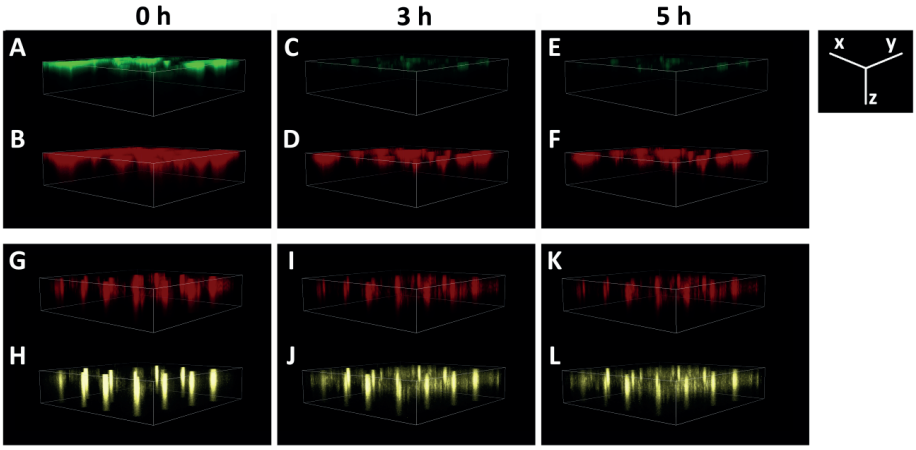


Figure 5. CLSM 3D images of HA (green), DT (red) and Gib (yellow) localization into *ex vivo* human (fresh) skin after dMN arrays application for 20 min. Deposited HA **(A, C, E)** and DT **(B, D, F)** fluorescently labelled (HA-FAM and DT-AF647) into the skin after dissolution of hyaluronan dMNs loaded with DT; deposited DT **(G, I, K)** and gibbsite **(H, J, L)** fluorescently labelled (DT-AF647 and Gib-LMG) into the skin after dissolution of hyaluronan dMNs loaded with DT and gibbsite. Images related to time 0 h **(A, B, G, H)**, 3 h **(C, D, I, J)** and 5 h **(E, F, K, L)** are shown. Time 0 h refers to the beginning of the detection, starting after the dMN dissolution of 20 min and removal of the dMN array. The location of the skin surface is the xy area on top of the z-axis representing the depth of imaging (0.7 mm).

Finally, the amount of DT delivered into the skin after dMN array application using infrared labelled DT was determined. After 20 min of application in the skin, the dMNs containing a full or 1/3 dose of DT delivered respectively 0.32 ± 0.02 µg and 0.13 ± 0.04 µg of DT in *ex vivo* human skin and 0.35 ± 0.03 µg and 0.10 ± 0.01 µg of DT in *ex vivo* mouse skin (mean ± sd, n = 3).

3.4 dMN arrays and hMNs: single-full dose vs. repeated-fractional dose

The aim of this study was to compare RFrD with SFD administration of DT with or without adjuvant using dMN arrays and a hMN keeping the total dose of DT and antigen approximately the same.

Following prime vaccination by a hMN, IgG titers after DT RFrD were higher than DT SFD (Figure 6 A). To determine whether MN piercing itself has an effect on the immune response, a hMN group (PBS/PBS/DT SFD) consisting of two consecutive days of PBS injection and a third day of SFD DT injection was included. As the IgG titers were higher than that of the SFD injection, microneedle piercing as such seems to enhance the immune response.

Prime administration of DT by dMNs gave higher IgG responses than hMN injection (Figure 6 A). DT RFrD by dMNs did not significantly increase the IgG levels compared to DT SFD by dMNs, although there is a trend of a higher response and after RFrD there is less variation in the response. Additionally, the application of empty dMN arrays in the first two days and the SFD administration of the DT on the third day (E/E/DT SFD) showed a comparable IgG response as RFrD. The encapsulation of an adjuvant (poly(I:C) or gibbsite) together with DT in the dMNs, did not increase the DT-specific total IgG response when delivered as SFD or RFrD compared to the absence of an adjuvant. Finally, the administration of DT by dMNs gave a higher response than the control of DT-poly(I:C) injected subcutaneously and a response comparable to the positive control, DT-$AlPO_4$ sc, with a 15 times higher DT dose. Conversely, the hMN groups showed comparable response to the control of DT-PI sc and a significantly lower response than the positive control DT-$AlPO_4$ sc.

After the first boost, DT-specific total IgG titers increased (Figure 6 B) but the differences between the groups were similar as after the prime with a few changes. DT RFrD by dMNs was comparable to DT RFrD using hMN but still higher than PBS/PBS/DT SFD hMN group. Furthermore, the positive controls DT-PI and DT-$AlPO_4$ subcutaneously injected were comparable to all hMN and dMNs groups except to DT SFD hMN and DT SFD hMN and PBS/PBS/DT SFD hMN groups, respectively, which showed a significant lower response.

After the second boost (Figure 6 C) the titers of most groups further increased, although slightly. Apparently a plateau in the immune response was reached. After this second boost, for the first time the DT RFrD dMNs group developed a higher response than E/E/DT SFD dMNs.

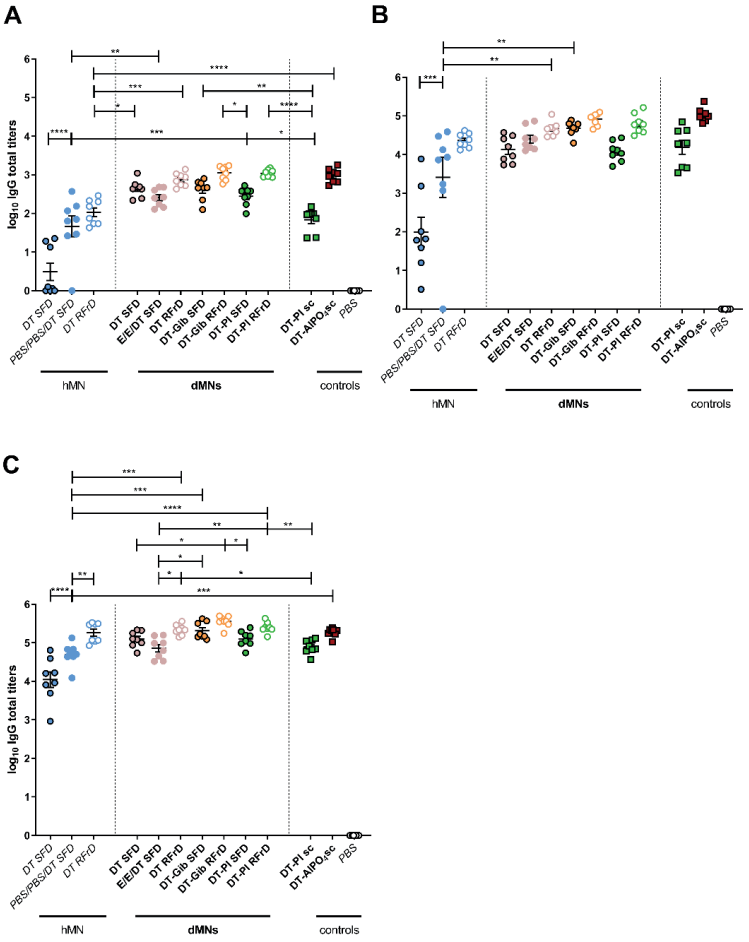


Figure 6. DT-specific total IgG antibody titers measured in BALB/c mice on day 21 **(A)**, day 42 **(B)** and day 63 **(C)**. Bars represent mean ± SEM, n = 8. *p < 0.05, **p < 0.01, ***p < 0.001, ****p < 0.0001. SFD, single-full dose; RFrD, repeated-fractional dose; dMNs, dissolving microneedles; hMN, hollow microneedle; DT, diphtheria toxoid; PI, poly(I:C); Gib, gibbsite; E, empty dMNs; $AlPO_4$, aluminum phosphate.

The IgG1/IgG2a ratios are depicted in Figure S2 in Supplementary material. DT vaccination by dMNs and addition of gibbsite or poly(I:C) as adjuvant modestly changed the IgG1/IgG2a ratio, shifting the balance slightly to Th1.

High levels of toxin-neutralizing antibodies were induced after vaccination by means of dMNs, regardless the dosing modality or the presence of an adjuvant, and by DT RFrD by

hMN (Figure 7). No adjuvant effect was observed after addition of PI in dMNs (DT SFD dMNs gave a similar response compared to DT-PI SFD dMNs and DT-PI SFD sc), but DT-PI RFrD dMNs resulted higher in response compared to DT-PI SFD dMNs and DT-PI SFD sc. In this case, the dosing modality made a difference in protection against the toxin, resulting a RFrD of DT-PI in a much higher toxin neutralization.

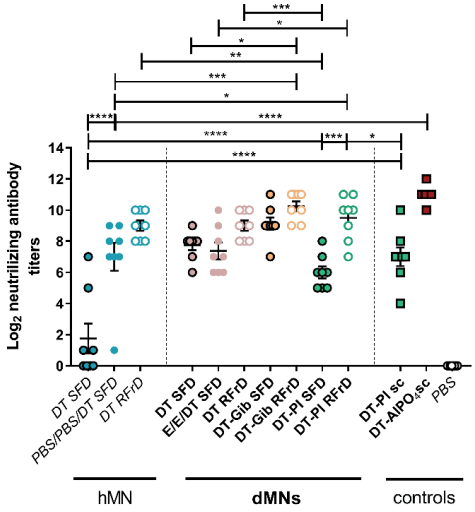


Figure 7. DT-neutralizing antibody titers. Results are shown for serum collected on day 63. Bars represent mean ± SEM, n = 8. *p < 0.05, **p < 0.01, ***p < 0.001, ****p < 0.0001. SFD, single-full dose; RFrD, repeated-fractional dose; dMNs, dissolving microneedles; hMN, hollow microneedle; DT, diphtheria toxoid; PI, poly(I:C); Gib, gibbsite; E, empty dMNs; $AlPO_4$, aluminum phosphate.

4. DISCUSSION

Repeated-fractional doses effect

The aim of this study was to obtain insight in whether dermal vaccination by RFrD of DT enhances the specific IgG response compared to that after SFD antigen dermal administration. The present study corroborated existing data [12, 24] by showing a superior response by RFrD compared to SFD of antigen after vaccination by hMN. In the present study less consecutive days of administration were used as in the previous studies: 33% in each consecutive day during 3 days vs 4, 7 and 8 days in the previous studies. Furthermore, low responders seemed to benefit more from the RFrD regime and it was demonstrated that consecutive skin piercing by hMN (PBS/PBS/DT SFD) could enhance the immune response compared to a DT SFD only by hMN. Piercing of the skin may cause some cell death or other local damage resulting in the release of damage-associated molecular patterns (DAMPs) and subsequent attraction of antigen presenting cells to the immunization area [25]. However,

application of empty dMN arrays (E/E/DT SFD), inducing an even higher number of piercings in the skin compared to a hMN (16 dMNs per array vs 1 hMN) and applied by a 20 minutes pressure on the skin potentially leading to skin inflammation [25, 26]. This did not enhance the response further compared to a SFD antigen administration by dMNs. This may be explained by a maximal level of immunity reached after prime for the E/E/DT SFD group due to the skin piercing by the first empty array application inducing release of DAMPs and then an immune response with no additional further effect after application of the other empty and then DT loaded dMN arrays.

dMNs vs a hMN

Vaccination by means of dMNs led to significantly higher response than by hMN, as already reported in our previous study [17], showing a faster increase in DT-specific IgG responses already after the first immunization. This can be related to several factors. First, the use of different MN types: a hMN injects the vaccine at a specific intradermal depth point (120 µm) while the longer dMNs (300 µm) release the antigen at various skin depths simultaneously possibly reaching a higher number of immune cells and involving different immune cell populations [27], although in literature no difference in the immune response is reported when comparing different injection depths [20]. Second, the number of needles piercing the skin (16 dMNs vs 1 hMN) and the pressure applied on the skin (20 minutes for the dMN array application and no pressure for the hMN) potentially causing inflammation and thus more release of DAMPs in a larger region, facilitating attraction of antigen presenting cells. Third, the presence of low molecular weight species of HA. Although high MW HA is considered immunologically inert, low molecular weight HA fragments, potentially present in the dMNs or generated *in vivo*, can elicit various proinflammatory responses leading to innate immune activation [28, 29], although this is not observed in recent studies in our group [30] and in literature [31]. Fourth, the prolonged exposure of the antigen during dMN dissolution to relevant immune cells may enhance the response [32]. Fifth, the presence of low responding and no-responding mice after prime vaccination in SFD by hMN: in a previous study [22] and in the adjuvants screening of the present study, the titers after DT vaccination by hMN resulted in an overall higher response being closer to the positive control DT-$AlPO_4$ than in the SFD vs RFrD immunization study.

Adjuvants vs repeated-fractional dosing by dMNs

Antigen dose sparing can be achieved with the use of adjuvants [10, 23]. Besides adjuvants (CpG, PI and CT) commonly used for experimental dermal vaccination [1, 4, 23], aluminum-based NPs (alumNPs), so far tested only for subcutaneous or intramuscular administration [10, 33, 34], were included for intradermal vaccination.

The selection, in the first immunization study by hMN, of the optimal adjuvants for DT vaccination by dMNs led to the choice of poly(I:C) and gibbsite. Poly(I:C) gave a more robust response after primary immunization, similar to CT, than other adjuvants and it has a better

feasibility for human vaccination than CT. The selection of gibbsite (in ratio 1:1 with DT) was based on the following considerations: i) its higher response among the DT adjuvanted with alumNPs and ii) dermal injection of gibbsite, as of boehmite too, did not induce any palpable persistent intradermal injection-site nodules in mice, as previously observed after intradermal injection of classical aluminum preparations [35].

The addition of adjuvants for intradermal vaccination by both hMN and dMNs did not enhance the IgG total levels further compared to unadjuvanted antigen indicating that the response reached already a plateau and any extra did not lead to a higher response. However, vaccination by dMNs, in the presence of poly(I:C) or gibbsite, shifted the Th2/Th1 balance to Th1. This was not observed using hMNs. This change in response may be related to the depot created in the skin after dMN dissolution leading to a sustained release of antigen and adjuvant [32].

In our study, similarly potent DT-specific IgG responses were observed upon intradermal vaccination by dMNs of SFD, RFrD and adjuvanted DT. This demonstrates that by using dMNs the immune response can be enhanced and the use of an adjuvant or prolonged antigen delivery by fractional dosing can be avoided, at least for potent antigens. An adjuvant-free vaccine would then avoid side-effects and potential stability problems related to the presence of the adjuvant [11, 36].

However, results from neutralizing antibody assay indicated a higher protection against diphtheria toxin for adjuvanted-DT RFrD dMNs compared to unadjuvanted DT in dMNs, hMN groups and even conventional injection of DT-PI. This may be related to a prolonged exposure of the antigen during and after dMN dissolution to relevant immune cells involved in the humoral protection as mentioned above.

Overall these observations lead to the conclusion that the combination of RFrD and adjuvant in dMNs, but not their separated use, can be very efficient in respect to the antibody response and the neutralization of the diphtheria toxin effect.

Finally, Joice et al [37] reported how extended-delivery vaccination by means of dMNs enables a single vaccination to generate immune responses equivalent to a two-dose vaccination regimen for vaccines as IPV, tetanus toxoid and influenza but the same extended-delivery vaccination does not enhance immune response to the live-attenuated measles vaccine. This demonstrates that RFrD of the antigen can lead to a superior immune response than SFD depending on the antigen type.

dMNs vs conventional subcutaneous injections

This study focused on minimally-invasive delivery for DT immunization by dMNs and it has been shown that vaccination by dMNs loading unadjuvanted DT led to comparable responses already after prime immunization as compared to invasive subcutaneous injections of DT-$AlPO_4$ with almost 15 and 415 times higher DT and adjuvant doses

respectively. These results corroborated existing data in literature where a comparable or even higher response was obtained after vaccination by dMNs than conventional subcutaneous injection [27, 38-41] and similar response was shown after vaccination with hMN in comparison with the above mentioned positive control [1, 22]. Higher IgG responses after prime and comparable responses after the two boost immunizations demonstrate the efficiency of a dermal vaccination by dMNs compared to subcutaneous injection of adjuvanted-DT (DT-PI sc).

Characterization of the alumNPs

Fabrication of dMN arrays and dMN interaction with the skin, regardless the formulation, was successful as previously demonstrated [17]. However, dissolution of DT-Gib was not complete after 20 minutes. This may be related to the particle aggregation observed in the alumNPs characterization studies. Aggregation is likely due to the pH, as the alumNPs are stable at pH<6 and aggregate above this value (H. Vrieling et al, manuscript in preparation).

Boehmite and gibbsite were characterized in the transmission electron microscope for their shape and size resulting in nm range [42, 43]. In the present study their size resulted in the µm range using dynamic light scattering (data not shown). This suggests that particle aggregation occurred. Besides the presence of DT and the concentration of alumNPs, the buffer composition also had a role on the zeta potential: PB lowered the zeta potential more than the histidine buffer. A possible explanation can be found in the phosphate groups from PB exchanging with hydroxyl groups of alumNPs so that a mixture of aluminum oxyhydroxide and aluminum phosphate is obtained.

5. CONCLUSION

In conclusion, when using hMN a delivery of the antigen over multiple days can enhance the immune response more than a SFD delivery. The SFD vaccination by dMNs can enhance a much higher response than hMN, however fractional delivery administration by using dMNs does not lead to a superior response. Moreover, dMNs demonstrate no further increase in response by co-encapsulation of the adjuvant and a comparable or even higher response than, respectively, the current benchmarks: $AlPO_4$ adsorbed DT and DT-PI administered subcutaneously. These findings demonstrate the potential of dMNs as vaccine delivery device addressing to a SFD administration of an adjuvant-free vaccine to have a fast and high functional response.

Acknowledgements

We thank Amy Kogelman from Intravacc for her help with the neutralizing antibody assay.

REFERENCES

1. G. Du, M. Leone, S. Romeijn, G. Kersten, W. Jiskoot, J.A. Bouwstra, Immunogenicity of diphtheria toxoid and poly(I:C) loaded cationic liposomes after hollow microneedle-mediated intradermal injection in mice, Int J Pharm, 547 (2018) 250-257.
2. H. Jiang, Q. Wang, X. Sun, Lymph node targeting strategies to improve vaccination efficacy, J Control Release, 267 (2017) 47-56.
3. L.J. Peek, C.R. Middaugh, C. Berkland, Nanotechnology in vaccine delivery, Adv Drug Deliv Rev, 60 (2008) 915-928.
4. M. Leone, J. Monkare, J.A. Bouwstra, G. Kersten, Dissolving Microneedle Patches for Dermal Vaccination, Pharm Res, (2017).
5. E. Larraneta, M.T. McCrudden, A.J. Courtenay, R.F. Donnelly, Microneedles: A New Frontier in Nanomedicine Delivery, Pharm Res, 33 (2016) 1055-1073.
6. K. van der Maaden, W. Jiskoot, J. Bouwstra, Microneedle technologies for (trans)dermal drug and vaccine delivery, J Control Release, 161 (2012) 645-655.
7. N. Li, L.H. Peng, X. Chen, S. Nakagawa, J.Q. Gao, Transcutaneous vaccines: Novel advances in technology and delivery for overcoming the barriers, Vaccine, 29 (2011) 6179-6190.
8. Y.C. Kim, J.H. Park, M.R. Prausnitz, Microneedles for drug and vaccine delivery, Adv Drug Deliv Rev, 64 (2012) 1547-1568.
9. H.S. Gill, M.R. Prausnitz, Coated microneedles for transdermal delivery, J Control Release, 117 (2007) 227-237.
10. S.G. Reed, M.T. Orr, C.B. Fox, Key roles of adjuvants in modern vaccines, Nat Med, 19 (2013) 1597-1608.
11. O.S. Kumru, S.B. Joshi, D.E. Smith, C.R. Middaugh, T. Prusik, D.B. Volkin, Vaccine instability in the cold chain: mechanisms, analysis and formulation strategies, Biologicals, 42 (2014) 237-259.
12. P. Schipper, K. van der Maaden, S. Romeijn, C. Oomens, G. Kersten, W. Jiskoot, J. Bouwstra, Repeated fractional intradermal dosing of an inactivated polio vaccine by a single hollow microneedle leads to superior immune responses, J Control Release, 242 (2016) 141-147.
13. P.A. Buining, C. Pathmamanoharan, J.B.H. Jansen, H.N.W. Lekkerkerker, Preparation of Colloidal Boehmite Needles by Hydrothermal Treatment of Aluminum Alkoxide Precursors, J Am Ceram Soc, 74 (1991) 1303-1307.
14. A.M. Wierenga, T.A.J. Lenstra, A.P. Philipse, Aqueous dispersions of colloidal gibbsite platelets: synthesis, characterisation and intrinsic viscosity measurements, Colloid Surface A, 134 (1998) 359-371.
15. A.N. de Belder, K.O. Wik, Preparation and properties of fluorescein-labelled hyaluronate, Carbohydr Res, 44 (1975) 251-257.
16. I. Mile, A. Svensson, A. Darabi, M. Mold, P. Siesjo, H. Eriksson, Al adjuvants can be tracked in viable cells by lumogallion staining, J Immunol Methods, 422 (2015) 87-94.
17. M. Leone, M.I. Priester, S. Romeijn, M.R. Nejadnik, J. Monkare, C. O'Mahony, W. Jiskoot, G. Kersten, J.A. Bouwstra, Hyaluronan-based dissolving microneedles with high antigen content for intradermal vaccination: Formulation, physicochemical characterization and immunogenicity assessment, Eur J Pharm Biopharm, 134 (2019) 49-59.
18. M. Leone, B.H. van Oorschot, M.R. Nejadnik, A. Bocchino, M. Rosato, G. Kersten, C. O'Mahony, J. Bouwstra, K. van der Maaden, Universal Applicator for Digitally-Controlled Pressing Force and Impact Velocity Insertion of Microneedles into Skin, Pharmaceutics, 10 (2018).
19. K. van der Maaden, E. Sekerdag, W. Jiskoot, J. Bouwstra, Impact-insertion applicator improves reliability of skin penetration by solid microneedle arrays, Aaps J, 16 (2014) 681-684.
20. P. Schipper, K. van der Maaden, S. Romeijn, C. Oomens, G. Kersten, W. Jiskoot, J. Bouwstra, Determination of Depth-Dependent Intradermal Immunogenicity of Adjuvanted Inactivated Polio Vaccine Delivered by Microinjections via Hollow Microneedles, Pharm Res, 33 (2016) 2269-2279.
21. K. van der Maaden, S.J. Trietsch, H. Kraan, E.M. Varypataki, S. Romeijn, R. Zwier, H.J. van der Linden, G. Kersten, T. Hankemeier, W. Jiskoot, J. Bouwstra, Novel hollow microneedle technology for depth-controlled

microinjection-mediated dermal vaccination: a study with polio vaccine in rats, Pharm Res, 31 (2014) 1846-1854.
22. P. Schipper, K. van der Maaden, V. Groeneveld, M. Ruigrok, S. Romeijn, S. Uleman, C. Oomens, G. Kersten, W. Jiskoot, J. Bouwstra, Diphtheria toxoid and N-trimethyl chitosan layer-by-layer coated pH-sensitive microneedles induce potent immune responses upon dermal vaccination in mice, J Control Release, 262 (2017) 28-36.
23. Z. Ding, E. Van Riet, S. Romeijn, G.F. Kersten, W. Jiskoot, J.A. Bouwstra, Immune modulation by adjuvants combined with diphtheria toxoid administered topically in BALB/c mice after microneedle array pretreatment, Pharm Res, 26 (2009) 1635-1643.
24. P. Johansen, T. Storni, L. Rettig, Z. Qiu, A. Der-Sarkissian, K.A. Smith, V. Manolova, K.S. Lang, G. Senti, B. Mullhaupt, T. Gerlach, R.F. Speck, A. Bot, T.M. Kundig, Antigen kinetics determines immune reactivity, Proc Natl Acad Sci U S A, 105 (2008) 5189-5194.
25. A.C.I. Depelsenaire, S.C. Meliga, C.L. McNeilly, F.E. Pearson, J.W. Coffey, O.L. Haigh, C.J. Flaim, I.H. Frazer, M.A.F. Kendall, Colocalization of cell death with antigen deposition in skin enhances vaccine immunogenicity, J Invest Dermatol, 134 (2014) 2361-2370.
26. S.C. Meliga, C. Flaim, M. Veidt, M.A.F. Kend, The Mechanical Stress Caused by Micro-Projection Arrays Penetrating the Skin for Vaccine Delivery, Australian Journal of Multi-Disciplinary Engineering, 10 (2013).
27. K. Matsuo, Y. Yokota, Y. Zhai, Y.S. Quan, F. Kamiyama, Y. Mukai, N. Okada, S. Nakagawa, A low-invasive and effective transcutaneous immunization system using a novel dissolving microneedle array for soluble and particulate antigens (vol 161, pg 10, 2012), J Control Release, 184 (2014) 9-9.
28. C. Termeer, F. Benedix, J. Sleeman, C. Fieber, U. Voith, T. Ahrens, K. Miyake, M. Freudenberg, C. Galanos, J.C. Simon, Oligosaccharides of Hyaluronan activate dendritic cells via toll-like receptor 4, J Exp Med, 195 (2002) 99-111.
29. C.C. Termeer, J. Hennies, U. Voith, T. Ahrens, J.M. Weiss, P. Prehm, J.C. Simon, Oligosaccharides of hyaluronan are potent activators of dendritic cells, J Immunol, 165 (2000) 1863-1870.
30. M. Leone, S. Romeijn, B. Slutter, C. O'Mahony, G. Kersten, J.A. Bouwstra, Hyaluronan molecular weight: Effects on dissolution time of dissolving microneedles in the skin and on immunogenicity of antigen, Eur J Pharm Sci, 146 (2020) 105269.
31. E.J. Oh, K. Park, K.S. Kim, J. Kim, J.A. Yang, J.H. Kong, M.Y. Lee, A.S. Hoffman, S.K. Hahn, Target specific and long-acting delivery of protein, peptide, and nucleotide therapeutics using hyaluronic acid derivatives, J Control Release, 141 (2010) 2-12.
32. D. Gatto, S.W. Martin, J. Bessa, E. Pellicioli, P. Saudan, H.J. Hinton, M.F. Bachmann, Regulation of memory antibody levels: the role of persisting antigen versus plasma cell life span, J Immunol, 178 (2007) 67-76.
33. G. Crepeaux, H. Eidi, M.O. David, E. Tzavara, B. Giros, C. Exley, P.A. Curmi, C.A. Shaw, R.K. Gherardi, J. Cadusseau, Highly delayed systemic translocation of aluminum-based adjuvant in CD1 mice following intramuscular injections, J Inorg Biochem, 152 (2015) 199-205.
34. R.K. Gupta, Aluminum compounds as vaccine adjuvants, Adv Drug Deliver Rev, 32 (1998) 155-172.
35. M. Vogelbruch, B. Nuss, M. Korner, A. Kapp, P. Kiehl, W. Bohm, Aluminium-induced granulomas after inaccurate intradermal hyposensitization injections of aluminium-adsorbed depot preparations, Allergy, 55 (2000) 883-887.
36. M.L. Mbow, E. De Gregorio, N.M. Valiante, R. Rappuoli, New adjuvants for human vaccines, Curr Opin Immunol, 22 (2010) 411-416.
37. J.C. Joyce, H.E. Sella, H. Jost, M.J. Mistilis, E.S. Esser, P. Pradhan, R. Toy, M.L. Collins, P.A. Rota, K. Roy, I. Skountzou, R.W. Compans, M.S. Oberste, W.C. Weldon, J.J. Norman, M.R. Prausnitz, Extended delivery of vaccines to the skin improves immune responses, J Control Release, 304 (2019) 135-145.
38. V. Bachy, C. Hervouet, P.D. Becker, L. Chorro, L.M. Carlin, S. Herath, T. Papagatsias, J.B.

Barbaroux, S.J. Oh, A. Benlahrech, T. Athanasopoulos, G. Dickson, S. Patterson, S.Y. Kwon, F. Geissmann, L.S. Klavinskis, Langerin negative dendritic cells promote potent CD8+ T-cell priming by skin delivery of live adenovirus vaccine microneedle arrays, Proc Natl Acad Sci U S A, 110 (2013) 3041-3046.

39. C. Edens, M.L. Collins, J.L. Goodson, P.A. Rota, M.R. Prausnitz, A microneedle patch containing measles vaccine is immunogenic in non-human primates, Vaccine, 33 (2015) 4712-4718.
40. A. Pattani, P.F. McKay, R.F. Donnelly, M.J. Garland, K. Migalska, C.M. Cassidy, R. Malcolm, R.J. Shattock, R.M. Curran, Microneedle Mediated Intradermal Delivery of Adjuvanted Recombinant HIV-1 CN54gp140 Effectively Primes Mucosal Boost Inoculations, Aids Res Hum Retrov, 27 (2011) A69-A69.
41. Z. Zhu, X. Ye, Z. Ku, Q. Liu, C. Shen, H. Luo, H. Luan, C. Zhang, S. Tian, C. Lim, Z. Huang, H. Wang, Transcutaneous immunization via rapidly dissolvable microneedles protects against hand-foot-and-mouth disease caused by enterovirus 71, J Control Release, 243 (2016) 291-302.
42. P.A. Buining, A.P. Philipse, H.N.W. Lekkerkerker, Phase-Behavior of Aqueous Dispersions of Colloidal Boehmite Rods, Langmuir, 10 (1994) 2106-2114.
43. A.A. Verhoeff, R.P. Brand, H.N.W. Lekkerkerker, Tuning the birefringence of the nematic phase in suspensions of colloidal gibbsite platelets, Mol Phys, 109 (2011) 1363-1371.

SUPPLEMENTARY MATERIAL

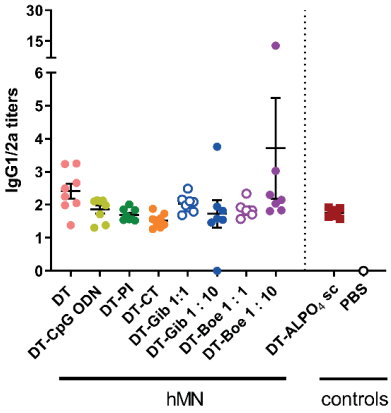


Figure S1. DT-specific IgG1 and IgG2a ratio titers on day 63. Bars represent mean ± SEM, n = 8. No significant difference among the groups was found ($p > 0.05$). hMN, hollow microneedle; DT, diphtheria toxoid; PI, poly(I:C); CT, cholera toxin; Gib, gibbsite; Boe, boehmite; $AlPO_4$, aluminum phosphate.

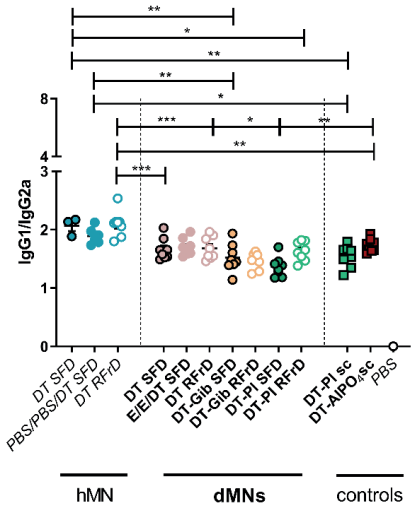


Figure S2. DT-specific IgG1 and IgG2a ratio titers measured in BALB/c mice on day 63. Bars represent mean ± SEM, n = 8. *$p < 0.05$, **$p < 0.01$, ***$p < 0.001$. SFD, single-full dose; RFrD, repeated-fractional dose; dMNs, dissolving microneedles; hMN, hollow microneedle; DT, diphtheria toxoid; PI, poly(I:C); Gib, gibbsite; E, empty dMNs; $AlPO_4$, aluminum phosphate.

Chapter 7

Summary, prospects and conclusion

SUMMARY

Vaccination is one of the most effective method for reducing infection-related deaths and morbidity around the world. The principle of vaccination was first published by Edward Jenner in 1796 [1] and, since the advent of the microbiology era in the second half of the 19th century, numerous types of vaccines have been developed and licensed for both human and veterinary use.

Many factors have an impact on vaccination coverage [2-4]. These include costs, concerns about vaccine safety and efficacy by the general public [5], religious believes, the spread of mis-information by “anti-vax” groups [6]. Some other factors are related with the way vaccines are administered. Injected vaccines cause discomfort by a substantial part of the target group. Furthermore, needlestick injuries and re-use of needles and syringes are health risks for medical personnel as well as the vaccinated. To overcome these problems, vaccination in a minimally invasive and pain-free manner may improve vaccination coverage.

Microneedle-based dermal immunization is a promising alternative to the classical conventional administration of vaccine by means of hypodermic needles such as intramuscular and subcutaneous injections. The skin is an excellent immune competent organ containing many antigen presenting cells, such as Langerhans cells and dendritic cells, to induce an effective immune response. This is a consequence of the fact that the skin, differently than muscle and subcutaneous tissue, is directly exposed to the surrounding environment and protects the body against pathogens, not only by forming an effective physical barrier but also by extensive immune surveillance just beneath the barrier.

Of the several types of microneedles [7], the focus of this thesis is on the development of dissolving microneedles, using hyaluronan as matrix polymer.

This thesis starts with a detailed overview of dissolving microneedle research and development (*Chapter 2*), describing methods to produce dissolving microneedles and their challenges, as well as the microneedle characterization methods and antigen stability aspects. Furthermore, this chapter contains a detailed overview of the immunogenicity of several antigens encapsulated in dissolving microneedles. Immune responses generated after immunization by dissolving microneedles have been compared with conventional injection. Frequently, the responses after dermal immunization are at least comparable to conventional injection. Additionally, several factors influencing the immunogenicity have been discussed: besides the use of conventional adjuvants, the microneedle design such as needle spacing and needle geometry may also influence the immunogenicity. Finally, the current status of the clinical development of dissolving microneedles is discussed. Dissolving microneedle devices are in early clinical development [8, 9] and may reach the market within a decade.

The research described in *Chapter 3* focuses on the development of a digitally-controlled microneedle applicator to insert microneedles into the skin via impact insertion (velocity) or via pressing force insertion. Six microneedle arrays with different geometries, needle density and/or consisting of different materials were applied onto *ex vivo* human skin varying velocities and pressing forces to assess differences in penetration efficiency of the skin and antigen delivery in the skin. Application of microneedle arrays by impact application, with a specific angle of application, could generate a more efficient piercing of the skin than application via pressing force. The delivery of the antigen in the skin could be increased by increasing the velocity or pressure, demonstrating the importance of a controlled application of the microneedle array on the skin by means of an applicator.

In *Chapter 4* a novel mold design is described for the manufacturing of dissolving microneedles by micromolding, avoiding waste of antigen in the backplate. During the original manufacturing one backplate with 9 arrays was produced. This single backplate resulted in non-homogeneous antigen distribution between arrays. The new method eliminates this problem as one mold contains 9 separate templates for the arrays. Using this mold, dissolving microneedles with increasing antigen loading were fabricated to assess the physicochemical effects of maximal antigen content. Dissolving microneedles could be fabricated with an ovalbumin:hyaluronan ratio of 1:1 (w/w), with excellent sharpness and efficient skin piercing properties, even after storage at high temperature and high humidity. The protein did not aggregate during the fabrication of dissolving microneedles. However, when using the same skin dissolution time, increased antigen loading led to a decrease in dissolution volume of microneedles in *ex vivo* human skin. Finally an immunization study in mice by using dissolving microneedles induced antibody responses comparable to those obtained by conventional immunization and there was a faster antibody response compared to dermal immunization by means of a single hollow microneedle.

In *Chapter 5* the optimal hyaluronan molecular weight for the fabrication of dissolving microneedles with regard to microneedle integrity and immune modulating properties was identified. These studies were initiated as it was reported that low MW HA showed immune modulating properties. Hyaluronan ranged from a molecular weight of 4.8 kDa up to 1.8 MDa and all demonstrated to be inert material. No effects on the antibody response generated in mice or on the CD4 T-cell responses after immunization or after *in vitro* stimulation with the model antigen ovalbumin were detected. However, not all the hyaluronan molecular weights of the selected range were suitable for microneedle fabrication: too high molecular weight resulted in a too viscous formulation to be used for micromolding while too low molecular weight generated fragile microneedle arrays showing a lack of structure. Furthermore, longer application time of dissolving microneedles in the skin was necessary for a complete dissolution of high hyaluronan molecular weight dissolving microneedles than for low hyaluronan molecular weight ones, leading to the selection of the 20 kDa HA to fabricate dissolving microneedles.

The aim of *Chapter 6* was to determine whether repeated-fractional intradermal administration of the antigen diphtheria toxoid could enhance the response compared to a single administration in the presence or absence of adjuvants with both hollow and dissolving microneedles. After a selective immunization screening, poly(I:C) and gibbsite, a nanoparticulate alum based adjuvant, were selected as adjuvants and encapsulated with diphtheria toxoid in dissolving microneedles in full or fractional diphtheria toxoid(-adjuvant) dose. Regardless the composition, it was possible to fabricate sharp dissolving microneedles capable to penetrate the skin and dissolve within 20 minutes depositing the intended diphtheria toxoid(-adjuvant) dose. Vaccination by dissolving microneedles without adjuvant, led to a superior response as compared to a hollow microneedle. Repeated dosing with dissolving microneedles did not further increase the immune responses. However, repeated-fractional dosing with a hollow microneedle led to a higher immune response than single-full dose and reached the same level of response as using dissolving microneedles. Furthermore, adjuvanted diphtheria toxoid co-encapsulated in dissolving microneedle did not increase further the immune response. The response after applying dissolving microneedles without adjuvant was comparable to conventional subcutaneous injections of diphtheria toxoid-$AlPO_4$ in a 15 times higher antigen dose as well as diphtheria toxoid-poly(I:C) in a similar antigen dose. In conclusion, single-full dermal dose diphtheria toxoid administration by means of dissolving microneedle led to a superior response without the use of adjuvants. Based on results in this study, it may be possible that immunization by dissolving microneedle will result in efficient immune responses while only using a single administration with a lower antigen dose as compared to subcutaneous administration.

PROSPECTS

Dissolving microneedles: challenges and next steps in development

Although dissolving microneedles as vaccine delivery device have huge potential, pharma companies are still facing hurdles that must be overcome. Before vaccine-loaded dissolving microneedles will appear as licensed products, the accuracy of vaccine delivery need to be increased and the ease of application of microneedle arrays on the skin need to be improved. To achieve this, the research should focus on i) the formulation of a vaccine product, not only taking into account the shelf life of the final product, but also antigen loss during manufacturing should be acceptable, ii) increase in antigen loading and its stability in dMNs, iii) an efficient insertion, and dissolution, of the microneedle in the skin, iv) product sterility for which new production procedures have to be developed, v) adjuvants that may need to be added for less immunogenic antigens, vi) the scale-up of the manufacturing process.

A first challenge encountered during the fabrication of dissolving microneedles, especially in micromolding, is the **loss of antigen** in the backplate of the microneedle array, that increases the cost of vaccination. In the literature hardly any data are available on formulation volume

and antigen amount used for the fabrication of dMN array, the antigen amount present in the dMN tips and on the dose delivered in the skin. This would highlight the important drawback related to a low fabrication efficiency in terms of antigen incorporation. In this thesis we attempted to optimize the PDMS mold design to overcome this problem. However, future research should keep focus on developing methods to cast the vaccine formulation only in the microneedle tips of the mold in order to reduce vaccine loss in the backplate [10, 11]. This would make vaccination using dissolving microneedles more affordable, especially for developing countries.

In Chapter 4 of the present thesis, increase in **antigen loading** in dMNs has been investigated and it was observed that, up to a weight ratio antigen:hyaluronan of 1:1, it was still possible to fabricate sharp dMNs resulting in **antigen stability** after fabrication. However, these studies have been conducted using OVA, a very stable model antigen. Thus, several hurdles related to the antigen loading in dMNs should be taken into account, such as antigen stability when working with less stable antigens, solubility issues when high antigen concentration is needed to deliver sufficient antigen dermally for a proper response, etc. It is known that the physical stability of the antigen is relevant to avoid uncontrolled immune response, thus these aspects should trigger new studies to explore themes hardly reported in literature.

Another critical issue is an efficient and complete microneedle insertion into the skin. When the microneedles have a geometry and length causing an incomplete insertion in the skin, this results in **incomplete dissolution**. This could lead to inconsistent dosing and waste of antigen. Furthermore vaccinees should wear patches long enough to ensure complete microneedle dissolution avoiding failure in the vaccine delivery related to the dissolution [12]. Patches may be removed too early, introducing an unwanted variable in the delivery of the vaccine. To overcome these problems of too early removal of the patch or incomplete microneedle insertion into the skin, some ideas have been proposed, such as i) arrow-head dissolving microneedles [13] composed of polymer arrowheads that, upon insertion in the skin, separate from the metal shaft on which they are mounted and remain embedded in the skin for subsequent dissolution and drug release and ii) patchless dissolving microneedle with a system capable of inserting drug-loaded dissolving microneedles in the skin as individual microneedles [14]. However, these ideas have their drawbacks including i) generation of long microneedles (>600 μm [13]) that, although potentially enhancing the immune response more than short microneedles [15], are more likely to induce pain [16], ii) use of a device for the dissolving microneedle insertion in the skin that may need trained personnel and can increase costs for their application. It would be then necessary to work on the choice of the matrix material and the formulation composition in order to reach very short application time (1-2 minutes) needed for the dissolution of the dMNs. In this regard, an application time of hours [12] would result in too long applications for a real-life vaccination.

It is important that microneedle products are sterile. In light of this, the **sterile manufacture** of microneedles is essential and should be performed accordingly to specific sterility requirements to guarantee product safety [17]. Sterilization methods should be incorporated in the manufacturing processes avoiding modification of the microneedle loaded vaccine and also an increase in manufacturing costs. For example, terminal sterilization using gamma irradiation, moist heat or microwave heating can be less expensive than aseptic manufacturing, however it can damage the microneedles or the product cargo. Several materials used for dissolving microneedle production have been shown to possess antimicrobial properties, showing no microbial growth upon storage and are, therefore, highly unlikely to cause skin or systemic infection [18]. In such cases, a fabrication of microneedles with the assurance of a low bioburden may be sufficient to avoid sterile manufacture and obtain regulatory approval.

For some less immunogenic antigens the addition of **adjuvants** may still be essential to obtain a high enough immune response. However, because of safety concerns, not all adjuvants are feasible for dermal application. An example is the classical aluminum preparations inducing palpable persistent intradermal injection-site nodules in mice [19]. On the one hand the avoidance of adjuvant would make the vaccine product less complex and thus less likely to undergo interactions affecting stability, on the other hand including adjuvants may lead to antigen dose sparing.

An important step to progress is the **scale-up** of the manufacturing process. Currently, an abundance of small-scale production methods are present in literature (see Chapter 2) by which a number of steps need to be undertaken (e.g. centrifuge and vacuum steps for the micromolding) that pose a challenge in terms of transfer to a larger scale. Furthermore, guidance related to good manufacturing practice, pharmacopoeial standards and appropriate quality control tests specific to microneedle devices are required [20]. Specific regulatory guidelines concerning packaging, disposal, assurance of correct use are needed. However, due to the innovative nature of the technology, the lack of regulation remains a barrier to the availability of a dissolving microneedle product. Although the use of dissolving microneedles for vaccination is promising, there are not yet dissolving microneedle products on the market. This is expected to change in the next decade as a high number of studies in the field continues to accumulate and some products are in clinical development [8, 9]. Currently some companies are setting up a production of dissolving microneedles for skin care cosmetics [21] and for delivery of biologics across the skin [22]. The latter with a successfully completed Phase 2a clinical evaluation.

Once manufacturing processes are optimized and regulatory hurdles are solved, vaccination by means of dissolving microneedles may become a keystone in improving vaccination coverage around the world.

The big potential of dissolving microneedles

Although dissolving microneedles may have still a long development route before being ready as product for marketing authorization, they have a great potential over the other microneedle types: dissolving microneedles consist of dry formulations which enhances the vaccine stability compared to liquid formulation used in traditional vaccination routes [23, 24]. Because of this increased stability, these microneedles could circumvent the need for a cold-chain supply and be ideal for vaccine campaigns in low income countries. This would significantly reduce vaccination costs for transportation and storage and therefore increase the vaccination coverage and the efficiency of vaccination programs.

Additionally, vaccination by means of dissolving microneedles showed, in most of the cases, a comparable or even higher response than by conventional injection (see *Chapter 2*). The antigen dose sparing, as illustrated by the results described in Chapter 6, provides a further strong potential of dissolving microneedles for dermal vaccination.

The importance of microneedle application

In this thesis, two microneedle types have been used for administration of vaccines: a hollow microneedle and dissolving microneedles. Both microneedle types require application devices.

Controlled and precise injection volume of the vaccine in the skin by means of a hollow microneedle may require a complex device with an applicator for controlled depth piercing of the skin and a pump for a controlled dermal microinjection.

Dissolving microneedles can be applied instantaneous and would take short time for dissolution in the skin. However, the use of an applicator may not be feasible in areas with a lack of infrastructure. Applicator failure or applicator loss may disrupt immunization programs locally. Additionally, a device for the application may increase the vaccination costs.

In this regard, an important improvement would be skin application of microneedles without the use of a device. This may avoid the need for trained personnel and should make self-administration possible especially in remote locations in the world or in case of pandemic disease outbreaks. Studies show that using an applicator improves the efficiency and reproducibility of microneedle insertion [25] and that short microneedles (300 µm), but also less sharp microneedles, may have a lower penetration efficiency in the skin than longer ones (>550 µm) [26-28] and thus the use of an applicator can be crucial for their efficient piercing in the skin. Manual application avoiding the use of an applicator is possible and successful [8, 9] if longer microneedles are used. In this case, long needles can still be considered much less invasive than hypodermic needles, keeping their advantage in a

reduced generation of pain sensation. Table 1 summarizes the pros and cons of applicator use in microneedle application.

Table 1. Advantages and disadvantages of manual application and application by the use of an applicator.

Manual application		Application by the use of an applicator	
Advantages	**Disadvantages**	**Advantages**	**Disadvantages**
Low production costs	Limitation in microneedle length: application of long microneedles only	No limitation in microneedle length (application of short microneedles)	Higher production costs of the system
No need for trained personnel	Use of long microneedles may generate pain sensation	High efficiency and reproducibility in microneedle piercing	Need for trained personnel
			More dependent on technology on site

The role of hyaluronan in vaccination by means of dissolving microneedles

As demonstrated in *Chapter 5*, the hyaluronan used as matrix material does not have an effect on the immune response after vaccination by dissolving microneedles despite the reported immune modulating properties of low molecular weight hyaluronan [29]. However, in literature hyaluronan conjugated with ovalbumin can activate naive dendritic cells *in vitro* more efficiently than ovalbumin only [30] and conjugation can increase the size of compounds to promote lymphatic delivery [31]. Furthermore, intramuscular injection of hyaluronan-ovalbumin conjugates induced a higher immune response than ovalbumin alone [30]. To this end, it would be interesting to encapsulate hyaluronan-antigen conjugates in dissolving microneedles and assess the immunogenicity.

CONCLUSION

The research described in this thesis showed that dissolving microneedles used for dermal delivery of vaccines can evoke an antigen specific immune response comparable with the conventional subcutaneous route. However, further research is needed to optimize this technology and overcome several manufacturing and application hurdles in order to translate research to commercial products beneficial for the patients.

REFERENCES

1. A.M. Stern, H. Markel, The history of vaccines and immunization: familiar patterns, new challenges, Health Aff (Millwood), 24 (2005) 611-621.
2. P.M. Frew, A.K. Fisher, M.M. Basket, Y. Chung, J. Schamel, J.L. Weiner, J. Mullen, S.B. Omer, W.A. Orenstein, Changes in childhood immunization decisions in the United States: Results from 2012 & 2014 National Parental Surveys, Vaccine, 34 (2016) 5689-5696.
3. C. Hough-Telford, D.W. Kimberlin, I. Aban, W.P. Hitchcock, J. Almquist, R. Kratz, K.G. O'Connor, Vaccine Delays, Refusals, and Patient Dismissals: A Survey of Pediatricians, Pediatrics, 138 (2016).
4. H.J. Larson, A. de Figueiredo, Z. Xiahong, W.S. Schulz, P. Verger, I.G. Johnston, A.R. Cook, N.S. Jones, The State of Vaccine Confidence 2016: Global Insights Through a 67-Country Survey, EBioMedicine, 12 (2016) 295-301.
5. J.S. Gerber, P.A. Offit, Vaccines and autism: a tale of shifting hypotheses, Clin Infect Dis, 48 (2009) 456-461.
6. Poland GA and Jacobson RM, Understanding those who do not understand: a brief review of the anti-vaccine movement, Vaccine, 19 (2001) 2440-2445.
7. K. van der Maaden, W. Jiskoot, J. Bouwstra, Microneedle technologies for (trans)dermal drug and vaccine delivery, J Control Release, 161 (2012) 645-655.
8. J. Arya, S. Henry, H. Kalluri, D.V. McAllister, W.P. Pewin, M.R. Prausnitz, Tolerability, usability and acceptability of dissolving microneedle patch administration in human subjects, Biomaterials, 128 (2017) 1-7.
9. N.G. Rouphael, M. Paine, R. Mosley, S. Henry, D.V. McAllister, H. Kalluri, W. Pewin, P.M. Frew, T. Yu, N.J. Thornburg, S. Kabbani, L. Lai, E.V. Vassilieva, I. Skountzou, R.W. Compans, M.J. Mulligan, M.R. Prausnitz, T.-M.S. Group, The safety, immunogenicity, and acceptability of inactivated influenza vaccine delivered by microneedle patch (TIV-MNP 2015): a randomised, partly blinded, placebo-controlled, phase 1 trial, Lancet, 390 (2017) 649-658.
10. L.Y. Chu, S.O. Choi, M.R. Prausnitz, Fabrication of dissolving polymer microneedles for controlled drug encapsulation and delivery: Bubble and pedestal microneedle designs, J Pharm Sci, 99 (2010) 4228-4238.
11. D.D. Zhu, Q.L. Wang, X.B. Liu, X.D. Guo, Rapidly separating microneedles for transdermal drug delivery, Acta Biomater, 41 (2016) 312-319.
12. S. Hirobe, H. Azukizawa, T. Hanafusa, K. Matsuo, Y.S. Quan, F. Kamiyama, I. Katayama, N. Okada, S. Nakagawa, Clinical study and stability assessment of a novel transcutaneous influenza vaccination using a dissolving microneedle patch, Biomaterials, 57 (2015) 50-58.
13. L.Y. Chu, M.R. Prausnitz, Separable arrowhead microneedles, J Control Release, 149 (2011) 242-249.
14. S.F. Lahiji, M. Dangol, H. Jung, A patchless dissolving microneedle delivery system enabling rapid and efficient transdermal drug delivery, Sci Rep, 5 (2015) 7914.
15. K. Matsuo, Y. Yokota, Y. Zhai, Y.S. Quan, F. Kamiyama, Y. Mukai, N. Okada, S. Nakagawa, A low-invasive and effective transcutaneous immunization system using a novel dissolving microneedle array for soluble and particulate antigens (vol 161, pg 10, 2012), J Control Release, 184 (2014) 9-9.
16. Y.C. Kim, J.H. Park, M.R. Prausnitz, Microneedles for drug and vaccine delivery, Adv Drug Deliver Rev, 64 (2012) 1547-1568.
17. M.T. McCrudden, A.Z. Alkilani, A.J. Courtenay, C.M. McCrudden, B. McCloskey, C. Walker, N. Alshraiedeh, R.E. Lutton, B.F. Gilmore, A.D. Woolfson, R.F. Donnelly, Considerations in the sterile manufacture of polymeric microneedle arrays, Drug Deliv Transl Res, 5 (2015) 3-14.
18. R.F. Donnelly, T.R.R. Singh, A.Z. Alkilani, M.T.C. McCrudden, S. O'Neill, C. O'Mahony, K. Armstrong, N. McLoone, P. Kole, A.D. Woolfson, Hydrogel-forming microneedle arrays exhibit antimicrobial properties: Potential for enhanced patient safety, Int J Pharmaceut, 451 (2013) 76-91.
19. M. Vogelbruch, B. Nuss, M. Korner, A. Kapp, P. Kiehl, W. Bohm, Aluminium-induced granulomas after inaccurate intradermal hyposensitization injections of aluminium-

adsorbed depot preparations, Allergy, 55 (2000) 883-887.
20. R.E. Lutton, J. Moore, E. Larraneta, S. Ligett, A.D. Woolfson, R.F. Donnelly, Microneedle characterisation: the need for universal acceptance criteria and GMP specifications when moving towards commercialisation, Drug Deliv Transl Res, 5 (2015) 313-331.
21. Nissha Co., Ltd., Dissolving Microneedle Patch, in:

    https://www.nissha.com/english/products/allproducts/dds.html, date of access January 2020.
22. Corium, Corium's MicroCor® system utilizes dissolving microstructures (microneedles) for innovative, needle-free delivery of biologics across the skin, in:

    http://www.coriumintl.com/home/technology/microcor/, date of access January 2020.
23. R.R. Thakur, I.A. Tekko, F. Al-Shammari, A.A. Ali, H. McCarthy, R.F. Donnelly, Rapidly dissolving polymeric microneedles for minimally invasive intraocular drug delivery, Drug Deliv Transl Res, 6 (2016) 800-815.
24. X. Chen, G.J. Fernando, M.L. Crichton, C. Flaim, S.R. Yukiko, E.J. Fairmaid, H.J. Corbett, C.A. Primiero, A.B. Ansaldo, I.H. Frazer, L.E. Brown, M.A. Kendall, Improving the reach of vaccines to low-resource regions, with a needle-free vaccine delivery device and long-term thermostabilization, J Control Release, 152 (2011) 349-355.
25. K. van der Maaden, E. Sekerdag, W. Jiskoot, J. Bouwstra, Impact-Insertion Applicator Improves Reliability of Skin Penetration by Solid Microneedle Arrays, Aaps J, 16 (2014) 681-684.
26. M.I. Haq, E. Smith, D.N. John, M. Kalavala, C. Edwards, A. Anstey, A. Morrissey, J.C. Birchall, Clinical administration of microneedles: skin puncture, pain and sensation, Biomed Microdevices, 11 (2009) 35-47.
27. F.J. Verbaan, S.M. Bal, D.J. van den Berg, J.A. Dijksman, M. van Hecke, H. Verpoorten, A. van den Berg, R. Luttge, J.A. Bouwstra, Improved piercing of microneedle arrays in dermatomed human skin by an impact insertion method, J Control Release, 128 (2008) 80-88.
28. F.J. Verbaan, S.M. Bal, D.J. van den Berg, W.H. Groenink, H. Verpoorten, R. Luttge, J.A. Bouwstra, Assembled microneedle arrays enhance the transport of compounds varying over a large range of molecular weight across human dermatomed skin, J Control Release, 117 (2007) 238-245.
29. A. D'Agostino, A. Stellavato, L. Corsuto, P. Diana, R. Filosa, A. La Gatta, M. De Rosa, C. Schiraldi, Is molecular size a discriminating factor in hyaluronan interaction with human cells?, Carbohyd Polym, 157 (2017) 21-30.
30. K.S. Kim, H. Kim, Y. Park, W.H. Kong, S.W. Lee, S.J.J. Kwok, S.K. Hahn, S.H. Yun, Noninvasive Transdermal Vaccination Using Hyaluronan Nanocarriers and Laser Adjuvant, Adv Funct Mater, 26 (2016) 2512-2522.
31. H. Liu, D.J. Irvine, Guiding principles in the design of molecular bioconjugates for vaccine applications, Bioconjug Chem, 26 (2015) 791-801.

Nederlandse samenvatting

SAMENVATTING

Vaccinatie is een van de meest effectieve methoden voor het verminderen van infectie-gerelateerde morbiditeit en mortaliteit. Het principe van vaccinatie werd voor het eerst gepubliceerd door Edward Jenner in 1796 [1] en, sinds de ontwikkeling van de microbiologie in de tweede helft van de 19e eeuw, zijn er talloze vaccins ontwikkeld en goedgekeurd voor zowel menselijk- als veterinair gebruik.

Verscheidene factoren kunnen de vaccinatiegraad beïnvloeden [2-4]. Hieronder vallen onder andere de kosten, zorgen van de bevolking aangaande de veiligheid en effectiviteit [5], religieuze overtuigingen, en de verspreiding van onjuist informatie door anti-vaxxers [6]. Andere factoren zijn gerelateerd aan de manier waarop de vaccinaties worden toegediend.
Het gebruik van injecteerbare vaccins wordt door een groot deel van de doelgroep gezien als hinderlijk. Daarnaast zorgen prikaccidenten en hergebruik van injectienaalden ook voor gezondheidsrisico's voor zowel het zorgpersoneel als de gevaccineerde. Om deze problemen te voorkomen, kan vaccinatie op een minimaal invasieve- en pijnvrije manier de vaccinatiegraad verbeteren.

Dermale immunisatie via micronaalden is een veelbelovend alternatief voor de klassieke toediening van vaccins door middel van intramusculaire en subcutane injecties. De huid is een immunocompetent orgaan welke veel antigeen-presenterende cellen bevat, zoals Langerhans cellen en dendritische cellen, om een effectieve immuunrespons op te wekken. Dit is een gevolg van het feit dat de huid, in tegenstelling tot spier- en onderhuids weefsel, direct is blootgesteld aan de omgeving en daarmee het lichaam beschermt tegen ziekteverwekkers, niet alleen door het vormen van een effectieve fysieke barrière, maar ook door de daaronder gelegen omvangrijke immuunbewaking.

Van de verschillende soorten micronaalden [7] ligt de focus van dit proefschrift op de ontwikkeling van oplosbare micronaalden, waarbij hyaluronzuur (HA) als matrixpolymeer wordt gebruikt.

Dit proefschrift begint met een gedetailleerd overzicht van onderzoek en ontwikkeling naar oplosbare micronaalden (*Hoofdstuk 2*), waarin methoden worden beschreven voor het produceren van oplosbare micronaalden, evenals de karakteriseringsmethoden en aspecten van antigeen-stabiliteit. Verder bevat dit hoofdstuk een gedetailleerd overzicht waarin de immunogeniciteit van verschillende antigene, welke ingekapseld zijn in oplosbare micronaalden, wordt beschreven. Hierin wordt het verschil in de opgewekte immuunrespons na immunisatie vergeleken tussen oplosbare micronaalden en conventionele injecties.
Hieruit blijkt dat de respons na dermale immunisatie i.h.a. op zijn minst vergelijkbaar is met conventionele injecties. Daarnaast worden verschillende factoren besproken die van invloed

zijn op de immunogeniciteit: naast het gebruik van adjuvantia (componenten die het aangeboren immuunsysteem stimuleren), kan het ontwerp van de micronaald zoals de naaldafstand en -geometrie ook van invloed zijn. Ten slotte wordt de huidige status van de klinische ontwikkeling van oplosbare micronaalden besproken. Deze bevindt zich nog in een vroeg stadium, maar vaccins geformuleerd in oplosbare micronaalden kunnen binnen een decennium op de markt verschijnen.

De studie beschreven in *Hoofdstuk 3* focust zich op de ontwikkeling van een digitaal aangestuurde micronaald applicator om de micronaalden in de huid te brengen via impact insertie (snelheid) of via statische kracht. Zes micronaald arrays met verschil in geometrie, naalddichtheid en/of bestaande uit verschillende materialen werden aangebracht op *ex vivo* humane huid met variërende snelheden en drukkrachten om het verschil in penetratie efficiëntie en antigeen afgifte te analyseren. Het aanbrengen van micronaald arrays door middel van impact insertie met een specifieke applicatiehoek resulteerde in een efficiëntere dermale penetratie in vergelijking met applicatie via statische kracht. De dosering in de huid wordt positief beïnvloed door het verhogen van de snelheid of de kracht, waarmee tevens het belang wordt aangetoond van het gebruik van een micronaald applicator voor een gecontroleerde toepassing in de huid.

In *Hoofdstuk 4* wordt een nieuw ontwerp beschreven voor het produceren van oplosbare micronaalden via micromolding, waarmee het verlies van antigenen aan structuren buiten de individuele micronaalden wordt verminderd. In het originele productieproces werd een gietvorm gebruikt waarin 9 arrays tegelijkertijd werden gemaakt, die aan de achterzijde verbonden werden een enkele matrix laag. Deze backplate zorgde voor een niet-homogene antigeen verdeling tussen de arrays. De nieuwe methoden voorkomt dit probleem doordat één gietvorm 9 afzonderlijke arrays bevat. Vervolgens werd met behulp van dit ontwerp onderzocht in welke mate oplosbare micronaalden met hogere antigeen dosis konden worden vervaardigd. Oplosbare micronaalden met een ratio ovalbumine:hyaluronzuur 1:1 (w/w) konden worden geproduceerd, welke uitstekende scherpte en penetratie efficiëntie vertoonden, zelfs na opslag bij hogere temperaturen en hoge luchtvochtigheid. Het modelantigeen aggregeerde niet tijdens het productieproces. Er was echter wel een verschil merkbaar in de oplosbaarheid van de micronaalden in de huid; een hogere antigeenbelading leidde tot een verminderd opgelost volume na eenzelfde insertietijd in *ex vivo* humane huid. Tenslotte toonde een immunisatiestudie in muizen aan dat oplosbare micronaalden een antilichaam respons induceerden welke vergelijkbaar is met conventionele immunisatie. Daarnaast ontwikkelde de antilichaam respons zich sneller in vergelijking met dermale immunisatie via een enkele holle micronaald.

In *Hoofstuk 5* werd het optimale molecuulgewicht (MW) van HA voor de vervaardiging van oplosbare micronaalden bepaald met betrekking tot micronaald integriteit en immuunmodulerende eigenschappen. Deze studies zijn uitgevoerd omdat eerdere publicaties aantoonden dat HA met een laag MW het aangeboren immuunsysteem zou

kunnen stimuleren. Het MW van hyaluronzuur varieerde tussen de 4.8 kDa tot 1.8 MDA, en allen waren immunologisch inert. Antilichaamresponsen noch CD4 T-cel responsen tegen het model antigeen ovalbumine werden beïnvloed door aanwezigheid van HA met verschillende MW. Echter niet alle moleculaire massa's van HA binnen het aangegeven bereik waren geschrikt voor de productie van micronaalden; een te hoog MW resulteerde in een te viskeuze formulering voor micromolding, terwijl een te laag MW zorgde voor fragiele micronaald arrays. Daarnaast vereisten oplosbare micronaalden met een hoog MW een langere insertietijd in de huid in vergelijking met de lage MW formuleringen, waardoor uiteindelijk 20 kDa werd geselecteerd voor de vervaardiging van oplosbare micronaalden.

Het doel van *Hoofdstuk 6* was om te bepalen of herhaalde fractionele intradermale toediening van difterietoxoïd zorgt voor een verbetering in respons in vergelijking met een enkele toediening in de aan- of afwezigheid van adjuvantia met zowel de holle- als de oplosbare micronaalden. Na een initiële screening werden poly(I:C) en gibbsiet, een adjuvant gebaseerd op aluminiumhydroxide, geselecteerd en ingekapseld met de difterietoxoïd in oplosbare micronaalden in volledige of herhaalde fractionele difterietoxoïd (-adjuvant) dosis. Ongeacht de samenstelling was het mogelijk om scherpe oplosbare micronaalden te vervaardigen, die in staat waren om de huid te penetreren en vervolgens binnen 20 minuten op te lossen en daarmee de difterietoxoïd (-adjuvant) dosis af te leveren. Vaccinatie door middel van oplosbare micronaalden zonder toegevoegd adjuvant leidde tot een verhoogde respons in vergelijking met toediening via een enkele holle micronaald. Herhaalde doseringen met oplosbare micronaalden zorgden niet voor een extra verhoging in de immuunreactie.
Echter, herhaalde fractionele doseringen met een holle micronaald leidde tot een hogere immuunrespons in vergelijking met een enkele volledige dosis, maar bereikte uiteindelijk hetzelfde responsniveau als toediening via oplosbare micronaalden. Daarnaast zorgde inkapseling van het adjuvant samen met difterietoxoïd in oplosbare micronaalden niet voor een verdere verhoging van de immuunrespons. De reactie na toediening van oplosbare micronaalden zonder adjuvant was vergelijkbaar met die van conventionele subcutane injecties van difterietoxoïd-AlPO4 in een 15 maal hogere antigeendosis, en difterietoxoïd-poly (I:C) adjuvant in een vergelijkbare dosis. Hieruit kan geconcludeerd worden dat dermale toediening van een enkele, volledige dosis difterietoxoïd via oplosbare micronaalden leidt tot een verbeterde respons, zelfs zonder het gebruik van adjuvantia. Op basis van de resultaten van dit onderzoek is het mogelijk dat immunisatie via oplosbare micronaalden zal resulteren in een efficiëntere immuunreactie, waarbij – in tegenstelling tot subcutane toediening - slechts één toediening met een lagere antigeen dosis vereist is.

PERSPECTIEF

Oplosbare micronaalden: uitdaging en volgende stappen in de ontwikkeling

Hoewel de verwachtingen hoog gespannen zijn om oplosbare micronaalden als vaccin te kunnen toepassen, moeten de farmaceutische bedrijven nog een aantal hordes nemen. Voordat de met vaccin geladen micronaalden op de markt zullen verschijnen, moet de toedieningsnauwkeurigheid verhoogd worden en de toediening van micronaalden arrays op de huid vereenvoudigd worden. Om dit te bereiken moet het onderzoek gericht zijn op i) de vaccinformulering met o.a. aandacht voor de stabiliteit, ii) efficiënte insertie en oplosbaarheid van de micronaalden in de huid, iii) steriliteit van het product, waarbij nieuwe productie stappen ontwikkeld moeten worden, iv) adjuvantia die mogelijk toegevoegd moeten worden voor minder immunogene antigenen, v) het productieproces waarbij ook het antigeenverlies tijdens de fabricage in beschouwing moet worden genomen.

Een eerste uitdaging waarmee we geconfronteerd worden tijdens de fabricage van de micronaalden is het verlies van het antigeen in de gietvorm, wat kostenverhogend werkt. Toekomstig onderzoek moet daarom gericht zijn om het vaccin voor in de punt van de naald te gieten [10,11]. Dit zou vaccinatie met behulp van micronaalden betaalbaar maken voor ontwikkelingslanden.

Een tweede kritisch punt is een efficiënte en volledige insertie in de huid. Wanneer als gevolg van de geometrie of een gebrek aan lengte een onvolledige insertie plaats vindt, zal de naald niet volledig oplossen en dit zou leiden tot een niet reproduceerbare toediening en verlies van antigenen. Dit gebeurt ook indien patiënten de pleister met micronaalden niet lang genoeg dragen totdat de micronaalden volledig opgelost zijn. Om dit probleem het hoofd te bieden zijn diverse voorstellen gedaan zoals i) een pijlvormig oplosbare kop van de naald [12] samengesteld uit een polymeer die bij insertie los laat van de metalen schacht waarmee het verbonden is en zo in de huid vastgehouden wordt, totdat de naald volkomen opgelost is en ii) micronaalden te gebruiken zonder pleister, zodat een systeem gebruikt kan worden waarbij alleen individuele, medicijn bevattende oplosbare naalden in de huid worden geïnjecteerd [13]. Hoe dan ook, hier kleven ook nadelen aan: i) langere micronaalden (>600 μm [12]) die hoewel potentieel meer dan kortere naalden [14] de immuunrespons verhogen, veroorzaken waarschijnlijk ook meer pijn [15], ii) het gebruik van een apparaat, speciaal voor de toediening van micronaalden, vereist getraind personeel, die de kosten van deze toepassing verder opdrijft.

Het is van belang dat de micronaalden steriel zijn. In dit licht bezien is steriele fabricage essentieel [16]. Sterilisatiemethoden moeten in het productieproces ingebouwd worden, zonder dat het vaccin gemodificeerd wordt. Dit kan kostenverhogend werken. Zo zal bijvoorbeeld eindtraps sterilisatie met behulp van gamma straling, hitte behandelingen al dan niet met behulp van een magnetron of autoclaaf, minder duur zijn dan aseptische bereiding. Dit kan echter de micronaalden en hun inhoud beschadigen. Sommige van de

gebruikte materialen bezitten antibacteriële eigenschappen. Zij laten geen groei van bacteriën zien bij langdurige opslag en zullen hoogst waarschijnlijk geen infecties in de huid veroorzaken [17]. In dit geval, wanneer de initiële contaminatie erg laag is, kan het voldoende zijn om zonder steriele fabricage de micronaalden goedgekeurd te krijgen.

Voor minder immunogene antigenen zal de toediening van adjuvantia essentieel zijn om voldoende immuunrespons op te wekken, maar vanwege veiligheidsvoorschriften zijn niet al die stoffen geschikt voor dermale toediening. Als voorbeeld kunnen de klassieke op aluminium gebaseerde adjuvantia dienen, die een hardnekkige ontsteking veroorzaken bij intradermale injectie in muizen [18]. Enerzijds zal het vermijden van adjuvantia het vaccin minder complex maken, anderzijds kan het leiden tot een lagere werkzaamheid.

Een belangrijke stap in de productontwikkeling is het opschalen van het bereidingsproces. Er zijn talrijke productiemethoden op kleine schaal beschreven (zie Hoofdstuk 2), die processtappen bevatten die moeilijk opschaalbaar zijn (bv. centrifuge en het gebruik van vacuüm). Bovendien zijn richtlijnen vereist met betrekking tot GMP, farmacopee referenties, en geschikte kwaliteitscontrole testen [19]. Speciale voorschriften over verpakking, verwijdering, en verzekering van correct gebruik zijn daarbij ook nodig. Door het innovatieve karakter van deze technologie blijft het gebrek aan regelgeving echter een barrière voor de beschikbaarheid van oplosbare micronaalden. Hoewel het gebruik van oplosbare micronaalden voor vaccinatie veelbelovend is, zijn er nog geen producten op de markt. Dit zal naar verwachting veranderen in het komende decennium, aangezien verscheidene producten in klinische ontwikkeling zijn [8,9]. Op dit moment zijn bedrijven bezig met het opzetten van een productielijn van oplosbare micronaalden voor huidverzorgingscosmetica [20] en voor de levering van biologische producten voor de huid [21]. Dit laatste met een succesvol afgeronde fase 2a klinische evaluatie.

Zodra de productieprocessen zijn geoptimaliseerd en de regulatoire hindernissen zijn opgelost, kan vaccinatie door middel van oplosbare micronaalden een hoeksteen in het verbeteren van de vaccinatiegraad over de hele wereld worden.

Het grote potentieel van oplosbare micronaalden

Hoewel oplosbare micronaalden nog een lange ontwikkelingsroute te gaan hebben, alvorens gereed te zijn als regulier product, vormen zij een groot potentieel boven andere micronaald types: oplosbare micronaalden bestaan uit droge formuleringen die i.h.a. een betere vaccinstabiliteit hebben dan vloeibare formuleringen, die in traditionele vaccinatieroutes gebruikt worden [22,23]. Door deze verhoogde stabiliteit kunnen deze micronaalden de noodzaak van een koude keten omzeilen en zijn ze ideaal voor vaccinatiecampagnes in ontwikkelingsladen. Dit zou de vaccinatiekosten voor vervoer en opslag aanzienlijk verminderen en daardoor de vaccinatiegraad en de efficiëntie van de vaccinatieprogramma's kunnen verhogen.

Bovendien laat vaccinatie door middel van oplosbare micronaalden in de meeste gevallen een vergelijkbare of zelfs hogere respons zien dan bij een conventionele injectie (zie Hoofdstuk 2). De besparing van de antigeendosis, zoals beschreven in Hoofdstuk 6, biedt een ander voordeel voor vaccinatie via de huid door oplosbare micronaalden.

Het belang van het toepassen van micronaalden

In dit proefschrift zijn twee soorten micronaalden beschreven voor het toedienen van vaccins: een holle micronaald en oplosbare micronaalden. Beide types vereisen toedieningsapparaten.

Het gecontroleerd en nauwkeurig injecteren van een specifiek volume van het vaccin in de huid door middel van een holle micronaald vereist een complex apparaat met een applicator en een pomp om tot een gecontroleerde diepte door te dringen in de huid.

Oplosbare micronaalden kunnen snel toegediend worden en het kost relatief weinig tijd om ze in de huid op te laten lossen. Het gebruik van een applicator is echter mogelijk niet haalbaar in gebieden met een gebrek aan infrastructuur. Technische storingen of verlies van de applicator kunnen de immunisatieprogramma's lokaal verstoren. Boven zal het gebruik van een apparaat voor de toepassing de vaccinatiekosten verhogen.

In dit opzicht zou het een belangrijke verbetering zijn als de micronaalden gebruikt kunnen worden zonder het gebruik van een applicator. Hierdoor kan de behoefte aan geschoold personeel worden vermeden en zou zelftoediening mogelijk worden, vooral op afgelegen plaatsen in de wereld of in het geval van het uitbreken van een pandemie. Studies tonen aan dat het gebruik van een applicator de efficiëntie en reproduceerbaarheid van het inbrengen van micronaalden verbetert[24] en dat korte micronaalden (300 µm), maar ook minder scherpe micronaalden, een lagere penetratie-efficiëntie in de huid kunnen hebben dan langere (>550 µm)[25-27] en dat het gebruik van een applicator bij kortere naalden dus cruciaal kan zijn voor efficiënte toediening in de huid. Handmatige toepassing, waarbij het gebruik van een applicator wordt vermeden, is mogelijk en succesvol [8, 9] indien langere micronaalden worden gebruikt. In dit geval kunnen lange naalden nog steeds beschouwd worden als minder invasief dan injectienaalden, en veroorzaken ze veel minder pijn. Tabel 1 geeft een overzicht van de voor- en nadelen van het gebruik van een applicator bij het aanbrengen van micronaalden.

Tabel 1. Voor- en nadelen van handmatig toediening en toepassing door middel van een applicator.

Handmatige toediening		Toepassen van een applicator	
Voordelen	**Nadelen**	**Voordelen**	**Nadelen**
Lagere productiekosten	Beperking in micronaald lengte: alleen lange micronaalden	Geen beperking in lengte (toediening van korte micronaalden mogelijk)	Hogere productiekosten
Geen getraind personeel nodig	Gebruik van langere micronaalden is pijnlijker	Efficiënter en reproduceerbaarder injectie	Getraind personeel nodig
			Afhankelijk van technologie ter plekke

De rol van hyaluronan bij vaccinatie door middel van oplosbare micronaalden

Zoals aangetoond in hoofdstuk 5, heeft het hyaluronzuur dat gebruikt wordt als matrixmateriaal geen effect op de immuunrespons na vaccinatie door oplosbare micronaalden, ondanks de gerapporteerde immuunmodulerende eigenschappen van hyaluronzuur met een laag molecuulgewicht [28]. Echter, volgens de literatuur kan hyaluronzuur geconjugeerd met ovalbumine dendritische cellen *in vitro* efficiënter activeren dan ovalbumine alleen [29] en conjugatie kan de toediening van grotere verbindingen via het lymfestelsel verbeteren[30]. Bovendien leidde intramusculaire injectie van hyaluronzuur-ovalbumine-conjugaten tot een hogere immuunrespons dan ovalbumine alleen [29]. Daartoe zou het interessant zijn om hyaluronan-antigeenconjugaten in te kapselen in oplosbare micronaalden om immunogeniciteit te bereiken.

CONCLUSIE

Het in dit proefschrift beschreven onderzoek toonde aan dat oplosbare micronaalden die gebruikt worden voor de afgifte van vaccins via de huid een antigeen specifieke immuunrespons kan oproepen die vergelijkbaar is met de conventionele subcutane route.
Er is echter verder onderzoek nodig om deze technologie te optimaliseren en verschillende productie- en toepassingshindernissen te overwinnen om het onderzoek te vertalen naar werkzame commerciële producten.

Curriculum Vitae

Mara Leone was born on the 20th of January 1987 in Avellino, Italy. After graduating from the Liceo Classico P.E. Imbriani summa cum laude in 2006, she started her study in Molecular and Diagnostic Biotechnologies at the faculty of Mathematic, Physic and Natural Sciences (University of Sannio, Benevento, Italy) where she obtained her Bachelor's degree in 2009 with honors (summa cum laude) and academic mention with a thesis in molecular biotechnology entitled "Endocrine disrupting chemicals: structure, mechanism of action and their effects on the thyroid gland". From 2009 to 2011 she studied Genetic Sciences and Technologies at the Biogem research center (University of Sannio, Benevento, Italy). During her study she did an internship in the field of Biochemistry, entitled "The role of cAMP on human keratinocytes in culture". In 2011 she obtained her Master's degree with honors (summa cum laude).

In parallel to the scientific studies, from 2002 to 2011 she studied classical piano at the National Conservatory of Music of Benevento, Italy obtaining her ten years degree in 2011 summa cum laude.

In 2011 she started her Masters in Opera Coach/Assistant Conductor and World Music respectively at the National Conservatory of Benevento, Italy and at the University of Arts (Codarts) in Rotterdam, The Netherlands.

After completing her musical studies in 2014, she started her internship at the Erasmus Medical Center of Rotterdam at the department of Neuroscience with a project focusing on the molecular and cellular mechanisms underlying learning and neurodevelopmental disorders.

In July 2014 she started her PhD project at Leiden University under the supervision of Prof. Dr. Joke Bouwstra and Prof. Dr. Gideon Kersten (Division of BioTherapeutics, Leiden Academic Centre for Drug Research (LACDR), Leiden University) which resulted in this thesis.

In June 2019 she started as Scientist at the Business Unit Formulation and Lyophilization at Coriolis Pharma, a biopharmaceutical research and development service in Munich, Germany.

List of publications

M. Leone, J. Monkare, J.A. Bouwstra, G. Kersten, Dissolving Microneedle Patches for Dermal Vaccination, Pharm Res, 34 (2017) 2223-2240.

M. Leone, B.H. van Oorschot, M.R. Nejadnik, A. Bocchino, M. Rosato, G. Kersten, C. O'Mahony, J. Bouwstra, K. van der Maaden, Universal Applicator for Digitally-Controlled Pressing Force and Impact Velocity Insertion of Microneedles into Skin, Pharmaceutics, 10 (2018).

M. Leone, M.I. Priester, S. Romeijn, M.R. Nejadnik, J. Monkare, C. O'Mahony, W. Jiskoot, G. Kersten, J.A. Bouwstra, Hyaluronan-based dissolving microneedles with high antigen content for intradermal vaccination: Formulation, physicochemical characterization and immunogenicity assessment, Eur J Pharm Biopharm, 134 (2019) 49-59.

M. Leone, S. Romeijn, B. Slutter, C. O'Mahony, G. Kersten, J.A. Bouwstra, Hyaluronan molecular weight: Effects on dissolution time of dissolving microneedles in the skin and on immunogenicity of antigen, Eur J Pharm Sci, 146 (2020) 105269.

M. Leone, S. Romeijn, G. Du, S.E. Le Devedec, H. Vrieling, C. O'Mahony, J.A. Bouwstra, G. Kersten, Diphtheria toxoid dissolving microneedle vaccination: Adjuvant screening and effect of repeated-fractional dose administration, Int J Pharm, 580 (2020) 119182.

G. Du, **M. Leone**, S. Romeijn, G. Kersten, W. Jiskoot, J.A. Bouwstra, Immunogenicity of diphtheria toxoid and poly(I:C) loaded cationic liposomes after hollow microneedle-mediated intradermal injection in mice, Int J Pharm, 547 (2018) 250-257.

G. Du, L. Woythe, K. van der Maaden, **M. Leone**, S. Romeijn, A. Kros, G. Kersten, W. Jiskoot, J.A. Bouwstra, Coated and Hollow Microneedle-Mediated Intradermal Immunization in Mice with Diphtheria Toxoid Loaded Mesoporous Silica Nanoparticles, Pharm Res, 35 (2018) 189.

J. Monkare, M. Pontier, E.E.M. van Kampen, G. Du, **M. Leone**, S. Romeijn, M.R. Nejadnik, C. O'Mahony, B. Slutter, W. Jiskoot, J.A. Bouwstra, Development of PLGA nanoparticle loaded dissolving microneedles and comparison with hollow microneedles in intradermal vaccine delivery, Eur J Pharm Biopharm, 129 (2018) 111-121.